Civil and Environmental Engineering Department

# Cold In-Place Recycling Characterization Framework and Design Guidance for Single or Multiple Component Binder Systems

**Report Written and Performed By:**
Ben C. Cox – Mississippi State University
Isaac L. Howard – Mississippi State University

**Final Report**
**FHWA/MS-DOT-RD-15-250-Volume 2**
**December 2015**

Mississippi State University
CMRC
Construction Materials Research Center
An Industry, Agency & University Partnership

## Technical Report Documentation Page

| | | |
|---|---|---|
| 1. Report No.<br>FHWA/MS-DOT-RD-15-250 Volume 2 | 2. Government Accession No. | 3. Recipient's Catalog No. |
| 4. Title and Subtitle<br><br>Cold In-Place Recycling Characterization Framework and Design Guidance for Single or Multiple Component Binder Systems | | 5. Report Date<br>December 18, 2015 |
| | | 6. Performing Organization Code |
| 7. Author(s)<br>*Ben C. Cox*, PhD Candidate, MSU<br>*Isaac L. Howard*, Materials and Construction Industries Chair, MSU | | 8. Performing Organization Report No. |
| 9. Performing Organization Name and Address<br>Mississippi State University (MSU)<br>Civil and Environmental Engineering Department<br>501 Hardy Road: P.O. Box 9546<br>Mississippi State, MS 39762 | | 10. Work Unit No. (TRAIS) |
| | | 11. Contract or Grant No. |
| 12. Sponsoring Agency Name and Address<br>Mississippi Department of Transportation (MDOT)<br>Research Division<br>P.O. Box 1850<br>Jackson, MS 39215-1850 | | 13. Type of Report and Period Covered<br>Final Report<br>January 2012 to December 2015 |
| | | 14. Sponsoring Agency Code |

Supplementary Notes: Work performed under Mississippi State University research project titled: *Full Depth Reclamation for High Traffic Applications.* The work performed for this report was under Mississippi Department of Transportation State Study 250 and principal investigator Isaac L. Howard. Two additional reports were performed as part of State Study 250, which were designated FHWA/MS-DOT-RD-15-250-Volume 1 and FHWA/MS-DOT-RD-15-250-Volume 3. Volume 1 deals with full-depth reclamation, while Volume 3 deals with infiltration and thin-lift asphalt concrete joints.

16. Abstract

This report focused on cold in-place recycling (CIR) and presented laboratory and field data collected during this multi-year study. The primary objective of this report was to characterize CIR properties that are important to design, construction, and performance in high-traffic applications. This report considers single component binder (SCB) or multiple component binder (MCB) systems used to stabilize reclaimed asphalt pavement (RAP) to produce CIR. Stated simply, a framework capable of encompassing any cementitious or bituminous binder within one protocol in an unbiased way did not exist prior to completion of the activities presented in this report to the author's knowledge. The primary conclusion from this report is that a framework capable of systematically addressing single or multiple component binder systems in an unbiased manner for CIR is feasible technically and from the standpoint of implementation. The framework prepares specimens at a 6% moisture content, compacts specimens 30 to 40 gyrations in a Superpave Gyratory Compactor, uses a maximum mixture specific gravity ($G_{mm}$) protocol developed in this research, uses AASHTO T269 or T331 to determine bulk mixture specific gravity ($G_{mb}$), cures specimens in a humid oven at 40 °C and 35-50% relative humidity, and tests specimens via APA wheel tracking and instrumented indirect tension. Overall, a blend of 1.5% cement and 3% emulsion by mass, while not the most economical blend tested, appeared to offer the best balance of rutting and cracking.

| | | | |
|---|---|---|---|
| 17. Key Words<br>Cold-in-Place Recycling, CIR, Portland Cement, Asphalt Emulsion, Universal Design Method, Rutting, Cracking, Wheel Tracking | | 18. Distribution Statement<br>No distribution restrictions. | |
| 19. Security Classif. (of this report)<br>Unclassified | 20. Security Classif. (of this page)<br>Unclassified | 21. No. of Pages<br>184 | 22. Price |

**Form DOT F 1700.7** (8-72) **Reproduction of completed page authorized**

# NOTICE

The contents of this report reflect the views of the author, who is responsible for the facts and accuracy of the data presented herein. The contents do not necessarily reflect the views or policies of the Mississippi Department of Transportation or the Federal Highway Administration. This report does not constitute a standard, specification, or regulation.

This document is disseminated under the sponsorship of the Department of Transportation in the interest of information exchange. The United States Government and the State of Mississippi assume no liability for its contents or use thereof.

The United States Government and the State of Mississippi do not endorse products or manufacturers. Trade or manufacturer's names appear herein solely because they are considered essential to the object of this report.

# TABLE OF CONTENTS

# LIST OF FIGURES

# LIST OF TABLES

# ACKNOWLEDGEMENTS

Thanks are due to many for the successful completion of this report. The MDOT Research Division is owed special thanks for funding State Study 250. James Watkins served as State Research Engineer for this project. The MDOT Project Engineer was Alex Middleton. Additionally, Jonathan Dixon, Durwood Graham, Nan Mitchell, Drew Parker, Matt Strickland, and Griffin Sullivan provided technical and logistical assistance for this project.

Ergon Asphalt & Emulsions, Inc. and Paragon Technical Services, Inc. assisted this project in a significant way. Most notably was the financial support within the *Ergon Asphalt & Emulsions Distinguished Doctoral Fellowship in Construction Materials* held by Ben C. Cox during the time frame of State Study 250. This fellowship was not associated with State Study 250, but its benefit was significant in that it provided a vehicle for Ben C. Cox to pursue graduate education, which benefitted a variety of activities including State Study 250. In addition to the aforementioned fellowship, technical support, testing, and raw materials were provided in-kind. Those deserving special thanks are Gaylon Baumgardner, Baxter Burns, John Dumas, Mike Hemsley, Mark Ishee, Paul Morris, and Trey Jordan.

The University of Florida (UF) was very helpful and forthcoming regarding past experiences with cracking characterization testing. Key individuals at UF were Dr. Reynaldo Roque, Dr. Jian Zou, and George Lopp. UF's technical guidance was extremely useful with regard to the authors being able to characterize in place recycled materials.

Burns Cooley Dennis, Inc. (BCD) assisted this report with sampling assistance, technical review of some parts of the project, and data taken during construction of US-49. Drs. L. Allen Cooley, Jr. and Randy Ahlrich provided the majority of the assistance received from BCD. Randy Battey of Gresham, Smith, and Partners (retired from MDOT) also provided technical assistance for US-49 activities. Dr. Colin S. Campbell of Decagon Devices, Inc. assisted with instrumented moisture testing and data analysis, and Dr. Kent Newman of the Engineer Research and Development Center (ERDC) provided technical review of some parts of this report.

Dr. Don Christensen provided the LTSTRESS.xls spreadsheet for use by the authors, and Dr. Jan DuBien (Mississippi State University Professor of Statistics) provided considerable technical review and guidance related to data analysis. APAC Mississippi, Inc. (Michael Bogue and Scott Glusenkamp), InstroTek, Inc. (Ali Regimand), and Holcim (US), Inc. (Tim Cost) provided in-kind materials, technical support, testing services, project information, and/or facilitated field work. Joe Ivy of Mississippi State University (MSU) facilitated laboratory and field work by maintaining laboratory equipment as well as designing and fabricating multiple pieces of equipment.

Several current and former MSU students assisted State Study 250 in a variety of manners, mostly as undergraduate or graduate research assistants. Among them are Graham Coffelt, Justin Cooper, Will Crawley, Web Floyd, Brad Hansen, Chase Hopkins, Dr. Robert James, Patrick Kuykendall, Alyssa Leard (Barksdale), Jon Love, Garrison Lipscomb, Drew Moore, Brad Robinson, Matt Roddy, Braden Smith, and Tim Woolman. The efforts of these individuals were vital to the completion of State Study 250.

# LIST OF SYMBOLS AND ACRONYMS

| | |
|---|---|
| *a* | Inside cross-sectional area, referring to MSP standpipe |
| *A* | Cross-sectional contact area, referring to MSP permeability |
| $A_s$ | Total area beneath thermal profile curve and a 0 °C reference temperature |
| $A_{\Delta T}$ | Total area between thermal profiles of a test specimen and inert reference |
| AADT | Annual average daily traffic |
| AASHTO | American Association of State Highway and Transportation Officials |
| *Abs* | Absorption |
| AC | Asphalt concrete |
| AC1 to AC8 | Asphalt concrete mixtures 1 to 8 |
| APA | Asphalt pavement analyzer |
| A/R | As-received |
| ASTM | American Society for Testing and Materials |
| Avg | Average |
| BBR | Bending beam rheometer |
| BCD | Burns Cooley Dennis, Inc. |
| BOP | Beginning of project |
| c | Portland cement and portland cement content |
| $C_1$ to $C_5$ | Regression constants |
| CCPR | Cold central-plant recycling |
| *CF* | Relative correction factor |
| *CI* | Cracking index, used in Chapter 9, similar to FE used throughout the report |
| C.I. | Confidence interval |
| COV | Coefficient of variation |
| CIR | Cold in-place recycling |
| CR | Moist curing room |
| CR1 to CR2 | Laboratory-produced crushed RAP materials 1 to 2 |
| *CR +#4* | Percentage of crushed material larger than 4.75 mm |
| CRIM | Complex refractive index model |
| CrRAP | Laboratory-produced crushed RAP |
| CTB | Cement-treated base |
| $d_0$ | FWD deflections under the center of loading |
| *D/B* | Dust to binder ratio |
| $D_{b\text{-}s}$ | Bulk density of LAC slab (dry mass divided by calculated volume) |
| $D_{HMA}$ | Asphalt concrete thickness |
| $D_p$ | Total pavement thickness |
| DCB | Density curve broke |
| DCSE | Dissipated creep strain energy |
| $DCSE_{min}$ | Minimum DCSE |
| DCT | Disc-shaped compact tension |
| DDC | Deformation differential curve |
| DGA | Dense graded asphalt |
| DNB | Density curve did not break, reported max density achieved |
| DO | Dry oven |
| $DO_{40C}$ | Dry oven curing at 40 °C |

| | |
|---|---|
| $DO_{60C}$ | Dry oven curing at 60 °C |
| DOT | Department of Transportation |
| D(t) | Creep compliance |
| d2*s* | Two-sigma limit, max allowable difference between two test results |
| e | Emulsion and emulsion content |
| *E* | Elastic modulus |
| EC | Evaluation criteria |
| EE | Elastic energy |
| EOP | End of project |
| ER | Energy ratio |
| ERDC | Engineering Research and Development Center |
| ESAL | Equivalent single axle load |
| FA | Fly ash |
| *FAA* | Fine aggregate angularity |
| FC | Field-compacted |
| FDR | Full-depth reclamation |
| FE | Fracture energy |
| FWD | Falling weight deflectometer |
| $G_b$ | Specific gravity of asphalt binder |
| $G_{cm}$ | Specific gravity of portland cement |
| $G_{HL}$ | Specific gravity of hydrated lime |
| $G_{mb}$ | Bulk specific gravity, always referring to a dry density |
| $G_{mb,dry}$ | Dry bulk specific gravity |
| $G_{mb,wet}$ | Wet bulk specific gravity |
| $G_{mm}$ | Mixture maximum specific gravity |
| $G_{mm,CIR}$ | Estimated $G_{mm}$ for a CIR mixture according to Equation 4.3 |
| $G_{mm,RAP}$ | $G_{mm}$ of RAP, typically referring to that measured by D6857 |
| $G_{sa}$ | Apparent specific gravity |
| $G_{sb}$ | Bulk specific gravity |
| $G_{se}$ | Effective specific gravity |
| $G_w$ | Specific gravity of water (0.997 g/cm$^3$ at 25 °C) |
| GC | Coarse gradation |
| GF | Fine gradation |
| $GS3_i$ | Observed raw GS3 reading at time *i* |
| $GS3_{i,corrected}$ | Temperature-corrected GS3 reading at time *i* |
| *GV* | Type I portland cement from Holcim, Saint Genevieve, MO |
| $h_1$ | Initial head during permeability testing |
| $h_2$ | Final head during permeability testing |
| h/d | Height to diameter ratio |
| HIR | Hot in-place recycling |
| HL | Hydrated lime and hydrated lime content |
| HLWT | Hamburg Loaded Wheel Tester |
| HLS | Hydrated lime slurry |
| HO | Humid oven |
| IDT | Indirect tensile |
| *Inf* | Infiltration rate |

| | |
|---|---|
| $J_c$ | Critical strain energy release rate |
| $k_{20}$ | ASTM PS129 permeability adjusted to 20 °C |
| LC | Laboratory-compacted |
| *LH* | Type I portland cement from Lehigh Cement, Leeds, AL |
| LVDT | Linear variable displacement transducer |
| $M_{bag}$ | Dry mass of D6857 vacuum sealing bags |
| $M_{dry}$ | Dry mass of D6857 $G_{mm}$ sample |
| $M_L$ | Mass loss |
| $M_r$ | Resilient modulus |
| $M_{r,total}$ | Total resilient modulus |
| $M_{sub}$ | Submerged mass of D6857 $G_{mm}$ sample and vacuum sealing bags |
| $M_1$ | Initial specimen mass (before Cantabro testing) |
| $M_2$ | Final specimen mass (after Cantabro testing) |
| max | Maximum |
| $Max\ Range_{10}$ | Max acceptable range of ten individual test results |
| *MC* | Moisture content, refers to moisture content in a generic sense |
| $MC_E$ | Moisture content estimated from *MC* estimation plots |
| $MC_M$ | Moisture content directly measured through oven drying |
| MCB | Multiple component binder |
| MDOT | Mississippi Department of Transportation |
| min | Minimum |
| *MLP* | Multilaboratory precision |
| *MS* | Marshall stability |
| MSU | Mississippi State University |
| *n* | Number of replicates |
| $N_{des}$ | Design gyration level |
| $N_{gyr}$ | Gyration level |
| *NG* | Nuclear gage |
| NMAS | Nominal maximum aggregate size |
| *N/S* | Not specified |
| OD | Outdoor |
| OGCF | Open graded friction course |
| *OMC* | Optimum moisture content |
| $P_{AC}$ | Asphalt binder content |
| $P_{AC\text{-}T164}$ | Asphalt binder content determined by AASHTO T164 |
| $P_{AC\text{-}T308}$ | Asphalt binder content determined by AASHTO T308 |
| $P_{ba,mix}$ | Absorbed asphalt binder content by mix mass basis |
| $P_{be}$ | Effective asphalt binder content |
| $P_{cm}$ | Percent of cement by mass of RAP |
| $P_{Em}$ | Percent of emulsion by mass of RAP |
| $P_{HL}$ | Percent of hydrated lime by mass of RAP |
| $P_{Res}$ | Percent of asphalt residue by mass of emulsion |
| $P_{0.075}$ | Percent passing 0.075 mm |
| $P_{12.5}$ | Number of passes at 12.5 mm rut |
| $P_{12.5\text{-}HLWT}$ | Number of HLWT passes at 12.5 mm rut |
| $P_{12.5\text{-}PW}$ | Number of PURwheel passes at 12.5 mm rut |

| | |
|---|---|
| PCI | Pavement condition index |
| PG | Performance grade |
| PTSi | Paragon Technical Services, Inc. |
| PW | PURWheel laboratory wheel tracker |
| $PW_{dry}$ | PURWheel testing following dry test protocols |
| $PW_{wet}$ | PURWheel testing following wet test protocols |
| QL | Quick lime |
| $R^2$ | Coefficient of determination |
| RAP | Reclaimed asphalt pavement |
| $RD_{APA}$ | APA rut depth |
| $RD_{HLWT}$ | HLWT rut depth |
| $RD_{PW}$ | PURWheel rut depth |
| R.H. | Relative humidity |
| $RL_{pre}$ | Remaining life pre-construction |
| $RL_{post}$ | Remaining life post-construction |
| *RMS* | Retained Marshall stability |
| $RR_{APA}$ | APA rutting rate |
| $RR_{PW}$ | PURWheel rutting rate |
| *RT* | Raveling test |
| R1 to R4 | RAP material 1 to RAP material 4 |
| $S_C$ | Slope of PURWheel rutting data in the creep region |
| $S_S$ | Slope of PURWheel rutting data in the stripping region |
| $S_t$ | Indirect tensile strength |
| $S_{t,corr}$ | Indirect tensile strength corrected for $V_a$ |
| $S_{t,f}$ | Fracture $S_t$ |
| $S_{t,ult}$ | Ultimate $S_t$ |
| SCB | Single component binder |
| SCBend | Semi-circular bend |
| S.D. | Standard deviation |
| SEM | Scanning electron microscope |
| SENB | Single edge notched beam |
| SGC | Superpave gyratory compactor |
| SHRP | Strategic highway research program |
| SIP | Stripping inflection point |
| $SN_{eff}$ | Effective structural number |
| *SOP* | Single-operator precision |
| SS 250 | MDOT State Study 250 |
| SSD | Saturated surface dry |
| SSE | Sum of squared errors of prediction |
| St. Dev. | Standard deviation |
| $t$ | Elapsed time between $h_1$ and $h_2$ in permeability testing |
| $t_{max}$ | Time in which $T_{max}$ occurs in thermal measurement testing |
| $T_{crit}$ | Critical cracking temperature |
| $T_i$ | Temperature at time $i$ |
| $T_{max}$ | Maximum measured temperature from thermal measurement testing |
| $T_r$ | Reference temperature |

| | |
|---|---|
| TSR | Tensile strength ratio |
| *TTF* | Temperature-time factor |
| UCS | Unconfined compressive strength |
| $UCS_{corr}$ | Unconfined compressive strength corrected for $V_a$ |
| US-45Alt | US Highway 45 Alt |
| US-49 | US Highway 49 |
| $V_a$ | Air voids |
| $V_{air}$ | Air volume, equal to $V_a$ if $V_{water}$ is zero |
| $V_{a\text{-}s}$ | LAC slab $V_a$ by T331 basis |
| $V_{a(T166)}$ | $V_a$ measured by AASHTO T166 |
| $V_{a(T269)}$ | $V_a$ measured by AASHTO T269 |
| $V_{a(T331)}$ | $V_a$ measured by AASHTO T331 |
| $V_{CIR}$ | CIR volume fraction |
| $V_{total}$ | Total volume |
| $V_{water}$ | Water volume |
| VBE | Volume of effective binder |
| *VMA* | Voids in mineral aggregate |
| *VMC* | Volumetric moisture content |
| *VFA* | Voids filled with asphalt |
| V.S. | Vacuum saturated |
| $W_{CIR}$ | CIR weight |
| $w_{NE}/cm$ | Non-evaporable water-cement ratio |
| $W_{total}$ | Total weight |
| $W_{water}$ | Water weight |
| XRD | X-ray diffraction |
| $\alpha$ | Empirical power parameter equal to 2 in CRIM |
| $\beta$ | Fitted constant in Equation 11.1 |
| $\gamma_d$ | Dry density |
| $\gamma_{d,max}$ | Maximum dry density |
| $\Delta T$ | Max temperature difference between test specimen and inert reference |
| $\varepsilon_{air}$ | Dielectric constant of air |
| $\varepsilon_{bulk}$ | Bulk dielectric permittivity |
| $\varepsilon_{CIR}$ | CIR dielectric constant |
| $\varepsilon_f$ | Horizontal strain at fracture stress in an IDT test |
| $\varepsilon_{ult}$ | Horizontal strain at ultimate stress in an IDT test |
| $\varepsilon_{water}$ | Dielectric constant of water |
| μ | Poisson's ratio |
| με | Microstrain |
| $\omega$ | Gravimetric moisture content |
| $\omega_{add}$ | Moisture content due to added water only |
| $\omega_{comp}$ | Post-compaction SGC specimen moisture content |
| $\omega_{mix,actual}$ | Actual moisture content of an uncompacted mixture |
| $\omega_{mix,target}$ | Target moisture content of an uncompacted mixture |
| $\omega_{total}$ | Total moisture content (added water, emulsion water, and RAP moisture) |
| 1*s* | One-sigma limit, max allowable standard deviation of a group of results |

# CHAPTER 1 – INTRODUCTION

## 1.1 General and Background Information

Cold in-place recycling (CIR) and full depth reclamation (FDR) are in-place pavement re-construction techniques recently used by the Mississippi Department of Transportation (MDOT) on US Highway 49 (US-49) in Madison County, Mississippi (Federal Aid Project number for US-49 was NH-008-03(032)). In-place recycling can provide an economical solution for pavements if used in conjunction with proper cementing blends and construction practices. In-place recycling may be necessary for use in high traffic applications in the coming years within MDOT projects. As such, MDOT funded State Study 250 (SS 250) at Mississippi State University (MSU), and this report presents laboratory and field data regarding CIR performed during this multi-year study.

## 1.2 Objectives and Scope

The primary objective of this report was to characterize CIR properties that are important to design, construction, and performance in high traffic applications. This report was part of State Study 250 (SS 250), which was reported in three volumes. This report (Volume 2) focuses on in-place recycled material consisting only of asphalt concrete layers; i.e. CIR. Volume 1 compliments Volume 2 in that it is also related to in-place recycling, but addresses FDR. Volume 3 is not related to in-place recycling, rather studies characteristics of thin-lift asphalt concrete joints over time. Specific aspects of SS 250 addressed in this report are summarized in the remainder of this section. Note that the descriptions provided are for Modification 1 of the FDR component of SS 250's Scope of Work, which was reviewed and approved by MDOT in late 2014.

A literature review (Chapter 2) was conducted to find information related to in-place recycling, with high traffic applications being of special interest. Chapters 3, 4, and 5 provide properties of materials sampled for further use, and describe the laboratory and field experimental programs utilized for CIR. Chapter 6 provides properties of asphalt concrete that was used in some manner in later chapters. Asphalt concrete properties of the upper layers of US-49 were used during CIR field assessments, and asphalt concrete properties of a group of additional mixtures were used for comparison to laboratory produced CIR with single and multiple component binder systems.

Chapter 7 provides a series of mix design and supporting test results based largely on existing in-place recycling test methods. Most of the information in this chapter was not directly mentioned in the project's scope of work, but was incorporated to help provide clarity and context to help accomplish the main objective of this study (i.e. to characterize CIR for high traffic applications). Some of the testing performed included multiple replicates prepared in traditional manners (e.g. proctor compacted) for assessing existing methods while considering variability. In a similar manner, Chapter 8 provides information on CIR moisture-density relationships which was informative for preparing specimens for characterization testing.

Chapter 9 screened several test methods of possible interest for characterizing CIR with single and multiple component binder systems. Protocols were sought that could be useful for CIR stabilized with all cement, all emulsion, or a combination of cement and

emulsion where both were used at dosages over 1% by mass. Several of the protocols investigated were aimed at durability and cracking.

Chapter 10 developed test protocols to determine the maximum mixture specific gravity of CIR for design and quality control purposes. None of the information in this chapter was directly mentioned in the project's scope of work, but developing this tool was useful for the process of integrating design and construction. This tool also helped to unify characterization of single and multiple component binder systems.

Chapter 11 provides a series of investigations aimed at better understanding of early age CIR behaviors. Curing characteristics and traffic opening were two of the main items considered in this effort. A field CIR project on US Highway 45 Alternate (US-45 Alt) and subsequent testing of materials sampled from this project were the focus of this investigation.

US-49 was evaluated to assess performance of in-place recycling in a high traffic application, but also to provide information suitable to help improve CIR practices going forward. One example is to evaluate performance of emulsion only and cement only CIR sections and determine whether a multiple component binder system would be more appropriate for high traffic applications. This information is provided in Chapter 12.

Chapter 13 is the most comprehensive chapter in the document. Therein, single and multiple component binder systems are evaluated in a variety of manners including wheel tracking with the PURWheel and Asphalt Pavement Analyzer. Wheel tracking includes wet and dry testing, as well as some testing at reduced loads to account for various pavement depths. Strength versus time, strength variability, and permeability/infiltration testing is also performed. Also, indirect tensile strength, creep compliance, and resilient modulus testing was performed on multiple blends of CIR.

Chapter 14 provides concluding statements and recommendations. Conclusions were made largely from the perspective of the research performed and findings of the CIR portion of SS 250. Recommendations were made largely from the perspective of implementation and increased use of CIR for high traffic applications. Chapter 15 provides a list of references.

# CHAPTER 2 – LITERATURE REVIEW

## 2.1 Overview of Literature Review

Cold in-place recycling mix design and characterization methods are of interest within this literature review. A history and background of in-place recycling (CIR and FDR) is provided for context (Section 2.2). Though this report focuses on CIR, CIR and FDR can be closely related and are both discussed (FDR to a lesser extent) in this literature review (Section 2.3). The current state of practice regarding DOT mix designs for bituminous and cementitious binders is discussed (Section 2.4).

Section 2.5 discusses multiple component binder systems for in-place recycling materials. Section 2.6 discusses moisture in CIR mixtures primarily as it relates to mixing and compaction. Section 2.7 discusses curing protocols. Section 2.8 discusses density, primarily relating to density measurement. Section 2.9 discusses performance characterization tests, and Section 2.10 discusses literature relating to field evaluations of in-service CIR pavements. Within many sections of this chapter, asphalt concrete is also discussed when beneficial in providing a frame of reference for evaluating CIR.

## 2.2 History and Background of In-Place Recycling

As noted by Rogge et al. (1992), the term cold recycling is frequently misunderstood because it has been used to describe different processes with sometimes substantially different design concepts and results. Therefore, it is necessary to establish standard terminology for each recycling technique. The following paragraph presents the most common in-place or cold recycling techniques as most commonly defined in literature and as used throughout this report.

In-place recycling typically refers to three techniques: cold in-place recycling (CIR), full-depth reclamation (FDR), and hot in-place recycling (HIR). HIR is not discussed in this report. Similarly, cold recycling typically refers to two techniques: cold in-place recycling and cold central-place recycling (CCPR). CCPR is not discussed in this report, except for aspects which are common or applicable to both CCPR and CIR. CIR is the focus of this literature review, but FDR is also discussed where pertinent as many of the same considerations apply. Currently, CIR is defined as a process where existing asphalt concrete layers are reclaimed, resized, stabilized, mixed, placed, and re-compacted. FDR is similar except some portion of underlying layers (e.g. aggregate base) is also recycled.

Though in-place recycling was documented as early as the 1940s, these techniques did not begin to emerge as viable rehabilitation alternatives until the late 1970s (Epps, 1980). Low-volume roads were the focus of these early recycling efforts. Note that definitions of the term low-volume vary. For example, Mamlouk (1991) referred to routes with an annual average daily traffic (AADT) of 400 or less as low-volume. Kim et al. (2010) and Chen et al. (2010) considered any route over 800 AADT to be high-traffic.

Scherocman (1983) states that many low-volume roads were aggregate surfaced as originally built. Over time, as traffic volumes increased, single or double chip seal surface treatments were commonly placed. In some cases, cold or hot mix asphalt layers were eventually constructed; in others, additional chip seal treatments were applied. While periodic motor grader shaping of aggregate pavements was relatively straightforward,

maintenance became more complicated and costly once bituminous layers were present, creating opportunities favorable for in-place recycling.

Prior to the advent of milling machines, various types of equipment were used for recycling operations. Tractor attachments with steel tines were used to scarify existing pavements, though this generally yielded large pavement chunks and tines often penetrated deeper than planned, increasing the amount of material which must be stabilized (Alcoke et al., 1979; Epps, 1980; Scherocman, 1983). Hammer-mills were often used to re-size chunks produced during scarification (Wood, 1980; Scherocman, 1983). Uniform mixing of stabilization binders was often difficult (Scherocman, 1983). Material spreading was usually accomplished via motor grader or traditional paver, and conventional compaction equipment was typically used (Scherocman, 1983). Pavement reclamation with modern milling machines, which are preferred over other pulverization and mixing equipment, was not conducted until approximately 1980.

Advantages of in-place recycling include ability to: improve structural capacity relative to existing capacity, treat most pavement distress types and severities, improve ride quality, and reduce material transportation costs (Epps, 1980). Economics was a major driving factor behind in-place recycling in early years (Scherocman, 1983). For example, Spelman (1983) estimated more than $10,000 per kilometer savings by using CIR instead of traditional re-construction in Massachusetts. Bradbury et al. (1991) documented 33% cost savings relative to traditional re-construction in Ontario. Scholz et al. (1991) estimated 40% cost savings relative to a typical 50 mm asphalt concrete overlay.

Disadvantages of in-place recycling with any binder type include: curing is generally required to achieve adequate strength or stability, curing is usually dependent on temperature and humidity, and quality control is not as enhanced as for traditional plant recycling (Epps, 1980). For example, Mamlouk and Ayoub (1983) stated rutting and instability were common distresses observed with bituminous-stabilized projects, generally a result of slow asphalt emulsion curing. From its implementation, difficulty in adequate quality control has been considered a major disadvantage (Bandyopadhyay, 1982). To some degree, this could have been partly due to the considerable variability observed among mix design methods in a survey conducted by Wood et al. (1988). At present, there is no commonly accepted mix design method, though methods have become increasingly similar, and it may be argued that quality control is still an area where notable improvements are needed.

Epps (1980) conducted a literature review and found that early in-place recycling specifications were largely developed from soil stabilization and quality control specifications. For example, field compaction was (and still is) typically required to yield a specified percentage of laboratory-compacted density (e.g. 93% of laboratory-compacted density was recommended by AASHTO (1998) rather than of a fixed reference density such as maximum mixture specific gravity ($G_{mm}$). Cementitious-stabilized mixtures have been traditionally designed following Proctor-based methods, while bituminous-stabilized mixtures have been traditionally designed following Marshall, HVEEM, and, to a considerably lesser degree, Superpave methods.

Throughout the many years of in-place recycling use, single component binder (SCB) systems have governed the market (Cox and Howard, 2013). SCB systems are defined in this report as those with either one binder or two if the secondary binder dosage is 1% or less. For example, either 4% portland cement or 3% asphalt emulsion with 1% hydrated lime would both be considered SCB systems. Multiple component binder (MCB) systems (e.g. 2.5%

emulsion with 2% cement) are a major focus of this report and have not been studied in great detail or utilized in practice.

## 2.3 CIR and FDR General Comparison

In recent years, the distinction between CIR and FDR has become clearer; however, cross-use of the terms has been observed in practice. In the case of this report, discussing both CIR and FDR is useful, not only to further clarify distinctions between the two, but also to provide insight to binder systems since bituminous binders are more frequently used with CIR and cementitious binders are more frequently used for FDR. Cox and Howard (2013) presents data from 81 CIR and 18 FDR references, which is discussed herein.

Figure 2.1 presents CIR and FDR gradations from literature where *n* equals the number of gradations reported. The maximum density line for a 19 mm nominal maximum aggregate (NMAS) gradation (most CIR and FDR gradations were 19 mm NMAS) is also plotted to provide a reference point for comparing Figure 2.1a to 2.1b. Generally, CIR gradations are coarser than FDR gradations. At 7.1% on average, FDR typically has more fines (particles finer than an 0.075 mm sieve, $P_{0.075}$) than CIR (0.6% on average).

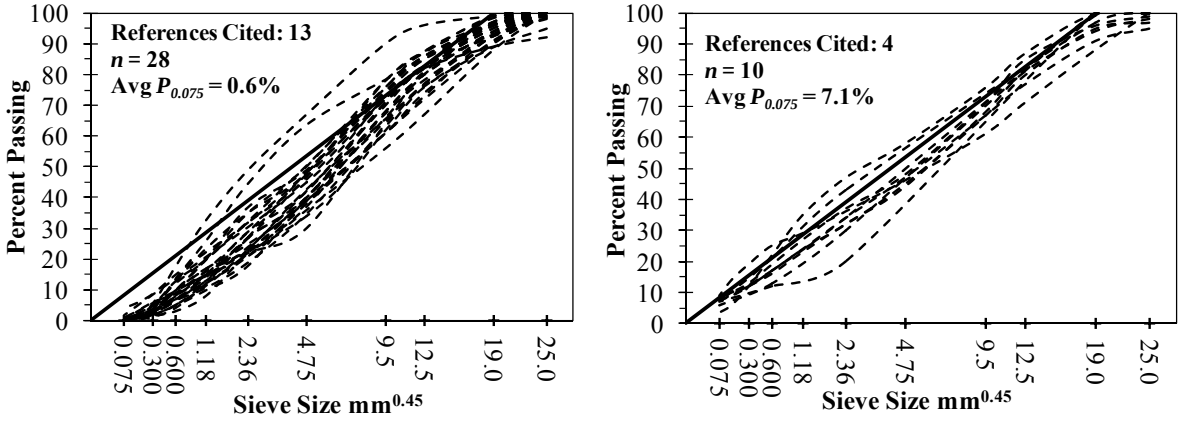


*a) CIR Gradations* *b) FDR Gradations*

**Figure 2.1. Comparison of CIR and FDR Gradations**

Figure 2.2 presents CIR and FDR histograms for AADT, layer thickness, and mixing and compaction moisture content. To compile these references into a consistent form, minor interpretation was required in some instances in Cox and Howard (2013); this should be noted but should not affect implications of Figure 2.2. Figures 2.2a and 2.2b indicate that AADT is not meaningfully different for CIR and FDR. AADT for both is generally less than 4,000 vehicles per day. Averages are similar at approximately 2,200 to 2,600. Figures 2.2a and 2.2b provide evidence that very few high-traffic in-place recycling projects have been conducted or studied, especially at US-49 traffic levels.

Figures 2.2c and 2.2d show that recycling depths for CIR and FDR are considerably different. By definition, it is intuitive that FDR recycling depths would, on average, be deeper than that of CIR. On average, FDR recycling depths, at approximately 22 cm, are more than twice that of CIR (approximately 8 cm).

Figure 2.2e and 2.2f show that moisture contents (*MC*'s) are also considerably different between CIR and FDR. The average FDR *MC* of approximately 7% is double the

3.5% average *MC* for CIR. Because FDR typically has a finer gradation, includes underlying base layers, and may have particles with some plasticity, it seems reasonable that FDR *MC*'s would be greater. It should be noted that water was accounted for differently in literature; therefore, an attempt was made in Cox and Howard (2013) to standardize all *MC*'s to total moisture content (i.e. added mixing moisture, water phase of asphalt emulsion, and existing moisture) for consistency. For Figure 2.2e and 2.2f, mixing *MC* and optimum *MC* (*OMC*) are considered equivalent.

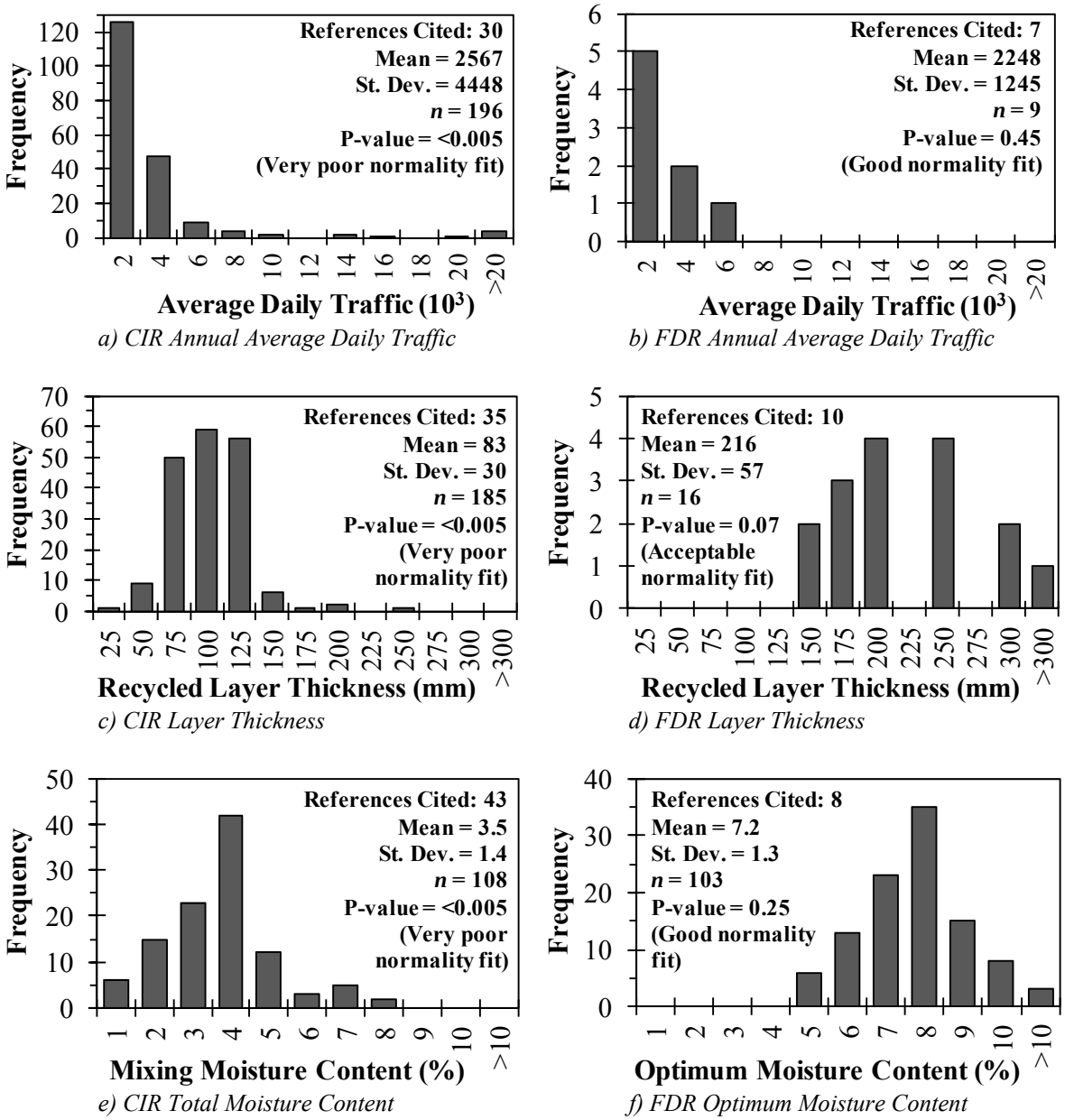


*a) CIR Annual Average Daily Traffic* *b) FDR Annual Average Daily Traffic*

*c) CIR Layer Thickness* *d) FDR Layer Thickness*

*e) CIR Total Moisture Content* *f) FDR Optimum Moisture Content*

**Figure 2.2. Comparison of CIR and FDR**

Table 2.1 presents a summary of binders and dosage rates observed in practice and research for CIR and FDR (Cox and Howard, 2013). CIR binders are more frequently bituminous (emulsion or foamed asphalt); whereas, FDR binders are more frequently

cementitious, particularly portland cement or fly ash. The average dosage rates for any binder increase from CIR to FDR, which again could be considered reasonable since FDR typically has a finer gradation and includes previously-unbound materials. In Cox and Howard (2013), 18% of CIR mixtures and 15% of FDR mixtures used a combination of binders. These blends were typically dominated by one binder with a small dosage of a secondary binder (e.g. 2.7% emulsion with 1% cement, which is an SCB system as defined in this report). Cox and Howard (2013) indicates that standard practice when cement or hydrated lime are included is to use 1 or 1.5% (but rarely more) dosage by mass.

**Table 2.1. Comparison of CIR and FDR Binder Dosage Rates**

| | | Emulsion | Foamed Asphalt | Cement | Hydrated Lime | Fly Ash |
|---|---|---|---|---|---|---|
| **CIR** | ***n*** | 145 | 37 | 29 | 12 | 11 |
| | **Mean (%)** | 1.9 | 2.3 | 1.5 | 1.2 | 8.8 |
| | **St. Dev. (%)** | 1.0 | 0.7 | 0.7 | 0.3 | 4.8 |
| | **Min (%)** | 0.3 | 1 | 0.5 | 0.75 | 3 |
| | **Max (%)** | 6.8 | 4.5 | 3 | 1.6 | 19 |
| | **Range (%)** | 6.5 | 3.5 | 2.5 | 0.85 | 16 |
| **FDR** | ***n*** | 24 | 7 | 55 | 7 | 41 |
| | **Mean (%)** | 3.6 | 3.0 | 4.3 | 2.7 | 11.8 |
| | **St. Dev. (%)** | 1.4 | 0.4 | 2.0 | 1.9 | 2.7 |
| | **Min (%)** | 1.25 | 2.5 | 1 | 1 | 5 |
| | **Max (%)** | 6 | 3.5 | 7 | 5.9 | 15 |
| | **Range (%)** | 4.75 | 1 | 6 | 4.9 | 10 |

*-- n = number of by-mass binder dosage values observed.*

## 2.4 State of Mix Design Practice

SCB systems are the predominant state of practice for CIR. Because of this, mix design methods are typically developed to be applied to one binder type, either bituminous or cementitious. These two mix design methodologies are almost completely in contrast to one another, which presents a challenge for MCB systems in that both binder types cannot be represented (either individually or collectively) in an unbiased manner.

DOT standard specifications and special provisions were reviewed in order to understand the current state of mix design practice. Mix design methods with asphalt emulsion and portland cement binders were the focus of this section. Nine emulsion and five cement design methods were reviewed; with regard to cement methods, one was for CIR and four were for FDR. The FDR design methods were included since cement CIR design methods were not readily available.

Tables 2.2 and 2.3 present summaries of emulsion and cement mix design methods, respectively, focusing on mix design components which are of interest to this report. A key observation is that methods are distinctly different between binder types but largely similar within a given binder type. Note that many DOT design specifications reference state test methods which are equivalent to various AASHTO and ASTM test methods. In these cases, Table 2.2 provides the AASHTO or ASTM designation, whichever is more prevalent, for ease of comprehension. In general, most state design methods in Table 2.2 are based off specification recommendations of Thomas and Kadrmas (2003).

**Table 2.2. Existing Emulsion Mix Design Methods**

| State | California (2005) | Illinois (2012) | Iowa (2008) | Kansas (2014) | Mississippi (2010a) | Montana (2015) | New York (2010)[b] | Texas (2004) | Virginia (2014) |
|---|---|---|---|---|---|---|---|---|---|
| Designation | LP-8 | S.P. LR 400-5 | I.M. 504 App. B | C.M. Part V-5.3.4 | S.P. 907-425-1 | S.P. 405-2 | Proposed Spec. | S.S. 3254 | S.P. S315X01-1214 |
| Mixing & Compaction *MC* | Expected *MC* during milling, typically 1.5 to 2.5% | *MC* needed for emulsion dispersion | 1.5% *MC* | Expected *MC* during milling, typically 1.5 to 2.5% | T180 Proctor-determined *OMC* | Expected *MC* during milling | Expected *MC* during milling, typically 1.5 to 4.5% | Expected *MC* during milling, typically 1.5 to 2.5% | T180 Proctor-determined *OMC* |
| Compaction | 75-blow Marshall or 30-gyration SGC | 30-gyration SGC | 30-gyration SGC | 30-gyration SGC | 30-gyration SGC | 30-gyration SGC | 75-blow Marshall or 30-gyration SGC | 35-gyration SGC | 75-blow Marshall or 30-gyration SGC |
| Curing | 60 °C to constant mass (in 16 to 48 hrs) | *N/S* | 60 °C for 48 hrs | 60 °C to constant mass (in 16 to 48 hrs) | *N/S* | 60 °C to constant mass (in 16 to 48 hrs) | 60 °C to constant mass (in 16 to 48 hrs) | 60 °C to constant mass (in 16 to 48 hrs) | 60 °C to constant mass |
| Density | T209[a] $G_{mm}$, T166[a] $G_{mb}$, report $V_a$ | T209[a] $G_{mm}$, T331[a] or T166[a] $G_{mb}$, report $V_a$ | T166[a] $G_{mb}$ | T209[a] $G_{mm}$, T166[a] $G_{mb}$, report $V_a$ | *N/S* | T209[a] $G_{mm}$, T166[a] $G_{mb}$, report $V_a$ | T209 $G_{mm}$, T166 $G_{mb}$, report $V_a$ | T209[a] $G_{mm}$, T166[a] $G_{mb}$, report $V_a$ | *N/S* |
| Design Binder Content Selection Tests [test criteria in brackets] | **1.** T245 *MS* [5.56 kN min at 40 °C] | **1.** T245[a] *MS* [5.56 kN min, *NS*] | **1.** T245[a] *MS* [4.45 kN min at 40 °C] | **1.** T245[a] *MS* [4.45 kN min at 40 °C] | **1.** MT-59 boil test [60% min] | **1.** T245 *MS* [5.56 kN min at 40 °C] | **1.** T245 *MS* [5.56 kN min at 40 °C] | **1.** T245[a] *MS* [11.12 kN min at 40 °C] | **1.** T245 *MS* [5.56 kN min at 40 °C] |
| | **2.** T245 *RMS* [70% min at 40 °C after V.S. and 24 hr soak] | **2.** T245[a] *RMS* [70% min, *N/S*] | **2.** T245[a] *RMS* [70% min at 40 °C after V.S. and 24 hr soak] | **2.** T245[a] *RMS* [70% min at 40 °C after V.S. and 24 hr soak] | **2.** MT-63 $S_t$ and TSR [310 kPa and 55%] | **2.** T245 *RMS* [70% min at 40 °C after V.S. and 24 hr soak] | **2.** T245 *RMS* [70% min at 40 °C after V.S. and 24 hr soak] | **2.** T245[a] *RMS* [70% min at 40 °C after V.S. and 24 hr soak] | **2.** T245 *RMS* [70% min at 40 °C after V.S. and 24 hr soak] |
| | **3.** D7196[a] *RT* [2% max, 20-gyr, cured at 21 °C for 4 hrs] | **3.** *RT* [2% max, at 10 °C] | **3.** D7196[a] *RT* [2% max, 20-gyr, cured at 10 °C for 4 hrs] | **3.** D7196[a] *RT* [2% max, 20-gyr, cured at 21 °C for 4 hrs] | **3.** Marshall quotient [61.3 kN/cm] | **3.** D7196 *RT* [5% max, 20-gyr, cured at 21 or 10 °C for 4 hrs] | **3.** D7196 *RT* [5% max, 20-gyr, cured at 10 °C for 4 hrs at 50% R.H.] | **3.** D7196 *RT* [2% max, 20-gyr, cured at 10 °C for 4 hrs at 50% R.H.] | **3.** D7196 *RT* [2% max, 20-gyr, cured at 10 °C for 4 hrs at 50% R.H.] |
| | | | **4.** T322 $T_{crit}$ [-20 °C max] | **4.** T322[a] $T_{crit}$ [less than LTPPBind 98% reliability low temp at top of CIR layer] | | **4.** T322 $T_{crit}$ [-31 °C max] | **4.** T322 $T_{crit}$ [-20 °C max] | **4.** T322 $T_{crit}$ [report only]<br>**5.** Tex-226-F $S_t$ [276 kPa min]<br>**6.** Tex-242-F HLWT [5,000<$P_{12.5}$<15,000] | **4.** T322 $T_{crit}$ [less than LTPPBind 98% reliability low temp at top of CIR layer] |

*a) Denotes equivalent ASTM, AASHTO, or state test method used*

*b) New York DOT proposed specification as per Cross et al. (2010)*

Regarding mixing and compaction *MC*, little attention is generally given to the *MC* used in laboratory design. The amount of water added usually targets the *MC* expected to be due to water added at the milling head in reclaiming operations. This ranges from 1.5 to 4.5% in Table 2.2 but is generally between 1.5 and 2.5%. Note that this does not include water present in asphalt emulsion (i.e. 3% emulsion adds approximately 1% additional moisture). Woods et al. (1988) observed from surveys that 1 to 2% moisture was usually introduced at the milling head for lubrication and dust control. In a few cases, *OMC* is determined by modified Proctor compaction.

Regarding compaction, nearly all states in Table 2.2 reference 30-gyration (gyr) Superpave gyratory compactor (SGC) compaction, with the exception of Texas which specifies 35 gyrations. Several states still allow for 75-blow Marshall compaction, though SGC compaction has become more prevalent. Note that 100 mm diameter specimens are typically compacted; however, some tests specified require 150 mm diameter specimens also.

Regarding curing, aside from the few states where curing protocols were not specified (*N/S*), all states reviewed call for 60 °C dry oven curing. The general goal of all curing methods is to achieve constant mass (i.e. essentially all water is removed), which is more representative of ultimate cure properties. Curing is generally limited to no more than 48 hours but more than 16 hours, and constant mass is generally defined as no more than 0.05% mass change in 2 hours.

Regarding density, most states require maximum and bulk specific gravity ($G_{mm}$ and $G_{mb}$) to be measured and air voids ($V_a$) to be reported, but they have no influence on the mix design. For full pay, field density, as measured by nuclear gage, is generally required to be 97 or 98% of either a test-strip density, field Proctor density, or laboratory bulk density. Therefore, while AASHTO T209 and T166 are often measured, they have little bearing on quality control. Note that most states requiring T166 specify that submerged masses be recorded at 1 minute instead of 4 minutes in order to minimize water absorption.

Design binder contents are selected based on several test criteria. All Table 2.2 states require Marshall stability in some form. Most states require T245 Marshall stability (*MS*) to be 5.56 kN (1,250 lbs) minimum when measured at 40 °C (conditioned for 2 hours at 40 °C). Moisture susceptibility testing is generally in the form of retained Marshall stability after being vacuum saturated (V.S.) (following T283 protocols) to 55 to 75% saturation, soaked in a 25 °C water bath for 23 hours, and soaked in a 40 °C water bath for the 24$^{th}$ hour to bring specimens to test temperature (some states specify 30 minutes instead of 1 hour). All states requiring retained Marshall stability (*RMS*) specify 70% *RMS* minimum.

Most states require early-age traffic-opening durability be evaluated with the raveling test (*RT*), generally ASTM D7196 or equivalent. These specimens are 150 mm in diameter and are compacted and cured differently. They are SGC-compacted 20 gyrations and then cured at either room temperature (i.e. 21 °C) or 10 °C for 4 hours (some states also specify 50% relative humidity (R.H.)). The ring weight is generally removed from the wet-track abrasion head so that the final mass is 0.6 kg (1.32 lbs). Tests are conducted for 15 minutes, and the final mass loss is generally to be less than 2%.

Many states also require AASHTO T322 low-temperature creep compliance testing for determination of the critical cracking temperature ($T_{crit}$). These specimens are generally compacted to 115 mm tall with batched masses adjusted to target the $V_a$ measured for the optimum emulsion content based on *MS* and *RMS* testing. Specimens are sliced to obtain two 50 mm thick slices per specimen. Generally, testing is conducted at three temperatures (e.g.

0, -10, and -20 °C). The temperature at the intersection of the thermal stress curve (derived from compliance data) and indirect tensile (IDT) strength ($S_t$) curve is taken as $T_{crit}$, which must be lower than the 98% reliability low-end temperature at the top of the CIR layer determined from LTPPBind.

Although not as common, Texas requires a minimum $S_t$ of 276 kPa at room temperature with a 50 mm/min loading rate. Mississippi requires 310 kPa $S_t$ minimum as well as a minimum tensile strength ratio (TSR) of 55%. Texas also requires CIR mixtures to meet Hamburg Loaded Wheel Tester (HLWT) thresholds. The number of passes to 12.5 mm of rutting ($P_{12.5}$) must be between 5,000 and 15,000 at the recommended emulsion content.

Within Table 2.2 design methods, practices vary regarding addition of cementitious binders. Several states do not specify any type of additional stabilizer such as cement or lime (e.g. Virginia, Iowa). Others state that cement and lime can be used but do not specify limitations or provide guidance on dosages (e.g. New York). Mississippi requires 1% hydrated lime by mass in all mixtures. Others allow cement but limit it to 1% maximum by mass and also limit the ratio of residual asphalt emulsion to cement. For example, Illinois requires residual asphalt content to be three or more times cement content, and California requires residual asphalt content to be 1.8 times cement content at a minimum.

Table 2.3 presents a summary of cement CIR and FDR mix design methods. There is almost no commonality between Tables 2.2 and 2.3. *OMC* and maximum dry density ($\gamma_{d,max}$) are determined by Proctor compaction for all Table 2.3 states. Mix design specimens are predominantly standard Proctor compacted, extruded, and then moist cured. Traditional curing in a moist curing room at room temperature is common as is curing in a sealed bag to maintain moisture. California cures specimens in sealed bags as well but at 40 °C. Unconfined compressive strength (UCS) is generally measured after 7 days of curing. Design cement contents are typically taken as those which provide a minimum 2,068 kPa (300 psi) but no more than some maximum UCS. Maximum UCS values vary but are generally around 3,447 kPa (500 psi).

**Table 2.3. Existing Cement Mix Design Methods**

| State | Alabama (2009) | California (2013) | Mississippi (2010b) | Pennsylvania (2012)[a] | New York (2014) |
|---|---|---|---|---|---|
| Designation | ALDOT-416 | Caltrans | S.P. 907-499-1 | Pub 30, Bulletin 5 | GEM-27 |
| Type | FDR | FDR | CIR | FDR | FDR |
| Mixing & Compaction *MC* | T134 Proctor-determined *OMC* | Proctor-determined *OMC* | MT-9 Proctor-determined *OMC* | T134 Proctor-determined *OMC* | T99 Proctor-determined *OMC* |
| Compaction | Standard Proctor (100 mm dia., 3 layers, 25 blows) | Modified Proctor (100 mm dia., 5 layers, 25 blows) | Standard Proctor | Standard Proctor (100 mm dia., 3 layers, 25 blows) | Standard Proctor (100 mm dia., 3 layers, 25 blows) |
| Curing | Moist cure in sealed bag at 21 °C for 7 days | Sealed in bag at 40 °C for 7 days | Moist cure at 23 °C and 95% R.H. for 14 days | Moist cure in sealed bag at 23 to 25 °C and 95% R.H. for 7 days | Moist cure at 23 °C and 95% R.H., cure time *NS* |
| Density | $\gamma_{d,max}$ | $\gamma_{d,max}$ | $\gamma_{d,max}$ | $\gamma_{d,max}$ | $\gamma_{d,max}$ |
| Design Binder Content Selection Tests [test criteria in brackets] | D1633 7-day UCS [2,068 kPa min, 2,758 kPa max] | D1633 7-day UCS [2,068 kPa min, 4,137 kPa max] | MT-25 14-day UCS [2,068 kPa min] | D1633 7-day UCS [2,068 kPa min, 3,447 kPa max] | D1633 UCS [2,413 kPa min, 5,516 kPa max] |

*a) Pennsylvania requirements are those found in Morian et al. (2012), which is a Pennsylvania DOT research report where Pub 30, Bulletin 5 (Pennsylvania's FDR design method) was revised.*

## 2.5 Multiple Component Binder Systems

Table 2.4 presents a summary of findings relating to MCB systems and associated performance aspects relative to emulsion-only or cement-only SCB systems. Table 2.4 shows that MCB behavior has been documented; however, most studies primarily focused on bituminous stabilization and considered cementitious binders as an additive. In doing so, specimen fabrication, curing, and testing protocols were generally those typically associated with emulsion mix design practices. Consequently, efforts generally focused on improving emulsion's properties with cementitious addition as long as effects were not adverse, which was often around 1 or 1.5% cement. This aligns with trends discussed in Section 2.3.

Table 2.4 demonstrates the ability of cementitious binders to improve resilient modulus ($M_r$), strength, moisture resistance, and rutting. It also draws attention to the negative impacts of cementitious binders, specifically relating to fatigue and thermal cracking resistance. A key observation from Table 2.4 is that MCB systems have not been greatly studied from a perspective of symmetry and balance (i.e. cement SCB, cement-dominated MCB, balanced cement and emulsion MCB, emulsion-dominated MCB, and emulsion SCB).

Several researchers have studied interactions between cement and emulsion binders in MCB systems. Brown and Needham (2000) conducted scanning electron microscope (SEM) testing of MCB aggregate mixtures. Results suggested cement was relatively unaffected by the presence of emulsion and cured in much the same manner as it would in normal concrete, indicating it would act as a binder to some extent. Montepara and Giulianai (2001) used X-ray diffraction (XRD) to study cement and emulsion interactions. XRD patterns of cement or emulsion SCB and cement-emulsion MCB mixtures overlapped completely, indicating a lack of chemical interaction. However, cement and emulsion MCBs exhibited synergistic attributes (e.g. cement aided emulsion breaking and curing).

Thomas et al. (2000) discussed a CIR project on US Highway 283 in Kansas. Two sections were constructed for side-by-side comparison of a fly ash SCB and an emulsion-hydrated lime slurry MCB. The motivation for this experimental project was related to past experiences with both binders. Kansas utilized emulsion CIR for many years with good results on many projects; however, rutting and stripping problems were encountered with some projects. These issues ultimately resulted in the Kansas DOT discontinuing use of emulsions for CIR in 1992 and specifying Class C fly ash as the only approved CIR additive. Rutting and stripping problems were alleviated with fly ash, especially when traffic was permitted on the CIR layer before surface treatment application, but premature cracking problems were encountered.

Mallick et al. (2002a) documents an FDR project in Maine where four sections were constructed. Three SCB sections were built with the following binders: 7% water, 5% cement, and 3.4% emulsion. One MCB section was built with 3.4% emulsion and 2% hydrated lime. Mallick et al. (2002a) conducted a structural evaluation one year after construction and ranked the four sections by cost per mile and effective cost per mile (Table 2.5). Effective cost per mile is defined as the cost per mile per 1,000 equivalent single axle load (ESAL) increase in performance life relative to pre-construction. The emulsion and lime MCB was the least economical blend per mile but was the most economical blend when performance life was also considered. Ultimately, Mallick et al. (2002a) recommended the MCB blend for consideration in future in-place recycling projects.

**Table 2.4. Multiple Component Binder Summary**

| Reference | RAP/Agg | Binders Studied | Findings |
|---|---|---|---|
| Terrel and Wang (1971) | 0/100 | 7e;<br>7e with 0.5, 1, 1.5, & 3c | -- Ultimate $M_r$ (triaxial) was increased up to 200% with increasing cement content<br>-- Cement accelerated curing |
| Schmidt et al. (1973) | 0/100 | 7.5e;<br>7.5e with 1.3 & 3c | -- Cement increased $M_r$<br>-- Increasing cement decreased fatigue resistance<br>-- Cement accelerated curing and improved moisture resistance |
| Head (1974) | 0/100 | 7e;<br>7e with 1 & 2c | -- 1c increased *MS* ~2 to 3 times<br>-- 2c increased *MS* ~3 to 4 times |
| Brown and Needham (2000) | 0/100 | 8e;<br>8e with 1, 2, 3, & 4c | -- Above 200 initial με, cement decreased fatigue life; below 200 initial με, cement (up to 3%) increased fatigue life<br>-- Cement improved moisture resistance |
| Zawadzki (2000) | ~30/70 | 3e with 2, 3, & 4c;<br>4e with 2, 3, & 4c;<br>5e with 2, 3, & 4c | -- $M_r$ (23 °C) increased considerably with cement and decreased slightly with increasing emulsion; total range was ~7 GPa (2c5e) to 20 GPa (4c3e)<br>-- *MS* (60 °C) increased with increasing cement and/or decreasing emulsion; total range was ~13 kN (2c5e) to 45 kN (4c3e)<br>-- $S_t$ (23 °C) increased with increasing cement and/or decreasing emulsion; total range was ~400 kPa (2c5e) to 1125 kPa (4c3e) |
| Thomas et al. (2000) | 100/0 | 1.5e1.5HLS; 10FA | -- $T_{crit}$ values were -27 °C (1.5e1.5HLS) and -12 °C (10FA) |
| Du and Cross (2006) | 100/0 | 1.5e;<br>1.5e with 1.5HL & 1.14QL | -- APA rut depths were 6.5 mm (1.5e) versus 4.5 mm (1.5e1.5HL) and 3.8 mm (1.5e1.14QL) |
| Niazi and Jalili (2009) | 80/20 | 3.5e;<br>3.5e with 2c, 2HLS, & 2HL | -- $M_r$ increased 175% (2c) and 130% (2HLS, 2HL) from 1190 MPa (3.5e)<br>-- $S_t$ increased 170% (2c), 140% (2HLS), and 100% (2HL) from 245 kPa (3.5e)<br>-- *MS* increased 150% (2c) and 140% (2HLS, 2HL) from 8.3 kN (3.5e)<br>-- Cementitious binders greatly increased *RMS* and TSR<br>-- Wheel-tracking rut depths decreased 60% (2c), 50% (2HLS), and 40% (2HL) from 12.5 mm |
| Kavussi and Modarres (2010b) | 100/0 | 4e;<br>4e with 1, 2, & 3c | -- Fatigue life increased with increasing cement content below 250 με and decreased with increasing cement content above 250 με |

*-- $M_r$ = resilient modulus -- $T_{crit}$ = critical cracking temperature -- MS = Marshall stability -- RMS = retained MS*
*-- $S_t$ = indirect tensile strength -- TSR = tensile strength ratio -- APA = Asphalt Pavement Analyzer*
*-- RAP/Agg refers to relative amounts of RAP and aggregate utilized (e.g. 0/100 is an aggregate-only mixture, 80/20 is 80% RAP and 20% aggregate).*
*-- Binder blends identified by number (dosage percentage) and letter (binder type) designations for emulsion (e), cement (c), hydrated lime (HL), hydrated lime slurry (HLS), quick lime (QL), and fly ash (FA). For example, 1.5e1.5HLS is 1.5% emulsion with 1.5% hydrated lime slurry.*
*-- HLS dosages refer to the effective lime dosage (e.g. 1.5% HLS implies 1.5 grams of lime in dry form per 100 grams of RAP).*

**Table 2.5. Cost Data from Mallick et al. (2002a)**

| Section | $RL_{pre}$ (ESALs) | $RL_{post}$ (ESALs) | Cost per Mile | Effective Cost per Mile |
|---|---|---|---|---|
| 7% Water | 8,100,000 | 18,400,000 | $24,100 | $2.40 |
| 5% Cement | 8,100,000 | 21,200,000 | $38,800 | $2.90 |
| 3.4% Emulsion | 9,300,000 | 18,400,000 | $41,200 | $4.00 |
| 3.4% Emulsion with 2% Hydrated Lime | 6,900,000 | 31,000,000 | $44,700 | $1.80 |

*-- Effective cost per mile is cost per mile per 1,000 ESAL increase in remaining life after CIR construction*
*-- $RL_{pre}$ = pre-construction remaining life -- $RL_{post}$ = post-construction remaining life*

Mallick et al. (2002c) studied several of the binder blends presented in Mallick et al. (2002a) as well as several additional blends. Blends tested in the laboratory were as follows: 7% water, 5% cement, 3% emulsion, 3% emulsion with 2% cement, 3% emulsion with 2% hydrated lime, and 3% emulsion with 2% cement and with 2% hydrated lime. Resilient modulus and wet APA rutting tests were conducted. The 3% emulsion with 2% hydrated lime blend provided the overall best rutting performance and strength/modulus improvement rate. The 3% emulsion with 2% cement blend provided comparable results.

## 2.6 Moisture

This section focuses on moisture as it relates to mixing and compaction of CIR mixtures. Anderson et al. (1985) noted that adequate water must be added to facilitate field mixing and compaction; however, more water is generally needed for mixing than compaction. Anderson et al. (1985) deals primarily with bituminous-stabilized CIR and does not consider cementitious-stabilized CIR. Moisture also plays a notable role in the curing of CIR mixtures; curing is discussed in the following section alongside any moisture-related aspects of curing.

Multiple methods for determining design *MC*'s have been used in practice and research. Early *MC* determination methods were usually based on coating tests. For example, Kandhal and Koehler (1987) selected the *MC* which visually provided 90% coating minimum when the emulsion content was fixed at 2.5%.

Fixed *MC*'s are commonly documented and generally range from 2 to 5% (e.g. Mamlouk and Ayoub, 1983; Scholz et al., 1991; Khosla and Bienvenu, 1996; Kim et al., 2011). These values are on the order of values commonly used in current DOT emulsion CIR design methods (Table 2.2). Marshall design principles are often used to select *MC*'s which optimize both density and strength or stability (e.g. Lee et al., 2001; Carter et al., 2010). Proctor-based moisture-density relationships have also been used to select *OMC* (e.g. Kim and Lee, 2006; Martinez et al., 2007).

Kim et al. (2007) attempted to determine an *OMC* for the CIR material studied but found no discernible *OMC*. Kim et al. (2007) stated the issue could be due to RAP's coarseness and lack of fines. Ultimately, a *MC* of 4.0% was selected, which is close to the average CIR *MC* based on Figure 2.2e.

Generally, Proctor compaction methods yield high *MC*'s such as those in the right tail of Figure 2.2e. For gyratory compaction at these *MC*'s, SGC molds and base plates have been perforated by some to allow for moisture drainage during compaction (Mallick et al., 2002b; Santagata et al., 2010; Bang et al., 2011). At Proctor-level *MC*'s, water was expelled, bringing into question its necessity. O'Leary and Williams (1992) suggested too much

moisture could inhibit field compaction (assuming water is not expelled) since excess water volume in the mixture could prevent densification of the particle matrix. For example, Babei and Walter (1989) recommended *MC* be limited to 4% maximum to satisfy compaction and void content requirements.

## 2.7 Curing

As discussed in Section 2.4, curing protocols generally target ultimate cure properties for either cement or emulsion SCB systems. Consequently, this goal leads to curing protocols which are vastly different between cement and emulsion SCBs. Further, current curing protocols represent a favorable environment for one binder and an unfavorable for the other.

Bituminous-stabilized mixtures are most commonly cured in a 60 °C oven (e.g. Mamlouk and Ayoub, 1983; Lee et al., 2001; Salomon and Newcomb, 2000; Cross, 2002). Other researchers have also used 40 °C oven curing (e.g. Kandhal and Koehler, 1987; Lee and Kim, 2003). Room temperature curing has also been utilized, generally when early-age properties are of interest (e.g. Steward, 1987; Cross, 1999a; Cross, 1999b; Moore et al., 2011).

Cementitious-stabilized mixtures are typically moist-cured at room temperature (e.g. Lewis et al., 2006; Berthelot et al., 2010). Cement mixtures have also been cured at room temperature and humidity (e.g. Litzka and Haslehner, 1995). When cementitious binders are added to bituminous-stabilized CIR, oven curing is generally utilized (e.g. Cross, 2002; Pasetto et al., 2004).

Field curing of CIR mixtures is similar to laboratory curing in that cement and emulsion protocols differ from each other. Cement mixtures are generally primed with an emulsion prime coat to retain moisture and are cured for a specified time (e.g. 7 days, 14 days). Emulsion mixtures are generally cured until the *MC* drops below a set threshold. Rogge et al. (1992) recommended a 1.5% *MC* threshold based on experience in Oregon. This seems to be one of the first documented references to the 1.5% *MC* threshold which is commonly used.

Lee et al. (2009), Kim and Lee (2011b), and Woods et al. (2012) studied the 1.5% *MC* criteria by instrumenting field CIR layers with moisture and temperature sensors at various depths. Collectively, this group (University of Iowa Department of Civil and Environmental Engineering) appears to be the only group who has documented CIR pavement layer instrumentation at present. In all, five foamed asphalt and two emulsion CIR projects were instrumented with $ECH_2O$ sensors (note that Woods et al. (2012) does not specify sensor type used, though it is likely the same as those used by Lee et al. (2009) and Kim and Lee (2011b)).

Discussion with the corresponding authors revealed that sensors were installed after compaction of CIR layers. Sensors were installed with their factory calibrations which, by default, are calibrated to report volumetric *MC* (*VMC*), primarily for mineral soil applications. Laboratory experiments were conducted after field data collection in order to correlate *VMC* to *MC* (gravimetric), which was ultimately reported in the published documents.

Except for rainfall events, sensor outputs were generally fairly constant throughout curing for all projects studied. Sensors were sensitive to rainfall; *MC* after rainfall generally ranged from 8 to 16% but was nearly 22% in several cases. Note that 22% moisture by mass

(*MC*, gravimetric) would be nearly 50% *VMC* since the specific gravity ratio of CIR to water is usually greater than 2 to 1. *MC*'s this high seem questionable and could perhaps be related to the field *VMC* to laboratory *MC* correlation. Pockets of air voids adjacent to the sensors due to post-compaction sensor installation could have also affected readings. Nonetheless, *MC* after rainfall generally decreased back to a baseline *MC* which was generally around 2 to 6% moisture depending on the project. EC$H_2O$ *MC*'s for all but one CIR project were above 2% when the projects were overlaid with their respective surface treatments.

## 2.8 Density

Many years of study with pavement materials demonstrate the importance of adequate density as it is directly related to performance. A critical component in terms of controlling density is the ability to effectively and efficiently measure density. Generally speaking, CIR densities in the field are measured by nuclear gage and referenced against test strip densities or laboratory-compacted bulk densities (e.g. Bradbury et al., 1991). In some cases, especially when Proctor $\gamma_{d,max}$ is the reference density, achieved field densities exceed laboratory densities considerably. For example, Gumbert and Harris (1993) do not specify which laboratory compaction method was used but report field core densities which were 100 to 108% of laboratory densities. This is a common observation among those who use Proctor compaction. In cases such as this, consideration of a different reference density approach may be warranted. To this end, this report focuses on using $G_{mm}$ as a more suitable reference density and also evaluates various methods for measuring $G_{mm}$ and $G_{mb}$ applicable to multiple binder systems. Literature review is presented for asphalt concrete (AC) $G_{mm}$, CIR and RAP $G_{mm}$, AC $G_{mb}$, and CIR $G_{mb}$.

### 2.8.1 Asphalt Concrete Maximum Specific Gravity

AASHTO T209 is the most widely accepted method for measuring asphalt $G_{mm}$; it is well-established and fairly reliable. Other methods such as ASTM D6857 have also been studied. D6857 is a test method for measuring $G_{mm}$ via vacuum sealing with such devices as the CoreLok®. Rajagopal and Crago (2007) investigated similarities of T209 and D6857. Statistical analysis conducted on the testing of four Ohio asphalt mixtures (33 replicates were tested in all) determined T209 and D6857 were not significantly different at a 5% significance level.

Sholar et al. (2005) conducted a larger study of D6857 and FM 1-T209, which is a Florida DOT method equivalent to T209 and is further denoted T209 for discussion. When T209 was conducted, the supplemental saturated surface dry (SSD) dry-back procedure outlined in T209 was also performed and is further denoted $T209_{SSD}$. Note that $T209_{SSD}$ yields higher $G_{mm}$ values than T209. Five AC mixtures were tested at ten replicates each. Mixtures varied with respect to NMAS, gradation, aggregate type, and aggregate water absorption.

For all practical purposes, T209 and D6857 yielded similar $G_{mm}$ values for all five AC mixtures tested. However, Sholar et al. (2005) stated that the dry-back procedure may be necessary with high-absorption aggregate mixtures (even with D6857) as they cannot be accurately characterized otherwise. Further testing with $T209_{SSD}$ supported this argument.

For the very low (i.e. less than 1%) absorption (*Abs*) granite AC mixture, $T209_{SSD}$ and D6857 yielded similar $G_{mm}$ results with an average difference of 0.001 g/cm$^3$. However, $T209_{SSD}$ and D6857 were significantly different at a 5% significance level for all four limestone mixtures. The limestone mixtures tested had aggregate absorptions denoted as medium (2 to 3% *Abs*) and high (5 to 6% *Abs*). D6857 $G_{mm}$'s were higher than that of $T209_{SSD}$ by 0.002, 0.004, 0.011, and 0.033 g/cm$^3$.

Additionally, D6857 standard deviations were significantly greater (5% significance level) than those of $T209_{SSD}$, suggesting greater variability with D6857. Sholar et al. (2005) proposed the greater variability encountered with D6857 was due to operator unfamiliarity with the test. This issue could perhaps be overcome with additional experience.

Doyle et al. (2012) compiled a database of all MDOT asphalt mix designs between 2005 and 2010 (further referred to as the MDOT database). Figure 2.3 presents $G_{mm}$ distributions by NMAS for MDOT database mixtures. Since all RAP materials (i.e. major components in CIR mixtures) were at one time new AC mixtures, Figure 2.3 $G_{mm}$ values should also provide a reasonable representation of RAP $G_{mm}$ values to be expected.

RAP $G_{mm}$ is generally more difficult to measure than AC $G_{mm}$ because microcracks in the binder film, cracked aggregates, and uncoated particles are more likely to be encountered with RAP; therefore, Figure 2.3 could serve as a reasonableness assessment when evaluating measured RAP $G_{mm}$ values. For example, the 95% confidence interval (C.I.) for Figure 2.3a is 2.293 to 2.469. Reasonable RAP $G_{mm}$ values are likely to fall within this range; results outside this range could indicate a questionable test result or test method.

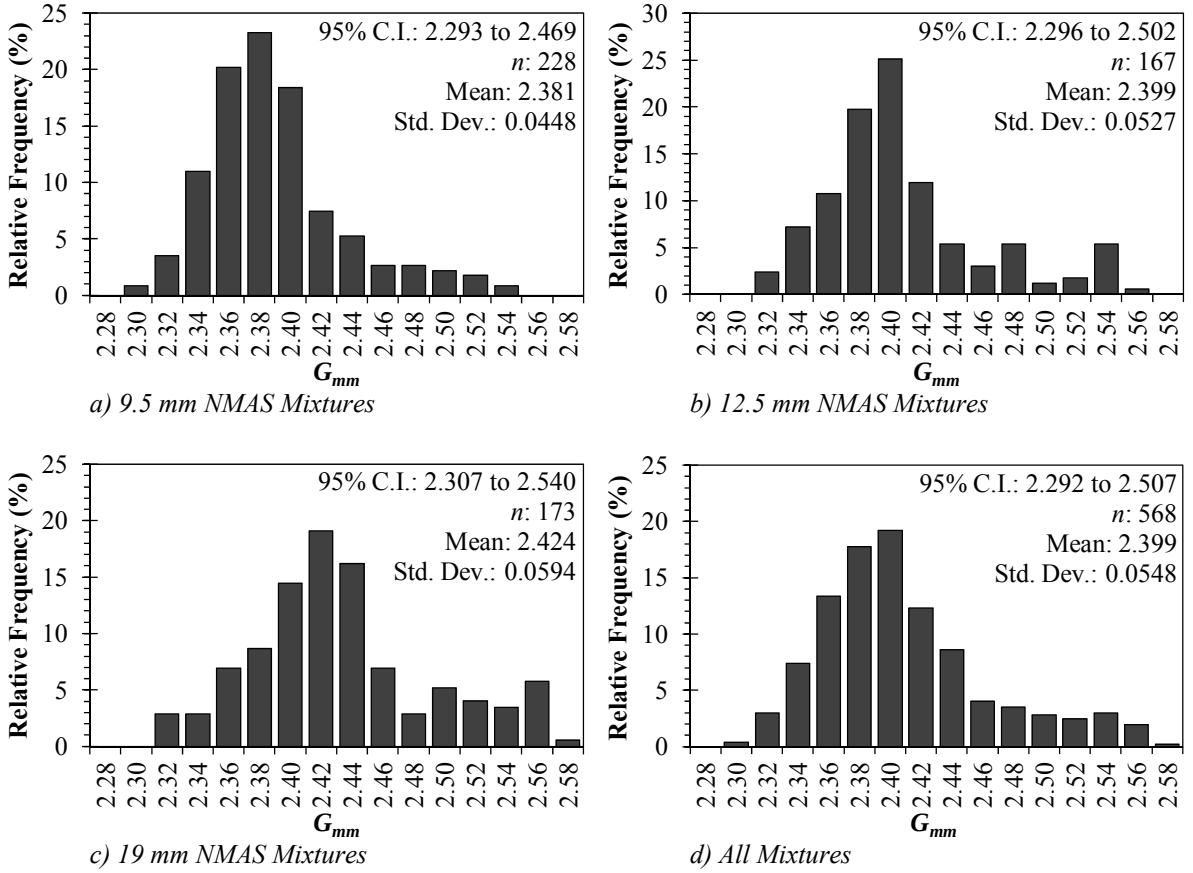


**Figure 2.3. $G_{mm}$ Distribution of MDOT Database Asphalt Mixtures**

### 2.8.2 RAP and CIR Maximum Specific Gravity

CIR $G_{mm}$ for emulsion-stabilized mixtures has traditionally been measured using ASTM D2041, a test method similar to AASHTO T209 (e.g. Cross and Ramaya, 1995; Khosla and Bienvenu, 1996; Santagata et al., 2010). A relatively standard practice in design methods such as those in Table 2.2 is to perform D2041 on emulsion-stabilized CIR after the loose mixture is cured to constant mass at 60 °C (0.05% mass change in 2 hours). Tests are normally conducted at the highest emulsion content considered in the mix design (usually in the 3 to 4% range). $G_{mm}$ for CIR at lower emulsion contents is normally back-calculated, though specific procedures for doing so are not usually described. A key concern with this approach is that it may not be appropriate for directly measuring $G_{mm}$ at lower emulsion contents or for additional binder types (e.g. cement) which is a major focus of this report.

In addition to the AC mixtures discussed in the previous section, Sholar et al. (2005) also studied a low absorption (1 to 2% *Abs*) limestone RAP. The average difference between either T209 or $T209_{SSD}$ and D6857 was 0.002 g/cm$^3$. The small difference between D6857 and both T209 methods was attributed to the low absorption value of the RAP's limestone aggregate. As in Section 2.8.1, standard deviation was slightly higher with D6857 than with T209 or $T209_{SSD}$.

Bang et al. (2011) studied FDR and used D6857 to measure $G_{mm}$. However, motivation for using D6857 over T209 (or any other method) was not provided. Additionally, D6857 results were not compared to that of any other method. Similarly, Chen et al. (2010) used D6857 to determine CIR $G_{mm}$ of field-cored materials, though $G_{mm}$ was not the focus of the study and reasoning for D6857 being used was not provided.

### 2.8.3 Asphalt Concrete Bulk Specific Gravity

Howard and Doyle (2014) presents approximately 2,500 $G_{mb}$ data points coupled with an in-depth literature review. Overall, AASHTO T331 (CoreLok® vacuum sealing) evaluated favorably against T166 (traditional SSD method) and T269 (dimensional measurement method). For typical AC mixtures, the T166 2% water absorption limit can be easily exceeded at $V_a$ levels of 8 to 9%. Howard and Doyle (2014) developed correlations between T166 and T331 of the form of Equation 2.1. These were used to compare T331- and T166-calculated $V_a$'s at typical mix design levels (4%), performance testing levels (7%), and moderately high construction acceptance levels (10%).

$$V_{a(i)} = C_1\left(V_{a(T166)}\right) + C_2 \tag{2.1}$$

Where,
$V_{a(i)} = V_a$ measured by method $i$ (e.g. $V_{a(T269)}$, $V_{a(T331)}$)
$V_{a(T166)} = V_a$ measured by AASHTO T166
$C_1$, $C_2$ = regression constants

While $V_a$'s were dependent on NMAS and gradation (e.g. fine, coarse), calculated $V_{a(T331)}$'s were almost always greater than $V_{a(T166)}$. On average, T331 yielded higher air voids relative to T166 as follows: 0.8% at mix design $V_a$ levels, 1.2% at performance testing $V_a$

levels, and 1.2 to 1.6% at upper-end construction acceptance $V_a$ levels. For fine-graded mixtures with low $V_a$'s, T331 and T166 often yielded approximately equivalent results.

### 2.8.4 CIR Bulk Specific Gravity

For those sources which measured and reported $G_{mb}$ rather than dry density ($\gamma_d$), T166, T269, or T331 was typically used. Recall that T166 is the most prevalent method used in current DOT mix designs (Table 2.2). Some sources which reported $G_{mb}$ values did not specify which method was used (e.g. Carter et al., 2010; Chan et al., 2010; Schwartz and Khosravifar, 2013). Several sources in this section relate to FDR for which $G_{mb}$ measurements are likely similar to that of CIR. Example references for each method are as follows:

- T166: Cross (2002), Cross (2003), Skok et al. (2008), Chen et al. (2010)
- T269: Kim and Lee (2006), Kim et al. (2007), Kim and Lee (2008), Kim et al. (2008), Kim et al. (2009), Kim and Lee (2011a)
- T331: Cross (2002), Mallick et al. (2002a), Mallick et al. (2002b), Cross (2003), Bang et al. (2011)

Ranges of documented air voids including those of field cores and laboratory specimens as well as those measured by various methods are presented in Table 2.5. These ranges should be considered an approximate $V_a$ representation since air voids were measured by different methods and on various specimen types (i.e. field cores versus laboratory specimens). While approximate, Table 2.5 provides a frame of reference for $V_a$'s documented in literature.

**Table 2.5. Documented $V_a$ Ranges for In-Place Recycling**

| $V_a$ Range | Source |
|---|---|
| 2.0 to 14.0% | Mallick et al. (2002b) |
| 4.5 to 14.3% | Chen et al. (2010) |
| 5.8 to 10.0% | Kim and Lee (2011a) |
| 6.0 to 10.0% | Kim and Lee (2006) |
| 6.3 to 22.4% | Bang et al. (2011) |
| 6.9 to 13.3% | Cross and Ramaya (1995) |
| 7.4 to 22.9% | Scholz et al. (1991) |
| 8.0 to 17.0% | Kim et al. (2007) |
| 8.8 to 14.7% | Yan et al. (2009) |
| 8.9 to 14.4% | Carter et al. (2010) |
| 9.0 to 13.8% | Niazi and Jalili (2009) |
| 9.1 to 14.3% | Forsberg et al. (2002) |
| 9.2 to 17.9% | Kim et al. (2008) |
| 9.4 to 15.2% | Cross (1999b) |
| 9.7 to 14.2% | Cross (2002) |
| 13.7 to 16.4% | Schwartz and Khosravifar (2013) |
| 16.0 to 22.5% | Marcandali da Silva et al. (2013) |

A key observation from Table 2.5 is that the lowest documented $V_a$'s are considerably lower than those typically observed with asphalt concrete. However, CIR $V_a$'s are usually greater than that of conventional asphalt (Scherocman, 1983). This is logical considering CIR

mixtures would be more difficult to compact for multiple reasons (e.g. RAP particles are generally more angular, no additional heat is applied, etc.). Since CIR $V_a$'s as low as those in Table 2.5 would be fairly difficult to achieve (but are reported), further investigation of density measurement methods appears warranted.

Mallick et al. (2002b) initially used T331 to measure $G_{mb}$ on freshly-compacted FDR specimens as it was suspected they would break down when submerged in water as required by T166. Cross (2002, 2003) expressed concerns that T166 may not be suitable for CIR since the 2% water absorption limit would likely be exceeded given CIR's $V_a$'s typically exceed the 8 to 9% range previously mentioned by Howard and Doyle (2014). This perspective was also supported by NCHRP Synthesis 421 on in-place recycling (Stroup-Gardiner (2011)). Cross and Ramaya (1995) used ASTM D2726 (T166 equivalent) but reported difficulty in accurate $V_a$ determination due to the high void contents. Likewise, many Table 2.5 $V_a$'s are well above the range at which 2% water absorption can occur with T166; therefore, T166 use for measuring CIR $G_{mb}$ is discouraged by the authors of this report.

## 2.9 Performance Characterization Tests

Multiple performance characterization tests are reviewed in this section and are considered in this report since a key goal of this report is to provide an extensive characterization of CIR materials. Tests reviewed include tests traditionally used to characterize CIR materials (e.g. Marshall stability) as well as those which are relatively uncommon for CIR but have been used to characterize asphalt concrete (e.g. IDT fracture energy). Most tests discussed in this section also include some discussion in reference to asphalt concrete in order to provide context.

### 2.9.1 Cantabro

Cantabro abrasion loss testing is often used to evaluate relative durability of open-graded friction course (OGFC) mixtures. The test is conducted in a Los Angeles abrasion drum without the charge of steel spheres where specimens are subjected to 300 revolutions. Durability is characterized by percent mass loss ($M_L$) after testing. Watson et al. (2004) recommended a maximum 20% $M_L$ for OGFC.

In more recent years, the Cantabro test has also been used to evaluate conventional asphalt concrete (i.e. dense-graded asphalt) (e.g. Doyle and Howard, 2011). It has been shown to be a useful durability index for asphalt mixtures and is relatively economical and efficient to perform. Howard et al. (2013a) cites $M_L$ values ranging from 6 to 16% for typical MDOT asphalt mixtures. Doyle and Howard (2016) performed over 400 asphalt concrete Cantabro tests to further assess its suitability for conventional asphalt concrete.

Results of Doyle and Howard (2016) were grouped into four key findings. First, Cantabro testing was sensitive to volume of effective binder (VBE), $V_a$, binder grade, and amount of gravel in the mixture. Second, variability testing of large sample sizes (30 replicates) indicated three replicates were sufficient for reasonable results. Third, Cantabro testing was sensitive to oven conditioning protocols (e.g. AASHTO R30). Fourth, Cantabro testing was sensitive to RAP content. Aside from work for SS 250 presented later in this report, CIR Cantabro testing does not appear documented in literature.

### 2.9.2 Bending Beam Rheometer

The bending beam rheometer (BBR) has been used for many years to test asphalt binder beams for determination of low-temperature binder properties. In more recent years, BBR testing has also been conducted with asphalt mixture beams (i.e. beams sawn from asphalt concrete SGC specimens or field cores). Considerable efforts have been made in terms of evaluating its practicality and feasibility, controllable variability, and theoretical validity (e.g. Zofka et al., 2005; Marasteanu et al., 2009).

BBR mixture beam testing has been used to evaluate stiffness and *m-value* responses of high-RAP asphalt concrete (Doyle and Howard, 2013b). It has also been used to characterize rejuvenation of pavements after seal treatment application (e.g. Braham et al., 2014; Cox et al., 2015a). Aside from work for SS 250 presented later in this report, BBR mixture beam testing with CIR does not appear documented.

### 2.9.3 Hamburg Loaded Wheel Tester

The Hamburg Loaded Wheel Tester (HLWT) is a wheel tracker that is commonly used to evaluate asphalt concrete rutting potential and moisture susceptibility. Steel wheels apply 700 N of force directly to test specimen surfaces which are typically submerged in 50 °C water. A standard test is conducted for 20,000 passes or, equivalently, 10,000 cycles.

Aschenbrener (1995) documents maximum rut depth ($RD_{HLWT}$) criteria after 20,000 passes of 4 mm (Hamburg, Germany) and 10 mm (Colorado DOT). It was also noted that well-performing pavements, when tested in the HLWT, generally exhibit stripping inflection points (SIPs) at 10,000 passes or more. Conversely, the Texas DOT specifies that a mixture must withstand a minimum number of passes before reaching a $RD_{HLWT}$ of 12.5 mm ($P_{12.5\text{-}HLWT}$) (Rand, 2006). Minimum $P_{12.5}$ values are 10,000 passes for mixtures with PG 64 binders and 15,000 passes for PG 70 binders. Recall that Texas requires $P_{12.5}$ to be between 5,000 and 15,000 for CIR mixtures (Table 2.2). Aside from companion documents previously published from this research study and Texas DOT's design method (Texas, 2004), CIR HLWT testing does not appear documented in literature.

### 2.9.4 Fatigue

Fatigue testing is somewhat common for conventional asphalt concrete. Flexural beam fatigue tests are somewhat common, and loaded wheel fatigue tests are relatively uncommon. In terms of asphalt concrete, loaded wheel fatigue testing is discussed in lieu of flexural beam fatigue testing since loaded wheel fatigue equipment was available to the researchers for this report.

Howard et al. (2013a) conducted loaded wheel fatigue testing in the APA. Tests were conducted at 20 °C for 50,000 cycles (i.e. 100,000 passes) or until failure, which was defined as 1 mm change in deflection within one pass. At a 1,100 N wheel load, conventional asphalt concrete and high-RAP asphalt concrete behaved similarly, generally lasting 50,000 cycles without failure. Further testing of conventional asphalt concrete at additional $V_a$ levels indicated APA fatigue testing was fairly sensitive to $V_a$.

Wu et al. (2014) also conducted asphalt concrete APA fatigue tests but modified the test setup for a more traditional theoretical analysis approach. Fatigue beams were

instrumented to obtain stress and strain values. Rather than a 1 mm deflection failure criteria, a more traditional criteria of 50% stiffness reduction was used. Cycles to failure for mixtures tested ranged from approximately 30,000 to 120,000 cycles.

With the exception of work for SS 250 presented later in this report, CIR loaded wheel fatigue testing does not appear documented in literature. CIR flexural beam fatigue testing has been documented (Schmidt et al., 1973) but not to the extent which IDT fatigue testing has been documented (e.g. Scholz et al., 1991; Brown and Needham, 2000; Yan et al., 2010; Kavussi and Modarres, 2010b; Modarres et al., 2011). Both stress-controlled and strain-controlled IDT fatigue tests have been conducted similarly to IDT $M_r$ tests generally at a loading frequency of 1 Hz with a 0.1 second load duration, an intermediate test temperature (e.g. 20 °C).

Schmidt et al. (1973) studied fatigue characteristics of cement-modified emulsion aggregate mixtures in comparison to cement mixtures, emulsion mixtures, and conventional asphalt mixtures. While CIR was not studied, Schmidt et al. (1973) provided some of the first documentation regarding cement and emulsion MCB systems. Therein, flexural beam fatigue testing was conducted for conventional hot mix asphalt (5% asphalt content) as well as mixtures stabilized with 5% cement, 8.4% emulsion with 1.3% cement, and 8.4% emulsion. Emulsion content was selected to provide 5% residual asphalt for comparison to the hot mix asphalt.

Fatigue loads were applied for 0.1 second durations at a frequency of 100 loadings per minute and were adjusted to yield bending strains of either 150 or 300 με. Mix stiffness versus fatigue applications to failure plots demonstrated that conventional hot mix had greater fatigue resistance than all other mixtures. At 300 με, the emulsion SCB mixture produced better fatigue results than the cement-emulsion MCB mixture for all mixture stiffnesses. At 150 με, fatigue performance favored the emulsion SCB at high mixture stiffnesses and the cement-emulsion MCB at low mixture stiffnesses. The cement SCB was only tested at 300 με. Results were less reliable; however, trends were that it was extremely sensitive to small changes in mixture stiffness and fatigue behavior was least favorable relative to other mixtures tested.

Though the cement-emulsion MCB generally exhibited less favorable fatigue behavior, Schmidt et al. (1973) stated its fatigue disadvantages should be considered in tandem with its $M_r$ advantages. With the higher $M_r$ of the cement-emulsion MCB, tensile strains would be less for a given applied load. An elastic layer program was used to estimate layer thicknesses needed for equal fatigue lives. Analysis was conducted assuming a 40 kN load at a tire pressure of 550 kPa, a 7.5 cm surface layer with $M_r$ of 1,034 MPa and Poission's ratio (μ) or 0.40, and a subgrade with $M_r$ of 41 MPa and μ of 0.50. The cement-emulsion MCB layer thickness needed to maintain equal fatigue lives was two-thirds that of the emulsion SCB mixture. Similarly, general trends in Brown and Needham (2000) indicated cement-emulsion MCBs would, at the tensile strain levels normally occurring in pavements, exhibit improved fatigue lives since their increased stiffness would cause a reduction in strain magnitude.

### 2.9.5 Marshall Stability

Marshall stability (*MS*) has traditionally been the main property used to select design binder contents for bituminous-stabilized CIR mixtures. Typically, *MS* is performed at a load

rate of 50 mm/min and a test temperature of 40 °C. Yan et al (2009) recommended a minimum 6 kN *MS* at 40 °C in a Chinese performance specification, as well as a 75% minimum retained stability (*RMS*). Similarly, Thomas and Kadrmas (2003) recommended a minimum 5.56 kN *MS* at 40 °C, as well as a 70% minimum *RMS*. Table 2.6 provides a compilation of *MS* and *RMS* values from literature.

**Table 2.6. Literature CIR Marshall Stability Values**

| Reference | Test Temp (°C) | Field/ Lab | Binders Studied | *MS* (kN) | *RMS* (%) |
|---|---|---|---|---|---|
| Dudley et al. (1987) | 60 | Lab | 5.2e, 6.8e, 8.3e | 2.35, 1.90, 2.02 | --- |
| | | Lab | 5.8e, 6.3e, 7.8e | 0.22, 0.51, 0.48 | --- |
| Scholz et al. (1991) | 60 | Field | 1e | 3.09 to 8.06 | --- |
| | | Lab | 1e | 2.72 to 5.22 | --- |
| | | Field | 1.9e | 2.25 to 7.10 | --- |
| | | Lab | 1.9e | 3.83 to 5.81 | --- |
| Niazi and Jalili (2009) | 60 | Lab | 3.5e | 8.3 | 57 |
| | | Lab | 3.5e2c | 12.7 | 83 |
| | | Lab | 3.5e2HL | 11.8 | 77 |
| | | Lab | 3.5e2HLS | 11.6 | 69 |
| Forsberg et al. (2002) | 40 | Lab | 1.3e to 2e | 9.31 to 9.39 | 42 to 50 |
| | | Lab | 2e, 2.7e, 3.4e | 7.22 to 9.67 | 66 to 92 |
| Yan et al. (2009) | 40 | Lab | 3e2c | 6.61 to 13.44 | 89 to 114 |
| | | Lab | 3.5e2c | 6.67 to 11.78 | 86 to 89 |
| | | Lab | 4e2c | 5.79 to 12.94 | 77 to 99 |
| | | Lab | 4.5e2c | 10.71 | 97 |
| | | Lab | 5e2c | 5.56 | 115 |

*-- Binder blends designated by dosage and binder as in Table 2.4*

### 2.9.6 Asphalt Pavement Analyzer Rutting

The Asphalt Pavement Analyzer (APA) is a wheel tracker that has been used for several years by multiple DOTs to evaluate asphalt mixture rutting potential. The APA applies wheel loads of 445 N to pressurized rubber hoses (689 kPa) which directly contact test specimens. Tests are generally conducted for 8,000 cycles (16,000 passes), and rut depth ($RD_{APA}$) is measured continuously during testing. In Mississippi, tests are conducted at 64 °C, the upper PG temperature for the region.

Typically, 8,000-cycle pass or fail $RD_{APA}$ criteria are used by DOTs for conventional asphalt mixtures. For example, Buchanan et al. (2004) recommended 4 to 6 mm maximum $RD_{APA}$ for high traffic mixtures in Mississippi and 12 mm for standard and medium traffic mixtures. Brown et al. (2001) suggested an 8 mm $RD_{APA}$ criteria.

Du and Cross (2007) tested three CIR mixtures stabilized with 1.5% emulsion, 1.5% emulsion with 1.5% hydrated lime, and 1.5% emulsion with 1.14% quick lime. $RD_{APA}$ at 8,000 cycles ranged from 3.7 to 6.7 mm. Cross (1999b) tested six CIR mixtures (test temperature was 40 °C). Three were stabilized with emulsion only; the other three were identical but with 1% lime added in the form of hydrated lime slurry (HLS). Emulsions tested were CMS-1, CSS-1, and HFE-150, which were all tested at 1.5% dosages. $RD_{APA}$ at 8,000 cycles ranged from 7.0 to 8.0 mm for emulsion mixtures and 5.5 to 6.2 mm for emulsion-HLS mixtures. In addition to results presented in Cross (1999b), Cross (1999a) obtained a 1.2 mm $RD_{APA}$ for CIR stabilized with 10% Class C fly ash.

### 2.9.7 PURWheel

The PURWheel laboratory wheel tracker (PW) was originally developed in the 1990s at Purdue University, and the original model was donated to Mississippi State University in 2007 where it was rebuilt and modified. Renovation of the PW, as well as a detailed description of all test protocols, is provided in Howard et al. (2010). Test protocols of the renovated equipment are as follows: pneumatic rubber tires pressurized to 862 kPa apply wheel loads of 1,750 N, resulting in approximate contact pressures of 630 kPa (gross) and 850 kPa (net). Test duration is 20,000 passes (10,000 cycles). Tests are conducted at 64 °C similar to APA tests and can be conducted dry or submerged in 64 °C water (wet). Rut depth ($RD_{PW}$) at 12.5 mm ($P_{12.5\text{-}PW}$) is a key test result reported. $P_{12.5\text{-}PW}$ criteria have not been developed for asphalt mixtures.

Howard et al. (2012) documents an emergency paving study where a Mississippi parking lot was paved with three hot-mixed warm-compacted asphalt mixtures at four haul times varying by mixture. Asphalt mixtures utilized a PG 67-22 asphalt binder, and the mix design was produced three ways: with neat binder, with foamed asphalt, and with Evotherm 3G$^{TM}$. Each mixture was hauled for various times prior to placement ranging from 1.0 to 10.5 hours. Slabs cut from the parking lot and tested in the PW yielded $P_{12.5\text{-}PW}$ values ranging from 8,200 to 20,000 passes (dry) and 3,200 to 12,700 passes (wet).

Doyle and Howard (2013a) studied various wheel tracking tests including the PW. Three control mixtures (conventional hot mix asphalt) were selected to represent a range of current Mississippi mixtures. Four high-RAP warm mix asphalts were tested with two utilizing 25% RAP and two utilizing 50% RAP. Control mixture $P_{12.5\text{-}PW}$ values ranged from 425 to 20,000 passes (dry) and 500 to 20,000 passes (wet). Note that one control mixture exhibited considerably low $P_{12.5\text{-}PW}$ values around 500 passes dry and wet; the other two control mixtures averaged approximately 20,000 passes dry and 17,000 passes wet. High-RAP mixture $P_{12.5\text{-}PW}$ values ranged from 19,100 to 20,000 passes (dry) and 7,950 to 13,600 passes (wet).

### 2.9.8 Indirect Tensile Strength

IDT strength can be measured with ease and has often been reported in literature (Table 2.7). In this case, IDT strength is calculated at the peak load ($S_{t,ult}$). Tests are generally conducted near room temperature at a 50 mm/min load rate and with no deformation measurements. Kavussi and Modarres (2010a) performed IDT testing of cement-emulsion CIR. In most cases, COV was less than 10%; the maximum COV of all specimens was 14.4%. Yan et al. (2009) recommended a minimum 0.5 MPa $S_t$ at 15 °C in a Chinese performance specification.

**Table 2.7. Literature CIR $S_t$ Values**

| Reference | Test Temp (°C) | Load Rate (mm/min) | Field/ Lab | Binders Studied | $S_t$ (kPa) |
|---|---|---|---|---|---|
| Dudley et al. (1987) | --- | --- | Lab | 4.3e, 6.8e, 8.3e | 510, 421, 586 |
| | | | | 5.8e, 6.3e, 7.8e | 145, 172, 372 |
| Cross (1999b) | --- | --- | Lab | 1.5e | 201 to 242 |
| | | | | 1.5e1HLS | 268 to 365 |
| Niazi and Jalili (2009) | 25 | 50 | Lab | 3.5e | 245 |
| | | | | 3.5e2c | 419 |
| | | | | 3.5e2HL | 344 |
| | | | | 3.5e2HLS | 249 |
| Yan et al. (2009) | 15 | --- | Lab | 3e2c | 370 to 630 |
| | | | | 3.5e2c | 540 to 600 |
| | | | | 4e2c | 560 to 750 |
| | | | | 4.5e2c | 610 |
| | | | | 5e2c | 700 |
| Apeagyei and Diefenderfer (2013) | 25 | 50 | Field | 2a1c, 2.25a1c, 2.5a1c | 316 to 665 |
| Marcandali da Silva et al. (2013) | --- | 50 | Lab | 2.5e, 3e, 3.5e | 350 to 360 |

*-- Binder blends designated by dosage and binder as in Table 2.4 -- a = foamed asphalt binder*

### 2.9.9 Resilient Modulus

Resilient modulus ($M_r$) determined in the IDT configuration is a relatively common property reported for CIR mixtures. The test is currently governed by ASTM D7369 which specifies the application of 100 load cycles with data recorded over the last 5 cycles. Each cycle consists of a 0.1 second haversine load pulse with a 0.9 second rest at a small contact load. $M_r$ is calculated from load, vertical deformation, and horizontal deformation data. Table 2.8. presents $M_r$ data compiled from literature.

**Table 2.8. Literature CIR $M_r$ Values**

| Reference | Test Temp (°C) | Field/ Lab | Binders Studied | $M_r$ (MPa) |
|---|---|---|---|---|
| Scholz et al. (1991) | 23 | Field | 1e | 1,668 to 3,626 |
| | | Lab | 1e | 1,523 to 3,261 |
| | | Field | 1.9e | 3,475 to 5,012 |
| | | Lab | 1.9e | 2,840 to 5,378 |
| Niazi and Jalili (2009) | 25 | Lab | 3.5e | 1,189 |
| | | Lab | 3.5e2c | 2,086 |
| | | Lab | 3.5e2HL | 1,575 |
| | | Lab | 3.5e2HLS | 1,520 |
| Apeagyei and Diefenderfer (2013) | 20 | Field | 2a1c, 2.25a1c, 2.5a1c | 2,861 to 5,169 |

*-- Binder blends designated by dosage and binder as in Table 2.4 -- a = foamed asphalt binder*

### 2.9.10 Creep Compliance

Creep compliance (D(t)) of asphalt mixtures is most commonly determined in the IDT configuration according to AASHTO T322. Compliance is often thought of as the inverse of modulus (i.e. strain divided by stress rather than stress divided by strain), which generally true for linearly elastic materials but not for viscoelastic materials. For viscoelastic materials, compliance can be thought of as the inverse of modulus for general discussion purposes (e.g. high modulus and low compliance are similar).

Creep and IDT strength tests were originally developed during the Strategic Highway Research Program (SHRP) in order to characterize low-temperature cracking (single-event thermal cracking). For creep tests, IDT specimens instrumented with linear variable differential transducers (LVDTs) are loaded with a constant load for 100 (or 1,000) seconds. Vertical and horizontal deformations are recorded throughout testing for D(t) calculation. Tests are generally conducted at 0, -10, and -20 °C. $S_t$ is obtained after creep testing but at a load rate of 12.5 mm/min rather than 50 mm/min as at 25 °C.

Test development is primarily discussed in Lytton et al. (1993). Thermal stress development in an asphalt mixture is governed by its viscoelastic properties, in this case relaxation modulus. The mixture's fracture properties control cracking development when a mixture is subjected to specified thermal stress levels. Therefore, these two properties must be measured in order to predict and control thermal cracking. Thermal cracking potential is typically characterized by critical cracking temperature ($T_{crit}$), which is defined as the point at which thermal stress exceeds mixture strength (i.e. intersection of thermal stress curve and $S_t$ curve). Lower $T_{crit}$'s are more likely to exhibit favorable thermal cracking behaviors.

Note that creep stiffness (inverse of compliance) is frequently used by engineers to approximate relaxation modulus, though it has its limitations. Direct measurement of relaxation modulus via relaxation tests (i.e. constant strain, time-dependent stress) is not ideal since this would require direct tension testing which necessitates non-traditional specimen geometries which are glued to end platens. Attachment to end platens is time consuming and often results in alignment errors and stress concentrations, especially at low temperatures. Alternatively, creep compliance can be determined with relative ease in the IDT configuration, and relaxation modulus can be calculated through viscoelastic theory, as the two are inversely related through their Laplace transforms.

Creep compliance curves are calculated over a range of test times, generally 100 seconds for asphalt concrete, at several temperatures. Each compliance curve can be shifted to a single reference temperature (generally -20 °C) by shifting the time to a reduced time via shift factors. In this way, a compliance master curve can be constructed, and a master relaxation modulus curve can be developed.

Christensen (1998) presents data analysis techniques for determining thermal stress and $T_{crit}$ and developed an Excel data analysis template titled "LTSTRESS". Thermal stresses are calculated in one direction since two- and three-dimensional stress calculations are substantially difficult. Christensen (1998) describes thermal stress calculations which require the following parameters to be defined: mixture coefficient of thermal expansion (α), starting pavement temperature for cooling cycle, pavement cooling rate, and step size for numerical integration. The current version of LTSTRESS, last modified in 2013, assigns values to these parameters of $2.28 \times 10^{-5}$ m/m/°C, 10 °C, 5.6 °C/hr, and 2 °C, respectively. Christensen (1998) presents $T_{crit}$ values for two asphalt mixtures tested which were -15 and -12 °C.

NCHRP 530 (Christensen and Bonaquist, 2004) describes creep testing theory, previous related research, and recommended T322 modifications. Key points are provided herein. Specimen conditioning times should be approximately 3 hours to achieve through-specimen temperature equilibrium. A repeatability study with asphalt concrete indicated coefficients of variation (COVs) for $S_t$ and D(t) were 7% and approximately 8 to 11%; the d2s value for $T_{crit}$ was 2.9 °C. Fracture IDT strength ($S_{t,f}$), which occurs prior to the ultimate IDT strength ($S_{t,ult}$), can fairly reliably be determined as 78% of $S_{t,ult}$; this prevents the need for instrumented $S_t$ tests and can protect LVDTs from potential damage. Christensen and

Bonaquist (2004) recommended test temperatures be linked with binder grade; for PG XX-28 and PG XX-22 binders, temperatures of 0, -10, and -20 °C were recommended.

Thomas et al. (2000) conducted IDT creep and strength testing for two CIR mixtures in Kansas, one stabilized with 1.5% emulsion plus 1.5% HLS and the other stabilized with 10% Class C fly ash. Testing was conducted according to TP9, which was the provisional test method in use prior to T322. Cores with a 150 mm diameter were sliced to 50 mm thickness and tested at 0, -10, -20, and -30 °C. $T_{crit}$ values for emulsion and fly ash CIR materials were -27 °C and -12 °C, respectively. The emulsion CIR with HLS exhibited greater resistance to thermal cracking.

Forsberg et al. (2002) conducted IDT creep and strength testing for two CIR mixtures used in Minnesota to rehabilitate Blue Earth County State Aid Highway 20. Two key goals of this study were to promote: 1) engineered emulsions with improved chemistry, and 2) a new mix design process which was more performance-oriented. One mixture was a conventional CIR mixture with a 1.5% design emulsion content. The second mixture was designed using a new process resulting in a 3.25% design engineered emulsion content. The primary advantage stated with the engineered emulsion was that its improved chemistry allowed for a higher dosage without balling up and resulting in workability and coating issues. Among other properties measured, thermal cracking was investigated with TP9 at test temperatures of -20, -30, and -40 °C. $T_{crit}$ values for the conventional and engineered emulsion CIR mixtures were -30 and -34 °C, respectively, indicating the engineered emulsion design provided better thermal cracking resistance, due primarily to its higher dosage made possible by its improved chemistry.

### 2.9.11 Instrumented Indirect Tensile Testing

Multiple test methods capable of characterizing cracking behaviors were reviewed in this study. Ultimately, instrumented IDT testing was selected for CIR characterization and is the only test method discussed in great detail. However, brief descriptions of other test methods considered are provided alongside explanation as to why they were not used in this report.

The single-edge notched beam (SENB) test has been studied to a moderate degree (e.g. Artamendi and Khalid, 2006). A 30 by 5 by 6.5 cm asphalt mixture beam with a notch cut in the bottom middle of its span is loaded in a three-point bending configuration to failure. Stress intensity factors and fracture energy are commonly calculated test results. Mull et al. (2006) stated difficulties could be encountered since beams may sag under self-weight, especially at warmer temperatures. Additionally, the large specimen size has generally discouraged SENB use in favor of tests which can be conducted on SGC-compacted specimens or on cores. The SENB was not utilized in this report primarily due to impracticality of the specimen sizes.

The disc-shaped compact tension (DCT) test (e.g. Wagoner and Buttlar, 2007; Zofka and Braham, 2009) was originally proposed as an alternative to the SENB test. It differs from all other cracking characterization tests presented in that only tensile loadings are applied. Load versus crack mouth opening displacement plots are generally used to determine fracture toughness or fracture energy.

The semi-circular bend (SCBend) test (e.g. Molenaar et al., 2002; Wu et al., 2005; Mohammed et al., 2013) is similar to the SENB configuration except the test is conducted on

a 150 mm diameter specimen sliced in half to form a semi-circle. Stress intensity factor, fracture energy, and critical strain energy release rate ($J_c$) are often calculated. While both DCT and SCBend tests have shown promise with conventional asphalt mixtures, extensive drilling and/or sawing are required to produce test specimens. Based on attempts in this report to saw CIR specimens, sawing is prohibited by some SCB and MCB systems tested herein; therefore, DCT and SCBend tests were not utilized.

Instrumented IDT tests appeared most promising since sawing is not a requirement to produce test specimens. The University of Florida in particular has researched IDT cracking tests in considerable detail and was consulted by the authors of this report for guidance. IDT testing, which has been discussed to some degree in Section 2.9.10, is relatively simple and produces reasonable stress states. These two factors have led to fairly widespread use of the test, especially for determining $S_t$ as discussed in Section 2.9.8 (Roque and Buttlar, 1992). While ultimate IDT strength ($S_{t,ult}$) is most common, many researchers have suggested $S_{t,ult}$ alone is not a reliable indicator of cracking behaviors (e.g. Kim and Wen, 2002; Marasteanu et al., 2007).

Much of the foundational groundwork for instrumented IDT testing was laid out in Roque and Buttlar (1992) and Lytton et al. (1993). It was noted that the stress state near the center of the specimen resembles the actual stress state in the bottom layer of a typical loaded asphalt pavement (i.e. horizontal tension combined with vertical compression). Additionally, as temperature decreases (less than 30 °C was discussed), asphalt behaves more and more as a linearly elastic material meaning material response becomes less dependent on stress state. Therefore, this suggests determination of properties from IDT testing is reasonable even though the resulting stress state is not purely tension.

Roque and Buttlar (1992) summarized issues with the existing IDT measurement and analysis system at the time. It was common to report horizontal and vertical deformations based on specimen exteriors (i.e. load strip to load strip), but these measurements lead to significant errors due to damage by the loading strips. For example, Molenaar et al. (2002) noted that a wedging effect near the loading strips often occurs at 15 °C or greater which would severely impact load strip to load strip deformation measurements. Alternatively, Roque and Buttlar (1992) proposed using gage-point-mounted LVDTs and recommended a 38 mm gage length for 150 mm diameter specimens.

Roque and Buttlar (1992) also developed several correction factors to address errors associated with apply 2-D plane stress calculations to 3-D specimens of finite thickness. Correction factors were developed to correct for bulging of specimen faces. Similarly, correction factors were used to correct 2-D plane stresses and strains to corrected stresses and strains at the center of specimen faces. Kim and Wen (2002) used 3-D finite element modeling to quantify errors associated with neglecting correction factors. Approximately 2.5% error was incorporated; therefore, Kim and Wen (2002) ignored correction factors entirely.

Kim and Wen (2002) found that neither $S_{t,ult}$ nor horizontal strain at peak stress ($\varepsilon_{ult}$) correlated well to fatigue cracking of WesTrack mixtures. However, fracture energy (FE) has been shown to correlate well with field cracking (e.g. Kim and Wen, 2002; Zhang et al., 2001). Fracture energy calculated from instrumented IDT tests is defined as the area under the IDT stress-strain curve up to the point of fracture. The point of fracture is determined by plotting the deformation differential curve (DDC), which is the vertical minus horizontal deformations; its peak corresponds to the point of fracture, which should occur prior to the

ultimate, or peak, load (Buttlar et al., 1996; Roque et al., 1997; Koh and Roque, 2010). Koh and Roque (2010) conducted dog-bone direct tension testing which yielded a one-to-one FE correlation with IDT tests. This supported FE as a fundamental mixture property which is independent of specimen geometry, loading mode, and loading rate. Birgission et al. (2003, 2007) reported FE values for asphalt concrete ranging from 0.8 to 1.4 kJ/m$^3$ (test temperatures of -10, 0, and 10 °C) and 2.0 to 7.4 kJ/m$^3$ (test temperatures of 10 °C), respectively.

Zhang et al. (2001) and Roque et al. (2002) presented a cracking threshold concept in which dissipated creep strain energy (DCSE) is calculated by subtracting elastic energy (EE) from FE according to Equations 2.2 and 2.3. Figure 2.4 illustrates a stress-strain curve with key parameters identified. The single-event cracking failure threshold for critical load applications is represented by FE, and DCSE represents the cracking threshold for continuous repeated loading. DCSE was also shown to be a fundamental mixture property (Zhang et al., 2001).

$$EE = \frac{1}{2}\frac{S_{t,f}^{\ 2}}{M_r} \tag{2.2}$$

$$DCSE = FE - EE \tag{2.3}$$

Where,
EE = elastic energy (kJ/m$^3$)
$S_{t,f}$ = IDT fracture strength (MPa)
$M_r$ = IDT resilient modulus (GPa)
DCSE = dissipated creep strain energy (kJ/m$^3$)
FE = fracture energy (kJ/m$^3$)

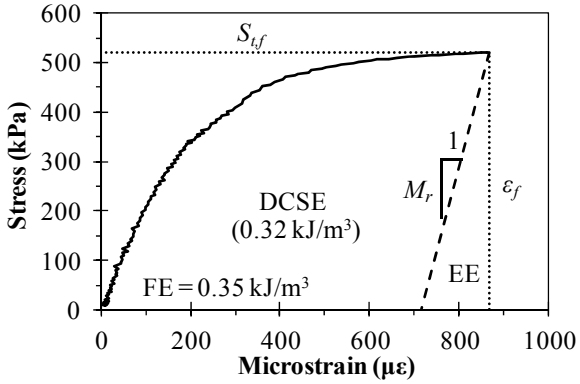


**Figure 2.4. Example Illustrated IDT Stress-Strain Curve for CIR**

Roque et al. (2004) developed the energy ratio (ER) concept. ER is the ratio of DCSE for a given mixture to a minimum DCSE (DCSE$_{min}$) which empirically accounts for D(t), $S_t$, and pavement structure. Field results indicated that an ER greater than 1 coupled with DCSE between 0.75 and 2.5 kJ/m$^3$ (test temperature of 10 °C) exhibited satisfactory cracking performance. Aside from work for SS 250 presented later in this report, instrumented fracture-oriented IDT testing with CIR does not appear documented.

## 2.10 In-Service Performance Evaluation

### 2.10.1 Distress Surveys

Badaruddin and McDaniel (1992) conducted a 5-year survey of a widening project on SR-38 (AADT of 1,500) in Indiana where two sections were built. CIR (binder type not specified) was utilized in one section and was overlaid with conventional asphalt. The other was a traditional trench widening with an asphalt overlay. Recycling depths were approximately 15 cm yielding a CIR thickness of approximately 12.5 cm after widening from 6.1 to 7.3 m; other layer thicknesses were not provided. Pavement condition index (PCI) values at 5 years were 70 to 75 for the CIR section and 57 to 59 for the overlay section. The CIR section exhibited higher PCI values as well as fewer observed distresses than the conventionally rehabilitated section.

Kim et al. (2010) conducted distress surveys on 26 emulsion-stabilized CIR pavements in Iowa. CIR thickness averaged approximately 10 cm and was overlaid with approximately 5 to 6 cm of asphalt concrete. Routes studied were mostly county roads and city streets but also included several state highways and two US highways. AADT ranged from 130 to 6,200 and averaged approximately 1,100. All routes except one had AADT levels less than 2,000. PCI data and falling weight deflectometer (FWD) data (discussed in Section 2.10.2) were presented for CIR pavement ages ranging from 1 to 19 years.

A first distress survey was conducted on CIR pavements 1 to 10 years of age (denoted short-term), and a second survey was conducted at 10 to 19 years of age (denoted long-term). Figure 2.5a plots PCI versus pavement age for both surveys and illustrates the trend in decreasing PCI over time. Shahin (2006) provides a PCI rating scale as follows: 85 to 100 (good), 70 to 85 (satisfactory), 55 to 70 (fair), 40 to 55 (poor), 25 to 40 (very poor), 10 to 25 (serious), and 0 to 10 (failed). Most Figure 2.5a PCI values are fair or better.

Figure 2.5b shows the PCI distribution for short-term and long-term surveys. Short-term data averaged 91 and was skewed towards higher PCI values. Approximately 60% of short-term PCIs were between 90 and 100, and 27% were between 80 and 90. Long-term PCIs were fairly evenly distributed from 48 to 98 and were 74 on average.

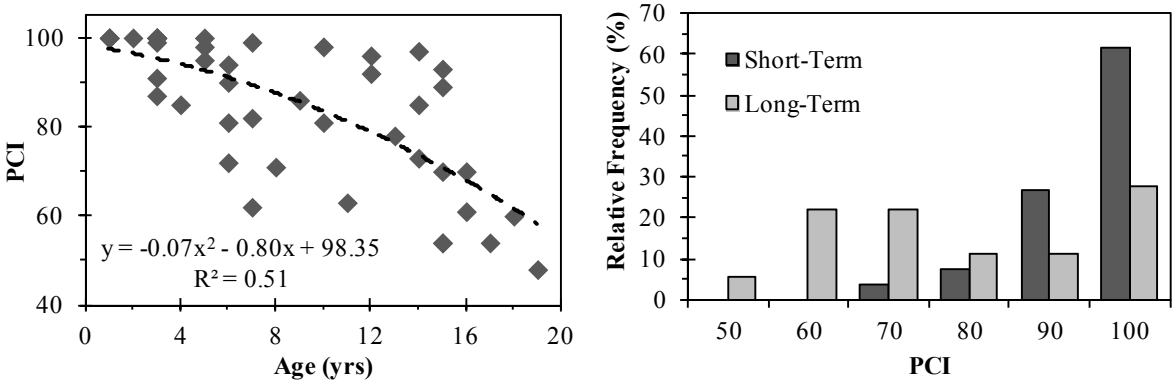


*a) PCI vs. Age* *b) PCI Relative Frequency Histogram*

**Figure 2.5. PCI Data from Kim et al. (2010)**

Chen et al. (2010) performed statistical analysis on data from 24 of the 26 CIR pavements studied in Kim et al. (2010). Laboratory testing of cores was also used in the

analysis in attempts to quantify relationships between factors such as traffic and material properties to pavement performance. Three multiple regression models were developed considering all routes simultaneously, only low traffic routes (AADT less than 800), and only high traffic routes (AADT greater than 800). Corresponding $R^2$ values were 0.59, 0.52, and 0.65, respectively. Overall, models indicated that better pavement performance was associated with lower CIR (recall that all CIR was emulsion-stabilized) modulus (values in data set were back-calculated from FWD testing and ranged from 1,390 to 30,100 MPa) and higher T166 $V_a$ (values in data set were measured on cores and ranged from 4.5 to 14.3%). Regression models also indicated a higher amount of accumulated traffic was associated with lower relative pavement performance.

### 2.10.2 Falling Weight Deflectometer

Table 2.9 presents FWD data obtained from literature with the aim of providing a broad range of deflections. Observations are ranked by effective structural number ($SN_{eff}$) as defined in the AASHTO 1993 pavement design guide (AASHTO, 1993). In some cases, $M_r$ or $SN_{eff}$ was not provided and was calculated according to Appendix L5 in AASHTO (1993). Multiple route types (e.g. county road, interstate) and structures (e.g. composite, FDR) were included to provide a broad data set. Specific details from each reference are largely omitted as they are not the focus.

**Table 2.9. FWD Literature Summary**

| Source | State | Route Type and Description | $D_{HMA}$ (cm) | $D_p$ (cm) | $M_r$ (MPa) | $d_0$ (mils) | $SN_{eff}$ |
|---|---|---|---|---|---|---|---|
| Howard and Warren (2009) | AR | Frontage road | 6 | 22 | 77 | 48 | 1.1[c] |
| Howard and Warren (2009) | AR | Frontage road | 6 | 32 | 77 | 34 | 1.8[c] |
| Noureldin et al. (2005) | IN | State route | 20 | 37 | 28 | 14 | 2.9 |
| Noureldin et al. (2005) | IN | State route | 28 | 48 | 42 | 10 | 5.0 |
| Kim et al. (2010) | IA | Low-volume road, emulsion CIR (max) | 5 | 37 | 17 | 22 | 5.2[c] |
| Chen et al. (2011) | TX | State route, CTB, Un-cracked | 8 | 56 | 154 | 7.9 | 5.2[c] |
| Noureldin et al. (2005) | IN | Multiple interstates (min) | 20 | 49 | 42 | 4.8 | 5.5 |
| Smith et al. (2008) | GA | County road, Lime-stabilized FDR | 8 | 44 | 251[c] | 3.8 | 6.1[c] |
| Kim et al. (2010) | IA | Low-volume road, emulsion CIR (median) | 5 | 36 | 27 | 13 | 6.3[c] |
| Chen et al. (2011) | TX | State route, CTB, Cracked | 8 | 56 | 154 | 5.4 | 6.5[c] |
| Noureldin et al. (2005) | IN | US Highway | 25 | 60 | 63 | 4.0 | 6.5 |
| Noureldin et al. (2005) | IN | Multiple interstates (avg) | 28 | 62 | 63 | 3.1 | 6.9 |
| Zhang et al. (2008) | LA | Multiple HMA pavements | *n/a* | *n/a* | 47 | 7.0 | 7.3 |
| Chen (2007) | TX | Farm to Market, Lime-stabilized base | 4 | 55 | 105[a] | 6.0 | 7.3[c] |
| Howard and Cox (2016) | MS | US Highway, cement FDR (avg) | 11 | 52 | 216 | 3.4 | 7.8 |
| Zhang et al. (2008) | LA | Multiple composite pavements | *n/a* | *n/a* | 45 | 5.3 | 8.2 |
| Noureldin et al. (2005) | IN | Multiple interstates (max) | 38 | 76 | 77 | 2.0 | 8.5 |
| Kim et al. (2010) | IA | Low-volume road, emulsion CIR (min) | 11 | 72 | 65 | 6.5 | 8.9[c] |

*a) $M_r$ was not provided in Chen (2007); default value of 105 MPa was used to calculate $SN_{eff}$.*
*b) Chen (2007) reported $d_0$ for a 44.5 kN (10 kip) loading; therefore, $SN_{eff}$ calculations use 44.5 kN as well.*
*c) Values calculated according to AASHTO (1993) Appendix L5 by authors of this report.*
*-- $D_{HMA}$ = asphalt concrete thickness*
*-- $D_p$ = total pavement thickness*
*-- $M_r$ = resilient modulus (subgrade in this case)*
*-- $d_0$ = deflection under center of loading*
*-- $SN_{eff}$ = effective structural number*
*-- CTB = cement-treated base*

Though not possible in some cases, attempts were made to report Table 2.9 values in a consistent manner. For example, efforts were made to ensure all deflections ($d_0$) were under the center of loading normalized to 40 kN and corrected to 20 °C. In some cases, data was summarized in Table 2.9 for brevity. For example, Kim et al. (2010) and Noureldin et al. (2005) reported FWD data for 18 CIR projects and 5 interstates, respectively, but only minimum (min), maximum (max), and average (avg) or median values are shown in Table 2.9.

Overall, $d_0$ values in Table 2.9 range from 2 to 48 mils. Corresponding $SN_{eff}$ values ranged from 1.1 to 8.9. While approximate when multiple studies are coupled together and some details are not available or uniformly handled, $d_0$ and $SN_{eff}$ values, as well as the relationship between the two, should be reasonable for the purposes of providing a frame of reference in this report.

Regarding layer coefficients, O'Leary and Williams (1992) cites multiple layer coefficients for emulsion-stabilized CIR. Values cited from a Purdue University study ranged from 0.17 to 0.44 with an average of 0.29. New Mexico used 0.25; with UCS greater than 1,720 kPa, 0.30 appeared to be a valid estimate. Oregon stated CIR layer coefficients may be considered equivalent to that of convention hot mix asphalt. Khosla and Bienvenu (1996) determined layer coefficients of 0.45 for CIR with CMS-2 emulsion and 0.28 to 0.36 for CIR with HFRA (high-float recycling agent).

# CHAPTER 3 – MATERIALS TESTED

## 3.1 Overview of Materials Tested

This chapter describes all materials tested in this report: asphalt concrete, reclaimed asphalt pavement (RAP), and stabilization additives (either bituminous or cementitious). Material sources, sampling, property test methods and results, and general descriptions are provided in this chapter. Testing in this report evaluates combinations of the materials described in this chapter to improve understanding of cold in-place recycling.

## 3.2 Asphalt Concrete

Eight asphalt concrete materials were tested in this report. Two materials (*US-49-BM* and *US-49-SM*) were those used in US-49 construction. Four materials (*ERDC-A* through *ERDC-D*) were used in a warm mixed asphalt (WMA) airfield study at the Engineering Research and Development Center (ERDC) and were also evaluated in MDOT State Study 266. Lastly, two materials were sawn from field-aged pavements, *Hwy 45* and *Hwy 41*. These eight mixtures are denoted AC1 to AC8. Table 3.1 provides properties of all asphalt concrete materials, and subsequent sections provide further details regarding each material.

### 3.2.1 US-49 Asphalt Concrete

*US-49-BM* (AC1) and *US-49-SM* (AC2) were hot mixed asphalt (HMA) materials used during US-49 construction. *US-49-BM* was a high-traffic (85 design gyrations ($N_{des}$)) polymer-modified 19 mm nominal maximum aggregate size (NMAS) mixture which comprised the US-49 base course placed on top of CIR or FDR layers. *US-49-SM* was a high-traffic (85 $N_{des}$) polymer-modified 9.5 mm NMAS mixture which comprised the US-49 surface course. Some US-49 mixtures were field compacted and are distinguished from laboratory compacted mixtures by an "FC" subscript (e.g. $AC1_{FC}$).

Loose asphalt mixture for laboratory-compacted mixtures was sampled from the paver or the plant and placed into 20 L metal buckets. Buckets were brought to the laboratory, allowed to cool, and reheated as necessary over a considerable period of time for specimen production. US-49 asphalt materials were tested to provide information relevant to the overall US-49 performance evaluation. Field-compacted mixtures were obtained via coring for a performance evaluation after some time of service as described in Chapter 5.

### 3.2.2 ERDC Asphalt Concrete

*ERDC-A* through *ERDC-D* (AC3 to AC6) were airfield mixtures studied in a full-scale comparison of HMA and WMA conducted at ERDC in Vicksburg, MS. All ERDC mixtures were designed with an $N_{des}$ of 75. *ERDC-A*, with a target compaction temperature of 146 °C, was the only HMA studied. All other mixtures had a target compaction temperature of 116 °C and employed the following WMA additives: Sasobit® (*ERDC-B*), Evotherm™ (*ERDC-C*), and Foam (*ERDC-D*). Loose mixture sampling and handling procedures were similar to those described in the previous section. ERDC asphalt was tested to provide a reference data set for comparison to CIR performance properties.

**Table 3.1. Asphalt Concrete Mixture Properties**

| | Asphalt Concrete ID | AC1 | AC2 | AC3 | AC4 | AC5 | AC6 | AC7 | AC8 |
|---|---|---|---|---|---|---|---|---|---|
| | **Asphalt Mixture** | ***US-49-BM*** | ***US-49-SM*** | ***ERDC-A*** | ***ERDC-B*** | ***ERDC-C*** | ***ERDC-D*** | ***Hwy 45*** | ***Hwy 41*** |
| **Percent Passing** | **25 mm** | 100 | 100 | 100 | 100 | 100 | 100 | 100 | 100 |
| | **19 mm** | 100 | 100 | 100 | 100 | 100 | 100 | 100 | 100 |
| | **12.5 mm** | 89.4 | 100 | 96.0 | 96.0 | 96.0 | 96.0 | 100 | 99.7 |
| | **9.5 mm** | 78.9 | 99.7 | 84.5 | 84.5 | 84.5 | 84.5 | 95.0 | 95.6 |
| | **4.75 mm** | 51.0 | 90.5 | 68.2 | 68.2 | 68.2 | 68.2 | 63.0 | 68.2 |
| | **2.36 mm** | 34.6 | 55.9 | 53.5 | 53.5 | 53.5 | 53.5 | 42.0 | 46.1 |
| | **1.18 mm** | 24.4 | 34.4 | 38.3 | 38.3 | 38.3 | 38.3 | 30.0 | 34.7 |
| | **0.60 mm** | 18.5 | 18.1 | 27.9 | 27.9 | 27.9 | 27.9 | 23.0 | 27.8 |
| | **0.30 mm** | 9.9 | 11.9 | 14.7 | 14.7 | 14.7 | 14.7 | 15.0 | 16.7 |
| | **0.15 mm** | 6.7 | 7.9 | 6.8 | 6.8 | 6.8 | 6.8 | 11.0 | 9.6 |
| | **0.075 mm** | 5.2 | 5.8 | 4.9 | 4.9 | 4.9 | 4.9 | 9.5 | 8.0 |
| **Aggregate** | $G_{sb}$ | 2.497 | 2.515 | 2.609 | 2.609 | 2.609 | 2.609 | --- | --- |
| | $G_{sa}$ | 2.627 | 2.637 | 2.688 | 2.688 | 2.688 | 2.688 | --- | --- |
| | ***Abs* (%)** | 1.99 | 1.83 | 1.15 | 1.15 | 1.15 | 1.15 | --- | --- |
| | ***CR +#4* (%)** | 90.0 | 91.6 | 95.5 | 95.5 | 95.5 | 95.5 | --- | --- |
| **Binder** | **RAP Content (%)** | 15.0 | 10.0 | 0.0 | 0.0 | 0.0 | 0.0 | --- | --- |
| | **RAP $P_{AC}$ (%)** | 5.6 | 5.6 | --- | --- | --- | --- | --- | --- |
| | **Total $P_{AC}$ (%)** | 4.9 | 5.8 | 5.3 | 5.3 | 5.3 | 5.3 | 6.8 | 6.8 |
| | **PG or Continuous Grade[a]** | 76-22 | 76-22 | 67-22 | 67-22 | 67-22 | 67-22 | 95-10 | --- |
| | **Warm Mix Technology** | --- | --- | --- | Sasobit® | Evotherm™ | Foam | --- | --- |
| **Mixture** | $G_{mm}$ | 2.387 | 2.379 | 2.461 | 2.461 | 2.461 | 2.461 | 2.381 | 2.316 |
| | $G_{se}$ | 2.560 | 2.587 | 2.668 | 2.668 | 2.668 | 2.668 | --- | --- |
| | $P_{ba,mix}$ | 0.97 | 1.08 | 0.83 | 0.83 | 0.83 | 0.83 | --- | --- |
| | $P_{be}$ | 3.93 | 4.72 | 4.47 | 4.47 | 4.47 | 4.47 | --- | --- |
| | ***D/B*** | 1.34 | 1.24 | 1.00 | 1.00 | 1.00 | 1.00 | --- | --- |
| | ***VMA*** | 12.7 | 14.6 | 14.3 | 14.3 | 14.3 | 14.3 | --- | --- |
| | ***VFA*** | 68.5 | 72.6 | 72.0 | 72.0 | 72.0 | 72.0 | --- | --- |

*a) PG purchase grade is reported for AC1 to AC6. Grade for AC7 is continuous grade.*

*-- AC1 and AC2 properties were obtained from the mix design.*

*-- AC3 to AC6 mixture properties were obtained from the mix design. MSU used $G_{mm}$ of 2.460 which was measured by T209 on plant-produced mixture.*

*-- AC7 and AC8 properties were measured at MSU; $P_{AC}$ (T164 extraction and recovery with a blend of 85% toluene and 15% ethanol); $G_{mm}$ (T209).*

### 3.2.3 Field-Sawn Asphalt Concrete

*Hwy 45* (AC7) and *Hwy 41* (AC8) were field pavements that had been in service for some time (Figure 3.1). *Hwy 45* materials were obtained from an abandoned portion of Highway 45 in Crawford, MS, while *Hwy 41* materials were obtained from an in-service portion of Highway 41 near Okolona, MS.

Materials were obtained by sawing slabs approximately 76 cm (*Hwy 45*) or 30 cm (*Hwy 41*) square from areas where minimal cracks and other distresses were present. Slabs were sawn across the entire lane width using a walk-behind wet saw and then carefully removed to prevent damage. Slabs were loaded into a trailer, returned to the laboratory, cleaned, dried, and stored until needed for testing. Field-aged pavements were used in some portions of Chapter 10 but were not tested for performance properties.


**Figure 3.1. Field-Aged Pavements Tested**

## 3.3 Reclaimed Asphalt Pavement

Multiple field-reclaimed and laboratory-crushed RAP materials were tested in this report. Four of these RAP materials were used when their properties were relevant. A few other RAP materials were used for incidental purposes (e.g. I-55 RAP in Chapter 9) and are not described in this section. Two field-reclaimed RAP materials were obtained from CIR projects, and two were obtained in more traditional manners (e.g. from a mill and overlay project). Field-reclaimed RAP materials are identified in this report as R1 to R4. Two laboratory-simulated RAP materials were produced by crushing *Hwy 45* and *Hwy 41* asphalt concrete and are identified in this report as CR1 and CR2. Table 3.2 provides properties for all RAP materials, while subsequent sections provide further details regarding each material.

### 3.3.1 Field-Reclaimed RAP Obtained from CIR Projects

#### 3.3.1.1 R1

RAP identified as R1 was obtained from a CIR project conducted on US Highway 49 (US-49) in Madison County, MS in 2010. Details regarding the construction and field evaluation of US-49 are provided in Chapter 5. RAP used in laboratory activities was sampled during Stage 2 (Chapter 5) of US-49 construction. Approximately 2,700 kg of R1 was sampled and tested in the laboratory at its as-received (A/R) gradation.

Six bulk samples were randomly obtained from US-49 as shown in Table 3.3. Three samples collectively referred to as R1 were taken from the CIR portion of US-49; these are *Hwy 49-A(1)* to *Hwy 49-A(3)*. Three other samples were taken from the FDR portion of US-49 (*Hwy 49-B(1)* to *Hwy 49-B(3)*); Volume 1 of this report deals with US-49 FDR. Bulk samples were obtained by both MSU and Burns Cooley Dennis, Inc. (BCD) prior to incorporation of any stabilization additives. Stationing, distance from beginning of project

(BOP), and lane information are provided for reference. It should be noted that *Hwy 49-A(3)* sampling location data was incorrect as it indicated the sample was obtained from FDR portions. However, gradation and material properties indicated the sample was in fact obtained from CIR portions as intended thus sampling location data was disregarded.

**Table 3.2. RAP Properties**

| **Category** | | CIR-Milled | | Traditionally-Milled | | | | Lab-Crushed | |
|---|---|---|---|---|---|---|---|---|---|
| **RAP ID** | | R1 | R2 | R3 | | | R4 | CR1 | CR2 |
| **Source** | | US-49 | US-45Alt | Lowndes Co. Stockpile | | | *Hwy 41* | *Hwy 45* | *Hwy 41* |
| **Gradation ID** | | A/R | A/R | A/R[a] | GF | GC | A/R | A/R | A/R |
| **Percent Passing (Bulk RAP)** | **25 mm** | 100 | 100 | 100 | 100 | 100 | 100 | 100 | 100 |
| | **19 mm** | 99.4 | 98.5 | 99.5 | 99.7 | 93.3 | --- | --- | --- |
| | **12.5 mm** | 94.4 | 88.7 | 94.4 | 96.5 | 78.3 | 89 | 67 | 58 |
| | **9.5 mm** | 85.4 | 73.1 | 85.4 | 90.5 | 64.5 | --- | --- | --- |
| | **4.75 mm** | 55.3 | 41.0 | 55.3 | 68.0 | 34.0 | 48 | 24 | 22 |
| | **2.36 mm** | 37.6 | 24.8 | 37.6 | 49.0 | 21.3 | 27 | 11 | 12 |
| | **1.16 mm** | 27.7 | 17.6 | 23.3 | 30.4 | 13.2 | --- | --- | --- |
| | **0.60 mm** | 19.3 | 12.9 | 14.8 | 19.5 | 8.4 | --- | --- | --- |
| | **0.30 mm** | 7.5 | 7.9 | 7.6 | 10.2 | 4.3 | --- | --- | --- |
| | **0.15 mm** | 3.3 | 5.7 | 3.3 | 4.6 | 1.9 | --- | --- | --- |
| | **0.075 mm** | 1.5 | 4.9 | 1.5 | 2.3 | 0.8 | --- | --- | --- |
| **Percent Passing (Extracted Aggregate)** | **25 mm** | 98.7 | 100 | 100 | 100 | 100 | 100 | 100 | 100 |
| | **19 mm** | 97.6 | 100 | 99.4 | 99.5 | 99.6 | 100 | 100 | 100 |
| | **12.5 mm** | 96.0 | 96.7 | 99.0 | 98.9 | 97.6 | 99.3 | 99.8 | 99.8 |
| | **9.5 mm** | 88.9 | 87.2 | 95.4 | 95.7 | 90.5 | 95.1 | 93.4 | 96.7 |
| | **4.75 mm** | 62.6 | 58.1 | 71.3 | 78.9 | 61.3 | 67.3 | 62.1 | 69.8 |
| | **2.36 mm** | 47.5 | 42.2 | 51.9 | 60.2 | 41.8 | 43.3 | 39.1 | 47.9 |
| | **1.16 mm** | 39.9 | 35.2 | 38.0 | 45.3 | 31.1 | 32.3 | 27.2 | 36.0 |
| | **0.60 mm** | 33.3 | 29.5 | 29.4 | 35.9 | 24.8 | 26.2 | 20.4 | 28.8 |
| | **0.30 mm** | 19.4 | 19.7 | 19.4 | 24.3 | 16.5 | 17.5 | 14.3 | 17.8 |
| | **0.15 mm** | 14.0 | 14.1 | 12.6 | 16.5 | 10.8 | 11.2 | 9.9 | 10.2 |
| | **0.075 mm** | 9.9 | 11.3 | 10.1 | 13.3 | 8.8 | 9.7 | 8.0 | 8.5 |
| **$P_{AC\text{-}T308}$ (%)** | | 5.1 | --- | 6.2 | 6.5 | 5.7 | 5.7 | 7.6 | 7.6 |
| **$P_{AC\text{-}T164}$ (%)** | | 4.8 | 5.1 | 5.6 | 6.2 | 4.9 | 5.4 | 6.8 | 6.8 |
| **RAP $G_{mm}$** | | 2.447 | 2.374 | 2.373 | 2.367 | 2.383 | 2.382 | 2.393 | 2.329 |
| **RAP $G_{sb}$** | | 2.385 | --- | 2.292 | 2.282 | 2.274 | --- | --- | --- |
| **RAP $G_{sa}$** | | 2.464 | --- | 2.382 | 2.374 | 2.375 | --- | --- | --- |
| **RAP *Abs* (%)** | | 1.3 | --- | 1.7 | 1.7 | 1.9 | --- | --- | --- |
| **Agg NMAS** | | 12.5 | 12.5 | 9.5 | 9.5 | 9.5 | 9.5 | 9.5 | 9.5 |
| **Agg $G_{sb}$** | | 2.567 | --- | 2.468 | 2.463 | 2.452 | 2.507 | 2.511 | 2.496 |
| **Agg $G_{sa}$** | | 2.627 | --- | 2.589 | 2.592 | 2.573 | 2.614 | 2.629 | 2.614 |
| **Agg *Abs* (%)** | | 0.8 | --- | 1.9 | 2.0 | 1.8 | 1.6 | 1.7 | 1.7 |
| **Agg *FAA* (%)** | | 41 | --- | 43 | 43 | 42 | 43 | 43 | 44 |

*a) R3 as-received (A/R) gradation is that which matches the R1 gradation at controlled sieve sizes.*
*-- Washed gradations for bulk RAP and extracted aggregates determined by ASTM C117 and C136.*
*-- $P_{AC\text{-}T308}$: NCAT ignition oven asphalt content (AASHTO T308). No aggregate correction factor was used.*
*-- $P_{AC\text{-}T164}$: Asphalt content by extraction (AASHTO T164). A blend of 85% toluene and 15% ethanol was used.*
*-- $G_{mm}$: maximum theoretical specific gravity determined via Corelok® vacuum sealing (Chapter 10).*
*-- Bulk ($G_{sb}$) and apparent ($G_{sa}$) specific gravity and absorption (Abs) determined by ASTM C127 and C128.*
*-- Fine aggregate angularity (FAA) determined by ASTM C1252 Method C.*

**Table 3.3. US-49 Sampling Summary**

| Sample | Station | BOP Distance | Lane |
|---|---|---|---|
| *Hwy 49-A(1)* | 715+32 | 0.08 km | North-Outside |
| *Hwy 49-A(2)* | 475+00 | 13.93 km | South-Outside |
| *Hwy 49-A(3)* | --- | --- | --- |
| *Hwy 49-B(1)* | 925+33 | 6.49 km | South-Inside |
| *Hwy 49-B(2)* | 927+50 | 6.55 km | North-Inside |
| *Hwy 49-B(3)* | 871+50 | 4.84 km | South-Outside |

*-- Sample A(1) and A(2) taken by MSU; samples A(3), B(1), B(2), and B(3) taken by BCD.*
*-- Total project length was 14.8 km.*

Table 3.4 provides moisture content (*MC*) data for R1 samples upon arrival to the MSU laboratory where six replicates (*n*) were tested per sample. Upon arrival, R1 was spread on the floor indoors and fan-dried to minimal *MC* (i.e. 0.25% or less). Once dry, R1 was sieved into six size fractions and stored in 19 L plastic buckets until needed for testing. Material retained on the 25 mm sieve was discarded. R1 size fractions were controlled at the following sieve sizes: 12.5 mm, 9.5 mm, 4.75 mm, 2.36 mm, and 0.075 mm (e.g. material finer than 2.36 mm but larger than 0.075 mm constituted one size fraction). In all, six individual size fractions were created for gradation consistency during batching and testing.

**Table 3.4. As-Received R1 Moisture Contents**

| Sample | *n* | Avg *MC* (%) | *MC* Range (%) |
|---|---|---|---|
| *Hwy 49-A(1)* | 6 | 3.9 | 3.6 to 4.2 |
| *Hwy 49-A(2)* | 6 | 3.4 | 3.1 to 3.8 |
| *Hwy 49-A(3)* | 6 | 5.0 | 4.3 to 5.9 |

### 3.3.1.2 R2

RAP identified as R2 was obtained from a CIR project conducted on US Highway 45 Alt (US-45Alt) in Monroe County, MS in 2014. Details regarding the construction and field evaluation of *Hwy 45Alt* are provided in Chapter 5. One site was sampled which was in the northbound inside lane at station 512+50, which was approximately 2.8 km from the BOP as measured in the outside lane by vehicle odometer. Sampling site coordinates were 33° 49' 49" N and 88° 44' 9" W.

At the sampling site, twenty 19 L buckets of RAP (approximately 1,000 kg) were sampled prior to incorporation of stabilization additives. At the time of sampling, unstabilized RAP had been spread relatively uniformly across the width of the lane. The twenty buckets were sampled at twenty locations spaced approximately 4.5 meters apart longitudinally over a 90-meter distance. At each sampling location, one bucket was completely filled with RAP; care was taken to partition off each location and sample the full depth of milled material.

Upon arrival to the laboratory, R2 was neither sieved nor dried as was R1. Instead, RAP was tested one bucket at a time since each bucket theoretically made up a representative sample. Prior to use, a bucket was uniformly mixed and randomly split into required batch sizes with the use of a sample splitter. *MC*s were taken from each bucket for the purpose of calculating corrected batch weights of RAP, water, and stabilization additives during specimen fabrication. The average R2 *MC* upon arrival was approximately 3.5%. R2 samples used for Table 3.2 property testing were dried to constant mass at 52 °C. Note that R2's $P_{0.075}$

was 4.9%, which was high relative to other RAP materials. Though this value appears questionable, no apparent issues with testing or data analysis were discovered.

### 3.3.2 Field-Reclaimed RAP Obtained in Traditional Manners

#### 3.3.2.1 R3

RAP identified as R3 was obtained from an APAC Mississippi's RAP stockpile in Lowndes County, MS. It was obtained primarily to provide additional material for laboratory experiments since quantities of RAP obtained from CIR projects were limited. RAP was sampled from the stockpile by the plant loader operator as in normal plant operations and was dumped into either 189 L barrels or a trailer. RAP was fan-dried in the laboratory similarly to R1 and was sieved into the six size fractions used for R1.

R3 was tested at three gradations which were all fabricated and did not represent the R3 stockpile gradation. The primary gradation fabricated was the R1 as-received gradation, which, for purposes of this report, is also deemed the as-received gradation for R3. Note that sieve sizes not controlled (e.g. 1.16 mm sieve) may have different percentages passing between, for example, R1 and R3. In addition, two other gradations, fine (GF) and coarse (GC), were fabricated in attempts to bound gradations observed in literature (Figure 2.1).

The original stockpile gradation for R3 was relatively coarse; therefore, in testing A/R and GF gradations with R3, the size fraction between 2.36 mm and 0.075 mm was depleted at a faster rate. Therefore, a second R3 sample was obtained, dried, and sieved with the primary goal of supplementing the critical size fraction. This was considered viable since the second sample was also from Lowndes County. To support this thought, a small experiment was conducted (results shown in Table 3.5). Three blends (Blends 1 to 3) were fabricated where the 2.36 to 0.075 mm size fraction was composed of only Sample 1, only Sample 2, or an even proportion of both. Based on $G_{mm}$, all blends were practically identical.

**Table 3.5. Results of R3 Blending Investigation**

| RAP Blend ID | | Blend 1 | Blend 2 | Blend 3 |
|---|---|---|---|---|
| **Sample 1 to 2 Ratio for 2.36 to 0.075 mm Size Fraction** | | 100% Sample 1 | 50% Sample 1<br>50% Sample 2 | 100% Sample 2 |
| **RAP $G_{mm}$** | | 2.369 | 2.371 | 2.368 |
| **$P_{AC}$ (%)** | | 5.6 | 5.7 | --- |
| **Percent Passing (Extracted Aggregate)** | **25 mm** | 100 | 100 | --- |
| | **19 mm** | 99.8 | 100 | --- |
| | **12.5 mm** | 99.1 | 99.6 | --- |
| | **9.5 mm** | 95.4 | 95.9 | --- |
| | **4.75 mm** | 71.3 | 71.6 | --- |
| | **2.36 mm** | 51.9 | 52.3 | --- |
| | **1.16 mm** | 38.0 | 39.5 | --- |
| | **0.60 mm** | 29.4 | 31.9 | --- |
| | **0.30 mm** | 19.4 | 21.3 | --- |
| | **0.15 mm** | 12.6 | 13.3 | --- |
| | **0.075 mm** | 10.1 | 9.8 | --- |
| **Agg $G_{sb}$** | | 2.468 | 2.457 | --- |
| **Agg *FAA* (%)** | | 42.5 | 41.5 | --- |

*-- $G_{mm}$ determined by D6857 (Chapter 10), $P_{AC}$ determined by T164, Gradation determined by C117 and C136, $G_{sb}$ determined by C127 and C128, FAA determined by C1252 Method C.*

In order to most effectively use R3, the optimum ratio of Samples 1 to 2 was 57 to 43, respectively (i.e. 43% of the 2.36 to 0.075 mm fraction was Sample 2). This ratio was bracketed by Table 3.5 Blends 1 and 2, which, in addition to $G_{mm}$, were tested for $P_{AC}$ and aggregate gradation and properties. Asphalt content, gradation, $G_{sb}$, and *FAA* were not meaningfully different, indicating R3 batched with the blended (Samples 1 and 2) size fraction were not greatly different than when only Sample 1 was present. Samples 1 and 2 were stored separately and were not blended until batching; all blended batches included 57% Sample 1 and 43% Sample 2.

In addition, R3 Sample 2 RAP particles larger than 25 mm were laboratory-crushed in an LA Abrasion drum with the charge of steel spheres. This laboratory-crushed material was then sieved, and only the 2.36 mm to 0.075 mm size fraction was kept. Some R3 was batched with this laboratory-crushed 2.36 to 0.075 mm size fraction and is hereafter referred to as R3 with laboratory-crushed material. This material was primarily used for development of laboratory test protocols but was also used to a small extent to supplement the $G_{mm}$ investigation in Chapter 10.

#### 3.3.2.2 R4

RAP identified as R4 was obtained from a mill and overlay project on *Hwy 41* near Okolona, MS. Milled RAP was sampled into buckets directly off the elevator belt of the milling machine. The sampling location was within several hundred meters of the sampling location for AC8 (Section 3.2.3).

Upon arrival to the laboratory, R4 was dried under fans and sieved. Material retained on the 25 mm sieve was discarded, and the remaining material was stored in four size fractions similar to practices discussed in previous sections. R4 size fractions were partitioned by the 12.5, 4.75, and 2.36 mm sieves. R4 was tested at its as-received gradation.

### 3.3.3 Laboratory-Simulated RAP Obtained by Crushing

#### 3.3.3.1 CR1

RAP denoted as CR1 was laboratory-produced by crushing *Hwy 45* slabs sampled as discussed in Section 3.2.3. Prior to crushing, slabs were broken into chunks and placed in a freezer overnight, which facilitated crushing. The material was removed from the freezer and immediately crushed in a jaw crusher at Paragon Technical Services, Inc. (PTSi). Particles larger than 25 mm were run through the crusher again.

The rapid thawing of frozen material produced considerable condensation or sweating. Therefore, crushed RAP was fan dried before sieving. CR1 was sieved into the same four size fractions as R4. CR1 was tested at its as-received gradation.

#### 3.3.3.2 CR2

RAP denoted as CR2 was laboratory-produced by crushing *Hwy 41* slabs sampled as discussed in Section 3.2.3. Crushing occurred in an identical manner to that of CR1. Similarly, CR2 was fan dried after crushing and sieved into four size fractions. CR2 was tested at its as-received gradation.

## 3.4 Stabilization Additives

### 3.4.1 Bituminous

Two asphalt emulsions were used in this research. The first emulsion tested was an engineered emulsion manufactured by Ergon Asphalt & Emulsions, Inc. and supplied by Paragon Technical Services, Inc. (PTSi) in small quantities as needed. The emulsion classified as a CSS-1h emulsion and was referred to by PTSi as FDR-EE or CIR-EE depending on the application. This emulsion was used during US-49 construction and is the primary emulsion used in this research as it was used for all emulsion-stabilized CIR mixtures regardless of RAP material. Average CIR-EE properties provided by PTSi are shown in Table 3.6.

**Table 3.6. Average CIR-EE Properties**

| Property | Result |
|---|---|
| Sieve (%) | 0.01 |
| 25 °C SFS Viscosity (sec) | 40 |
| Particle Size (μm) | 2.68 |
| Emulsion pH | 2.38 |
| Emulsion Residue (%) | 63.3 |

*-- pH determined according to T200; Saybolt Furol Seconds (SFS) viscosity determined according to T72; sieve and residue determined according to T59; particle size determined using a MalvernMastersizer Micro-P and manufacturer protocols.*

The second emulsion tested was used as a prime coat during US-45Alt construction and is classified as an AE-P emulsion by MDOT designations. The AE-P emulsion was used in this research in only a handful of cases to seal the surfaces of compacted cement-stabilized CIR specimens to replicate the prime coat on US-45Alt. A single sample of AE-P emulsion was obtained from the Ergon refinery in Vicksburg, MS. Table 3.7 provides the MDOT specifications for AE-P found in Section 702, Table III of the Mississippi Standard Specifications (MDOT, 2004).

**Table 3.7. MDOT Specifications for AE-P**

| | Specification Requirements | |
|---|---|---|
| **Test Method and Property** | **Min.** | **Max.** |
| T59 25 °C SFS Viscosity (sec) | 10 | 50 |
| T59 5-Day Settlement (%) | --- | 5 |
| T59 Total Distillate (%, weight) | --- | 55 |
| T59 Oil Distillate (%, volume) | --- | 12 |
| T50 60 °C Float Test (sec) | 20 | --- |
| T44 Solubility in TCE (%) | 97.5 | --- |

*-- T59 performed on asphalt emulsion; T44 and T50 performed on emulsion residue from T59 distillation to 260 °C.*

Emulsions were stored in 3.8 L plastic containers at room temperature. Prior to use, emulsions were heated to 60 °C based on practices recommended by PTSi. In general, emulsion samples were considered suitable for use for two months from the date of production based on PTSi guidance and were used without any property verification. During this two-month period, emulsion sample containers were periodically rolled end over end to

facilitate gentle agitation and reduce settling. Emulsion samples not completely used after two months were considered still useable as long as ASTM D6933 sieve test results were less than 0.10%. For an emulsion sample older than two months, a sieve test was performed prior to its use each day that CIR materials were mixed. Use of emulsions older than two months was uncommon as most samples were depleted within two months.

### 3.4.2 Cementitious

Table 3.8 provides properties of the ASTM C150 Type I portland cements tested herein. The *GV* cement was used during the construction of US-49. Two *GV* samples were received from the plant; properties of the first sample are shown in Table 3.8. The *LH* cement was used during the construction of US-45Alt and was sampled from the cement spreader during field construction. The *LH* cement was used to stabilize R2 (US-45Alt) only; the *GV* cement is the primary cement used in this research and was used to stabilize all other materials. Cement samples were stored in the laboratory in sealed plastic buckets to limit exposure to humidity.

**Table 3.8. Portland Cement Properties**

| Source | *GV*[a] | *LH*[b] |
|---|---|---|
| $SiO_2$ (%) | 20.0 | 20.4 |
| $Al_2O_3$ (%) | 4.5 | 4.6 |
| $Fe_2O_3$ (%) | 3.1 | 3.4 |
| CaO (%) | 64.2 | 63.1 |
| MgO (%) | 2.3 | 3.0 |
| $SO_3$ (%) | 3.2 | 2.9 |
| $C_3S$ (%) | 62 | 56 |
| $C_2S$ (%) | 9 | 16 |
| $C_3A$ (%) | 6 | 6 |
| $C_4AF$ (%) | 9 | 10 |
| Limestone (%) | 3.3 | 1.2 |
| LOI (%) | 2.7 | 1.8 |
| Blaine ($m^2$/kg) | 383 | 397 |
| Initial Vicat (min) | 90 | 102 |
| Air (%) | 7 | 7 |
| 1-Day Strength (MPa)[c] | 16 | 16 |
| 3-Day Strength (MPa)[c] | 30 | 25 |
| 7-Day Strength (MPa)[c] | 36 | --- |
| HoH, 7-Day (kJ/kg) | 344 | 406 |

*a) GV = Holcim Cement, Saint Genevieve, MO*
*b) LH = Lehigh Cement, Leeds, AL*
*c) 1-, 3-, and 7-day compressive strengths according to ASTM C109*

Hydrated lime was used as an anti-stripping agent for emulsion CIR mixtures which did not incorporate cement as a binder (i.e. emulsion SCB systems). As standard practice for MDOT hot mix asphalt, hydrated lime was also used during the construction of the emulsion CIR section of US-49.

In the early stages of State Study 250, the potential of utilizing thermal measurements for early age and/or traffic opening purposes was considered. Once the idea of a universal

framework suitable for any type of binder system became the focus of State Study 250, thermal measurements became less appealing. The remainder of this section presents the thermal measurement data collected as part of State Study 250 and provides brief details on how the data was collected. In addition, data is presented herein for US-49 FDR materials which were the focus of State Study 250 report Volume 1.

The overall goal of thermal measurement testing was to determine if the same thermal testing techniques developed in State Study 206 (Howard et al., 2013c) could apply to in-place recycled materials. Thermal measurement testing was conducted on a total of 54 specimens (27 US-49 CIR and 27 US-49 FDR). Thermal profile measurements were conducted using the *GV* cement at three cement contents (c's). Testing was also conducted at three different initial material temperatures of 10, 21, and 32 °C, but the ambient temperature during thermal measurement was kept constant at 21 °C. For each combination of material type, cement content, and initial material temperature, three replicates were tested.

Thermal profile testing was conducted in the same manner as State Study 206 and Sullivan (2012). All materials and equipment were conditioned overnight to the appropriate initial material temperature. Specimens were mixed, compacted using the PM device described in part in Chapter 4 (see State Study 206 and Sullivan et al. 2015 for additional details), and placed in the thermal measurement device within 20 minutes of cement addition. Inert reference specimens (unstabilized material) were also conditioned and placed in the thermal measurement device for comparison to cement-stabilized specimens. Thermal profile measurements were conducted over a 24 hour period before specimens were removed, measured for density, and placed in a moist curing room. After 7 days of moist curing, specimens were tested for UCS. Raw test data can be found in Sullivan (2012). Table 3.9 contains the thermal profile and UCS results.

**Table 3.9. Thermal Profile and UCS Results**

| Material | Initial Material Temp (°C) | Test Temp (°C) | c (%) | $T_{max}$ (°C) | $t_{max}$ (hr) | $\Delta T$ (°C) | $A_s$ (°C-hr) | $A_{\Delta T}$ (°C-hr) | UCS (kPa) |
|---|---|---|---|---|---|---|---|---|---|
| CIR | 10 | 21 | 3.6 | 21.5 | 23.9 | 2.1 | 374 | 13.9 | 1214 |
| | | 21 | 4.4 | 22.1 | 24.0 | 2.6 | 377 | 16.4 | 1477 |
| | | 21 | 5.2 | 23.1 | 23.9 | 3.4 | 406 | 41.0 | 2115 |
| | 21 | 21 | 3.6 | 25.8 | 12.7 | 3.8 | 597 | 75.5 | 1175 |
| | | 21 | 4.4 | 26.6 | 13.8 | 4.5 | 611 | 88.4 | 1507 |
| | | 21 | 5.2 | 26.7 | 12.9 | 4.8 | 613 | 93.1 | 1881 |
| | 32 | 21 | 3.6 | 30.3 | 5.5 | 1.5 | 680 | 44.2 | 1306 |
| | | 21 | 4.4 | 30.9 | 7.7 | 3.7 | 693 | 62.7 | 1657 |
| | | 21 | 5.2 | 31.0 | 5.3 | 1.6 | 689 | 51.5 | 2076 |
| FDR | 10 | 21 | 4.0 | 20.6 | 24.0 | 1.9 | 384 | 57.0 | 1756 |
| | | 21 | 4.8 | 21.1 | 23.8 | 2.3 | 392 | 57.7 | 2200 |
| | | 21 | 5.7 | 21.8 | 23.3 | 2.9 | 416 | 66.2 | 2488 |
| | 21 | 21 | 4.0 | 24.7 | 9.6 | 3.5 | 576 | 67.6 | 1898 |
| | | 21 | 4.8 | 25.7 | 10.8 | 4.4 | 594 | 85.4 | 2144 |
| | | 21 | 5.7 | 25.8 | 9.9 | 4.6 | 594 | 85.0 | 2062 |
| | 32 | 21 | 4.0 | 31.0 | 1.8 | 0.4 | 671 | 42.8 | 1708 |
| | | 21 | 4.8 | 31.6 | 4.2 | 2.9 | 691 | 67.0 | 1841 |
| | | 21 | 5.7 | 32.0 | 4.2 | 3.8 | 691 | 75.0 | 2071 |

*-- c = cement content by mass of unstabilized material. Chapter 4 further defines terminology used herein.*

Five thermal measurement variables were analyzed: 1) the maximum measured temperature ($T_{max}$); 2) the time in which $T_{max}$ occurred ($t_{max}$); 3) the maximum temperature difference between the test specimen and inert reference specimen ($\Delta T$); 4) the total area beneath the thermal profile curve and a 0 °C reference temperature ($A_s$); and 5) the total area between the test specimen thermal profile and the reference specimen thermal profile ($A_{\Delta T}$). Test variables of most value in State Study 206 were $T_{max}$, $\Delta T$, and $A_s$.

From Table 3.9, it appears that the initial material temperature has a significant effect on the thermal measurement results. This observation was also seen in data analysis from State Study 206. Overall, the results show that it is feasible to conduct thermal measurement testing on in-place recycled materials, but the results are subject to the same limitations as discussed in State Study 206.

# CHAPTER 4 – EXPERIMENTAL PROGRAM - LABORATORY

## 4.1 Laboratory Experimental Program Overview

The experimental program was developed to evaluate key components of CIR laboratory mix design and to characterize a variety of SCB and MCB systems. Testing goals were to establish a universal CIR design framework appropriate for any SCB or MCB system and to demonstrate sustainability advantages with MCB systems. Terminology used in this report is described in Section 4.2. Section 4.3 discusses asphalt concrete specimen production procedures. Section 4.4 discusses CIR specimen production procedures including mixing, compaction, curing, and density determination. In this report, specimen production generally refers to batching, mixing, compacting, curing or aging, and measuring density; specimen preparation refers to steps required to prepare a specimen for a particular test method. Section 4.5 discusses twelve test methods utilized in this report as well as test-specific preparation procedures.

## 4.2 Terminology

Terminology used to identify asphalt concrete specimens tested in this report generally includes asphalt concrete ID (AC1 to AC8), target air void level (4, 7, or 10%), and/or length of aging (0 or 2 years). As discussed in Section 3.2.1, some US-49 mixtures (AC1 and AC2) were field compacted then sampled during US-49 field investigations and are denoted with an "FC" subscript. Specifics regarding asphalt concrete terminology are provided at the beginning of each results chapter which includes asphalt concrete.

CIR specimens in this report are labeled according to RAP source (R1 to R4 and CR1 to CR2), gradation (A/R, GF, and GC), and binder system. Binder systems were identified by the by-mass dosage and type of binder: portland cement (c), asphalt emulsion (e), and hydrated lime (HL). For example, R3(GF)-2.5c2e refers to R3 batched to the GF (fine) gradation and stabilized with 2.5% portland cement and 2% emulsion.

## 4.3 Asphalt Concrete Specimen Production

### 4.3.1 Asphalt Concrete Batching

Laboratory-compacted asphalt concrete materials were plant mixed rather than laboratory mixed. Asphalt concrete was stored in metal buckets in the laboratory until needed for specimen production. Buckets were heated one at a time until mixture temperature was just high enough to facilitate batching into covered metal pans. Generally, a given bucket was only heated once, and asphalt was batched into metal pans (generally one specimen per pan) until the entire bucket was used. In some cases, batched pans were allowed to cool and were later reheated for specimen production, while in others, batched pans were kept in the oven until the compaction temperature was reached, at which point specimens were compacted.

### 4.3.2 Asphalt Concrete Compaction

Asphalt concrete specimens were either compacted in the Pine Superpave gyratory compactor (SGC) described in Section 4.4.2.1 or the Linear Asphalt Compactor (LAC) described in Section 4.4.2.2. Asphalt concrete SGC specimens were compacted to a target height and density or with a specified compactive effort (i.e. a set number of gyrations ($N_{gyr}$)). Asphalt compaction temperatures were either hot or warm mix temperatures ranging from 116 to 149 °C, depending on the mixture. Following compaction, asphalt specimens were immediately extruded from SGC molds and allowed to cool to room temperature under fans before handling or testing.

Asphalt concrete LAC slabs were compacted with 18 roller passes and a hydraulic pressure of 2413 kPa (350 psi). Target thickness was 7.6 cm, and target $V_a$ was 7.5 ± 1.0% on a T331 basis, which is approximately 7.0 ± 1.0% on a T166 basis. LAC compaction temperatures for asphalt concrete were identical to SGC compaction temperatures. Prior to compaction, the LAC mold was heated to compaction temperatures via an infrared heat lamp.

### 4.3.3 Asphalt Concrete Density Measurement

Density was measured on all asphalt concrete specimens. T209 was used to determined $G_{mm}$. T331 was used to determine $G_{mb}$ and calculate $V_a$. Methods in Doyle and Howard (2014) were used to calculate LAC slab $V_a$ (similar to method in Section 4.4.4.2).

### 4.3.4 Asphalt Concrete Field Aging

Approximately half of all ERDC asphalt concrete SGC specimens tested in this report were field aged for two years. Specimens were exposed to rain and sunlight; however, specimens were placed in PVC sleeves so that only the top face was exposed to direct sunlight. Aged and un-aged ERDC specimens are denoted 2-yr and 0-yr, respectively.

## 4.4 CIR Specimen Production

### 4.4.1 CIR Batching and Mixing

RAP materials were batched either directly into metal mixing buckets or into large plastic freezer bags and stored for later mixing. Predominantly, RAP was batched from individual size fractions (recall a sample splitter was instead used to batch R2 as discussed in Chapter 3). All stabilization additives were batched as a percentage of dry RAP mass. Water was batched as a percentage of dry solids (i.e. RAP, cement, hydrated lime, emulsion residue) and included the water in the emulsion (i.e. the total water added included both batch water and emulsion water). Figure 4.1a shows water and cementitious stabilization additives pre-batched into sealed plastic containers. Emulsion was not pre-batched; it was maintained at 60 °C and batched into the mixing bucket partway into the mixing process.

Materials were mixed for four minutes at room temperature in either a 19 L (Figure 4.1a) or 38 L (Figure 4.1b) bucket mixer using a mixing paddle and trowel (Figure 4.1c). The mixer was turned on, water was poured over the RAP, and a stopwatch was started. Water and RAP were mixed for one or two minutes, depending on whether or not emulsion was

added to that batch. If emulsion was added, the mixer was stopped at 1 minute, the bucket was removed and placed on a scale, a depression was formed in the middle of the bucket, the correct mass of emulsion was poured into the depression (Figure 4.2), and then mixing of RAP, water, and emulsion resumed for one minute. At two minutes, cementitious additives were gradually added without stopping the mixer, and mixing continued for two additional minutes. In Chapter 7, total mixing time for mixtures including emulsion was shortened to two minutes (added emulsion at 60 seconds and cementitious additives at 90 seconds) to comply with current DOT practices.

*a) Bucket Mixer (19 L)* *b) Bucket Mixer (38 L)* *c) Mixing Tools*

**Figure 4.1. CIR Mixing Equipment**

**Figure 4.2. Emulsion Batched into Mixing Bucket**

Most batches were mixed using the smaller 19 L bucket mixer. Slabs compacted in the LAC were mixed in the 38 L bucket mixer. Because of the large amount of material required, LAC slabs were mixed in two rounds (i.e. two half batches were mixed one after the other). Otherwise, mixing operations were identical to those discussed in the previous paragraph.

### 4.4.2 Compaction of CIR Test Specimens

Multiple compactors and compaction methods were employed in this study. The SGC and the LAC were the two primary compactors used. CIR specimens were also compacted with Proctor compaction (standard and modified) and with the plastic mold (*PM*) compaction method developed during MDOT State Study 206 (Howard et al., 2013c). Specific details regarding compaction with each device are provided in following subsections.

CIR specimens were compacted immediately after materials were thoroughly mixed as described in Section 4.4.1. In most cases, two or three specimens were compacted from one batch of mixed CIR material. The target time to compact all specimens in a batch was 20 minutes from the time that cementitious binders were incorporated. The average time to compact an entire batch in this study was approximately 12 minutes. The 20 minute target was exceeded in a few cases but not by a significant amount (e.g. 2 minutes).

After compaction, CIR specimens were normally placed in their respective curing environments immediately. Generally, specimens were supported when being carried from the compaction area to the curing environment to facilitate careful handling of freshly-compacted specimens. Smaller specimens (e.g. SGC specimens) were placed onto 15 by 15 cm stainless steel expanded metal (12.7 mm number 18 style) plates for support; these were usually left with the specimen for the first day of curing before being retrieved. Larger specimens (e.g. LAC slabs) were supported by solid aluminum plates.

#### 4.4.2.1 SGC Compaction

Two SGCs were used during this study (Figure 4.3): a Troxler 4140 and a Pine AFGC 125X. Typical compaction parameters were used for both SGCs (i.e. 1.25° external angle and 600 kPa compaction pressure). Both 100 and 150 mm diameter specimens were compacted. CIR compaction was initially conducted with the Troxler SGC; however, equipment malfunctions were common and resulted in the Pine SGC being used for CIR compaction.


*a) Troxler 4140* *b) Pine AFGC 125X*

**Figure 4.3. Superpave Gyratory Compactors**

CIR SGC specimens were compacted with a specified compactive effort, or $N_{gyr}$. CIR specimens were compacted at room temperature; additionally, SGC molds and other compaction equipment were maintained at room temperature. Paper discs, or release papers, were not placed between the material and SGC compaction plates as is typical for asphalt concrete. Following compaction, CIR specimens were immediately extruded from SGC molds, weighed, measured in some cases (i.e. specimen height or thickness), and promptly placed in specified curing environments.

#### 4.4.2.2 LAC Compaction

The Linear Asphalt Compactor (LAC) shown in Figure 4.4 was used during this study to produce laboratory-compacted slabs. Full details regarding the LAC can be found in the operator's manual (Doyle and Howard, 2014); an overview of key LAC components is provided herein. The LAC produces slabs which are 29.3 cm wide by 62.4 cm long and can

range from 3.8 to 10.2 cm thick. Compactive effort is applied by a hydraulic cylinder with which hydraulic pressure can be regulated and adjusted as needed. This compactive effort is applied to the mixture via a roller and a series of vertical steel plates.

**Figure 4.4. Linear Asphalt Compactor**

CIR slabs were compacted with 30 roller passes and a hydraulic pressure of 2930 kPa (425 psi). This combination of roller passes and hydraulic pressure was utilized as it produced $V_a$'s generally on the order of those at 30 gyrations with SGC compaction. Target thickness was either 6.3 cm or 7.6 cm, depending on testing envisioned. As with SGC compaction, all aspects of LAC compaction were conducted at room temperature immediately after mixing of CIR materials.

#### 4.4.2.3 Standard Proctor Compaction

Standard Proctor compaction was used in this report for RAP and CIR moisture-density relationship evaluations and for producing UCS specimens. In both cases, a manual (technician-operated) standard Proctor hammer was used. The hammer had a mass of 2.5 kg (5.5 lb) and was dropped from a height of 30.5 cm (12 in) from the material's surface.

For moisture-density relationship evaluations, Mississippi test method MT-8, a modification of AASHTO T99, was followed for unstabilized RAP, and MT-9, with some modifications, was followed for stabilized CIR. A typical Proctor compaction mold was used with a height of 116.4 mm, inside diameter of 152.4 mm, and volume of 2.124 ($10^{-3}$) $m^3$. For the 152.4 mm diameter mold, compaction was conducted in 4 layers with 56 blows per layer as per MT-8 and MT-9.

Note that MT-9 calls for a 152.4 mm diameter mold with a volume of 2.832 ($10^{-3}$) $m^3$, which corresponds to a height of 155.2 mm; instead, the 116.4 mm tall mold was used in all cases as this was typical of MDOT practices. Further, MT-9 states materials are to be mixed with stabilization additives, and each Proctor point is to reuse the same material; thus, some Proctor points are compacted several minutes after stabilization additives are incorporated. In this report, each Proctor point, except for a few exploratory cases, was batched, mixed, and compacted separately (i.e. no stabilized material was reused). Several exploratory Proctor tests reused stabilized material and also evaluated the automatic Texas hammer for comparison.

For producing UCS specimens, MT-8 protocols were used in conjunction with a 101.6 mm diameter mold. Mold height and volume were 116.4 mm and 0.934 ($10^{-3}$) $m^3$, respectively. For the 101.6 mm mold, compaction was conducted in 3 layers with 25 blows

per layer. Between each layer, the surface was scarified to slightly break up the surface and better promote uniform compaction. A straightedge was used to strike off excess material, and the specimen was generally immediately extruded and transported to its curing environment. With coarser gradations tested, specimens were often too fragile to be immediately extruded; instead, specimens were left in the mold under a damp towel approximately 2 hours before being extruded and placed into curing.

#### 4.4.2.4 Modified Proctor Compaction

Modified Proctor compaction according to T180 was used in this report for producing UCS specimens. A manual (technician-operated) modified Proctor hammer was used with a mass of 4.5 kg (10 lb) and a drop height of 45.7 cm (18 in). As with UCS specimens produced by standard Proctor compaction, a 101.6 mm diameter Proctor mold was used. Compaction was conducted in 5 layers with 25 blows per layer. Layer scarification, strike-off and extruding procedures were identical to those in Section 4.4.2.3.

#### 4.4.2.5 Plastic Mold Compaction

The plastic mold (*PM*) compaction device used in this report was developed at Mississippi State University and is documented in great detail in Sullivan (2012) and Howard et al. (2013c). The *PM* device consists of a split mold and removable collar in which a 7.6 by 15.2 cm plastic cylinder mold can be inserted, allowing a specimen to be compacted inside the plastic mold. The *PM-P* device is one configuration of the *PM* device in which it is affixed to a steel base plate and compaction is conducted with a modified Proctor hammer. Figure 4.5 provides photographs of the *PM-P* device with the split mold closed and open.

Prior to compaction, a plastic mold was inserted inside the split mold, the split mold was closed and secured, and the collar was placed on top of the split mold. Note that plastic molds were modified slightly to allow specimens to be extruded after curing (see Howard et al. (2013c) for details). Specimens were compacted in 3 layers and were scarified at each layer interface. Compaction effort of 5 blows per layer with the modified Proctor hammer was used in parts of Howard et al. (2013c) as well as in this report. This study also investigated compaction efforts of 10 and 25 blows per layer. Following compaction, specimens were not extruded prior to curing but were cured in the plastic molds.

*a) PM-P Closed* *b) PM-P Open* *c) PM-P w/ Mod. Hammer*

**Figure 4.5. *PM-P* Compaction Device**

### 4.4.3 Curing of CIR Test Specimens

Five curing environments were used in this study. Four laboratory curing methods were employed using various combinations of temperature and humidity. Outdoor curing was also conducted. Specific details regarding each curing environment are provided in the following subsections.

Generally, specimens were cured for specified periods of time. Cure times studied in this report include 1, 3, 7, 14, 28, 56, 90, 120, and 180 days. Tolerances on cure times adhered to cure time tolerances for portland cement concrete provided in ASTM C39. Tolerances for cure times not listed in C39 were determined by interpolation or extrapolation. Once removed from curing, a target timeframe was established in which all remaining preparation and testing procedures for a given specimen were completed (i.e. from removal from curing to discarding). For specimens cured 7 days or less, 8 hours were allowed; for specimens cured 14 days or longer, 24 hours were allowed, though this was sometimes exceeded at the later cure times (e.g. 180 days) since it did not violate C39 tolerances. Included in this target timeframe was a 2.5 hour normalization period where specimens were allowed to come to room temperature.

In Chapter 7, emulsion SCB specimens were cured to constant mass rather than for a fixed period of time. Specimens cured to constant mass were weighed every two hours until the percent mass loss (Equation 4.1) in a two hour period was less than 0.05%. Specimens cured to constant mass were cured a minimum of 16 hours but no longer than 48 hours. Once removed from curing, specimens underwent a 12 to 24 hour "cool-down" period as is prescribed in traditional DOT mix design methods for emulsion SCBs.

$$P_{ML} = \frac{M_i + M_{i+2}}{M_{i+2}} \times 100 \tag{4.1}$$

Where,
$P_{ML}$ = percent mass loss in a two hour period of dry oven curing
$M_i$ = specimen mass at time $i$
$M_{i+2}$ = specimens mass two hours after time $i$

#### 4.4.3.1 Humid Oven

Humid oven (HO) curing was the predominant means of curing specimens in this study. HO curing was conducted in a 40 °C oven maintained at approximately 35 to 50% relative humidity (R.H.). Figure 4.6 shows a humid oven filled with specimens. An Omega HH314A humidity and temperature data logger was mounted to the side of the oven, and the probe was positioned at approximately two-thirds the height of the oven.

Several trials were conducted at the beginning of the study where humidity was evaluated as a function of water surface area, water tray placement, and oven vent positions. Ultimately, two trays of water which were 61 by 61 cm square and 10 cm deep (yielding a combined water surface area of 0.75 $m^2$ for both trays) were placed at the bottom and middle of the oven, and all oven vents were completely closed. Water level in the trays was checked periodically and refilled as necessary, which was usually about once per week.


**Figure 4.6. Humid Oven**

The oven in Figure 4.6 was used throughout the entire study; however, a second oven was needed at one point for additional capacity. Therefore, a second humid oven (same make and model) was configured identically to the one in Figure 4.6, and the oven vents were adjusted until the second oven's R.H. approximately matched the first. Figure 4.7a shows the humidity distribution from the entire study for the first and primary oven; Figure 4.7b shows the humidity distribution for the second oven compared to the distribution for the first oven during the same time period. Readings were recorded at 30 minute intervals. Note that a small percentage of readings were considerably less than 30% R.H.; these readings typically coincided with the opening of an oven to add or remove specimens, at which point humidity decreased considerably.

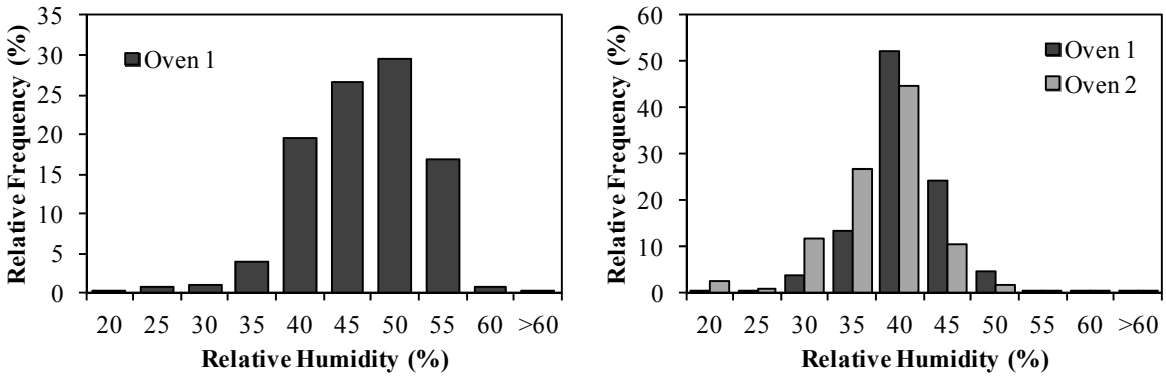


*a) Oven 1 RH from Feb 2013 to Oct 2015* *b) Ovens 1 and 2 RH from Jan to Apr 2015*

**Figure 4.7. Humid Oven Relative Humidity Distribution**

### 4.4.3.2 Dry Oven

Dry oven (DO) curing was conducted at two temperatures in this report. DO curing was similar to that depicted in Figure 4.6 but without water trays. Chapter 7 utilizes 60 °C dry oven curing ($DO_{60C}$) where specimens were cured to constant mass. All other dry oven curing was conducted at 40 °C ($DO_{40C}$) for specified cure times (e.g. 14 days).

#### 4.4.3.3 Moist Curing Room

A moist curing room (CR) such as those commonly used for curing of cementitious-stabilized mixtures was utilized. The curing room was maintained at 100% RH with an Aquafog misting fan (Figure 4.8a). Temperature was continuously monitored with a SPER Scientific Model 800024 data logger at 60 minute intervals. Figure 4.8b shows the distribution of curing room temperatures during the period of the study when the curing room was used for CIR specimens.

Specimens were set on shelves in the curing room. These shelves were wooden and were covered with stainless steel expanded metal (12.7 mm number 18 style). Wooden dowels (6.3 mm diameter) were placed between wooden shelves and expanded metal racks to act as spacers and prevent specimens from sitting in any standing water that may have pooled on a shelf. Figure 4.8a shows an example of one shelf next to the Aquafog misting fan.

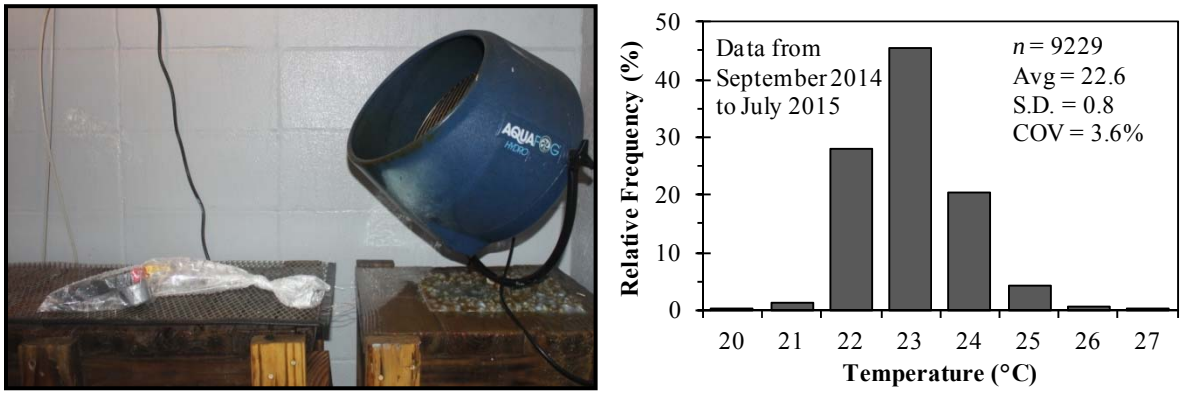


*a) Curing Room* *b) Curing Room Temperature Distribution*

**Figure 4.8. Moist Curing Room Photograph and Temperature Distribution**

#### 4.4.3.4 Ambient Laboratory

CIR $G_{mm}$ samples presented in Chapter 10 were cured in ambient laboratory conditions (i.e. room temperature, some humidity). Loose materials were spread in a thin layer on pans and sat on laboratory workspaces such as countertops. Generally, fans were placed next to pans to generate air flow over the samples.

#### 4.4.3.5 Outdoors

Outdoor (OD) curing was used in this report as an approximation of field curing conditions. Specimens were placed outdoors near the MSU laboratory in an area located between two buildings which received sunlight a few hours per day. Figure 4.9 provides two photographs of specimens during outdoor curing.

Specimens were cured fully-supported (e.g. on oven shelves or expanded metal racks) on wooden or plastic pallets and were exposed to sunlight but not rain. At night or when raining, pallets were stored close to one of the buildings under an overhead awning. Pallets were moved away from the building during the day to receive sunlight. At the end of the day or when rainfall started (whichever came first), pallets were moved under the awning again.

Two rounds of outdoor curing, both lasting 14 days, were conducted in this study. The first, denoted $OD_1$, was from September 1, 2014 to September 15, 2014, and the second, denoted $OD_2$, was from June 22, 2015 to July 6, 2015. Table 4.1 provides a summary of weather data from both OD curing rounds. $OD_2$ timing was coordinated so that weather conditions were relatively similar to that of $OD_1$.


**Figure 4.9. Outdoor Curing**

**Table 4.1. Outdoor Curing Weather Data Summary**

| | | | **$OD_1$** | | **$OD_2$** | |
|---|---|---|---|---|---|---|
| **Variable** | | | Weather Station (3.6 mi WSW) | Omega HH314A (Ambient) | Weather Station (3.6 mi WSW) | Omega HH314A (Ambient) |
| Daily Temp (°C) | Avg | Mean | 24.5 | 27.8 | 24.9 | 27.3 |
| | | St. Dev. | 2.2 | 0.8 | 1.9 | 3.2 |
| | High | Mean | 30.6 | 38.8 | 30.1 | 37.2 |
| | | St. Dev. | 3.0 | 5.5 | 3.0 | 9.2 |
| | Low | Mean | 19.6 | 23.4 | 20.2 | 22.7 |
| | | St. Dev. | 2.0 | 0.8 | 1.8 | 1.9 |
| Daily Relative Humidity (%) | Avg | Mean | 79.6 | 67.5 | 81.1 | 83.9 |
| | | St. Dev. | 4.5 | 6.1 | 4.7 | 12.7 |
| | High | Mean | 99.2 | 84.7 | 99.6 | 98.0 |
| | | St. Dev. | 2.1 | 3.7 | 1.6 | 3.9 |
| | Low | Mean | 52.4 | 48.0 | 57.8 | 51.3 |
| | | St. Dev. | 9.7 | 11.8 | 9.6 | 28.1 |
| Daily Wind Speed (mph) | Avg | Mean | 2.4 | --- | 2.4 | --- |
| | | St. Dev. | 1.3 | --- | 0.8 | --- |
| | High | Mean | 8.7 | --- | 9.0 | --- |
| | | St. Dev. | 2.4 | --- | 2.6 | --- |
| | Low | Mean | 0.5 | --- | 0.5 | --- |
| | | St. Dev. | 0.0 | --- | 0.0 | --- |
| Total Precipitation (cm) | | | 0.79 | --- | 12.42 | --- |

*-- Parentheses indicate data measurement locations for each data source. Weather station locations are in reference to test site locations (nearest available weather station data is reported).*

*-- Omega HH314A data recorded at 30-minute intervals adjacent to curing specimens.*

*-- For $OD_1$, Omega HH314A temperatures were average of the onboard temperature probe and an additional K-type thermocouple.*

*-- Omega HH314A data was not available for some days due to device malfunctions. All available data is reported, and data was only considered available if data was available for the entire day.*

### 4.4.4 CIR Density Measurement

#### 4.4.4.1 Maximum Specific Gravity

Maximum specific gravity ($G_{mm}$) was measured on RAP or CIR materials using either AASHTO T209 (Rice gravity) or ASTM D6857 (vacuum sealing method using the CoreLok® device). Figures 4.10a and 4.10b show typical T209 and D6857 equipment, respectively. RAP $G_{mm}$ samples were batched from individual size fractions, dry-mixed to a uniform state, then tested. CIR $G_{mm}$ samples were batched and mixed as in Section 4.4.1, cured according to Section 4.4.3.4, then tested. Most CIR $G_{mm}$ samples were cured 3 to 7 days so that samples were air dry; some samples were cured for specific periods of time (e.g. 28 days) as discussed in Chapter 10.


*a) AASHTO T209 Setup* *b) CoreLok® Device* *c) D6857 $G_{mm}$ Sample*

**Figure 4.10. $G_{mm}$ Testing Photographs**

AASHTO T209 was conducted according to specification. The supplemental dry-back procedure, also referred to as the saturated surface dry (SSD) procedure, was also conducted in some cases and is referred to as $T209_{SSD}$. This goal of this procedure is to adjust the measured $G_{mm}$ to account for any moisture that may have been absorbed into aggregate pores. It is typically used for asphalt concrete mixtures with high-absorption aggregates and was used in this case since RAP particles may have broken, or there may have been uncoated faces or microcracks in the binder film surrounding an aggregate.

ASTM D6857 was also conducted according to specification and the CoreLok operator's manual. Approximately 2,000 g of material (exact mass was recorded) was placed inside a textured vacuum sealing bag (textured side down to facilitate air removal), which was then placed inside a larger vacuum sealing bag (green bag in Figure 4.10c). All testing was performed with a vacuum dwell setting of 300 seconds, meaning the CoreLok maintained full vacuum for 300 seconds before sealing and venting.

After vacuuming, the sealed bag was submerged completely underwater and then cut open. Care was taken in cutting and opening the bag to prevent agitation and dispersion of fine particles from the bag. Material was gently kneaded to facilitate removal of any remaining entrapped air. Then, the bag was folded over and sat on the water bath scale, which was read as soon as the scale stabilized. Note that it was important to ensure that no

part of the bag, upon being fully submerged, floated above the water line as this would affect the submerged mass reading. D6857 $G_{mm}$ was calculated according to Equation 4.2.

$$G_{mm} = \frac{M_{dry}}{M_{bag} + M_{dry} - M_{sub} - \frac{M_{bag}}{0.903}} \tag{4.2}$$

Where,
$G_{mm}$ = maximum specific gravity
$M_{dry}$ = dry mass of $G_{mm}$ sample
$M_{bag}$ = dry mass of vacuum sealing bags
$M_{sub}$ = submerged mass of $G_{mm}$ sample and vacuum sealing bags

Chapter 10 of this report investigates CIR density measurement approaches and develops an equation (Equation 4.3) for calculating CIR $G_{mm}$ from D6857-measured RAP $G_{mm}$ and known CIR stabilization additive dosages and specific gravities. Development and validation of this equation is discussed in Chapter 10; however, Equation 4.3 was used throughout this study to determine CIR $G_{mm}$. Unless specifically stated otherwise, all $V_a$ values reported herein were calculated using Equation 4.3 $G_{mm}$ as the reference density.

$$G_{mm,CIR} = \frac{1 + \left[P_{cm} + w_{NE/cm}P_{cm}\right] + P_{HL} + P_{Em}P_{Res}}{\frac{1}{G_{mm,RAP}} + \left[\frac{P_{cm}}{G_{cm}} + \frac{w_{NE/cm}P_{cm}}{G_w}\right] + \frac{P_{HL}}{G_{HL}} + \frac{P_{Em}P_{Res}}{G_b}} \tag{4.3}$$

Where,
$G_{mm,CIR}$ = estimated maximum specific gravity for the CIR mixture
$P_{cm}$ = percent of cement by mass of RAP
$w_{NE/cm}$ = non-evaporable water-cement ratio
$P_{HL}$ = percent of hydrated lime by mass of RAP
$P_{Em}$ = percent of emulsion by mass of RAP
$P_{Res}$ = percent of asphalt residue by mass of emulsion
$G_{mm,RAP}$ = D6857 maximum specific gravity of RAP
$G_{cm}$ = specific gravity of portland cement
$G_w$ = specific gravity of water = 0.997 g/cm$^3$ at 25 °C
$G_{HL}$ = specific gravity of hydrated lime
$G_b$ = specific gravity of asphalt binder

#### 4.4.4.2 Bulk Specific Gravity

Four methods were used throughout this report to measure CIR bulk specific gravity ($G_{mb}$). First, AASHTO T166 (SSD method) was used in Chapter 7 to measure $G_{mb}$ according to traditional DOT design methods as shown in Table 2.2. T166 was followed with the one exception that specimens were submerged for 1 minute, rather than 4 ± 1 minutes, before recording submerged mass. This deviation is commonly specified in DOT design methods.

Second, AASHTO T269 (dimensional measurement method) was used to obtain $G_{mb}$ for nearly all specimens tested. Specimen heights were measured using calipers as shown in Figure 4.11. Specimen diameters were nominally taken as the diameter of a specimen's corresponding compaction mold (e.g. 100 mm). $G_{mb}$ was calculated using mass and caliper dimensions, which were obtained immediately after compaction or after curing. In either case, that $G_{mb}$ was taken as a wet $G_{mb}$ ($G_{mb,wet}$); dry $G_{mb}$ (simply referred to as $G_{mb}$) was calculated using specimen moisture content. Moisture contents (*MC*s) were determined several ways which are described at the end of this section.

**Figure 4.11. Caliper Dimensional Measurements**

Third, AASHTO T331 (CoreLok® vacuum sealing) was used to obtain $G_{mb}$ for nearly all specimens tested. Normal T331 test protocols were followed. However, specimens generally still contained some moisture from curing when T331 was performed; therefore, $G_{mb,wet}$ was measured rather than $G_{mb}$. As with T269, *MC* (discussed at the end of this section) was used to calculate $G_{mb}$.

During exploratory phases early in the study, concerns were raised that T331 vacuum sealing would draw water out of considerably moist specimens (e.g. those that had been in the curing room) and would affect volume measurement of the specimen when submerged in the water bath (i.e. add additional volume). A small experiment was conducted with twelve R3(A/R)-4.4 specimens to investigate this issue.

Specimens which had been cured in the curing room were selected since there was excess surface moisture, which would present the worst case scenario with respect to accurate vacuum sealing density measurements. Six specimens were tested for *MC* after curing, which was slightly greater than 7% on average.

Three specimens were tested via T331, dried in the CoreDry® device for 28 cycles, retested via T331, and then tested for *MC*. Final *MC* was 5.1% on average after this testing sequence; however, most moisture remaining was internal as specimen surfaces were relatively dry after 28 CoreDry cycles. $G_{mb,wet}$ was calculated for each T331 test; specimen volume was calculated by dividing dry mass and $G_{mb,wet}$. Changes in specimen volume were insignificant, likely caused by T331 variability or the process of handling and retesting a single specimen (e.g. particles being knocked off the specimen). If $G_{mb}$ was calculated by dividing dry mass by specimen volume for both volumes measured (i.e. pre-CoreDry and post-CoreDry), the maximum change in $G_{mb}$ for any of the three specimens tested was 0.002 g/cm$^3$, which would translate to less than 0.1% change in $V_a$.

The last three specimens were tested similarly to those in the previous paragraph except T331 was conducted after every 7 cycles in the CoreDry (28 cycles were still conducted in all). Five T331 tests were performed on each specimen. As in the previous paragraph, $G_{mb,wet}$ and specimen volume were calculated, then $G_{mb}$ was calculated using dry mass. The range of the five $G_{mb}$ values calculated per specimen was from 0.005 to 0.006 g/cm$^3$, depending on the specimen, which would translate to an 0.3% range in $V_a$. This degree of repeatability when considering all factors at play (e.g. test repeatability, changing *MC*, potential particle loss between tests due to handling) is extremely manageable for CIR.

In the fourth CIR density measurement method, dimensional measurements were used in conjunction with a T331 adjustment equation to calculate T331-based $V_a$'s for LAC slabs. Slab width, length, thickness, mass, and *MC* (a 2.5 cm slice was removed from LAC slabs when mass and dimensions were recorded in order to obtain *MC*) were measured and used to calculate slab dry bulk density ($D_{b\text{-}s}$). Equation 4.4 was used to calculate slab $V_a$ on a T331 basis (Doyle and Howard, 2014).

$$V_{a-s} = 89\left(1 - \frac{D_{b-s}}{G_{mm}}\right) \tag{4.4}$$

Where,
$V_{a\text{-}s}$ = LAC slab $V_a$ by T331 basis
$D_{b\text{-}s}$ = bulk density of LAC slab (dry mass divided by calculated volume)
$G_{mm}$ = mixture maximum specific gravity

Moisture contents for converting $G_{mb,wet}$ to $G_{mb}$ were determined in several ways throughout this report. Some specimens were broken up immediately after compaction and *MC* was measured on the entire specimen via 110 °C overnight oven drying. Some were tested immediately after density measurements (and curing and cool-down) and then broken up for *MC* measurement; this occurred in many cases where the prescribed test was quick and at room temperature (e.g. unconfined compression test). Predominantly, *MC* was measured on a small set of representative specimens and used to develop *MC* plots as shown in Figure 4.12. This was deemed reasonable since *MC* was generally very low after curing (with the exception of CR curing), especially for humid oven curing which was the predominant curing protocol used in this study. Hereafter, directly measured *MC* is denoted $MC_M$, while *MC* estimated from plots such as Figure 4.12 is denoted $MC_E$.

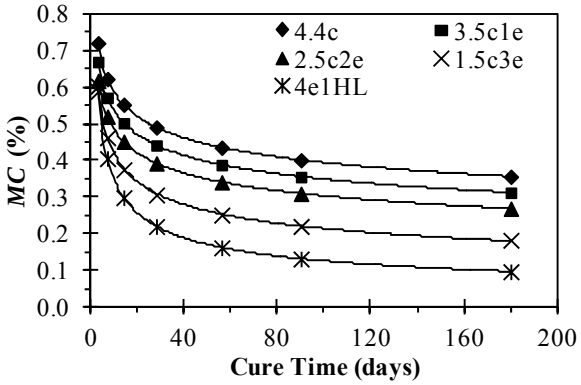


**Figure 4.12. R1(A/R) *MC* with Time after Humid Oven Curing**

The majority of $MC_E$ values estimated in this report used Figure 4.12. Power fit trendlines were developed for R1(A/R) with 4.4c, 2.5c2e, and 4e1HL binder combinations using humid oven data at 3, 7, and 14 days. Trends were extrapolated to other cure times and were interpolated for additional binder blends (e.g. 3.5c1e). $MC_E$ for other SCB blends (e.g. 3.5c) was taken to be the same as for 4.4c or 4e1HL blends, whichever was appropriate.

## 4.5 Test Methods

### 4.5.1 Marshall Stability Testing

Marshall stability (*MS*) testing was conducted largely in accordance with ASTM D6927, which replaced the commonly referenced ASTM D1559 (withdrawn in 1998). D6927 requires that specimens be oven conditioned for 2 hours prior to testing. Specimens (100 mm diameter) were removed from conditioning, placed in the Marshall breaking head, and loaded at 50 mm/min to maximum load. The elapsed time between removal from conditioning and maximum load application must be 30 seconds or less. Stability correction factors are applied to specimens with thicknesses other than 63.5 mm.

The Marshall loading frame used in this report is shown in Figure 4.13a. A 44.5 kN load cell and 50 mm stroke linear variable displacement transducer (LVDT) were used in conjunction with a Humboldt HM-2325A data logger to record load (stability) and displacement (flow). An Excel template was built to analyze stability data according to D6927 where stability and flow were taken at the point on the load-displacement curve which was shifted 6 flow units (1.5 mm) off the best tangent line. Figure 4.13b illustrates an example of this tangent offset analysis approach. *MS* by the tangent offset method was, on average, approximately 99% and 91% of the maximum *MS* for asphalt concrete and CIR testing in this report, respectively.

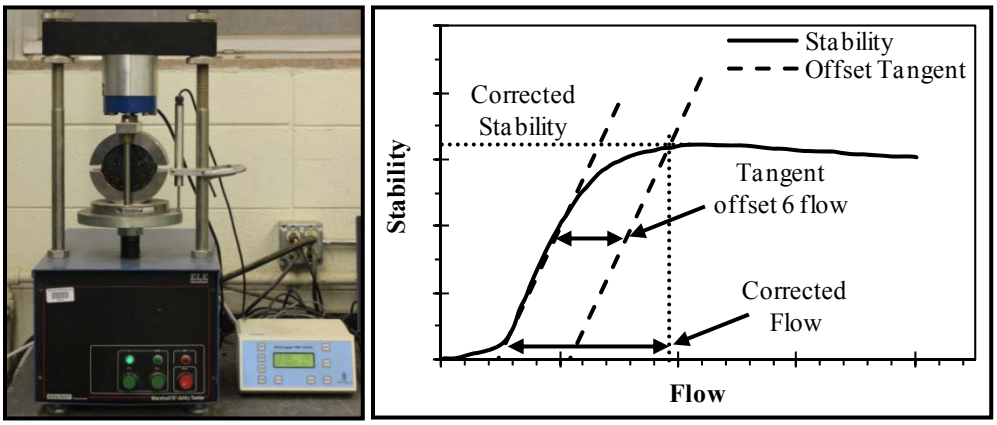


*a) Marshall Load Frame* *b) Illustration of Marshall Data Analysis (CIR Shown)*

**Figure 4.13. Marshall Stability Testing**

Asphalt concrete specimens were tested according to D6927, which requires oven conditioning at 60 °C. CIR specimens were tested similarly except oven conditioning was conducted at 40 °C according to typical DOT design methods (Table 2.2). The targeted minimum *MS* for CIR in this study was 5.56 kN (1,250 lbs). There were no target *MS* values for asphalt concrete as this data was used primarily as a reference for CIR.

Some specimens were tested for retained Marshall stability (*RMS*); with the exception of conditioning, these were tested and analyzed as described previously for *MS*. Specimens conditioned for *RMS* were vacuum saturated (following T283 protocols) to 55 to 75% saturation, soaked in a 25 °C water bath for 23 hours, and soaked in a 40 °C water bath for the 24$^{th}$ hour to bring specimens to test temperature. *RMS* was reported as a percentage of *MS* where 70% *RMS* was the targeted minimum *RMS* in this study. A few specimens were also tested which were placed in the 40 °C water bath for only 30 minutes before testing to investigate any differences between the two conditioning methods since some Table 2.2 states specify 30, rather than 60, minutes. No meaningful differences were observed; therefore, *RMS* testing in this report utilized the 60 minute protocol.

### 4.5.2 Unconfined Compression Testing

Unconfined compression (UC) testing was conducted in general accordance with ASTM D1633 and MT-26. Height to diameter (h/d) ratio was nominally 1.15:1 or 2:1. D1633 allows 2:1 ratio UC strength (UCS) to be converted to a 1.15:1 ratio equivalent by multiplying by 1.10, and vice versa by dividing by 1.10. Specific h/d ratios are provided in results chapters wherever UC results are presented. Actual h/d ratios varied slightly from nominal h/d ratios in some cases (e.g. field cores).

Figure 4.14 shows the two UC test frames used in this study. Most UC testing was on 100 mm diameter specimens and was conducted on the 44.5 kN capacity load frame (Figure 4.14a) at a standard load rate of 1.27 mm/min (0.05 in/min). Some 150 mm diameter specimens were tested and required a larger capacity load frame. The 100 kN capacity load frame shown in Figure 4.14 was used in these cases. The minimum load rate of the Figure 4.14 load frame was 5.08 mm/min (0.20 in/min). This load rate was used, and a paired experiment was conducted on a small set of specimens which determined the 100 kN load frame at 5.08 mm/min yielded, on average, UCS values 1.25 times that of the 44.5 kN load frame at 1.27 mm/min (data presented in Chapter 11).

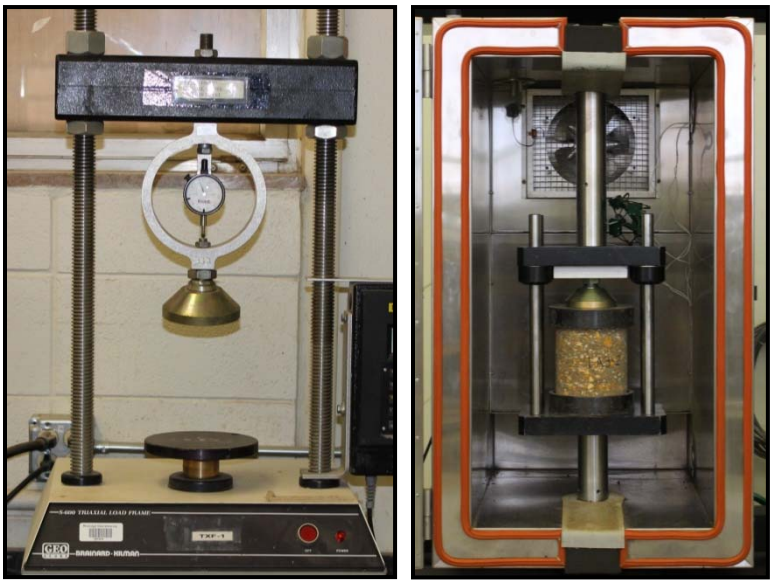

*a) 44.5 kN Capacity Load Frame* *b) 100 kN Capacity Load Frame*

**Figure 4.14. Unconfined Compression Test Setup**

### 4.5.3 Indirect Tensile Testing (Non-Instrumented)

Indirect tensile (IDT) testing in this section refers to non-instrumented IDT testing, in contrast to instrumented IDT testing discussed in Section 4.5.11. Testing was performed in accordance with loading procedures in AASHTO T283 with either the Marshall load frame (Figure 4.13a) or the 100 kN load frame (Figure 4.14b) in which an IDT breaking head was used in place of Marshall stability or UC breaking heads. Tests were conducted at 25 °C and a 50 mm/min load rate. Most non-instrumented IDT testing was on 100 mm diameter specimens, though some 150 mm diameter specimens were also tested (generally field cores).

### 4.5.4 Cantabro Testing

Cantabro testing was considered in this study for relative durability characterization of CIR mixtures. Cantabro testing was conducted in an LA Abrasion drum absent the charge of steel spheres for 300 revolutions at a specimen temperature of 25 ± 1 °C. Specimen mass was recorded before and after testing to calculate percent mass loss ($M_L$) according to Equation 4.5. Figure 4.15 shows several example asphalt concrete specimens.

$$M_L = \frac{M_1 - M_2}{M_1} \times 100 \tag{4.5}$$

Where,
$M_L$ = mass loss
$M_1$ = initial specimen mass (before testing)
$M_2$ = final specimen mass (after testing)

**Figure 4.15. Example Asphalt Concrete Cantabro Specimens (L: Untested, M: High $M_L$, R: Low $M_L$)**

### 4.5.5 Bending Beam Rheometer Testing

Bending beam rheometer (BBR) testing of mixture beams, in contrast to asphalt binder beams, is a fairly recent development but has been successfully documented. The feasibility of BBR testing of CIR mixture beams was explored in this study. Typically beams are sawn from 150 mm diameter specimens as illustrated with asphalt concrete in Figures 4.16a and 4.16b.


*a) Asphalt Concrete Slices* *b) Asphalt Concrete Beam* *c) CIR Slice & Broken Beam*

**Figure 4.16. Example BBR Specimen Preparation for Asphalt Concrete and CIR**

Full description of BBR beam preparation can be found in Howard et al. (2013b). Vertical saw cuts are first used to produce nominal 12 mm wide slices from 150 mm diameter specimens (Figure 4.16a). Then, slices are turned on their side and additional saw cuts (horizontal cuts with respect to original orientation) are used to produce nominal 7 mm thick beams. Attempts to saw CIR beams in this study were always unsuccessful. Vertical saw cuts were extremely difficult and usually unsuccessful, and horizontal saw cuts were always unsuccessful (Figure 4.16c).

### 4.5.6 Hamburg Loaded Wheel Testing

Hamburg Loaded Wheel Testing (HLWT) was conducted in accordance with AASHTO T324. Hamburg tests were performed in MSU's Asphalt Pavement Analyzer (shown in Figure 4.19 in Section 4.5.8), which can be configured with steel wheels required for Hamburg testing. Tests were conducted to 20,000 passes (i.e. 10,000 cycles) at a 50 °C test temperature (specimens were submerged in 50 °C water) with a wheel load of 705 N applied directly to test specimen surfaces. Specimens were 63 mm tall. Figure 4.17 shows example tested CIR specimens.

*a) Cement SCB* *b) Cement-Emulsion MCB* *c) Emulsion SCB*

**Figure 4.17. Example Tested CIR Hamburg Specimens**

### 4.5.7 Loaded Wheel Fatigue Testing

Fatigue specimens were sawn from slabs produced in the LAC. Sawn beam dimensions were nominally 29 by 12.5 by 7.6 cm. Tests were conducted in the APA with solid steel wheels directly contacting beam surfaces at loads of either 445 N or 1100 N. Beams were simply supported (i.e. supported on either end but not in the middle) and were tested at 20 °C with 1 cycle per second for 50,000 cycles (100,000 passes). The number of cycles to failure was reported with failure being defined as 1 mm change in deflection occurring in one pass. Example fatigue beams are shown in Figure 4.18.

*a) Untested Asphalt Concrete* *b) Tested CIR – Cement SCB* *c) Tested CIR – Emulsion SCB*

**Figure 4.18. Example Loaded Wheel Fatigue Beams**

### 4.5.8 Asphalt Pavement Analyzer Testing

Asphalt Pavement Analyzer (APA) testing was conducted according to AASHTO T340 using the APA equipment shown in Figure 4.19. Tests were conducted to 8,000 cycles (16,000 passes) at 64 °C. Vertical loads of 445 N were applied to rubber hoses which contacted specimen surfaces and were pressurized to 690 kPa. Specimens were generally 75 mm thick; specimens between 50 and 75 mm thick were grouted with Plaster of Paris in order to conform to APA molds as per T340. Thicknesses less than 75 mm were sometimes encountered with field cores. Rut depth ($RD_{APA}$) at 8,000 cycles was the primary result reported in this study. Figure 4.20 shows example tested CIR specimens.

**Figure 4.19. Asphalt Pavement Analyzer**

*a) Cement SCB* *b) Cement-Emulsion MCB* *c) Emulsion SCB*

**Figure 4.20. Example Tested CIR APA Specimens**

### 4.5.9 PURWheel Testing

Key PURWheel (PW) components are shown in Figure 4.21. Two independent loaded wheel carriages mounted with pneumatic rubber tires track LAC slabs 20,000 passes

(10,000 cycles) per test. Note that some CIR slabs were exposed to multiple tests (i.e. tracked more than 20,000 passes). Standard PW parameters are 862 kPa tire pressure, 1750 N wheel load, and 33 ± 2 cm/sec wheel speed. PW test specimens were LAC slabs that had been sawn in half (one half tested in one PW track). Note that CIR slabs were approximately 2.5 cm narrower than asphalt concrete slabs since a 2.5 cm slice was sawn off CIR slabs for *MC* measurement as discussed in Section 4.4.4.2; this should not have affected test results.

Figure 4.21b shows one wheel carriage and its tire print which results in contact pressures of approximately 630 kPa (gross) and 850 kPa (net) at the beginning of a test. Most testing was conducted at the standard PW load (1750 N); however, some CIR testing also investigated 50% and 80% test loads.

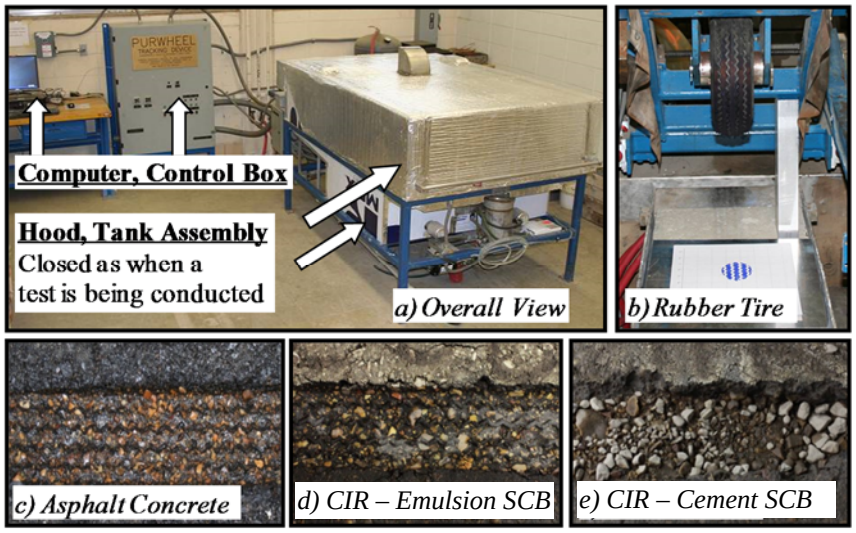


**Figure 4.21. PURWheel Photographs**

PW testing was conducted wet at 64 °C (i.e. submerged in 64 °C water). Wet PW ($PW_{wet}$) tests were conducted herein to evaluate wheel tracking in the presence of moisture. Except for AC1 and AC2 testing (Chapter 6), dry PW ($PW_{dry}$) testing was not utilized since it correlates reasonably well with the APA (Doyle and Howard 2013a).

Figures 4.21c to 4.21e show distresses for various representative mixtures after wet PW testing. The number of passes to 12.5 mm of rutting ($P_{12.5}$) was the primary test result reported. Note that moisture damage mechanisms likely differ between emulsion CIR and cement CIR. Emulsion CIR damage mechanisms are similar to that of asphalt concrete (i.e. stripping, non-stripping moisture damage, densification, mixture shear failure); whereas, cement CIR damage mechanisms are likely more related to pore pressure stresses caused when saturated specimens are loaded.

### 4.5.10 Permeability Testing

Permeability was measured on LAC slabs (sawn in half) immediately prior to conducting PW tests. Testing was conducted with the MSP-$L_L$ permeameter (i.e. large laboratory configuration of the Mississippi permeameter system) which is described in Volume 3 of the State Study 250 report alongside full test protocol details. Essentially, a

standpipe (Figure 4.22a) is sealed to the test surface (CIR slab in this case) via a neoprene gasket and a 445 N surcharge load.

The standpipe is filled with water to a mark at 25.4 cm of head, and the test is initiated. The time is recorded for the water to fall 12.7 cm to a lower mark, or the fall distance is recorded at 300 seconds, whichever comes first. Infiltration (*Inf*) was calculated and reported as in Equation 4.6.

Three successive replicates were performed one after another at each test location, and the results were averaged to form one test result. In nearly all cases, permeability decreased with each successive replicates; therefore, in cases where permeability was exceptionally low for the first replicate, the final two replicates were not conducted. Where pavements were impermeable, the final two replicates were not conducted. CIR slabs (half LAC slabs) were tested in three test locations on the top surface and three test locations on the bottom surface. Figure 4.22b illustrates testing of a fairly permeable CIR slab.

$$Inf = \frac{a}{At}(h_1 - h_2) \tag{4.6}$$

Where,
*Inf* = infiltration rate (cm/min)
$a$ = inside cross-sectional area of permeameter standpipe ($cm^2$)
$A$ = cross-sectional contact area ($cm^2$)
$t$ = elapsed time between $h_1$ and $h_2$ (min)
$h_1$ = initial head across the test specimen (cm)
$h_2$ = final head across the test specimen (cm)

*a) MSP Standpipe* *b) MSP-$L_L$ Testing of CIR Slab*

**Figure 4.22. Permeability Testing Photographs**

### 4.5.11 Instrumented Indirect Tensile Testing

Three tests were conducted in the instrumented IDT configuration: resilient modulus, creep compliance, and tensile strength with fracture energy. In some cases, only one or two of these three tests were conducted on a given specimen; in other cases, all three tests were conducted. When more than one of the three tests were conducted, they were conducted in the order presented in this section. All tests were conducted in an Interlaken Technology Corporation servo-hydraulic universal testing machine with an environmental chamber

(further denoted UTM) shown in Figure 4.23a. Note that the UTM used is also that shown in Figure 4.14b. Figure 4.23b shows the instrumented IDT configuration for a typical CIR specimen with four Epsilon 3910 extensometers (LVDTs) magnetically attached to steel gage points on both faces (one vertical and one horizontal LVDT per face). Details regarding specimen preparation and instrumentation are presented in the following subsection.

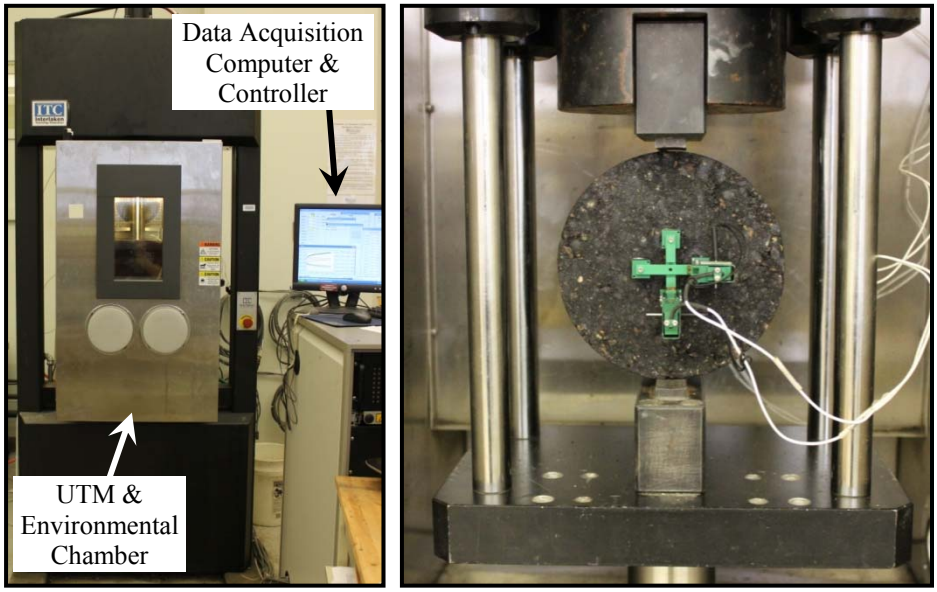


*a) Overall View* *b) Instrumented IDT Configuration*

**Figure 4.23. Interlaken UTM Configured for Instrumented IDT Testing**

#### 4.5.11.1 Specimen Preparation and Instrumentation

Preparation procedures for instrumented IDT specimens typically include sawing thin slices off either side of a 150 mm diameter specimen to achieve smooth faces on which gage points, and later LVDTs, can be mounted. Typical procedures were followed for asphalt concrete specimens, the specifics of which closely followed recommendations from the University of Florida. For SGC compacted asphalt concrete specimens, a 12.5 mm slice was sawn from the top of 63 mm tall specimens, and then the test specimen was sliced from the center of the original SGC specimen with a target thickness of 31 mm. After accounting for saw blade thickness, this left an approximately 12.5 mm slice at the bottom of the specimen. Field asphalt concrete cores were sliced to a target 31 mm thickness cut from the center of the core when possible.

Sawing of CIR specimens to produce smooth faces was prohibited by most binder combinations tested (similar to Section 4.5.5 BBR sawing attempts). Therefore, an alternate preparation procedure was developed for CIR specimens. Specimens were still compacted to 63 mm tall; the full specimen was ultimately tested (as opposed to the center 31 mm).

Since CIR specimens were not sawn, smooth faces for gage point mounting were not obtained; instead a high-speed drill press (Dremel 400 XPR set on speed 9 of 10) and a 16 mm diameter grinding stone attachment were used to polish mounting surfaces to which gage points were glued. Figure 4.24 shows the drill press used alongside an example CIR specimen with polished mounting points. Note additional steps were eventually adopted to CIR mounting point preparation procedures and are described in subsequent paragraphs.

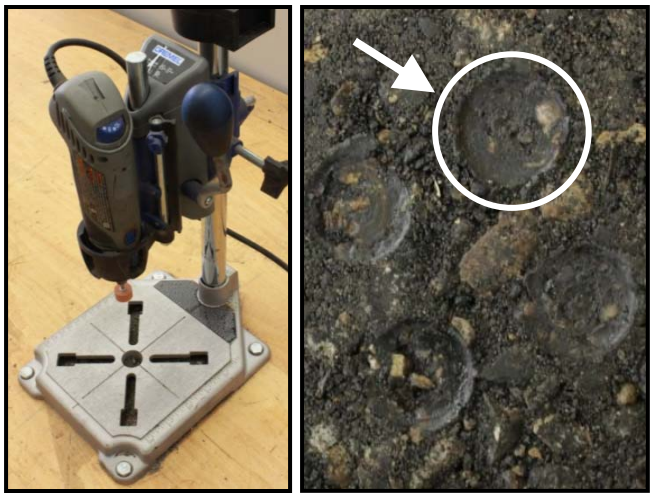

*a) Dremel and Drill Press* *b) Polished Mounting Points*

**Figure 4.24. CIR Gage Point Mounting Surface Polishing**

Gage points were nominally 6 mm tall and 8 mm diameter and were glued to specimens using the jig shown in Figure 4.25a. Multiple rapid-set two-part epoxies were tested at the beginning of this study to determine the most suitable epoxy for this purpose. Devcon 5 Minute Epoxy Gel exhibited the most favorable characteristics in terms of set time, strength, and consistency and was ultimately selected. It has the following properties: 17.2 MPa (2500 psi) strength, 5 minute handling time, 10 minute set time, and 1 hour cure time. Gage points were glued with a 38 mm gage length (one-fourth the diameter) to sliced asphalt concrete specimens with smooth faces (Figure 4.25b) or CIR specimens with polished mounting surfaces (Figure 4.25c). Specimens were given 15 minutes in the jig for epoxy to firmly set before being removed.

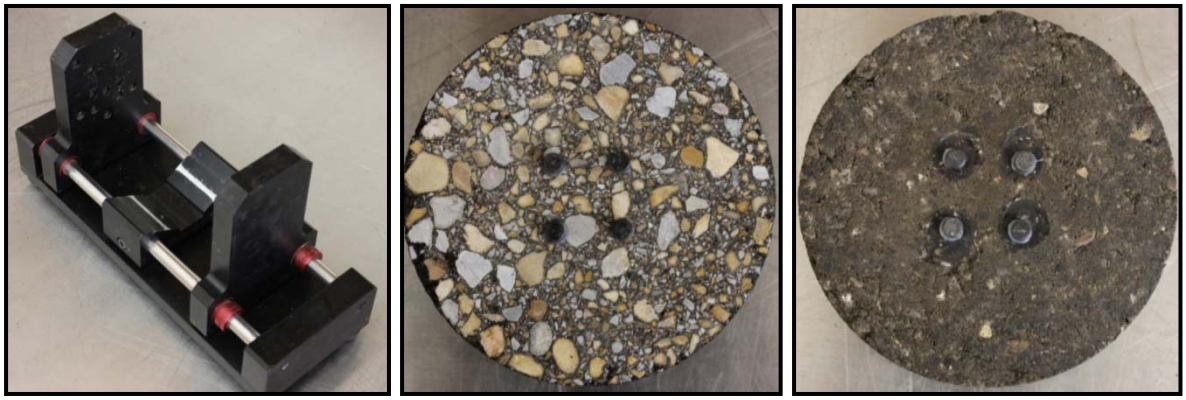

*a) Gage Point Gluing Jig* *b) Prepared Asphalt Concrete* *c) Prepared CIR*

**Figure 4.25. Gage Point Mounting**

As previously mentioned, additional preparation steps were later adopted for CIR specimens. The reason for this is that it was common for gage points to be easily dislodged due to CIR particles flaking off the surface, especially with cement-dominated binder blends. This generally occurred when LVDTs were being attached for testing, which was after the 2 to 4 hour temperature-conditioning period. Thus, specimens would have to be taken out of

conditioning, re-glued, and re-conditioned, which significantly lengthened the time elapsed from when the specimen was removed from curing and when it was tested.

To alleviate the issue described in the previous paragraph, a series of steps were implemented. First, CIR mounting surfaces were polished similarly as before (Figure 4.24b). Loose particles with the potential for dislodging later were then brushed away, which, in the most severe cases, resulted in mounting points resembling hollowed depressions (Figure 4.26a). Epoxy was applied to these polished surfaces and thoroughly spread as to lock all remaining surface particles in place (Figure 4.26b). After a minimum of 15 minutes, the epoxy was sanded flush with the specimen face (Figures 4.26c to 4.26e), and gage points were glued as normal (Figure 4.26f). Overall, the new protocol provided a more stable base and greatly decreased the number of dislocated gage points which had to be re-glued.

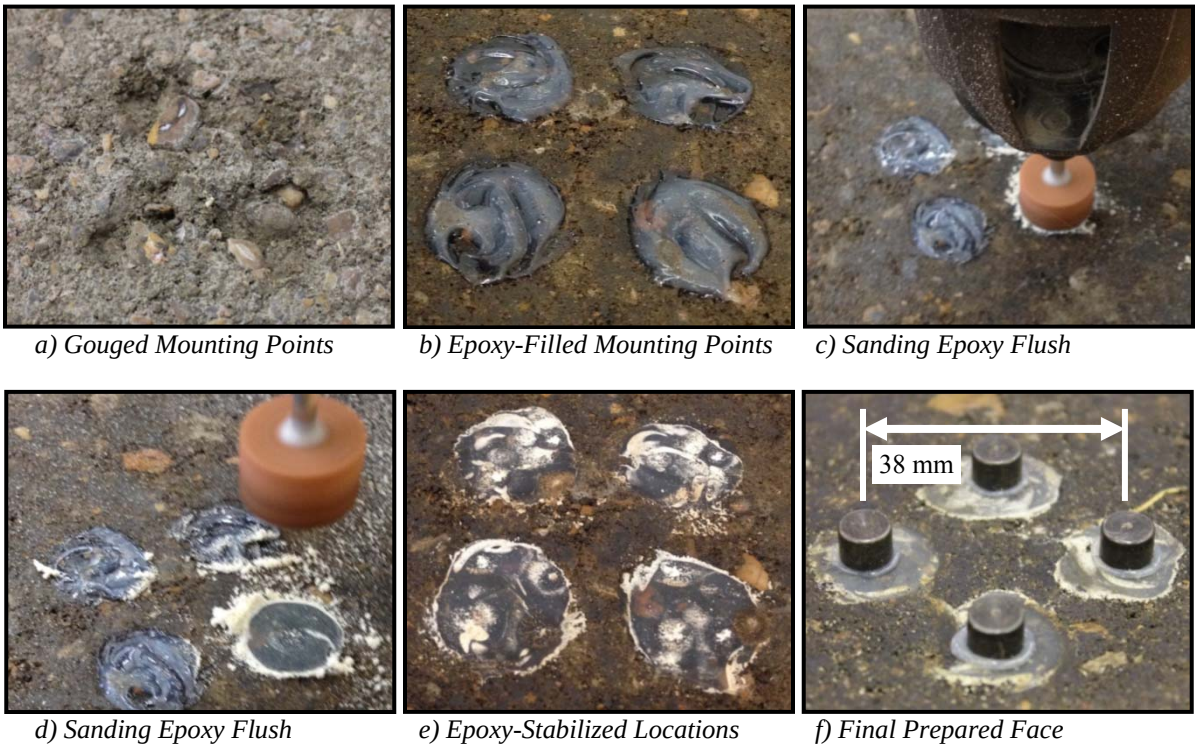


*a) Gouged Mounting Points* *b) Epoxy-Filled Mounting Points* *c) Sanding Epoxy Flush*

*d) Sanding Epoxy Flush* *e) Epoxy-Stabilized Locations* *f) Final Prepared Face*

**Figure 4.26. Additional CIR Gage Point Mounting Surface Preparation Steps**

The additional mounting surface preparation steps were implemented for all cement SCB systems and all cement-dominated MCB systems without discretion. With discretion, emulsion SCB and emulsion-dominated MCB systems were generally glued as in Figure 4.25 without conducting the steps in Figure 4.26, except for a few cases where Figure 4.26 steps were deemed useful.

It is worthwhile to mention several potential concerns with the Figure 4.26 process. Displacements and strains measured during the instrumented IDT tests presented are very small and vary through a specimen (i.e. strain at the surface of a specimen likely differs from strain at the center). Using epoxy to effectively immobilize parts of a specimen's surface (and sometimes at depths below the surface) likely affects strain measurement to some extent. While these effects are likely small to modest, they should be noted as they were not directly investigated in this study. This study focused on prevailing trends among various

CIR binder systems, which, as shown in results chapters, were extremely clear despite any effects associated with epoxy.

Prior to testing, gage-point-mounted specimens were conditioned to the corresponding test temperature. Four temperatures were used in instrumented IDT testing in this report. They were 20, 0, -10, and -20 °C, which are typical fatigue and low-temperature test temperatures for Mississippi's environment. A small experiment was conducted to determine the appropriate conditioning time for each test temperature. Results of this experiment are shown in Figure 4.27 and are discussed in the following paragraphs.

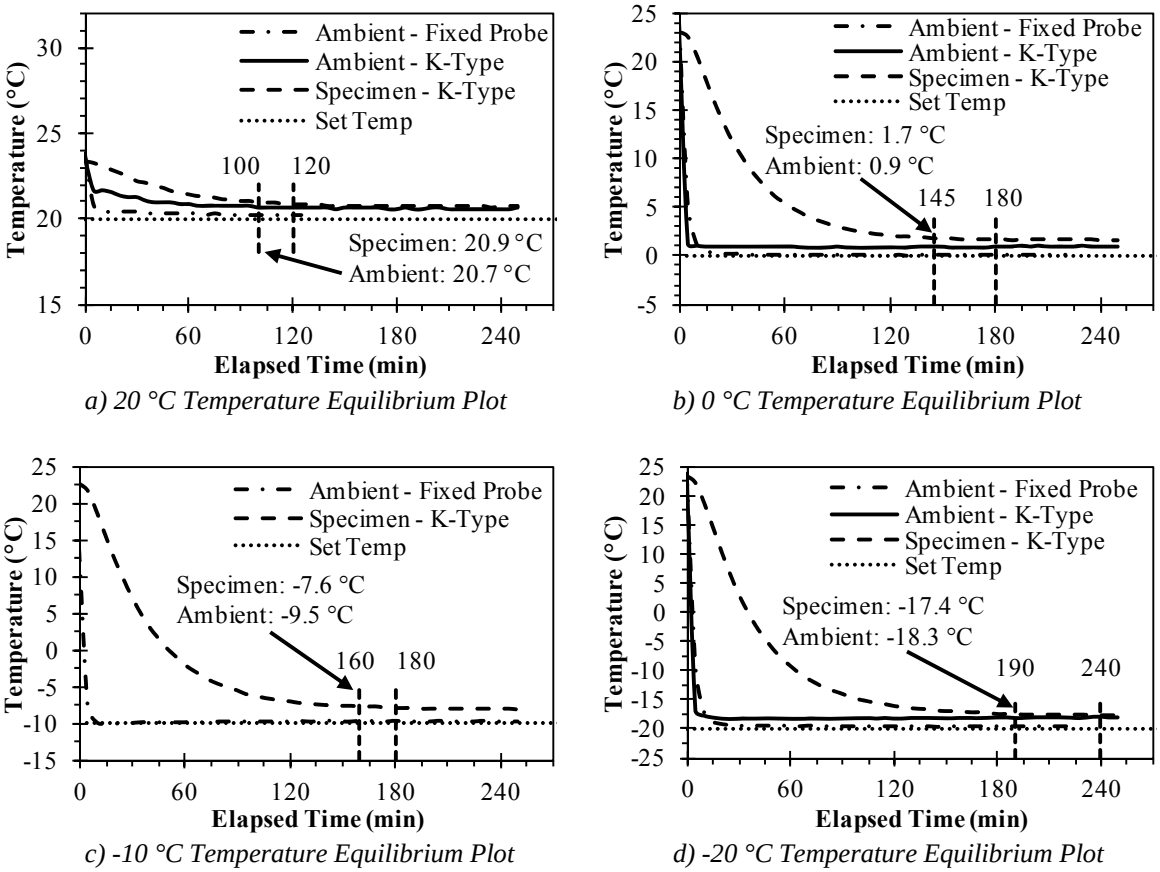


*a) 20 °C Temperature Equilibrium Plot*

*b) 0 °C Temperature Equilibrium Plot*

*c) -10 °C Temperature Equilibrium Plot*

*d) -20 °C Temperature Equilibrium Plot*

**Figure 4.27. Results of Temperature Conditioning Time Experiment**

A data logger was used to collect ambient temperature in the environmental chamber (the fixed probe of an Omega HH314A was originally used) and internal specimen temperature (a K-type thermocouple was embedded in a CIR specimen). Data logging was started within 5 seconds of placing the specimen and thermocouples in the environmental chamber. The first trial was at -10 °C (Figure 4.27c). Differences between the HH314A onboard probe and K-type temperatures were observed, which were thought to be due to differences in thermocouple type rather than the specimen not actually being at equilibrium. This was verified by adding a second ambient K-type thermocouple as shown in all other Figure 4.27 plots. The two K-type temperatures converged together but were always slightly higher (ambient temperatures differences ranged from 0.5 to 1.4 °C) than the HH314A temperature. Based on further investigation, differences between thermocouple readings and

the reported environmental chamber temperature (which was within ± 0.1 °C of the set temperature) were thought to be primarily due to thermocouple type and secondarily due to thermocouple placement in the environmental chamber. Ultimately, the slight discrepancies (e.g. 0.6 °C) were deemed inherent, but also non-meaningful, issues.

Because the K-type thermocouples read slightly high, it was not possible to use the as-reported specimen temperature by itself to determine required conditioning times. Instead, the derivative, or slope, was calculated for the specimen temperature curve on 5 minute intervals. A limiting threshold of 0.01 °C/min change was set, and this appeared to reasonably correlate with steady state temperature. Vertical dashed markers were used in Figure 4.7 (the earliest of the two) to denote the point at which 0.01 °C/min change or less was achieved.

The later dashed markers indicate the actual conditioning times ultimately used, which were 2, 3, 3, and 4 hours for 20, 0, -10, and -20 °C, respectively. Conditioning times were extended slightly from earlier dashed markers for two main reasons. First, rounding conditioning times up to the nearest hour seemed to be a logical decision. Second, temperature conditioning experiments were conducted with only one specimen in the environmental chamber. In many cases, specimens would be placed into conditioning at approximately 15 minute intervals if they were being conditioned immediately after gage points were mounted. Extending conditioning times slightly accounted for multiple specimens being in the chamber to some extent. For 0 °C temperatures and lower, specimens were often not put into conditioning until all gage points were mounted and were then allowed to condition overnight. Once specimens were conditioned, they were tested by one or more of the test methods presented in subsequent sections.

#### 4.5.11.2 Resilient Modulus Testing

Resilient modulus ($M_r$) testing was conducted according to ASTM D7369. Total $M_r$ ($M_{r,total}$), as opposed to instantaneous $M_r$, is reported herein and is calculated using total deformations (instantaneous recoverable plus time-dependent recoverable deformations). D7369 standard test parameters require application of 100 loading cycles (data recorded over the last 5) where each cycle consists of a 0.1 sec haversine load pulse with a 0.9 sec rest at a small contact load ($P_{contact}$). D7369 requires $P_{contact}$ to be 4% of the maximum load ($P_{max}$) so long as it is between 22 and 89 N. Note that the UTM control software utilized was not able to meet this criteria; $P_{contact}$ was pre-programmed to be 10% of $P_{max}$. $M_r$ load data was collected with a 22.2 kN capacity load cell.

For all mixtures, three replicates were tested to obtain a single $M_r$ value. Specimens were tested along two axes (rotated 90° from each other), and vertical and horizontal deformations were recorded on both faces for a total of 12 $M_r$ values (3 replicates, 2 axes, 2 faces) from which a 10% trimmed average was reported. An Excel spreadsheet was developed for this study to perform $M_r$ analysis according to D7369.

#### 4.5.11.3 Creep Compliance Testing

IDT creep compliance (D(t)) testing was conducted according to AASHTO T322. Creep tests were conducted for 1,000 seconds, which is permitted by T322 but is longer than

the standard 100 second test. Test loads for a mixture were selected to produce horizontal deformations between 1.25 and 19 μm at 1,000 seconds.

Test loads were applied over a two-second ramping period and then remained constant over the test duration (1,000 seconds). Ideally, the test load would be instantaneously applied; however, this is not possible due to equipment response limitations. At optimal controller gain settings, a two-second ramping period was found to be the best balance between applying load too slowly and applying it so quickly that the load overshot the target test load by a meaningful amount. As with $M_r$ testing, load data was collected with a 22.2 kN capacity load cell. Replication was identical to $M_r$ testing except only one axis was tested, resulting in 6 individual faces.

Data was analyzed two ways. First, an Excel spreadsheet was developed to analyze creep data according to T322. Second, the Excel spreadsheet LTSTRESS.xls, developed by Christensen (1998), was used. LTSTRESS both reduces raw D(t) data and calculates a thermal stress curve for critical cracking temperature ($T_{crit}$) determination (i.e. point at which thermal stresses exceed mixture strength). It was used in this report to determine $T_{crit}$. LTSTRESS was developed to analyze 100-second tests and was modified by the authors to accommodate 1,000-second tests.

#### 4.5.11.4 Instrumented Indirect Tensile Strength and Fracture Energy Testing

Instrumented IDT tests were performed according to T322 at load rates of 50 mm/min for 20 °C tests and 12.5 mm/min for 0, -10, -20 °C tests. Ultimate IDT strength ($S_{t,ult}$), fracture IDT strength ($S_{t,f}$), and fracture energy (FE) were calculated from load and deformation measurements. Note that, in this report, $S_t$ implies $S_{t,ult}$, while fracture IDT strength is always denoted $S_{t,f}$. FE, being the area under a stress-strain curve, was calculated by numerically integrating the stress-strain curve using Simpson's trapezoidal rule.

Three replicates (six faces) were tested as one test group, similarly to $M_r$ and creep tests. For the six FE results obtained, probable outliers were removed then the highest and lowest values were trimmed as long as at least three values remained. For example, if two outliers were removed, the two extremes would not be trimmed as this would leave only two values to be averaged.

An Excel spreadsheet was developed in which all results were calculated. The point of fracture for each face was determined using the DDC approach discussed in Section 2.9.11. The desired testing outcome (defined in T322) is when the DDC is positive and peaks prior to the ultimate load (designated Case 1). The least desirable testing outcome (defined in T322) is when the DDC is never positive, in which case the test is invalid and no result is produced (designated Case 4).

The authors often observed two testing outcomes in addition to those defined in T322. First, the DDC peaked after the ultimate load occurred (designated Case 2). Since stress-strain data was plotted up to the point of fracture, or the DDC peak, Case 2 generally resulted in unrealistic stress-strain plots because stress-strain data occurring far past the peak load was plotted, yielding inflated FE values. Figure 4.28a shows a typical Case 2 stress-strain plot before correction where data beyond the peak load is included, in which case strain accumulates quickly, resulting in a much higher FE for Face 2 than Face 1. When Case 2 was encountered, the stress-strain curve was corrected by truncating at the point of ultimate load, resulting in more reasonable FE values. Case 2 was considered undesirable but manageable.

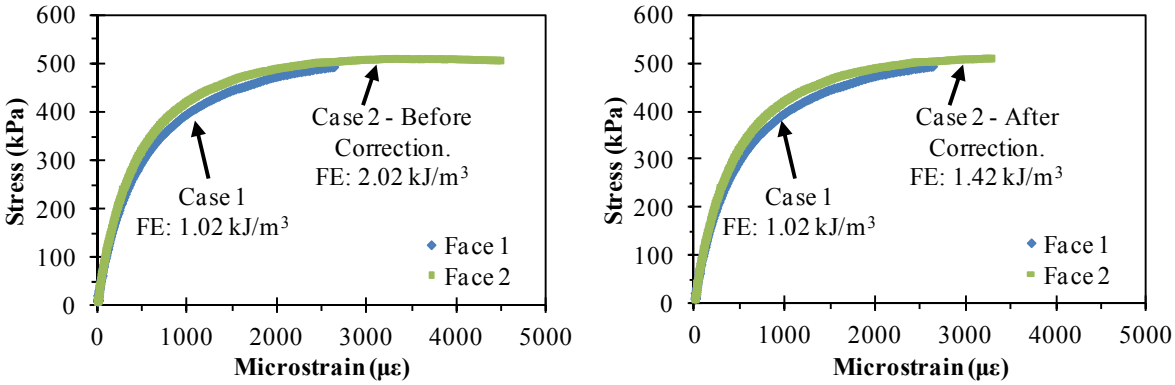


*a) Case 2 Stress-Strain Plot (Uncorrected)* *b) Case 2 Stress-Strain Plot (Corrected)*

**Figure 4.28. FE Case 2 Illustration (Emulsion SCB at 20 °C Shown)**

The other scenario encountered was slightly more complex. In some cases, strain during loading would increase, peak, and then decrease, as if the extensometer slipped (designated Case 3). This resulted in stress-strain plots which appeared to have backwards progressing strain as shown in Figure 4.29. Stress-strain curves such as this yielded negative accumulated area under the curve, which, in turn, produced negative FE values as shown.

When Case 3 was encountered, unreasonable data was removed, and the stress-strain plot was forecasted to the fracture stress using remaining deformation data. In Figure 4.29, Face 1 data up to approximately 200 με was considered reasonable and was used to forecast the stress-strain curve (gray line) to the fracture stress using regression. Since Case 3 results were expected to be less reliable, a limitation was put in place that no more than half of the final data values (after outlier removal and trimming of extremes) could be Case 3 values. If that limitation was exceeded, replacement specimens were made and tested.

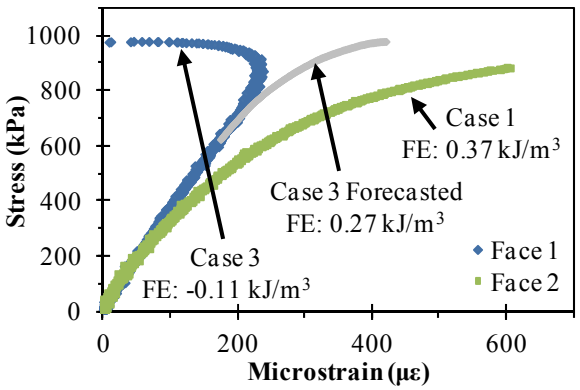


**Figure 4.29. FE Case 3 Illustration (Emulsion SCB at -10 °C Shown)**

Dissipated creep strain energy (DCSE) and energy ratio (ER) were also considered. DCSE was calculated according to Equation 2.3. ER, as calculated in Roque et al. (2004), was not appropriate for CIR because $DCSE_{min}$, one of the ER calculation inputs, was empirically developed for AC. Calculated $DCSE_{min}$ values were extremely high, were not reasonable for CIR, and would have yielded extremely low and also unreasonable ER values.

# CHAPTER 5 – EXPERIMENTAL PROGRAM - FIELD

## 5.1 Field Experimental Program Overview

Two field projects, US Highway 49 (US-49) and US Highway 45 Alt (US-45Alt), were studied in conjunction with this research. The US-49 CIR project was the larger of the two and a major component of State Study 250. The US-45Alt CIR project was used primarily in Chapter 11. This chapter provides an overview of each project, construction details, and field monitoring/testing activities.

## 5.2 US Highway 49 CIR Project

### 5.2.1 US-49 Project Overview

US-49 informally refers to MDOT Project No. NH-0008-03(032), between Flora and Yazoo City, MS that contained FDR and CIR sections and occurred during the 2010 construction season. The US 49 project was conducted on a 14.8 km (9.2 mile) section of high-traffic four-lane divided highway. At time of construction, US-49 had a traffic volume of 12,000 AADT with 14% trucks. The bid price was around $15 million; final project costs were around $16.5 million.

Two pavement structures, composite (i.e. asphalt concrete (AC) over portland cement concrete (PCC)) and full-depth AC, were present on US-49 prior to rehabilitation. The original jointed concrete slabs and full-depth AC sections were built in 1959 and 1980, respectively. Immediately prior to rehabilitation, several types of pavement distresses were present. Distresses included longitudinal cracking, potholes, transverse cracking with spalling, and rutting. Several patches existed in heavily distressed sections. The quantity and severity of distresses present, in MDOT's assessment, made US-49 a viable in-place recycling candidate since milling and overlaying was a less suitable option.

Since CIR and FDR were largely untested by MDOT prior to US-49, construction details of US-49 were documented by MDOT in Strickland (2010). Information was obtained from Strickland (2010) and other parties (e.g. MDOT engineers, consultants) and compiled herein into a summary of US-49 construction activities.

### 5.2.2 US-49 Construction Activities

#### 5.2.2.1 US-49 Construction Stages

US-49 was constructed in three stages to accommodate the removal and replacement of two northbound bridges. In stage 1, southbound lanes adjacent to the northbound bridges to be replaced were in-place recycled then overlaid with a nominal 7.6 cm base lift of 19 mm NMAS PG 76-22 AC (further denoted base mix). This was necessary to route traffic onto southbound lanes near the bridges in a head-to-head fashion, while allowing construction traffic to use northbound lanes during the bridge replacements. In stage 2, the remaining in-place recycling was conducted, which was most of the in-place recycling, and all in-place recycled material was overlaid with a nominal 7.6 cm thick lift of base mix. The two bridges were also re-constructed in stage 2. In stage 3, areas adjacent to the replaced bridges were

rebuilt with a traditional construction approach (AC over crushed stone), and a nominal 3.8 cm thick surface lift of 9.5 mm NMAS PG 76-22 AC (further denoted surface mix) was placed over the entire project.

Extended period lane closures were frequently used to facilitate construction in one lane and allow traffic in the adjacent lane. A lane under construction remained closed until in-place recycling was completed and the base mix was placed, at which point it was reopened and the other lane was closed. The only exception to this practice would have been near the bridge replacements where traffic was routed head-to-head on southbound lanes.

#### 5.2.2.2 Original and Modified US-49 Construction Plan

The original US-49 plan was to perform CIR at variable depths depending on underlying materials; 23 cm was targeted for full-depth AC sections, and 15 cm was targeted for composite sections. Northbound lanes were to be stabilized with 4% emulsion and 1% hydrated lime, while southbound lanes were to be stabilized with 4.4% cement by mass. However, during stage 2 of construction, problems were encountered in some full-depth AC areas where the existing subgrade was unable to support in-place recycling equipment.

It was decided that, in order to compensate for the insufficient subgrade strength, stabilization depths needed to increase and a supplemental agreement was developed to conduct cement-stabilized FDR instead of CIR in most full-depth HMA sections where concrete was not present. Note that some full-depth HMA sections (concrete not present) proceeded with CIR as originally planned. FDR stabilization was nominally 41 cm deep with 4.8% cement by mass; FDR construction details are provided in Volume 1 of the State Study 250 report. Strickland (2010) noted future in-place recycling efforts should conduct more extensive coring and materials testing prior to construction. Figure 5.1 shows the as-constructed layout of US-49, which was divided into six sections as discussed further in the following sections.

#### 5.2.2.3 US-49 Construction Processes

Hall Brothers Recycling & Reclamation, Inc. performed all US-49 recycling procedures. Figure 5.2 provides photographs of major CIR construction processes. First (not shown in Figure 5.2), the top 7.6 cm of existing asphalt pavement was milled and taken off site to establish a uniform grade. Second, hydraulic binders (cement or hydrated lime) were spread onto the milled surface with an auger system (Figure 5.2b). Next, a Caterpillar PR-1000 cold planing unit pulverized and reclaimed the existing pavement to 15 or 23 cm (Figure 5.2c). Reclaimed material was conveyed to a screening and crushing unit (Figure 5.2d) which fed into a pugmill (Figure 5.2e). Emulsion was stored in a tank and, where needed, was metered into the pugmill and mixed with reclaimed material.

The pugmill deposited material into a windrow which was smoothed with a Caterpillar 140H motor grader (Figure 5.2f). Smoothed material was compacted with a Rex® 3-70A compactor with steel wheels fitted with rectangular steel pads (Figure 5.2g). The 140H motor grader then smoothed the material a second time, and final compaction was performed with a Caterpillar CB-634D vibratory steel wheel roller (Figure 5.2h). For full pay, 97% of standard Proctor density was required.

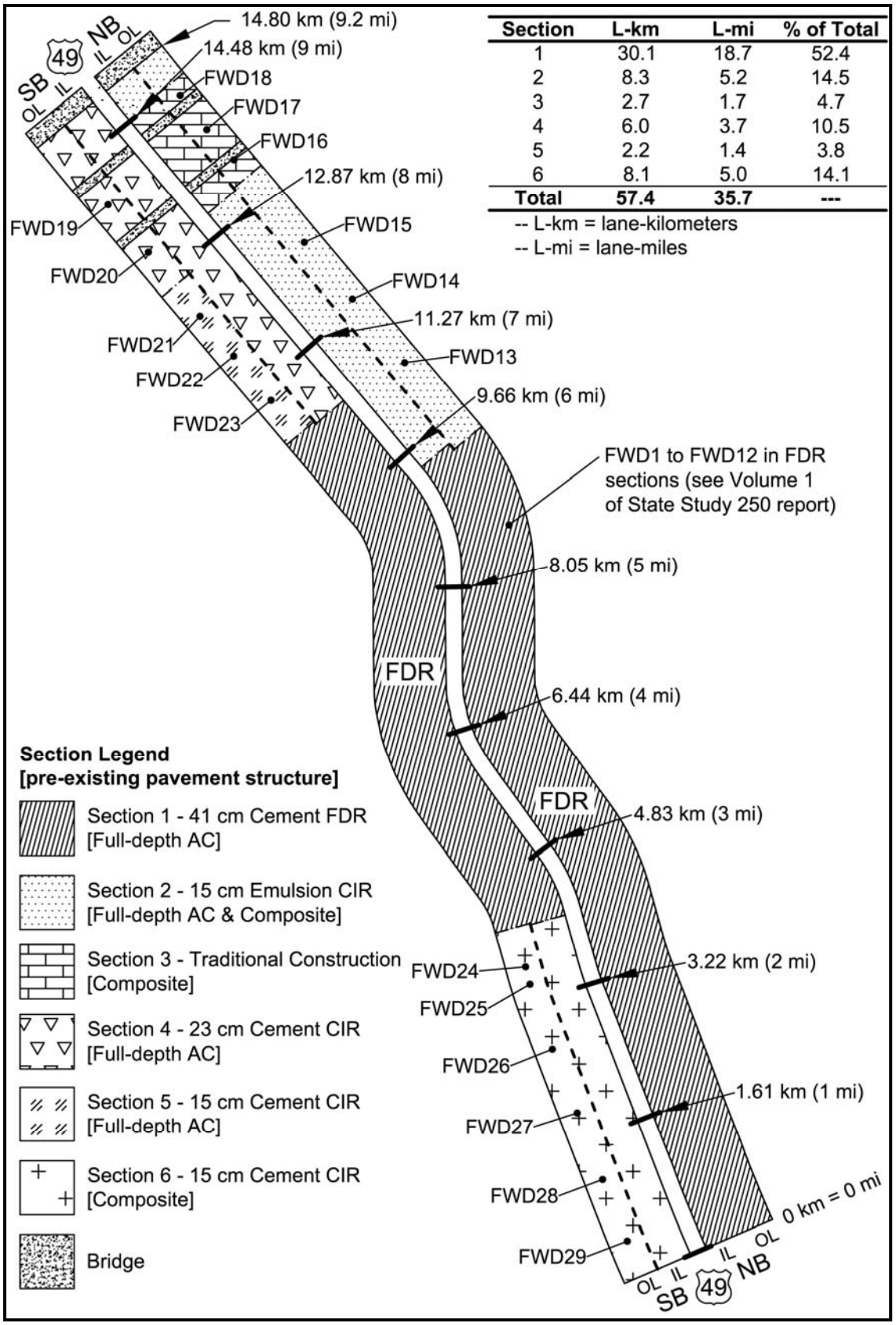


| Section | L-km | L-mi | % of Total |
|---|---|---|---|
| 1 | 30.1 | 18.7 | 52.4 |
| 2 | 8.3 | 5.2 | 14.5 |
| 3 | 2.7 | 1.7 | 4.7 |
| 4 | 6.0 | 3.7 | 10.5 |
| 5 | 2.2 | 1.4 | 3.8 |
| 6 | 8.1 | 5.0 | 14.1 |
| **Total** | **57.4** | **35.7** | **---** |

-- L-km = lane-kilometers
-- L-mi = lane-miles

**Figure 5.1. US-49 CIR Project Layout**

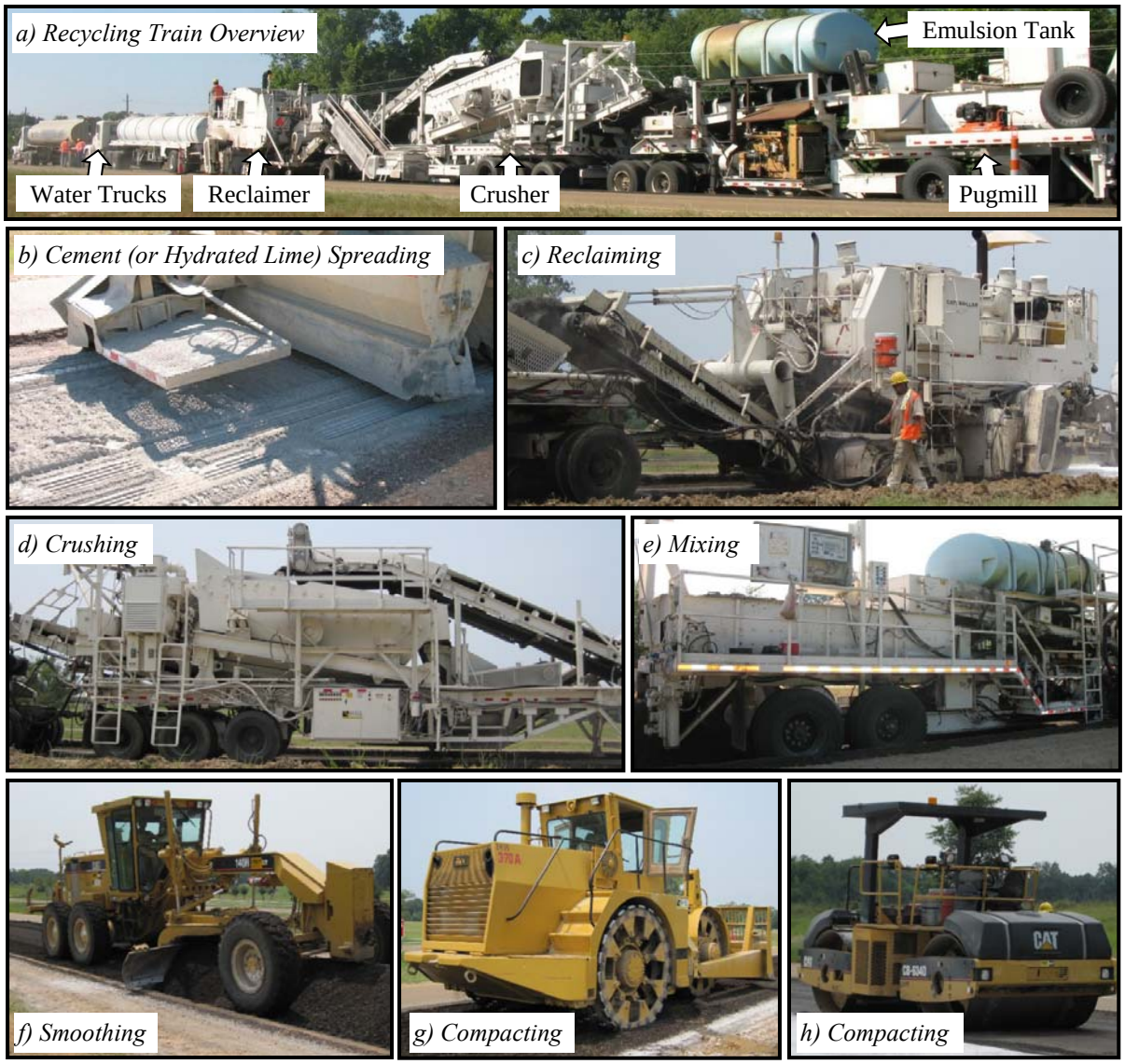


**Figure 5.2. US-49 CIR Construction Photos**

Curing specifications prior to AC overlay varied by binder type. Emulsion CIR cured until the moisture content was less than 2.5%. Cement CIR and FDR were sealed with a tack coat to minimize moisture loss and were cured for 7 days. CIR construction began in June 2010, and all CIR, FDR, and AC base course was placed by November 2010. Public traffic was allowed on the entire route around November 2010 with only the AC base course placed. The final AC surface course (stage 3) was placed between July and August of 2011. Note that during construction, MDOT and BCD obtained bulk RAP samples which were provided to MSU for testing as described in Section 3.3.1.1.

### 5.2.2.4 Final US-49 Section Details

Figure 5.1 presents the six as-built sections of US-49 and their locations. Figure 5.1 also provides the lane mileage for each section. Section 1 is the cement FDR section which

comprised approximately half of US-49 and is primarily documented in Volume I of the State Study 250 report.

Section 2 is emulsion CIR targeting a 15 cm thickness since concrete slabs were present (i.e. composite pavement). At least one area was encountered within Section 2 where concrete slabs were not present; the history of this area was unknown but was likely the result of previous rehabilitation efforts which called for slab removal and replacement with full-depth AC. Where full-depth AC was encountered in this section, CIR continued as originally planned as if concrete slabs were present (i.e. recycling depths were 15 cm rather than 23 cm).

Section 3 is traditional construction. Existing AC materials were removed down to existing concrete slabs. Serving as a crack mitigation layer, 15 cm of crushed stone base was placed on top of the concrete slabs. A total of 19 cm of 19 mm NMAS AC was placed in three lifts where the first 6.3 cm lift had PG 67-22 binder and the top two 6.3 cm lifts had PG 76-22 binder. The surface was the same as that used in stage 3 construction and was placed during stage 3 when the entire project was overlaid.

Sections 4, 5, and 6 are cement-stabilized CIR. Section 4 CIR thicknesses targeted 23 cm since no concrete slabs were present. No concrete slabs were present in Section 5; however, the target thickness was 15 cm instead of 23 cm. The reason for this deviation from original construction plans is unknown to the authors. Lastly, Section 6 CIR thicknesses targeted 15 cm since concrete slabs were present. Discussion with MDOT engineers indicated there was a tack coat (curing-related) application delay on the north end of the project, which would correspond most likely with Section 4 but possibly Section 5 as well. Exact records regarding location and length of delay were not kept, but it is believed that tack coat was applied the following day. By the time of tack coat application, MDOT engineers noted transverse shrinkage cracks were visible in the CIR layer, which should be considered when evaluating performance results.

### 5.2.3 US-49 Field Monitoring and Testing

Field monitoring and testing activities for US-49 were post-construction and consisted of three items: falling weight deflectometer (FWD) testing, automated road profiler distress surveys, and coring with subsequent laboratory characterization. MDOT periodically performed FWD testing on US-49 leading up to a more comprehensive field evaluation during the 2015 construction season (i.e. 5$^{th}$ construction season since the US-49 project). The more comprehensive evaluation occurred between May and June of 2015, which is referred to hereafter as 53 months after opening to public traffic.

#### 5.2.3.1 US-49 FWD Testing

MDOT collected FWD data when possible throughout the first 53 months of US-49's service life, with the final test date coinciding with the 53-month coring. Testing occurred at 24, 28, 34, 40, and 53 months (November 2012, March 2013, September 2013, March 2014, and June 2015). FWD testing times are also further denoted FWD Phases 1 to 5, respectively. A total of 29 FWD locations were tested on US-49 (denoted FWD1 to FWD29 in Figure 5.1). FWD1 to FWD12 were FDR test locations; FWD 13 to FWD29 were CIR locations. In

Sections 2, 5, and 6, at least three FWD locations were cored directly at the FWD drop location to assist FWD analysis.

Procedures documented in the *1993 AASHTO Pavement Design Guide* (AASHTO 1993), which is hereafter referred to as the *1993 Guide*, were used to analyze US-49 FWD data since a structural number (SN) approach was used within MDOT at the time the project was constructed. For each FWD location and test phase, deflections were normalized linearly to 40 kN (9 kips) using linear regression of data at all available applied FWD loads (target FWD loads ranged from 26.7 to 80.1 kN (6 to 18 kips)). In accordance with the *1993 Guide*, the deflection under the center of loading ($d_0$) was also corrected for temperature effects (the other measurements were not temperature corrected). Figure L5.5 of (AASHTO 1993) was used to determine temperature correction factors ($C$) to adjust to 20 °C ($d_{0\text{-}20}$). Measured asphalt surface temperatures were used as the Figure L5.5 input. This approach, while not ideal for temperature correction for US-49, incorporated cement stabilized base that was 25.4 cm thick with an elastic modulus of 5.86 GPa (850 ksi).

Due to the nature of US-49 CIR sections, US-49 CIR FWD data was less conducive to a detailed analysis than US-49 FDR data. Instead a more approximate analysis was conducted. This is discussed further in Chapter 12.

#### 5.2.3.2 US-49 Automated Road Profiling

MDOT conducted an initial distress survey where only mean roughness index (MRI) was measured in September of 2011 (10 months from opening to public traffic). Much of the northern portion of US-49 was not surveyed. Section 3 was not surveyed, and approximately 30, 75, and 30% of Sections 2, 4, and 5 were not surveyed.

MDOT conducted a second, more comprehensive pavement distress survey on April 23, 2015 (i.e. a 53 month survey) using their Pathrunner™ profiler, which is equipped with multiple computers for distress measurement. Data was collected in 152 m (500 ft) long units which were eventually merged to produce results by test section. Parameters considered were MDOT's pavement condition rating (PCR), mean roughness index (MRI), rutting, fatigue cracking, block cracking, longitudinal cracking, and transverse cracking. Each distress was quantified by severity level based on the Federal Highway Administration (FHWA) publication RD-03-031 (Miller and Bellinger 2003). MDOT's profiler was capable of measuring other distresses (e.g. edge cracking), but these were not reported since they were not observed. Note that PCR values are reported on a 0 to 100 scale where the thresholds for various condition ratings vary depending on route type. PCR is a composite index which combines roughness and distress into a single index and is calculated using an algorithm defined by MDOT.

#### 5.2.3.3 US-49 Field Coring and Associated Laboratory Testing

In all, 62 cores (100 or 150 mm diameter) were acquired from US-49 CIR and FDR sections. Cores were taken from all four lanes at locations which were spread longitudinally and distributed spatially in attempts to fully represent US-49. Cores up to 61 cm long were obtained using coring bit sleeve extensions. Additionally, a coring rig frame was designed by MSU and fabricated by a local machine shop which attached to the receiver hitch of a vehicle

and provided a stable base for cutting deep cores (Figure 5.3). Of the 62 cores, 12 were FDR, and 50 were CIR. Figure 5.4 shows representative cores from each section.

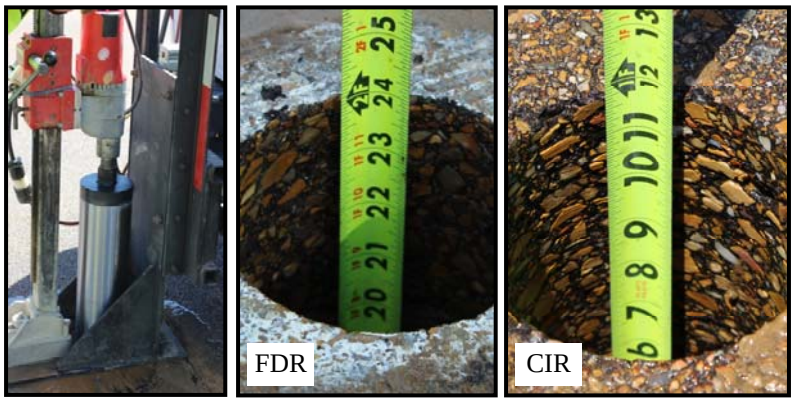


*a) Deep Coring* *b) 61 cm Core Depth* *c) 30 cm Core Depth*

**Figure 5.3. US-49 Deep Coring**

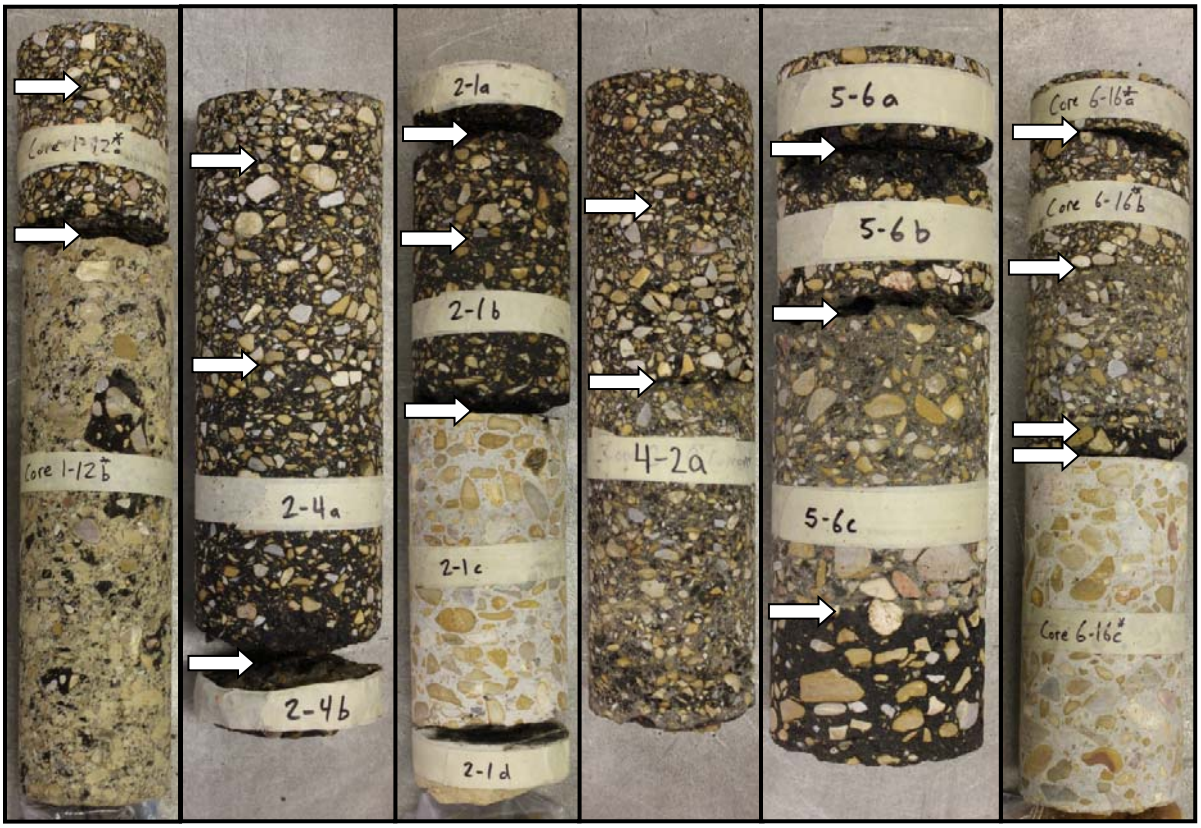


*a) Section 1* *b) Section 2* *c) Section 2* *d) Section 4* *e) Section 5* *f) Section 6*

**Figure 5.4. Representative Photos of 100 mm Diameter US-49 Cores**

Most cores were cut to a depth where the entire recycled layer could be retrieved, while cores obtained at FWD locations were cut to the subgrade; subgrade samples were taken out of nine of the core holes. Subgrade samples were combined to form six composite samples based on location taken and visual appearance. Subgrade soils were tested for basic

index properties, washed gradation, and Atterberg limits for soil classification and potential use in the FWD analysis.

Cores were visually examined, logged, and then sliced with a wet-cut masonry saw into individual test specimens. $G_{mb}$ was measured as per Section 4.4.4.2 for $V_a$ determination. Specimens were tested for multiple properties following Section 4.5 test protocols: $S_t$ (100 and 150 mm diameter), $M_r$, FE, APA rutting, and UCS. *MC* was measured on 100 mm diameter $S_t$ specimens and used to approximate *MC* for all other specimens.

$S_t$ and FE tests were conducted on specimens with target sliced thicknesses of 50 mm for both 100 and 150 mm diameters. $M_r$ testing was conducted on 150 mm diameter specimens prior to determining $S_t$ and FE. UCS tests were conducted on 100 mm diameter specimens nominally sliced to 115 mm. APA tests were conducted on 150 mm diameter specimens between 50 and 75 mm thick; specimens less than 75 mm thick were plastered to fit appropriately in APA molds.

Six replicates were tested at a minimum except for APA testing of cement CIR where two replicates were tested and UCS testing where three replicates were tested. Coring continued until minimum replication targets could be met, which required varying numbers of cores to be cut per section due to varying thicknesses and some cores being damaged or cracked.

Coring and subsequent testing for this volume of the State Study 250 report prioritized Sections 2, 5, and 6, as well as the AC base and surface mixtures. Section 1 cores and results are discussed in Volume 2 of the State Study 250 report. Section 3 was not cored. As it related to material properties measured on cores, Sections 4 and 5 were expected to be similar since the only meaningful difference between the two sections was layer thickness (23 cm compared to 15 cm). Two cores were cut from Section 4 for an estimate of as-built layer thickness. However, most coring was performed in Section 5 since its 15 cm thickness aligned more closely with typical CIR thicknesses (Figure 2.2c) and also provided more direct comparison to Section 6.

## 5.3 US Highway 45Alt CIR Project

### 5.3.1 US-45Alt Project Overview

In the 2014 construction season, a cement-stabilized CIR project was conducted on a 9.8 km (6.1 mile) section of US Highway 45 Alt under MDOT project STP-0079-02(016). The initial bid price was approximately $7.3 million; final project costs were approximately $7.5 million. US-45Alt was a high-traffic four-lane divided highway with an average daily traffic (ADT) volume of 9,200. The project was located in Monroe County, MS, with the beginning of the project occurring 6.0 km (3.8 miles) north of the Monroe-Clay County line. Project stationing (south to north from the beginning of project (BOP) to end of project (EOP)) is as follows: BOP: 453+50, Equation: 630+00 equals 30+00, and EOP: 175+00.

All four lanes were recycled and then paved with a 5.0 cm AC base course lift (12.5 NMAS, PG 76-22) and a 3.8 cm AC surface course lift (9.5 mm NMAS, PG 76-22). Recycling depths and techniques varied throughout the project. Existing pavement sections were either full-depth AC or composite pavement (i.e. AC over PCC). The field test location studied in this research was located in a composite pavement section, thus, full-depth AC sections are not discussed. The target asphalt recycling depth over concrete sections was 15 cm (i.e. the entire asphalt layer was recycled).

For northbound and southbound outer lanes, Class 9C soil was incorporated into the RAP during mixing operations. For northbound and southbound inner lanes, no virgin material was incorporated into the RAP. The field test location studied in this research was located in the northbound inner lane; therefore, only CIR materials with 100% RAP are discussed. No existing asphalt concrete in the inside lanes was milled and removed prior to recycling; all asphalt concrete present was recycled.

The target cement dosage was 4.2% by mass. This cement dosage was based on MDOT special provision S.P. 907-499-1 for cement CIR which requires the design cement dosage provide a minimum UCS by MT-25 of 2068 kPa (300 psi). The target moisture content was 11% based on a 10.9% MT-9 standard Proctor *OMC*.

### 5.3.2 US-45Alt Construction Activities

#### 5.3.2.1 US-45Alt Construction Processes

US-45Alt was constructed one lane at a time (traffic was controlled with extended period lane closures similar to US-49), working in sections within each lane. This section details the construction procedures which were used for the section where the field test site studied herein was located (i.e. station 512+50). These procedures were typical, but not necessarily the same, for the entire construction project. Figure 5.5 demonstrates key construction processes described in subsequent paragraphs.

On July 23, 2014, one day prior to cement stabilization, existing asphalt concrete was reclaimed to the depth of the underlying concrete pavement (approximately 15 cm). This material was spread evenly across the lane width and left overnight. On the morning of July 24, 2014, cement was spread (Figure 5.5a) over the loose RAP in four passes total (two towards the left side of the lane and two towards the right). A water truck applied water in a top-down application method (Figure 5.5b), and the material was mixed by a Caterpillar RM-250C (Figure 5.5c) and bladed by a Caterpillar 140H motor grader (Figure 5.5d). This sequence of water addition, mixing, and blading was repeated a second time before compaction began.

Compaction began 75 minutes after water was first added and 45 minutes after the final mixing pass of the reclaimer. Breakdown rolling was conducted with a vibratory sheepsfoot Caterpillar CP-563C roller (Figure 5.5e). Following breakdown rolling, a static pneumatic Caterpillar PS-360C roller and a vibratory/static Ingersoll Rand Pro-Pac Series 100 steel wheel roller were used in an alternating fashion (Figures 5.5e and 5.5f).

Compaction continued until a Troxler 3440 nuclear gage (*NG*) reported a dry density ($\gamma_d$) of 1.874 g/cm$^3$ (117.0 pcf), which was 97% (approximately) of the standard Proctor $\gamma_{d,max}$ of 1.937 g/cm$^3$ (120.9 pcf). Note that no correction factor was applied to nuclear gage readings. In all, compaction lasted 125 minutes. An additional pass of the water distributor was made approximately halfway through compaction. Final compacted thicknesses measured from cores which were obtained during post-construction monitoring and testing averaged 20 cm.

Within 24 hours of compaction, a prime coat was applied to the CIR surface in order to maintain moisture in the CIR layer needed for cement hydration. The AE-P emulsion described in Chapter 3 was used as the prime coat and was applied at a rate of 0.91 L/m$^2$ (0.2 gal/yd$^2$). The project required a minimum 14-day cure before trafficking or overlaying. On the afternoon of August 14, 2014, the topmost 5 cm were milled and removed from the CIR

layer, and 5 cm of base course AC was placed. The actual cure time for the CIR layer prior to overlay was 21 days. The exact timing of the surface course AC placement is unknown; however, it occurred within several days of the base course AC placement and is not greatly relevant to CIR curing behaviors. Figure 5.6 shows pictures of US-45Alt during key construction phases.

*a) Cement Spreading*

*b) Water Addition*

*c) Mixing*

*d) Blading*

*e) CP-563C Compaction (Background: PS-360C)*


*f) Pro-Pac Series 100 Compaction*

**Figure 5.5. Overview of US-45Alt Construction Sequence**

Figure 5.7 shows nominal layer thicknesses of the as-constructed pavement. Figure 5.7 thicknesses were measured on the northbound outside lane when the northbound inside

lane was being constructed. This report focuses on the inside lane, but outside lane thicknesses are shown as they were identical.

*a) CIR* *b) CIR – Primed* *c) Final AC Surface*

**Figure 5.6. Representative Photographs of US-45Alt Stages**

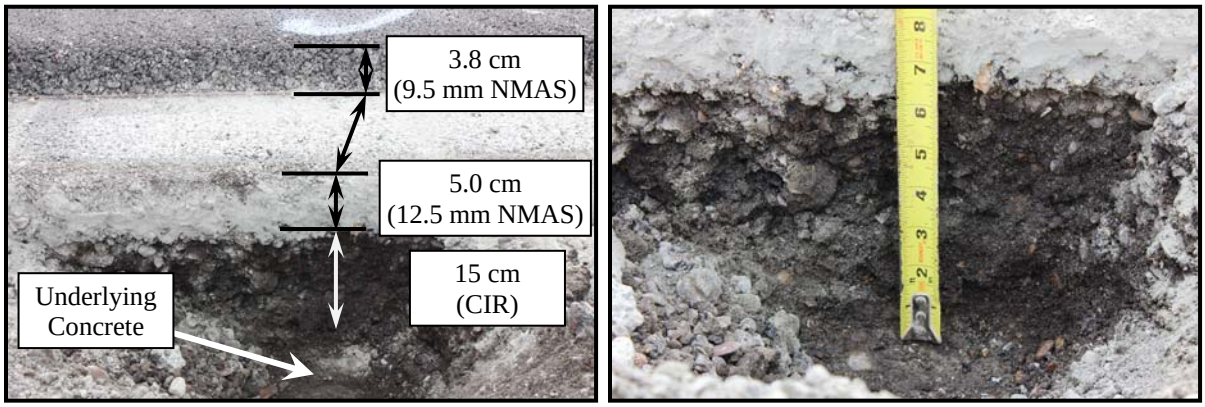


*a) Constructed Pavement Layers* *b) CIR Thickness*

**Figure 5.7. Final US-45Alt Pavement Layers (Northbound Outer Lane)**

### 5.3.2.2 US-45Alt Field Test Site and Objectives

With the guidance of the MDOT project inspector, a test site was selected in the northbound inside lane of US-45Alt where the CIR material was composed of 100% RAP. Two general criteria were considered in selecting the test site. First, it would ideally be located in a flat, straight section of the roadway with a wide shoulder for MSU vans, trucks, and equipment. Second, the test site must be located in a composite pavement section with concrete underlying the asphalt layers. The selected site was located at station 512+50, which was 2.82 km (1.75 miles) from the BOP as measured in the outside lane by vehicle odometer. The coordinates of the site were 33° 49’ 49” N and 88° 44’ 9” W.

Two key objectives were intended for the US-45Alt field test site. The first objective was to acquire approximately 450 kg (1,000 lbs) of RAP for further laboratory study. Twenty 19 L (5 gal) buckets of RAP were sampled from the spread material prior to the addition of cement. Samples were obtained in general accordance with ASTM D979 for sampling bituminous paving mixtures from the roadway prior to compaction. Each of the twenty buckets was considered one sample. The only deviation from D979 was that each sample was not taken in three increments from three locations; rather, a single location was selected for each sample, and the entire bucket was filled at that location. As in D979, care was taken to partition off each selected location and sample the full depth of the material. Samples were spaced approximately 4.5 meters apart over a 90-meter distance spanning the field test site.

Buckets were numbered in a south-to-north order from 1 to 20. In addition, a single bucket of *LH* cement was sampled from the cement distributor. Chapter 3 discusses handling of materials upon returning to the laboratory.

The second objective was to evaluate moisture (and associated early-age strength/stability) aspects during CIR compaction and curing. Moisture instrumentation was used in conjunction with cores cut at several time intervals to characterize the CIR moisture and strength during curing. Details of the second objective are discussed in the following two sections. Section 5.3.2.3 discusses the US-45Alt instrumentation utilized during construction; Section 5.3.3 discusses post-construction monitoring and testing of US-45Alt.

### 5.3.2.3 US-45Alt Instrumentation

US-45Alt was instrumented with temperature and moisture devices prior to construction to provide information related to the second US-45Alt objective. Three GS3 Ruggedized sensors (described later), which measure temperature, *MC*, and electrical conductivity, were used on US-45Alt. Figure 5.8 provides a drawing of the field test plan including instrumentation layout as well as locations which were cored after construction.

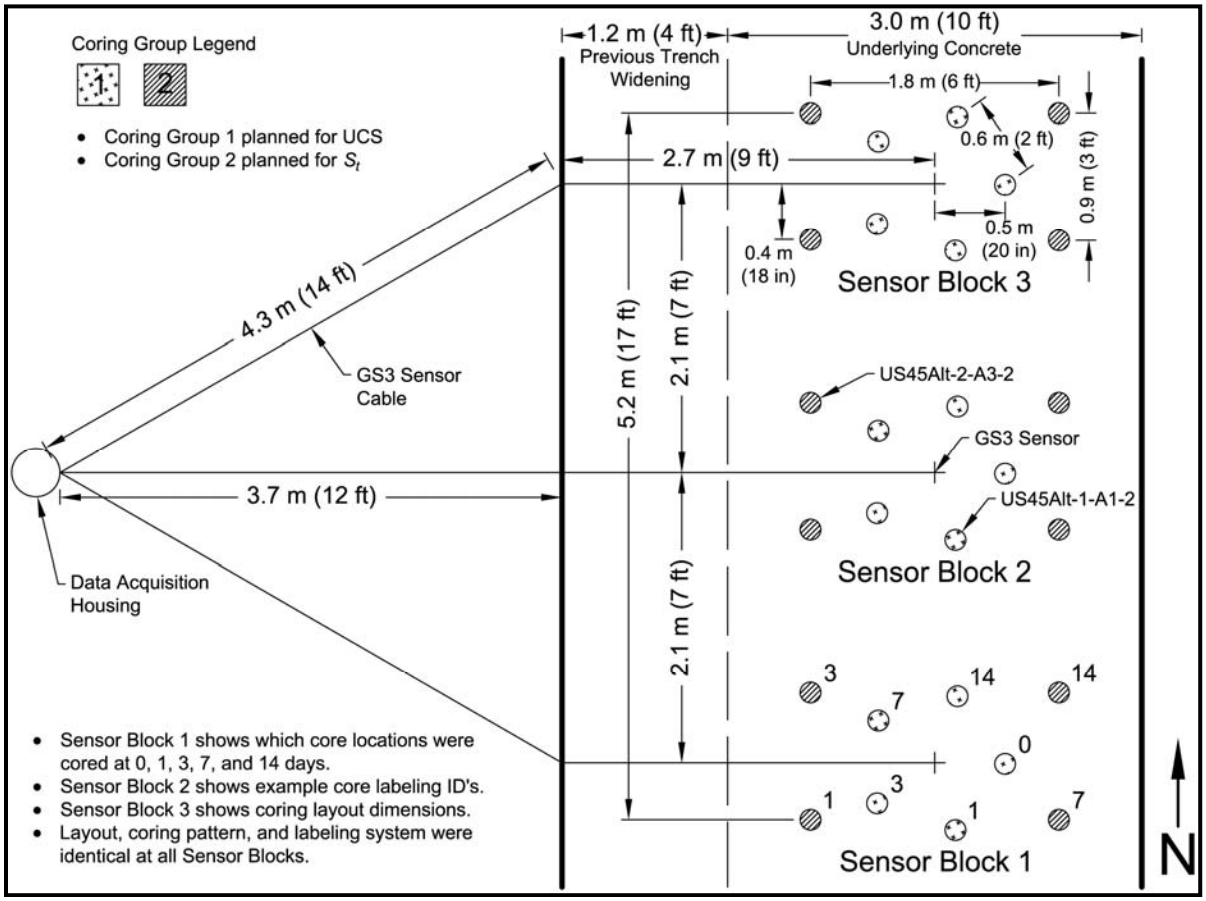


**Figure 5.8. Drawing of US-45Alt Field Test Plan**

Three blocks, referred to as Sensor Block 1 to Sensor Block 3, were laid out with one GS3 and nine coring locations per block. The nine coring locations were grouped by

anticipated testing (UCS or $S_t$) as shown in Figure 5.8. The total lane width was 4.2 m (14 ft), but the inside 1.2 m (4 ft) was a previously-conducted trench widening. The original concrete slab width was 3.0 m (10 ft). For consistency, the entire instrumentation and coring plan was limited to where there was underlying concrete. During construction, a test pit was dug to verify the presence and width of underlying concrete as shown in Figure 5.9.

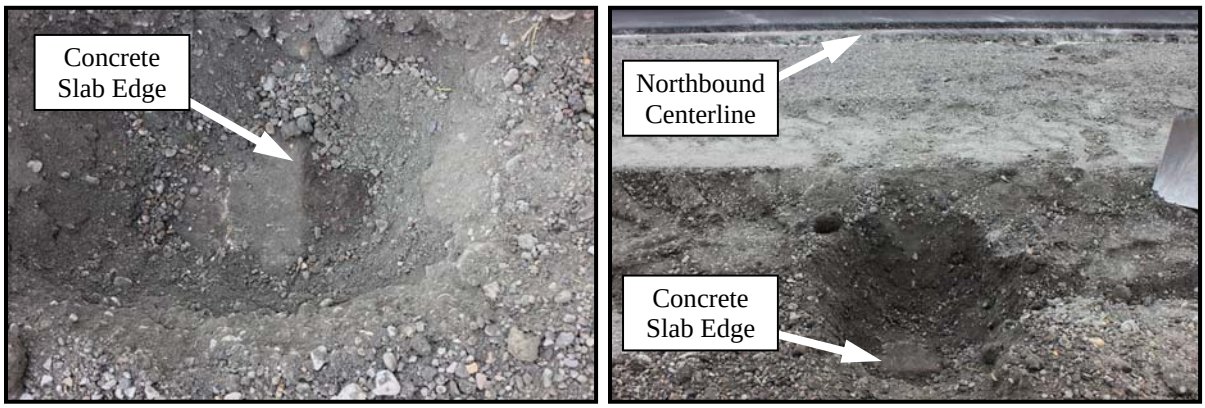


*a) Longitudinal Plan View* *b) Transverse View*

**Figure 5.9. Test Pit Showing the Underlying Concrete Layer Edge**

GS3 sensors were manufactured by Decagon Devices, Inc. with custom Ruggedized 7.6 m (25 ft) cables (Figure 5.10a). Of interest to this research, GS3's use a thermistor to measure temperature and a frequency domain sensor to measure volumetric *MC* (*VMC*). Electromagnetic fields measure the surrounding medium's dielectric permittivity (correlates to *MC*); sensors are calibrated to relate signal voltage to dielectric permittivity. GS3 sensors are typically used in mineral soil applications and are shipped with a generic dielectric-to-*VMC* calibration based on a wide variety of soil types. Given potential differences between mineral soil and CIR, GS3 sensors used herein were acquired from Decagon with no calibration (i.e. sensor output was raw data which could be later calibrated).

Figure 5.10 illustrates GS3 preparation prior to instrumentation. The 7.6 m cable was divided into two sections. The 2.7 m portion buried within the CIR layer was encased in Kearney AquaSeal™ which is commonly used for waterproofing or insulation of electrical components (Figures 5.10b and 5.10c). In this case, it was used to provide an extra layer of protection for the cable as well as seal off potential moisture flow paths along the cable. The remaining portion of the cable was encased in flexible vinyl tubing with a 19 mm (3/4 in) outer diameter and a 16 mm (5/8 in) inner diameter (Figure 5.10d), and the opening at each end of the vinyl tubing was sealed with silicone (Figures 5.10e and 5.10f). This tubing encasement was used as a precautionary measure to protect the cables from damage from any construction vehicles.

Figure 5.11 illustrates data logging equipment used as well as the housing unit fabricated to protect equipment from the weather (Figure 5.11a). GS3 data was recorded using a Decagon Em50 data logger (Figure 5.11b), while ambient temperature and humidity were measured with an Omega HH314A data logger (Figure 5.11c). In addition to the HH314A's permanently attached temperature and humidity probe, a separate K-type thermocouple was attached as a secondary ambient temperature measurement. Both data loggers were mounted inside the 20 L plastic bucket shown in Figure 5.11a; their cables were routed through two openings in the bucket's side which were sealed with silicone to prevent

moisture from entering the bucket (Figure 5.11d and 5.11e). A metal stake with a rain cover accompanied the plastic bucket for mounting of the ambient temperature and humidity measurement probe as shown in Figure 5.11f.

*a) GS3 Sensor with 7.6 m Ruggedized Cable*

*b) Kearney Aqua Seal™ Cut into Strips*

*c) Cable Portion Encased in Aqua Seal™*

*d) Cable Portion Encased in Flex Tubing*

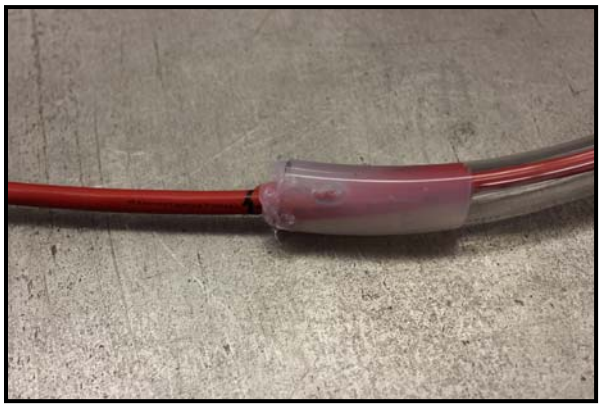

*e) Silicone Seal at End of Flex Tubing*

*f) Flex Tubing and Aqua Seal™ Junction*

**Figure 5.10. GS3 Sensor and Cable Preparation**

Figure 5.12 provides photos of the field test site during and after instrumentation. After final mixing passes but prior to compaction, three trenches were dug to the mid-depth of the CIR layer according to the Figure 5.8 drawing. Each sensor was laid in its

corresponding trench, protective materials covering the GS3 steel tines and the AquaSeal™ were removed, then the trenches were covered, and the GS3 locations were marked with orange paint. Figure 5.12d also shows the location of *NG* readings (orange rectangle near right side of photo) which were recorded after every roller pass crossing the location. The data acquisition housing was partially buried on the shoulder to reduce visibility and likelihood of being disturbed (Figure 5.12e). The coring layout from Figure 5.9 was painted on the pavement surface after compaction was finished.

*a) Data Acquisition Container*


*b) Decagon Em50 Data Logger for GS3 Sensors*

*c) Temperature and Humidity Data Logger*

*d) GS3 Cables Sealed with Silicone*

*e) Sealed Temperature and Humidity Cables*

*f) Mounted Temp/Humidity Instrumentation*

**Figure 5.11. Data Acquisition Setup**

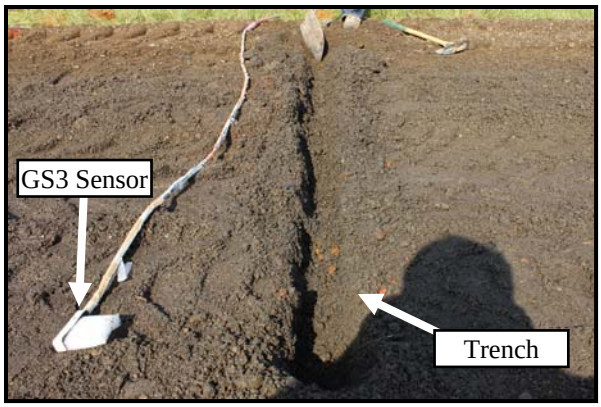


*a) Wrapped GS3 Sensor and Trench*

*b) Overview of Instrumentation Trenches*

*c) GS3 Sensor in Trench*

*d) GS3 and Nuclear Gage Locations*

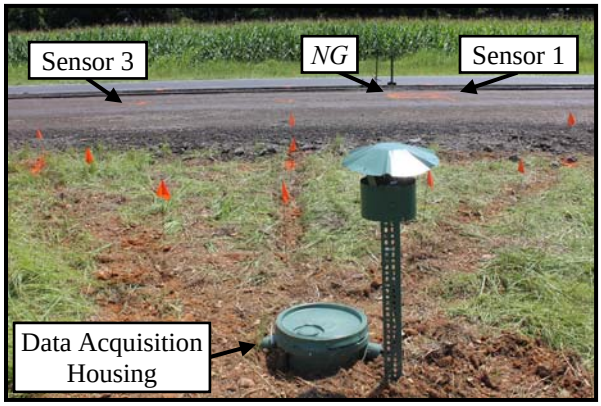


*e) Data Acquisition Layout*

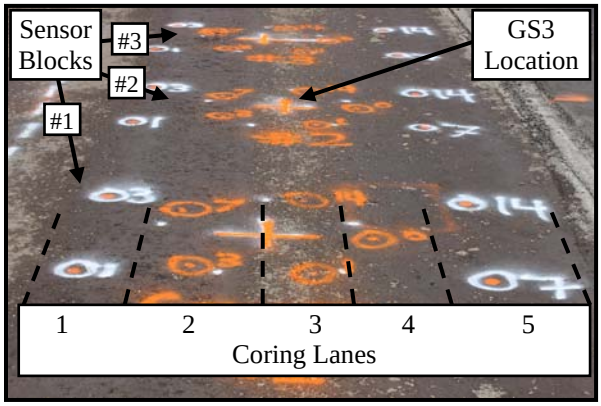


*f) Coring Plan*

**Figure 5.12. Instrumentation and Preparation of Field Test Site**

### 5.3.3 US-45Alt Field Monitoring and Testing

Field monitoring and testing activities for US-45Alt occurred during construction and up to one month after construction. Instrumentation data was recorded during compaction and throughout curing. During construction, samples of unstabilized RAP were obtained for later laboratory testing as previously discussed in Section 5.3.2.2. *MC* samples were obtained

at multiple points throughout construction as described in the following paragraph. Cores were also cut at multiple times after construction.

### 5.3.3.1 US-45Alt Instrumentation Data

Data logging with the Em50 and HH314A loggers was started with the first roller pass and was set to 1 minute intervals until compaction was finished. The data logging interval was changed to 30 minutes after construction. Approximately every three days, data loggers were inspected so that, in the event of a malfunction, the amount of data lost would be minimized. When loggers were inspected, batteries were also replaced, and data was downloaded to a computer. Data was recorded through the first 28 days post-construction; however, data from the first 14 days was of primary interest (Table 5.1).

**Table 5.1. Weather Data Summary for US-45Alt Monitoring Period**

| Variable | | | Weather Station (~16 mi ESE) | Omega HH314A (Ambient) | Decagon Em50 (Pavement) |
|---|---|---|---|---|---|
| Daily Temp (°C) | Avg | Mean | 24.8 | 27.2 | 36.3 |
| | | St. Dev. | 2.0 | 2.9 | 2.2 |
| | High | Mean | 30.9 | 36.4 | 43.3 |
| | | St. Dev. | 2.2 | 3.2 | 2.7 |
| | Low | Mean | 19.1 | 19.9 | 30.5 |
| | | St. Dev. | 2.1 | 3.4 | 1.8 |
| Daily Relative Humidity (%) | Avg | Mean | 76.2 | 73.6 | --- |
| | | St. Dev. | 5.3 | 5.2 | --- |
| | High | Mean | 98.3 | 99.6 | --- |
| | | St. Dev. | 3.1 | 1.0 | --- |
| | Low | Mean | 46.4 | 40.6 | --- |
| | | St. Dev. | 6.5 | 6.4 | --- |
| Daily Wind Speed (mph) | Avg | Mean | 3.8 | --- | --- |
| | | St. Dev. | 2.0 | --- | --- |
| | High | Mean | 10.8 | --- | --- |
| | | St. Dev. | 3.3 | --- | --- |
| | Low | Mean | 0.7 | --- | --- |
| | | St. Dev. | 0.5 | --- | --- |
| Total Precipitation (cm) | | | 0.15 | --- | --- |

*-- Parentheses indicate data measurement locations for each data source. Weather station locations are in reference to test site locations (nearest available weather station data is reported).*
*-- Omega HH314A and Decagon Em50 data recorded at 30-minute intervals.*
*-- Omega HH314A temperatures were average of the onboard temperature probe and an additional K-type thermocouple.*
*-- Omega HH314A data was not available for some days due to device malfunctions. All available data is reported, and data was only considered available if data was available for the entire day.*
*-- Dates: 7/24/14 to 8/7/14.*

Table 5.1 presents weather and temperature data from US-45Alt for the first 14 days after construction. Weather data was obtained from the nearest available weather station which was approximately 28 km (16 miles) east-southeast from the US-45Alt test site. Ambient field test site conditions were recorded with the HH314A data logger. Table 5.1 also presents internal pavement temperatures measured by the GS3 sensors and recorded by the Em50 data logger.

#### 5.3.3.2 US-45Alt Sampling, Coring, and Testing

Loose *MC* samples were obtained during construction. Unstabilized RAP *MC* samples were obtained at 7:30 AM the day of construction. Cement-stabilized (and mixed with water) *MC* samples were obtained at 9:10 AM immediately after mixing and again at 9:46 AM immediately prior to compaction. Five approximately 550 g *MC* samples were attained each time and placed in sealed containers until they could be returned to the laboratory, weighed, and dried.

Also during construction, 14 CIR specimens were compacted with field-mixed CIR material on the side of the road with the PM-P compaction device (Section 4.4.2.5). Three replicates each were compacted for 1, 3, 7, and 14 day cure times; two additional specimens were compacted in the event they were needed. Specimens remained at the US-45Alt test site throughout curing, sitting on a pallet which had been leveled. At 1, 3, 7, and 14 days, three specimens were brought to the laboratory, their density was measured (Section 4.4.4.2), and they were UC tested (Section 4.5.2, 44.5 kN load frame).

Immediately after compaction, the dry-cutting (with compressed air) of three 150 mm diameter cores was attempted for compacted *MC* data. Cutting 0-day cores was not successful, which is not surprising. Instead, loose mixture was recovered from the attempted core holes and as with other *MC* samples, was placed in sealed containers for transport to the laboratory.

At 1, 3, 7, and 14 days, six 150 mm diameter cores were dry-cut with compressed air according to the Figure 5.8 plan for a total of 24 cores. After cores were retrieved from their holes, they were photographed and heavily wrapped in plastic wrap to prevent moisture loss. Upon arrival at the laboratory, cores were unwrapped, dry-sliced to test specimen heights, measured for density (Section 4.4.4.2), tested for UCS (Section 4.5.2, 100 kN load frame) or $S_t$ (Section 4.5.3), then broken up for *MC* samples. From the time a core was unwrapped, it was sliced and tested as quickly as possible so that moisture loss prior to taking the wet weight for *MC* was minimized. Any condensate on the inside of the plastic wrap was also weighed and accounted for in the *MC*. Target slicing heights were 115 mm for $S_t$ specimens and 150 mm for UCS specimens. Actual sliced heights varied slightly depending on the nature of each core.

As with 0-day cores, issues were encountered with 1-day cores though to a lesser extent. Of the six cores attempted, two were retrieved intact, two were retrieved mostly intact, and two were broken into loose mixture. Of the four intact (or mostly intact) cores, three were Group 2 ($S_t$) and one was Group 1 (UCS). The one UCS core was mostly intact but not tall enough for UC testing; therefore, it was tested for $S_t$ (four replicates total instead of three). No notable issues were encountered for coring at 3, 7, and 14 days.

# CHAPTER 6 – ASPHALT CONCRETE RESULTS

## 6.1 Overview of Asphalt Concrete Results

Asphalt concrete results in this chapter are presented for the purpose of providing a reference data set for CIR mixtures in this report. Two groups of asphalt concrete mixtures were used for this purpose. The first group included the US-49 asphalt concrete mixtures (AC1 and AC2) which were laboratory compacted. The second group included all ERDC asphalt concrete mixtures (AC3 to AC6). Field-sawn asphalt concrete mixtures (AC7 and AC8) were tested for different purposes than asphalt concrete mixtures presented in this chapter and, therefore, are discussed in Chapter 10.

## 6.2 US-49 Asphalt Concrete Results

Table 6.1 presents strength and durability properties for laboratory-compacted US-49 asphalt concrete mixtures where target $V_a$ was 7.0 ± 1.0% on a T331 basis unless otherwise noted. Permeability was measured according to ASTM PS129 (see Volume 3 of the State Study 250 report). Darcy's hydraulic conductivity adjusted to 20 °C ($k_{20}$) by PS129 is reported.

**Table 6.1. US-49 Asphalt Concrete Strength and Durability Properties**

| | AC1 | | | | AC2 | | | |
|---|---|---|---|---|---|---|---|---|
| **Property** | **Avg** | **COV (%)** | ***n*** | ***$V_a$* (%)** | **Avg** | **COV (%)** | ***n*** | ***$V_a$* (%)** |
| $k_{20}$ ($10^{-5}$) (cm/sec) | 46 | 43 | 2 | 7.4 | 0 | --- | 2 | 6.9 |
| $M_L$ (%) | 15.5 | 10 | 3 | 5.0 | 11.0 | 15 | 3 | 4.4 |
| $S_t$ 25 °C (kPa) | 1936 | 7 | 2 | 3.3 | 1511 | 3 | 2 | 4.7 |
| $S_t$ 20 °C (kPa) | --- | --- | --- | --- | 1733 | 5 | 3 | 7.1 |
| $S_t$ 0 °C (kPa) | --- | --- | --- | --- | 2956 | 17 | 3 | 6.7 |
| $S_t$ -10 °C (kPa) | --- | --- | --- | --- | 3941 | 3 | 3 | 6.8 |
| $S_t$ -20 °C (kPa) | --- | --- | --- | --- | 4658 | 5 | 3 | 7.0 |
| $M_{r,total}$ 20 °C (GPa) | --- | --- | --- | --- | 11.7 | 18 | 3 | 7.1 |
| $M_{r,total}$ 0 °C (GPa) | --- | --- | --- | --- | 22.7 | 6 | 3 | 6.7 |
| $M_{r,total}$ -10 °C (GPa) | --- | --- | --- | --- | 26.2 | 22 | 3 | 6.8 |
| $M_{r,total}$ -20 °C (GPa) | --- | --- | --- | --- | 29.7 | 8 | 3 | 7.0 |
| FE 20 °C (kJ/m$^3$) | --- | --- | --- | --- | 2.87 | 9 | 3 | 7.1 |
| FE 0 °C (kJ/m$^3$) | --- | --- | --- | --- | 0.74 | 10 | 3 | 6.7 |
| FE -10 °C (kJ/m$^3$) | --- | --- | --- | --- | 0.68 | 2 | 3 | 6.8 |
| FE -20 °C (kJ/m$^3$) | --- | --- | --- | --- | 0.63 | 7 | 3 | 7.0 |
| $T_{crit}$ (°C) | --- | --- | --- | --- | -19.9 | --- | --- | --- |

*-- All $S_t$ testing performed on 150 mm diameter specimens.*

At less than 125 ($10^{-5}$) cm/sec, AC1 permeability was below typical thresholds. Cantabro $M_L$ and 25 °C $S_t$ were reasonable (target $V_a$ was 4.0 ± 1.0%). AC1 material quantities were limited, which ultimately resulted in instrumented IDT testing not being conducted for AC1. AC2 was impermeable. $S_t$ and $M_{r,total}$ increased as temperature decreased,

while FE decreased with temperature. $T_{crit}$ was -19.9 °C. Variability was reasonable as most COVs were less than 20%.

Table 6.2 presents HLWT results for mixtures compacted to 7.0 ± 1.0% $V_a$. Hamburg $P_{12.5}$ ($P_{12.5\text{-}HLWT}$) is commonly reported for HLWT testing; however, no mixtures tested reached rutting levels of 12.5 mm. All HLWT rut depths ($RD_{HLWT}$) were less than 6 mm.

**Table 6.2. US-49 Asphalt Concrete HLWT Results**

| | | | | $RD_{HLWT}$ (mm) by Passes | | | |
|---|---|---|---|---|---|---|---|
| **Mixture** | **Rep** | **Avg $V_a$ (%)** | **$P_{12.5\text{-}HLWT}$** | **5,000** | **10,000** | **15,000** | **20,000** |
| AC1 | 1 | 6.9 | --- | 2.8 | 3.5 | 4.1 | 4.3 |
| | 2 | 6.9 | --- | 5.3 | 5.9 | 6.3 | 6.3 |
| | **Avg** | **6.9** | **---** | **4.0** | **4.7** | **5.2** | **5.3** |
| AC2 | 1 | 6.9 | --- | 4.3 | 5.0 | 5.6 | 6.0 |
| | 2 | 6.9 | --- | 3.5 | 4.1 | 4.6 | 5.0 |
| | 3 | 6.7 | --- | 3.9 | 4.9 | 5.5 | 5.9 |
| | **Avg** | **6.8** | **---** | **3.9** | **4.7** | **5.2** | **5.6** |

Table 6.3 presents APA results for mixtures compacted to 7.0 ± 1.0% and 10.0 ± 1.0% $V_a$. APA rut depth ($RD_{APA}$) is reported alongside the APA rutting rate ($RR_{APA}$), which is reported in mm per 1,000 cycles (2,000 passes) from 2,000 to 8,000 cycles. Rut depths at 7% $V_a$ are manageable; rut depths at 10% $V_a$ are greater but reasonable.

**Table 6.3. US-49 Asphalt Concrete APA Results**

| | | | | $RD_{APA}$ (mm) by Cycles | |
|---|---|---|---|---|---|
| **Mixture** | **Rep** | **Avg $V_a$ (%)** | **$RR_{APA}$** | **2,000** | **8,000** |
| AC1 | 1 | 7.2 | --- | 2.6 | 4.4 |
| | 2 | 6.8 | --- | 2.0 | 3.4 |
| | 3 | 7.0 | --- | 3.0 | 4.1 |
| | **Avg** | **7.0** | **0.23** | **2.5** | **4.0** |
| | 1 | 10.3 | --- | 5.9 | 8.5 |
| | 2 | 9.9 | --- | 6.4 | 9.1 |
| | 3 | 10.0 | --- | 5.7 | 7.5 |
| | **Avg** | **10.1** | **0.38** | **6.0** | **8.4** |
| AC2 | 1 | 7.2 | 0.35 | 4.8 | 6.9 |
| | 2 | 6.9 | 0.38 | 4.4 | 6.7 |
| | 3 | 6.9 | 0.28 | 4.8 | 6.6 |
| | **Avg** | **7.0** | **0.34** | **4.7** | **6.7** |
| | 1 | 10.1 | 0.35 | 5.3 | 7.4 |
| | 2 | 9.9 | 0.47 | 5.9 | 8.9 |
| | 3 | 9.9 | 0.48 | 6.6 | 9.6 |
| | **Avg** | **10.0** | **0.43** | **5.9** | **8.6** |

Table 6.4 presents dry PURWheel ($PW_{dry}$) results. Two LAC slabs were sawn in half creating four test blocks or replicates. Both passes to 12.5 mm of rut ($P_{12.5\text{-}PW}$) and PW rutting rate ($RR_{PW}$), reported in mm per 1,000 passes (calculated from 4,000 to 16,000 passes), are provided. Rut depths ($RD_{PW}$) are provided at 5, 10, 15, and 20 thousand passes but also at 4,000 and 16,000 passes (2,000 and 8,000 cycles) to correspond to APA results.

Table 6.5 presents wet PURWheel ($PW_{dry}$) results. Again, four replicates were tested per mixture. In lieu of $RR_{PW}$, two other parameters are reported: the slope of data plotted in

the creep region ($S_C$), and, if stripping is present, the slope of data plotted in the stripping region ($S_S$). If stripping was observed, the stripping inflection point (SIP) is also reported.

**Table 6.4. US-49 Asphalt Concrete $PW_{dry}$ Results**

| | | | | | $RD_{PW}$ (mm) by Passes | | | | | |
|---|---|---|---|---|---|---|---|---|---|---|
| **Mixture** | **Rep** | **$V_a$ (%)** | **$P_{12.5\text{-}PW}$** | **$RR_{PW}$** | **4,000** | **5,000** | **10,000** | **15,000** | **16,000** | **20,000** |
| AC1 | 1 | 9.2 | 19100 | 0.39 | 6.4 | 7.1 | 9.4 | 11.2 | 11.6 | 12.9 |
| | 2 | 9.2 | 8900 | 0.88 | 7.0 | 8.1 | 13.2 | 17.0 | 17.6 | 20.2 |
| | 3 | 6.8 | --- | 0.26 | 3.9 | 4.3 | 5.8 | 6.9 | 7.1 | 7.8 |
| | 4 | 6.8 | --- | 0.16 | 2.8 | 3.1 | 4.0 | 4.6 | 4.8 | 5.3 |
| | **Avg** | **8.0** | **---** | **0.42** | **5.0** | **5.7** | **8.1** | **9.9** | **10.3** | **11.6** |
| AC2 | 1 | 6.9 | 14800 | 0.65 | 5.5 | 6.2 | 9.4 | 12.8 | 13.4 | 15.5 |
| | 2 | 6.9 | --- | 0.42 | 4.6 | 5.2 | 7.4 | 9.4 | 19.9 | 11.3 |
| | 3 | 6.6 | --- | 0.16 | 2.6 | 2.8 | 3.7 | 4.4 | 4.6 | 4.9 |
| | 4 | 6.6 | --- | 0.22 | 4.6 | 5.0 | 6.4 | 7.2 | 7.3 | 7.2 |
| | **Avg** | **6.8** | **---** | **0.36** | **4.3** | **4.8** | **6.7** | **8.5** | **11.3** | **9.7** |

**Table 6.5. US-49 Asphalt Concrete $PW_{wet}$ Results**

| | | | | | | | $RD_{PW}$ (mm) by Passes | | | |
|---|---|---|---|---|---|---|---|---|---|---|
| **Mixture** | **Rep** | **$V_a$ (%)** | **$P_{12.5}$** | **SIP** | **$S_C$** | **$S_S$** | **5,000** | **10,000** | **15,000** | **20,000** |
| AC1 | 1 | 9.4 | 3800 | 4000 | 2.85 | 4.48 | 17.3 | --- | --- | --- |
| | 2 | 9.4 | 4100 | --- | 2.97 | --- | 14.9 | --- | --- | --- |
| | 3 | 5.1 | 17600 | --- | 0.51 | --- | 7.0 | 9.4 | 11.6 | --- |
| | 4 | 5.1 | 10200 | 11000 | 0.90 | 3.77 | 7.9 | 12.2 | --- | --- |
| | **Avg** | **7.3** | **8925** | **---** | **1.81** | **---** | **11.8** | **10.8** | **11.6** | **---** |
| AC2 | 1 | 7.6 | 7800 | 6000 | 0.95 | 3.38 | 6.6 | --- | --- | --- |
| | 2 | 7.6 | 12900 | 12000 | 0.79 | 2.04 | 4.8 | 8.9 | 15.9 | --- |
| | 3 | 8.5 | 5100 | 5000 | 2.02 | 10.59 | 12.1 | --- | --- | --- |
| | 4 | 8.5 | 4900 | 5000 | 2.13 | 5.16 | 12.9 | --- | --- | --- |
| | **Avg** | **8.1** | **7675** | **7000** | **1.47** | **5.29** | **9.1** | **8.9** | **15.9** | **---** |

## 6.3 ERDC Asphalt Concrete Results

Table 6.6 provides test results for all ERDC asphalt concrete mixtures. Mixtures are categorized by field aging time (0-yr and 2-yr) as well as target $V_a$ level (4% and 7%). The minimum (min), maximum (max), and average (avg) are provided for all Table 6.6 data. Averages are also provided for all 0-yr and all 2-yr data.

**Table 6.6. ERDC Asphalt Concrete Average Test Results**

| | AC3 | | | | AC4 | | | | AC5 | | | | AC6 | | | | | | | | |
|---|---|---|---|---|---|---|---|---|---|---|---|---|---|---|---|---|---|---|---|---|---|
| | 0-yr | | 2-yr | | 0-yr | | 2-yr | | 0-yr | | 2-yr | | 0-yr | | 2-yr | | All Data | | | 0-yr | 2-yr |
| **Property** | **4%** | **7%** | **4%** | **7%** | **4%** | **7%** | **4%** | **7%** | **4%** | **7%** | **4%** | **7%** | **4%** | **7%** | **4%** | **7%** | **Min** | **Max** | **Avg** | **Avg** | **Avg** |
| $RD_{APA}$ (mm) | 5.3 | 4.9 | 6.1 | 8.4 | 3.9 | 4.6 | 3.2 | 4.7 | 6.1 | 8.8 | 6.8 | 8.8 | 3.0 | 5.6 | 4.7 | 6.0 | 3.0 | 8.8 | 5.7 | 5.3 | 6.1 |
| $PW_{wet}$ $P_{12.5}$ (passes) | --- | 7550 | --- | --- | --- | 7867 | --- | --- | --- | 5925 | --- | --- | --- | 5525 | --- | --- | 5525 | 7867 | 6717 | 6717 | --- |
| $M_{r,total}$ 20 °C (GPa) | 11.7 | 8.9 | 10.3 | 8.4 | 11.1 | 8.5 | 11.2 | 9.0 | 11.3 | 8.8 | 10.7 | 10.0 | 9.7 | 8.2 | 11.9 | 9.1 | 8.2 | 11.9 | 9.9 | 9.8 | 10.1 |
| $M_{r,total}$ 0 °C (GPa) | 26.6 | 20.7 | 26.4 | 21.6 | 33.6 | 20.2 | 26.6 | 21.2 | 29.1 | 20.0 | 25.1 | 21.6 | 27.6 | 21.1 | 24.2 | 22.9 | 20.0 | 33.6 | 24.3 | 24.9 | 23.7 |
| $M_{r,total}$ -10 °C (GPa) | 31.6 | 26.9 | 27.6 | 25.6 | 30.8 | 26.4 | 30.4 | 27.0 | 33.3 | 26.3 | 31.8 | 26.7 | 36.5 | 26.3 | 30.7 | 26.0 | 25.6 | 36.5 | 29.0 | 29.8 | 28.2 |
| $M_{r,total}$ -20 °C (GPa) | 36.4 | 28.3 | 33.5 | 28.5 | 33.5 | 29.1 | 32.4 | 30.3 | 35.9 | 27.9 | 33.1 | 30.3 | 37.2 | 30.3 | 33.1 | 30.1 | 27.9 | 37.2 | 31.9 | 32.3 | 31.4 |
| $T_{crit}$ (°C) | -17.4 | -19.8 | -16.2 | -15.5 | -14.4 | -16.4 | -12.0 | -14.5 | -16.5 | -20.9 | -17.1 | -15.0 | -15.2 | -18.8 | -17.1 | -15.3 | -20.9 | -12.0 | -16.4 | -17.4 | -15.3 |
| $S_t$ 25 °C (kPa) | 1869 | 1339 | 1936 | 1542 | 1620 | 1181 | 1972 | 1513 | 1741 | 1289 | 2050 | 1724 | 1469 | 1195 | 1956 | 1592 | 1181 | 2050 | 1624 | 1463 | 1786 |
| $S_t$ 20 °C (kPa) | 1979 | 1476 | 1330 | 1600 | 1794 | 1461 | 1176 | 1311 | 1897 | 1541 | 1714 | 1669 | 1792 | 1369 | 1658 | 1591 | 1176 | 1979 | 1585 | 1664 | 1506 |
| $S_t$ 0 °C (kPa) | 3809 | 2984 | 4002 | 2866 | 3814 | 2506 | 3881 | 2899 | 3660 | 3068 | 4335 | 2959 | 3731 | 2884 | 4031 | 2898 | 2506 | 4335 | 3395 | 3307 | 3484 |
| $S_t$ -10 °C (kPa) | 4846 | 3939 | 4618 | 3736 | 4511 | 3229 | 4481 | 3750 | 5584 | 3725 | 4412 | 3665 | 4890 | 4135 | 5106 | 4233 | 3229 | 5584 | 4304 | 4357 | 4250 |
| $S_t$ -20 °C (kPa) | 4917 | 4216 | 5264 | 3232 | 4585 | 3142 | 4449 | 3538 | 4890 | 4495 | 5575 | 4341 | 3653 | 3756 | 5228 | 3750 | 3142 | 5575 | 4314 | 4207 | 4422 |
| FE 20 °C ($kJ/m^3$) | 2.73 | 3.49 | 0.88 | 3.62 | 2.76 | 1.78 | 0.35 | 1.34 | 4.61 | 4.11 | 1.92 | 2.13 | 4.64 | 3.83 | 1.17 | 2.61 | 0.4 | 4.6 | 2.6 | 3.5 | 1.8 |
| FE 0 °C ($kJ/m^3$) | 0.97 | 1.18 | 1.29 | 0.85 | 1.13 | 0.79 | 0.89 | 0.92 | 1.12 | 1.02 | 1.68 | 0.80 | 1.21 | 0.85 | 1.02 | 0.54 | 0.5 | 1.7 | 1.0 | 1.0 | 1.0 |
| FE -10 °C ($kJ/m^3$) | 0.95 | 0.68 | 0.62 | 0.65 | 0.68 | 0.47 | 0.70 | 0.68 | 0.96 | 0.69 | 0.54 | 0.60 | 0.86 | 0.86 | 0.83 | 0.96 | 0.5 | 1.0 | 0.7 | 0.8 | 0.7 |
| FE -20 °C ($kJ/m^3$) | 0.56 | 0.58 | 0.72 | 0.31 | 0.48 | 0.31 | 0.56 | 0.37 | 0.61 | 0.77 | 0.96 | 0.59 | 0.34 | 0.48 | 0.82 | 0.34 | 0.3 | 1.0 | 0.6 | 0.5 | 0.6 |
| *MS* 60 °C (kN) | 17.3 | 12.7 | 18.5 | 11.3 | 14.0 | 7.8 | 17.5 | 11.5 | 11.9 | 8.2 | 16.3 | 12.1 | 12.5 | 7.7 | 13.9 | 9.9 | 7.7 | 18.5 | 12.7 | 11.5 | 13.9 |
| Flow 60 °C (2.5 mm) | 14.6 | 15.1 | 15.7 | 16.1 | 14.5 | 14.6 | 15.4 | 16.0 | 14.6 | 15.1 | 15.3 | 15.7 | 14.6 | 14.8 | 15.6 | 16.1 | 14.5 | 16.1 | 15.2 | 14.7 | 15.7 |

*-- 25 °C $S_t$ testing conducted on 100 mm diameter specimens. All other $S_t$ results are for 150 mm diameter specimens.*

# CHAPTER 7 – EVALUATION OF EXISTING SCB DESIGNS

## 7.1 Overview of Existing SCB Design Method Evaluation

This report focuses on investigating and establishing universal CIR design principles for any SCB or MCB system. A logical starting point is evaluating existing CIR design methods currently available for SCB systems. To this end, this chapter performs CIR mix design processes for SCB systems according to Tables 2.2 and 2.3. Information in Table 2.2 was considered collectively, and the most prevailing practices were used herein to form a single mix design method since most practices were fairly similar. Information in Table 2.3 was also considered collectively; however, two methods were selected since two distinct groups of design practices were observed in Table 2.3.

Section 7.2 presents results following traditional design methods for cement SCB systems, while Section 7.3 presents results for emulsion SCB systems. Each section also includes supplemental testing conducted for the purposes of better understanding existing methods as well as connecting these methods to other work presented in this report. Section 7.4 shifts focus towards universal CIR design. In all, this chapter presents results from 171 Marshall stability tests, 102 UC tests, and 141 IDT tests (non-instrumented).

## 7.2 Cement SCB Systems

### 7.2.1 Existing Cement Design Practices

Cement CIR design practices described in Table 2.3 were grouped into two approaches with respect to compaction and curing. Both compaction and curing approaches utilized UC testing to select the final design cement content. The first approach was to prepare specimens via standard Proctor compaction (Section 4.4.2.3) followed by 7 days of curing in a moist curing room such as the CR described in Section 4.4.3.3. The second approach was to prepare specimens via modified Proctor compaction (Section 4.4.2.4) followed by 7 days of curing in a sealed plastic bag at 40 °C.

Table 2.3 practices rely on Proctor moisture-density curves to determine the mixing and compaction *MC*. Testing in this chapter used a fixed 6% mixing and compaction *MC* based on work that is presented in Chapter 8 where CIR compaction was generally indifferent to *MC*.

Figure 7.1 presents UCS results for cement SCB systems. The following material and gradation combinations were tested at 3, 4, 5, and 6% cement: R1(A/R), R3(A/R), and R3(GC). UCS results for both compaction and curing approaches are shown where standard Proctor compaction followed by CR curing is denoted “Std, CR” and modified Proctor compaction followed by 40 °C curing in a sealed bag is denoted “Mod, 40 C Sealed.” For reference, minimum and maximum thresholds were plotted at 2,068 kPa (300 psi) and 3,447 kPa (500 psi) based on Table 2.3 criteria.

For all mixtures tested, the two compaction and curing approaches resulted in considerably different cement contents required to meet a minimum UCS of 2,068 kPa. A mix design conducted using the Mod, 40 C Sealed approach would require approximately 3.5 to 4.0% cement for the three mixtures tested. In contrast, the Std, CR approach would require

approximately 5.0 to 5.5% cement. In either case, trends are fairly consistent and straightforward with reasonably low variability.

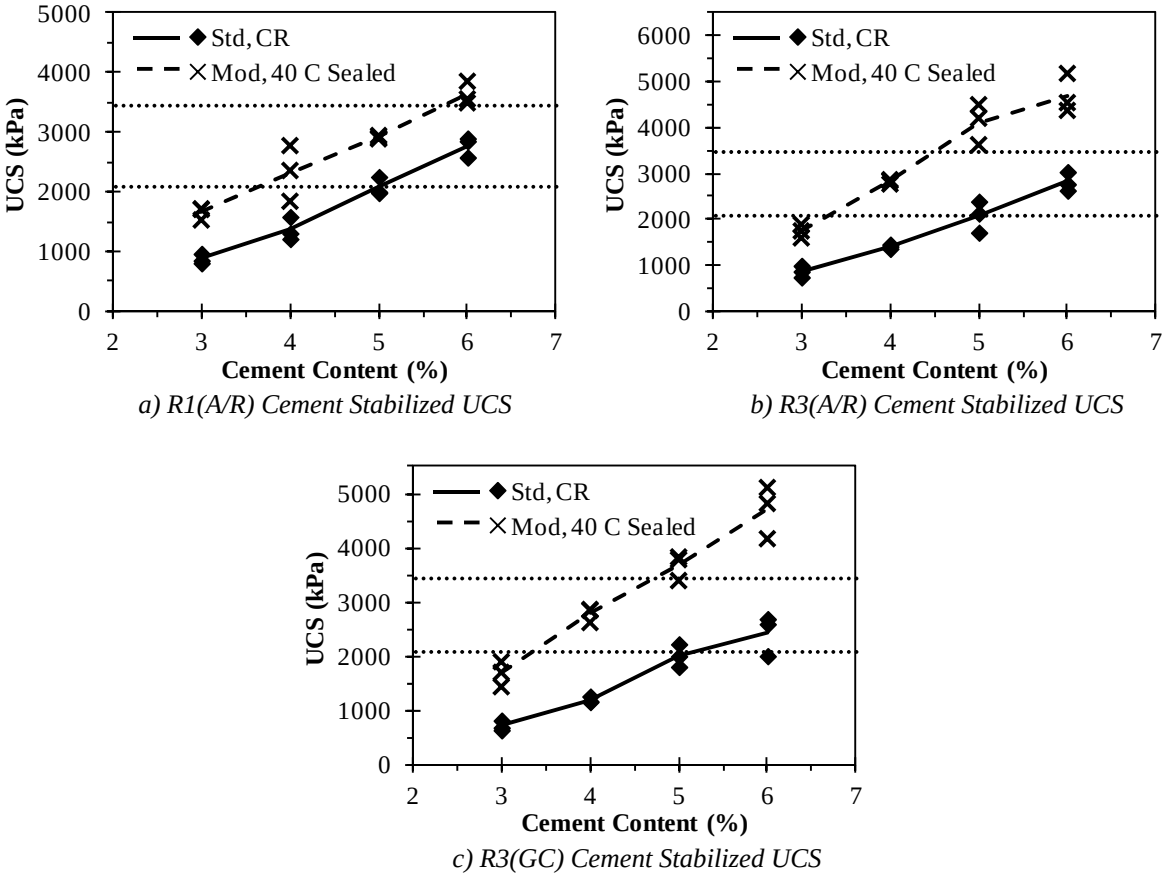


*a) R1(A/R) Cement Stabilized UCS*

*b) R3(A/R) Cement Stabilized UCS*

*c) R3(GC) Cement Stabilized UCS*

**Figure 7.1. Cement SCB Unconfined Compressive Strength**

Table 7.1 presents summary data for testing shown in Figure 7.1. Variability, characterized by COV, was reasonable in most cases. The highest COV observed was 20.1% with R1(A/R)-4c and the Mod, 40 C Sealed compaction and curing approach. On average, COV was approximately 9%.

Air voids ranged from 19.0 to 27.8% for standard Proctor compaction and 16.1 to 20.2% for modified Proctor compaction. Further, R1(A/R) exhibited the lowest $V_a$, followed by R3(A/R), and, lastly, R3(GC). The R3(GC) gradation exhibiting higher $V_a$ than R3(A/R) is reasonable since the gradation is coarser and would be more difficult to compact. However, differences between $V_a$ for R1(A/R) and R3(A/R) are less intuitive since both were batched to the same gradation (the US-49 as-received gradation). Ultimately this is believed to be primarily due to the inherent differences between R1 and R3 given they were reclaimed in different manners. R1, the US-49 RAP, was reclaimed at a relatively great depth (15 to 23 cm); R3, on the other hand, was obtained from an asphalt producer's stockpile meaning most of the RAP was likely obtained in shallow (e.g. 5 cm) mill-and-fill types of reclamation activities, which could possibly lead to different material characteristics (e.g. angularity). Within a single mixture and cement content, $V_a$ COVs were generally very low.

**Table 7.1. Summary of Properties for Std, Cr and Mod, 40 C Sealed Data**

| | | Cement Content (Std, CR) | | | | Cement Content (Mod, 40 C Sealed) | | | |
|---|---|---|---|---|---|---|---|---|---|
| **Mixture** | **Property** | **3%** | **4%** | **5%** | **6%** | **3%** | **4%** | **5%** | **6%** |
| R1(A/R) | UCS Avg (kPa) | 876 | 1370 | 2082 | 2779 | 1649 | 2324 | 2912 | 3634 |
| | UCS COV (%) | 9.2 | 14.0 | 7.2 | 6.2 | 6.4 | 20.1 | 1.0 | 5.3 |
| | $V_a$ Avg (%) | 21.6 | 20.6 | 20.4 | 19.0 | 17.1 | 17.0 | 16.3 | 16.1 |
| | $V_a$ COV (%) | 3.1 | 5.1 | 1.9 | 2.1 | 1.7 | 10.0 | 0.4 | 1.6 |
| R3(A/R) | UCS Avg (kPa) | 870 | 1413 | 2082 | 2816 | 1744 | 2824 | 4110 | 4700 |
| | UCS COV (%) | 14.4 | 3.2 | 16.4 | 7.3 | 8.4 | 1.7 | 10.8 | 9.0 |
| | $V_a$ Avg (%) | 25.3 | 24.1 | 23.4 | 22.5 | 19.4 | 18.5 | 17.9 | 16.9 |
| | $V_a$ COV (%) | 5.0 | 3.1 | 3.2 | 3.2 | 1.7 | 1.4 | 6.0 | 2.7 |
| R3(GC) | UCS Avg (kPa) | 717 | 1201 | 2015 | 2434 | 1680 | 2777 | 3669 | 4699 |
| | UCS COV (%) | 12.8 | 4.6 | 10.4 | 15.2 | 13.8 | 4.8 | 6.5 | 10.3 |
| | $V_a$ Avg (%) | 27.8 | 27.1 | 26.1 | 24.9 | 20.2 | 19.3 | 18.2 | 17.2 |
| | $V_a$ COV (%) | 0.8 | 2.0 | 2.9 | 2.8 | 3.4 | 4.3 | 3.3 | 5.7 |

*-- Three replicates tested in all cases.* *-- Air voids measured via T331 protocols in Section 4.4.4.2.*

Overall, UC testing of Proctor compacted specimens provided the ability, if so desired, to determine design cement content with relative ease. Design plots were clear without meaningful variability. Results presented in this section are useful for demonstrating a key point. Though this report is working towards a universal CIR design framework, existing SCB design methods are not, by any means, necessarily inadequate for their intended purpose (i.e. SCB design). They can, however, be limited in their ability to expand into universal design methods. For example, UC testing demonstrated its ability to differentiate cement contents; however, it would likely be much less informative for binder systems including emulsion. Also, quality control options are limited unless a group or agency desires to use the same Proctor compaction approach in the field to verify strengths.

### 7.2.2 Supplemental UC Testing

Testing in the previous section primarily followed key components of existing mix designs summarized in Table 2.3. During the Section 7.2.1 testing, two additional items of interest arose and were explored. Results of these two investigations are presented in this section since they did not specifically align with Section 7.2.1 objectives but do serve to supplement Section 7.2.1 results.

The first investigation dealt with the differences between the two compaction and curing approaches used in the previous section (Std, CR and Mod, 40 C Sealed). The Mod, 40 C Sealed approach yielded higher UCS values for a given cement content; both compaction (modified versus standard Proctor) and curing (higher versus moderate temperature) of the Mod, 40 C Sealed approach would facilitate higher UCS values. In order to isolate the effects of compaction method and curing protocol on UCS, additional testing was conducted with R1(A/R) where specimens were 1) compacted via standard Proctor compaction and cured in a sealed bag at 40 °C (Std, 40 C Sealed) and 2) compacted via modified Proctor compaction and cured in the curing room (Mod, CR). Results are shown in Figure 7.2 alongside previously-presented Std, CR and Mod, 40 C Sealed results for reference.

Figure 7.2 shows that UCS decreased slightly when modified Proctor compacted specimens were cured in the curing room rather than in a sealed bag at 40 °C. Likewise, UCS increased slightly when standard Proctor compacted specimens were cured at 40 °C in a sealed bag rather than in the curing room. Changes in UCS due to curing protocol were slight compared to changes in UCS due to compaction method.

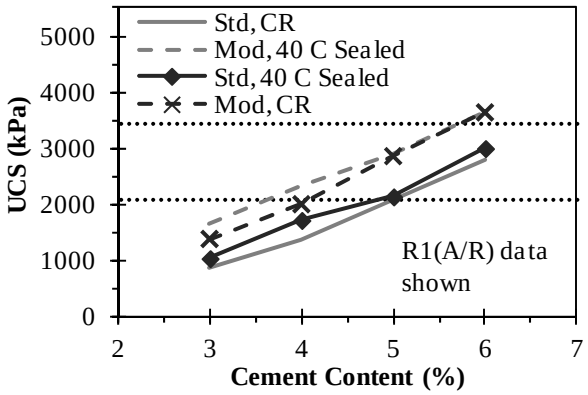


**Figure 7.2. Compaction and Curing Effects on UCS**

Overall, a key point is that UCS is noticeably dependent on specimen preparation method. If Std, CR is taken as the reference, other preparation approaches provided average relative UCS values (expressed as a percentage of Std, CR UCS values) of 111% for Std, 40 C Sealed; 131% for Mod, CR; and 148% for Mod, 40 C Sealed. Effectively, Figure 7.2 advocates for a universal design framework in which specimen preparation and testing protocols are standardized. Figure 7.2 demonstrates that a broad range of UCS values are producible for a given cement content depending on the specimen preparation method used, and this is only considering cement SCB systems. This issue would be further exaggerated if MCB or emulsion SCB systems were considered absent a universal design framework.

Compaction effects on UCS are likely related to specimen $V_a$. In Figure 7.1, $V_a$ was, on average, 5.8% lower for modified Proctor compaction than for standard Proctor compaction. Table 7.2 provides summary data for results presented in Figure 7.2. Again, modified Proctor compaction yielded lower $V_a$ than standard Proctor compaction by approximately 3.5% on average.

**Table 7.2. Summary of Properties for Std, 40 C Sealed and Mod, CR Data**

| | | Cement Content (Std, 40 C Sealed) | | | | Cement Content (Mod, CR) | | | |
|---|---|---|---|---|---|---|---|---|---|
| **Mixture** | **Property** | **3%** | **4%** | **5%** | **6%** | **3%** | **4%** | **5%** | **6%** |
| R1(A/R) | UCS Avg (kPa) | 1037 | 1718 | 2139 | 2999 | 1381 | 1999 | 2856 | 3637 |
| | UCS COV (%) | 4.7 | 12.3 | 9.5 | 6.7 | 3.4 | 1.3 | 7.5 | 4.6 |
| | $V_a$ Avg (%) | 20.8 | 18.9 | 19.5 | 18.5 | 17.1 | 15.7 | 15.5 | 15.1 |
| | $V_a$ COV (%) | 3.6 | 4.0 | 4.3 | 3.8 | 4.5 | 1.6 | 1.4 | 3.6 |

*-- Three replicates tested in all cases.* *-- Air voids measured via T331 protocols in Section 4.4.4.2.*

The second investigation dealt with comparing Proctor-compacted UC testing to SGC-compacted UC testing. Motivation for this related to MDOT utilizing SGC compaction during some aspects of US-49 design, MDOT expressed interest in moving forward with the

SGC for future CIR compaction, and the SGC provides a more versatile long-term solution with respect to a universal CIR design framework.

Figure 7.3 shows results of SGC-compacted UC testing overlaid next to standard and modified Proctor results from Section 7.2.1. Two replicates were compacted at each of three cement contents. First, for a fairly direct Proctor to SGC comparison, Proctor size (approximately 100 mm in diameter by 115 mm tall) specimens were SGC-compacted to 30 gyrations at 4% and 5% cement and then cured 7 days in the curing room. Second, 150 mm in diameter by 138 mm tall specimens were SGC-compacted to 35 gyrations at 4.8% cement (6% cement by volume) in order to replicate testing conducted by MDOT during US-49 design stages.

Figure 7.3 shows that SGC specimens compacted to 30 gyrations and CR cured yielded similar UCS values as the Mod, 40 C Sealed approach. Based on Figure 7.2 trends, SGC-compacted UCS values would likely shift up slightly and converge with Mod, 40 C Sealed results if SGC specimens had also been cured in a sealed bag at 40 °C. SGC 30-gyration $V_a$'s were 16.9% on average which were comparable to Mod, 40 C Sealed $V_a$'s of 16.6% on average.

UC tests on the 35-gyration specimens were conducted in the 100 kN load frame (Figure 4.14b) at 5.08 mm/min. As discussed in Chapter 4, UCS values obtained at the 5.08 mm/min load rate were approximately 1.25 times greater than at the 1.27 mm/min load rate. Since all other UC tests in this chapter were conducted at 1.27 mm/min, 5.08 mm/min UCS values were adjusted by dividing by 1.25 for more direct comparison. The adjusted average UCS at 4.8% cement was 3,290 kPa (average $V_a$ of 15.7%), which was noticeably higher than the UCS of 2,365 kPa reported by MDOT.

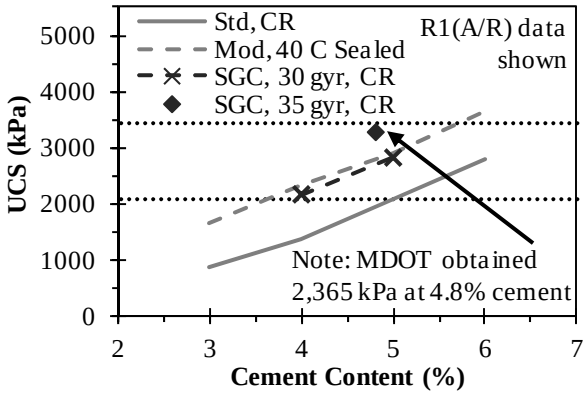


**Figure 7.3. UCS Comparison for Proctor and SGC Compaction**

Overall, the key finding from Section 7.2.2 is that UCS, while informative for cement SCB systems using Table 2.3 design approaches, demonstrated considerable dependency on specimen preparation approaches, even within cement SCB systems. If the practice of UC testing (or any testing for that matter) were extended to the opposite SCB system (emulsion in this case), direct comparisons between opposite SCB systems would only be possible if all specimen preparation procedures were identical (in contrast to preparing some cement SCBs with Std, CR; other cement SCBs with Mod, 40 C Sealed; and emulsion SCBs with a gyratory compaction and high-temperature curing approach). This demonstrates the

usefulness of a universal design framework even if just for the purpose of standardizing SCB design practices, not to mention MCB design practices.

## 7.3 Emulsion SCB Systems

### 7.3.1 Existing Emulsion Design Practices

Nearly all emulsion CIR design practices described in Table 2.2 utilized Marshall stability testing as the primary means of selecting design emulsion contents. Generally speaking, the optimum emulsion content selected based on *MS* was then tested to verify it met other requirements (e.g. 70% minimum *RMS*). For this reason, Marshall stability testing was the initial focus of testing in this section.

Marshall specimens (100 mm in diameter, 63 mm tall) were SGC-compacted to 30 gyrations and then cured at 60 °C to constant mass within 16 to 48 hours. After curing, specimens were allowed to cool for 12 to 24 hours. Density was measured via T166 and T331 then specimens were placed into a 40 °C oven for 2 hours to condition to the Marshall stability test temperature. Figure 7.4 presents Marshall stability results for R1(A/R), R3(A/R), and R3(GC).

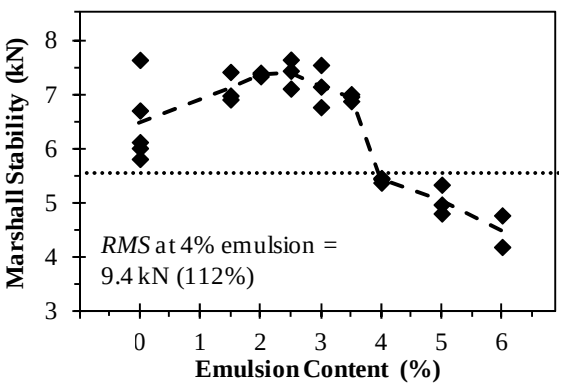


*a) R1(A/R) Emulsion Stabilized MS*

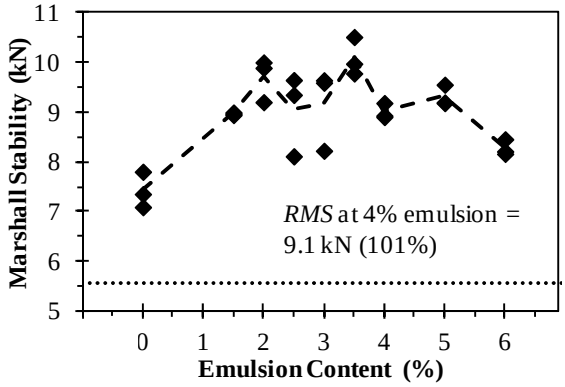


*b) R3(A/R) Emulsion Stabilized MS*

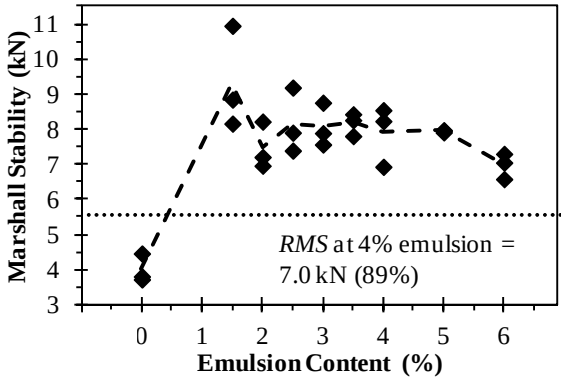


*c) R3(GC) Emulsion Stabilized MS*

**Figure 7.4. Emulsion SCB Marshall Stability**

Initially, emulsion contents from 1.5% to 4% in 0.5% increments were envisioned (1% hydrated lime was always included). For all mixtures, all emulsion contents between 1.5% and 4% yielded *MS* values well above the common 5.56 kN (1,250 lb) threshold (Table 2.2). However, a true optimum emulsion content was not always clearly identified. Further, the most optimum emulsion content from both a *MS* and economics perspective would be that which just exceeds the minimum threshold; even 1.5% emulsion exceeded the threshold by considerable margins, suggesting a more economical design is available.

To bracket *MS* behaviors, specimens were mixed, compacted, and cured as before but without emulsion or hydrated lime to determine the lowest possible *MS* for each mixture. For R1(A/R) and R3(A/R), *MS* with no stabilization additives remained above the design criteria, while *MS* for R3(GC) fell below the criteria. Curing to constant mass at 60 °C likely re-livened RAP binder slightly and helped provide stability even without emulsion. This finding reveals cause for concern regarding Marshall stability testing for CIR design. If the test and criteria intended to aid in selection of an emulsion content which provides optimum stability can be satisfied with no emulsion, perhaps alternative tests should be considered.

In a similar manner to the unstabilized *MS* testing, *MS* behaviors were bracketed on the upper end with unusually high 5 and 6% emulsion contents. In theory, emulsion content should eventually reach a point at which the emulsion phase of the mixture dominates the behavior resulting in *MS* decreases. This trend was generally observed in Figure 7.4, though *MS* fell below the 5.56 kN threshold only for R1(A/R) even though the emulsion contents tested were considerably greater than any dosage that would likely be used in practice.

Retained Marshall stability was measured at 4% emulsion for all mixtures. The 4% dosage was selected for *RMS* testing primarily because it was used during US-49 construction and also because other clearly distinguishable optimum emulsion contents were not observed. As shown in Figure 7.4, *RMS* values were 112, 101, and 89% of corresponding *MS* values. These were well above the 70% *RMS* criteria and were likely within the variability of the test given that the *RMS* values averaged just over 100%.

Table 7.3 provides key properties for specimens tested and presented in Figure 7.4. Notable observations from Table 7.3 include the following. Flow values did not vary greatly between emulsion contents and did not appear to follow any particular trend. T331 provided $V_a$'s which were 1.8% greater on average than those measured by T166. Air voids decreased approximately 5% for all mixtures from the 1.5% emulsion content to the 6.0% emulsion content.

Emulsion SCB design method testing was not conducted beyond Marshall stability and retained Marshall stability since several items of concern were encountered with Marshall testing. While CIR UC testing appears reasonable for its intended purpose (cement SCB systems), concern appears warranted regarding the ability of CIR Marshall testing to be informative, even for its intended purpose (emulsion SCB systems). Recall concerns were raised at the end of Section 7.2.2 for between-SCB evaluations based on UCS where compaction and curing protocols differed. The following section attempts to provide further insight to Marshall stability behaviors with several small investigations which extend beyond the scope of this section, which was primarily to carry out Table 2.2 with State Study 250 materials.

**Table 7.3. Summary of Properties for Figure 7.4 Data**

| | | Emulsion Content (%) | | | | | | | | |
|---|---|---|---|---|---|---|---|---|---|---|
| **Mixture** | **Property** | **0** | **1.5** | **2.0** | **2.5** | **3.0** | **3.5** | **4.0** | **5.0** | **6.0** |
| R1(A/R) | *MS* Avg (kPa) | 6.5 | 7.1 | 7.4 | 7.4 | 7.2 | 6.9 | 5.4 | 5.0 | 4.5 |
| | *MS* COV (%) | 11.5 | 3.9 | 0.5 | 3.6 | 5.4 | 0.9 | 0.8 | 5.4 | 9.2 |
| | Flow Avg (2.5 mm) | 14.3 | 14.3 | 14.2 | 14.0 | 14.2 | 14.3 | 13.6 | 14.5 | 14.7 |
| | Flow COV (%) | 4.0 | 0.4 | 6.3 | 2.2 | 2.0 | 4.5 | 2.9 | 2.1 | 6.3 |
| | T331 $V_a$ Avg (%) | --- | 16.8 | 15.9 | 15.5 | 15.0 | 14.3 | 15.0 | 12.5 | 11.9 |
| | T331 $V_a$ COV (%) | --- | 2.2 | 2.1 | 1.4 | 2.0 | 1.7 | 3.9 | 2.0 | 4.1 |
| | T166 $V_a$ Avg (%) | --- | 16.2 | 15.2 | 14.9 | 14.3 | 13.6 | 13.3 | 11.6 | 10.6 |
| | T166 $V_a$ COV (%) | --- | 2.0 | 1.0 | 2.1 | 1.7 | 1.4 | 2.9 | 2.2 | 5.2 |
| R3(A/R) | *MS* Avg (kPa) | 7.4 | 9.0 | 9.7 | 9.0 | 9.2 | 10.1 | 9.0 | 9.3 | 8.3 |
| | *MS* COV (%) | 4.9 | 0.3 | 4.5 | 9.0 | 8.8 | 3.8 | 1.7 | 2.2 | 1.9 |
| | Flow Avg (2.5 mm) | 17.1 | 15.8 | 16.6 | 16.2 | 15.8 | 16.0 | 15.4 | 16.7 | 16.0 |
| | Flow COV (%) | 15.3 | 2.6 | 0.0 | 1.9 | 1.9 | 2.5 | 6.8 | 6.2 | 0.6 |
| | T331 $V_a$ Avg (%) | --- | 20.4 | 20.2 | 20.7 | 19.8 | 18.3 | 18.4 | 17.2 | 15.8 |
| | T331 $V_a$ COV (%) | --- | 2.0 | 1.9 | 0.5 | 1.4 | 3.3 | 2.6 | 2.9 | 2.5 |
| | T166 $V_a$ Avg (%) | --- | 19.1 | 18.8 | 19.4 | 18.3 | 17.3 | 17.2 | 15.9 | 14.2 |
| | T166 $V_a$ COV (%) | --- | 2.6 | 1.6 | 0.5 | 2.4 | 3.6 | 2.1 | 3.3 | 3.2 |
| R3(GC) | *MS* Avg (kPa) | 4.0 | 9.3 | 7.5 | 8.2 | 8.1 | 8.2 | 7.9 | 8.0 | 7.0 |
| | *MS* COV (%) | 10.1 | 15.6 | 8.9 | 11.3 | 7.6 | 3.9 | 10.8 | 0.4 | 5.2 |
| | Flow Avg (2.5 mm) | 20.9 | 17.8 | 16.4 | 16.4 | 15.6 | 15.1 | 15.1 | 15.9 | 15.7 |
| | Flow COV (%) | 3.5 | 11.1 | 5.2 | 3.2 | 2.6 | 5.0 | 3.1 | 0.7 | 3.7 |
| | T331 $V_a$ Avg (%) | --- | 23.2 | 23.4 | 22.2 | 21.5 | 21.3 | 20.4 | 18.9 | 17.8 |
| | T331 $V_a$ COV (%) | --- | 1.8 | 1.2 | 1.0 | 2.8 | 0.8 | 6.1 | 1.4 | 0.3 |
| | T166 $V_a$ Avg (%) | --- | 19.9 | 19.6 | 19.1 | 18.6 | 18.1 | 17.0 | 16.3 | 15.2 |
| | T166 $V_a$ COV (%) | --- | 2.6 | 1.6 | 2.1 | 0.7 | 0.4 | 2.5 | 1.8 | 1.8 |

*-- Three replicates tested in all cases. In a few cases, more than three replicates were tested.*
*-- All blends included 1% hydrated lime except for the unstabilized (no emulsion) blend.*

### 7.3.2 Supplemental Marshall Stability Testing

This section builds on the previous section by attempting to explain and/or verify observed *MS* behaviors. First, *MS* was measured on R2(A/R) with no stabilization additives. This was conducted since R1(A/R) in the previous section was the only material from an actual CIR project. Testing R2(A/R) with no emulsion provided additional support for CIR project materials. Three R2(A/R) replicates were tested with no emulsion and yielded an average *MS* of 6.9 kN, which was, again, considerably above the 5.56 kN threshold. As previously stated, multiple materials being able to pass the *MS* criteria with no emulsion is a considerable cause for concern with future Marshall stability use within MDOT.

A repeatability experiment was conducted using R1(A/R) where an entire *MS* curve was constructed using emulsion contents of 1, 2, 3, 4, 5, and 6%. Two curves (in addition to the original presented in Section 7.3.1) were constructed using different samples of the CIR-EE emulsion. Figure 7.5 shows the two curves (denoted Trials 2 and 3) in addition to the original (denoted Trial 1). On average, Trial 2 yielded *MS* values below the 5.56 kN threshold for all emulsion contents tested. In contrast, Trial 3 yielded *MS* values even greater than those of Trial 1. Based on Figure 7.5, Marshall stability repeatability is concerning.

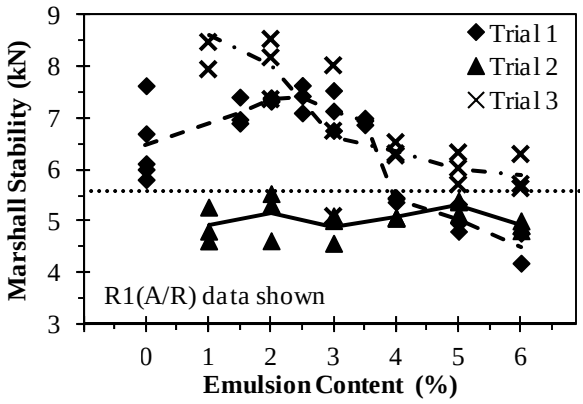


**Figure 7.5. Marshall Stability Repeatability**

Marshall stability variability was investigated by testing two 15-replicate data sets. One was at 2.5% emulsion, and the other was at 4% emulsion. At 2.5% emulsion, the average *MS* was 6.8 kN with a COV of 9.5%. At 4% emulsion, the average *MS* was 5.5 kN with a COV of 8.4%. COV appears reasonable for both emulsion contents. A 95% confidence interval was calculated for each emulsion content as well. For 2.5% emulsion, the C.I. was 5.5 to 8.1 kN, which is a fairly broad range; for 4% emulsion, the C.I. was 4.6 to 6.5 kN, which is a smaller, but still fairly broad, range. For comparison, the same two 15-replicate data sets were produced with different specimens and tested for indirect tensile strength ($S_t$). COV values were 9.7 and 6.0% for 2.5 and 4% emulsion contents, respectively. COVs between *MS* and $S_t$ results were comparable.

Lastly, the effect of cure time within the 16 to 48 hour curing constraints was investigated. Three replicates were tested at 8 hour intervals (i.e. 16, 24, 32, 40, and 48 hours). Figure 7.6 presents the results and shows there was a reasonable trend of increasing *MS* with cure time between the 16 and 48 hour window in which curing to constant mass is expected to occur. However, it is interesting to note that, on average, *MS* did not exceed 5.56 kN until specimens had been cured a full 48 hours. For most Marshall stability testing conducted in this chapter, curing to constant mass as defined in Equation 4.1 required about 24 hours, at which point Figure 7.6 data is well below 5.56 kN.

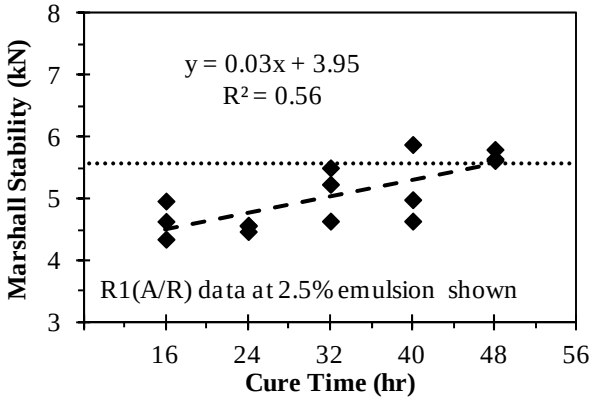


**Figure 7.6. Marshall Stability with Cure Time**

Overall, there appear to be factors at play which this section did not fully uncover though it did provide a modest amount of additional insight. For instance, undesirable *MS* behaviors observed in Section 7.3.1 do not appear to be heavily influenced by test variability or curing duration (at least in the range of cure times where specimens achieved constant mass). Repeatability does appear to be of concern and furthers the notion that Marshall stability may not be most suitable for CIR mix design procedures, even for emulsion SCB systems.

## 7.4 Transition Towards a Universal Design Framework

Key findings from Sections 7.2 and 7.3 are that existing design methods are reasonable for cement SCB systems, existing design methods are worth reconsidering for emulsion SCB systems, and neither existing design method is ideal for a universal CIR design framework capable of handling any binder system (SCB or MCB). UC testing does not appropriately characterize emulsion stabilized mixtures, and likewise, Marshall stability testing does not appropriately characterize cement stabilized mixtures.

Indirect tensile strength, for example, is one characterization test that, as shown in Figure 7.7, may be able to provide a link between emulsion and cement design methodologies. $S_t$ is commonly measured on bituminous materials as an indication of strength. While relatively uncommon for cement-stabilized materials, $S_t$ provides similar trends with cement content trends as UCS, but on a smaller scale. Overall, cement $S_t$ plots are as consistent as cement UCS plots, while emulsion $S_t$ plots are noticeably cleaner than emulsion *MS* plots.

In Figure 7.7, all specimens were SGC compacted to 30 gyrations, and then either cured to constant mass (emulsion SCB) or cured in the curing room (cement SCB). Because specimens were cured in different environments, it is not reasonable to state, for example, that 2.2% emulsion or 3.5% cement both provide an $S_t$ of 310 kPa for R1(A/R). In order to make such a statement, specimens would have to be handled identically in all facets (e.g. mixing, compaction, curing, testing). However, Figure 7.7 does demonstrate that a universal design framework in which a test can provide useful information for distinctly different binder types is feasible. The remainder of this report focuses primarily on developing the idea of a universal design framework and all components associated with that goal (e.g. consistent compaction and curing methods, etc.).

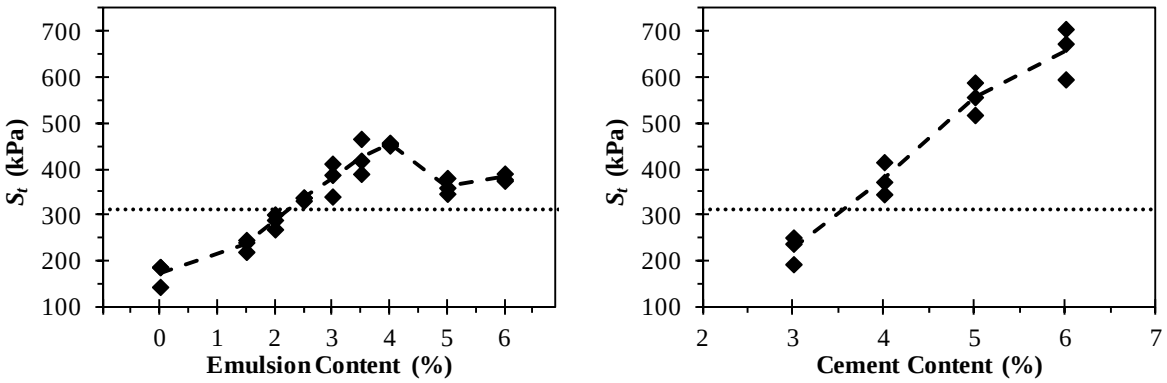


*a) R1(A/R) Emulsion Stabilized $S_t$*




*b) R1(A/R) Cement Stabilized $S_t$*

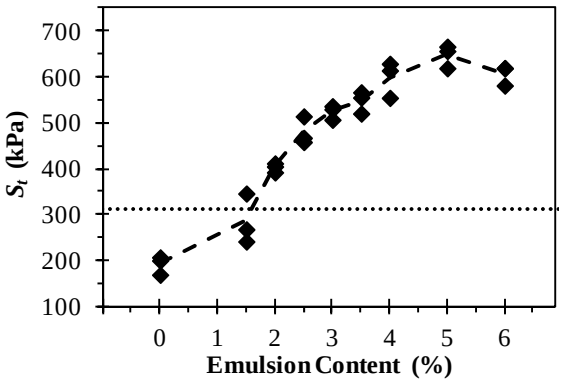


*c) R3(A/R) Emulsion Stabilized $S_t$*

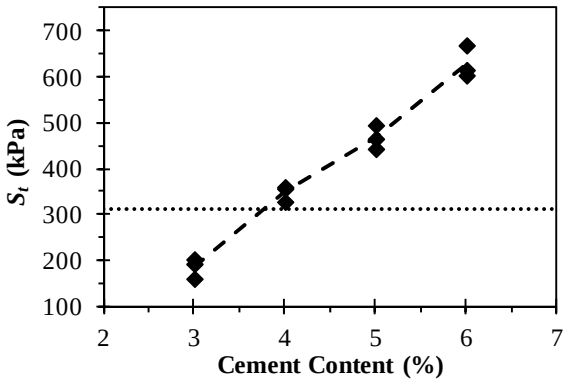


*d) R3(A/R) Cement Stabilized $S_t$*

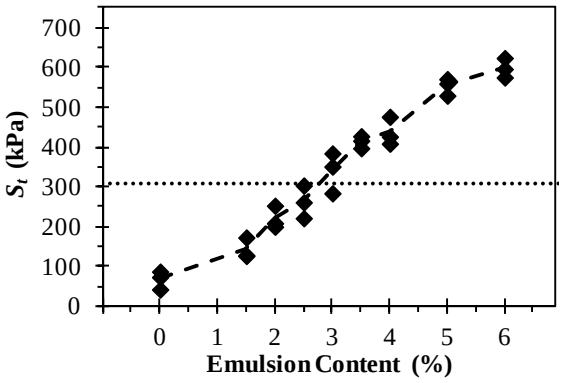


*e) R3(GC) Emulsion Stabilized $S_t$*

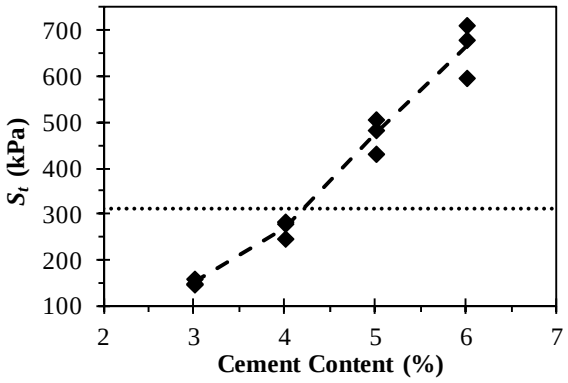


*f) R3(GC) Cement Stabilized $S_t$*

**Figure 7.7. SCB Indirect Tensile Strength**

# CHAPTER 8 – MOISTURE-DENSITY RELATIONSHIPS

## 8.1 Overview of Moisture-Density Relationships

The technical content contained in this chapter has been published by the American Society of Civil Engineers (ASCE) in the proceedings of the International Foundations Congress and Equipment Expo 2015 (Geotechnical Special Publication No. 256); accessible at: http://dx.doi.org/10.1061/9780784479087.035. With permission from ASCE the paper (Cox et al., 2015b) was reformatted and reproduced in Cox (2015). This chapter also contains all relevant moisture-density relationships from this work as it was collected for State Study 250.

Higher moisture contents (*MC*) and binder dosages are generally required for FDR than CIR (e.g. average FDR mixing *MC* is 7.2% versus 3.5% for CIR as shown in Figures 2.2e and 2.2f). Because FDR typically has a finer gradation, includes aggregate base, and may have particles with plasticity, this trend seems reasonable. Of interest to this chapter is that US-49 CIR activities incorporated *MCs* that were more representative of FDR. Also of interest to this chapter is investigating CIR moisture-density relationships using Proctor and SGC compaction.

This chapter has two objectives and two phases. The first objective was to investigate moisture-density relationships used in US-49 design and construction. To this end, Phase 1 performs complementary laboratory testing focusing on Proctor compaction related to US-49. The second and primary objective is to present CIR moisture-density relationships using the SGC since MDOT has expressed interest in its use for future in-place recycling projects. Ideally, the SGC would be used for all binders (e.g. cement, emulsion, hydrated lime, and combinations) to standardize protocols (at least to some extent) as this was not done for US-49 but would be a CIR advancement. To this end, Phase 2 utilized SGC specimens to evaluate SGC moisture-density relationships and compare them to Proctor compaction.

## 8.2 Phase 1: Compaction Efforts Related to US-49

### 8.2.1 US-49 Project Information Related to Compaction

Previous chapters documented most of the relevant US-49 project information, with those directly applicable to this chapter presented as follows. Pertinent MDOT special provisions during US-49 design and construction were S.P. 907-425-1 (emulsion) and S.P. 907-499-1 (cement). S.P. 907-425-1 (emulsion) requires *OMC* be obtained by Proctor compaction. S.P. 907-499-1 (cement) requires use of Mississippi Test Method MT-25, which entails Proctor compaction of unstabilized and stabilized material (MT-8, MT-9) and compressive strength (MT-26). For US-49, 97% of standard Proctor density was required in place for 100% pay. Maximum dry density is denoted as $\gamma_{d,max}$, while dry density is generically denoted $\gamma_d$. Other relevant terminology is as follows: $\omega_{add}$ is moisture content due to added water only, and $\omega_{total}$ is total moisture content including added water, water in the emulsion, and RAP moisture.

Table 8.1 presents all feasibly obtainable Proctor data from design and construction of US-49. Table 8.1 *OMC* values are more closely representative of FDR than CIR. It is also

noteworthy that single-point field Proctor *MC*s were, on average, 1.5% lower than the MDOT *OMC*, yet their densities were essentially identical (1980 versus 1970 kg/m$^3$).

CIR mix designs were performed by MDOT, BCD, and PTSi. For the cement design, 140 mm tall specimens (150 mm diameter) were SGC-compacted to 35 gyrations at the MT-8 *OMC* (7.4%), moist-cured seven days, then tested for unconfined compressive strength. The lowest cement content yielding 2068 kPa (300 psi) was selected (4.4%). For the emulsion design, PTSi constructed 30-gyration SGC moisture-density curves for RAP with 1.5% cement and reported 6.7% *OMC* and 1866 kg/m$^3$ $\gamma_{d,max}$. A 4% emulsion content was selected based on air voids, dry and wet indirect tensile strength, percent coating by boil test, Marshall stability and flow, and dynamic modulus. Emulsion water was subtracted from 6.7% to obtain 5.2% $\omega_{add}$, later rounded to 5%. Ultimately, 1% hydrated lime replaced the 1.5% cement to improve stripping performance, which was the failure mode in lower US-49 pavement layers prior to rehabilitation.

**Table 8.1. US-49 Moisture-Density Curve Data**

| | | | ***OMC* (%)** | | | | **$\gamma_{d,max}$ (kg/m$^3$)** | | | |
|---|---|---|---|---|---|---|---|---|---|---|
| **Binding Agent** | **Description** | ***n*** | **Mean** | **S.D.** | **Range** | **C.I.** | **Mean** | **S.D.** | **Range** | **C.I.** |
| *Results from Proctor Compaction Curves* | | | | | | | | | | |
| None | MDOT (design) | 1 | 7.4 | --- | --- | --- | 1968 | --- | --- | --- |
| 5.5% Cement[a] | BCD (design) 7/14/10 | 1 | 8.4 | --- | --- | --- | 1954 | --- | --- | --- |
| 4.4% Cement | MDOT (field) 6/23/10 to 8/13/10 | 12 | 7.9 | 0.52 | 1.6 | 6.8 - 8.9 | 1970 | 17.5 | 49.7 | 1935 - 2006 |
| 4% Emulsion + 1% Hyd. Lime | MDOT (field) 6/26/10 to 8/17/10 | 9 | 8.7 | 0.62 | 1.8 | 7.4 - 9.9 | 1855 | 10.6 | 35.2 | 1834 - 1876 |
| *Results from QC/QA Single-Point Field Proctor Tests*[b] | | | | | | | | | | |
| 4.4% Cement | BCD (field) 8/12/10 to 8/13/10 | 9 | 6.4 | 0.72 | 2.3 | 5.0 - 7.9 | 1980 | 39.2 | 110.5 | 1901 - 2058 |

*a) A terminology discrepancy led to BCD using 5.5% cement by mass as opposed to 4.4% by mass.*
*b) For single-point field Proctor tests, OMC and $\gamma_{d,max}$ refer to in-place moisture content (MC) and $\gamma_d$.*
*-- S.D. = Standard Deviation -- n = number of replicates -- C.I. = 95% Confidence Interval*

### 8.2.2 Proctor Compaction Testing and Results

Proctor compaction tests were performed according to Mississippi Test Method MT-8 (unstabilized materials) and MT-9 (stabilized materials) in the laboratory with US-49 RAP (denoted R1) at the bulk as-received gradation obtained from on-site sampling (denoted A/R) and also with R3 sieved and batched to the R1 A/R gradation. Three binder dosage combinations were used; two of them were those used for US-49, and a third employed a balanced blend of portland cement and emulsion.

Table 8.2 presents Proctor compaction results. R1(A/R) MT-8 $\gamma_{d,max}$ was 1974 kg/m$^3$, similar to the corresponding Table 8.1 value of 1968 kg/m$^3$. *OMC*, however, was lower by 1.2%. This is similar to the previously-mentioned 4.4% cement behavior in Table 8.1. This 4.4% cement behavior was consistent when Table 8.2 data for R1 (i.e. US-49) at 4.4% cement was incorporated. The *OMC* range increased from 1.5 to 2%, while the $\gamma_{d,max}$ range only increased from 10 kg/m$^3$ to 25 kg/m$^3$. Dry densities differing by 25 kg/m$^3$ (1.6 lb/ft$^3$) on a recycled material between three laboratories is very manageable. On the other hand, *OMC* values differing 2% is less manageable and brings to question the usefulness of Proctor-measured *OMC* for 100% RAP materials.

Testing the US-49 gradation with a different RAP source (i.e. R3) proved problematic across a wide range of binders, especially with emulsion included. Dry density continued to increase even at *MC*s where water was splattering and draining from the mold's base. Fine particles (i.e. high bitumen content particles) could have been escaping with the water, or some other behavior could have led to these results. Regardless, R3 data indicates an alternate compaction protocol (i.e. SGC) could be useful. A key Phase 2 question based on Tables 8.1 and 8.2 is what is moisture's role during SGC compaction for 100% RAP with varying binders and dosages.

**Table 8.2. Laboratory Proctor Compaction Results**

| Material | c (%) | e (%) | HL (%) | Method | *OMC* (%) | $\gamma_{d,max}$ (kg/m$^3$) | Curve Description |
|---|---|---|---|---|---|---|---|
| R1(A/R)[a] | 0 | 0 | 0 | MT-8 | 6.2 | 1974 | DCB - Typically shaped |
| | 4.4 | 0 | 0 | MT-9 | 5.9 | 1995 | DCB - Oddly shaped |
| | 2.3 | 2 | 0 | MT-9 | 6.6 | 1974 | DCB - Poorly shaped |
| | 0 | 4 | 1 | MT-9 | 4.9 | 1799[e] | DCB - Very slight break |
| R3(A/R)[b] | 0 | 0 | 0 | MT-8 | 7.8 | 1894 | DCB - Very slight break |
| | 4.6 | 0 | 0 | MT-9 | 7.3 | 1914 | DCB - Some scatter in data |
| | 2.4 | 2 | 0 | MT-9 | 8.7 | 1869 | DNB |
| | 2.4 | 2 | 0 | MT-9a[c] | 9.7 | 1859 | DNB |
| | 2.4 | 2 | 0 | MT-9b[d] | 9.3 | 1800 | DNB |
| | 0 | 4 | 1 | MT-9 | 8.6 | 1844 | DNB |

*a) RAP sampled from US-49 during construction.*
*b) RAP sampled from asphalt producer's stockpile.*
*c) Stabilized RAP re-used for each point on the Proctor curve.*
*d) Similar to (c) except compacted with automatic Texas hammer.*
*e) A new emulsion sample was used which was not used for all other Proctor data. This drastically decreased $\gamma_{d,max}$ for two replicates. Therefore, additional single-point Proctors were conducted with the new emulsion sample for R1(A/R) cement and cement/emulsion blends with 6% moisture. Relative to the original emulsion sample, $\gamma_d$ decreased 5.7% for the cement/emulsion blend and was unaffected for the cement blend. Further, 30-gyration SGC $\gamma_d$ changes were less than 1% between original and new emulsion samples. SGC $\gamma_d$'s at 6% moisture with the new emulsion sample were 2038, 2002, and 1984 kg/m$^3$ for cement, cement/emulsion, and emulsion blends, respectively. Unlike SGC compaction, Proctor compaction appeared sensitive to a different emulsion sample.*
*-- Cement (c), emulsion (e), and hydrated lime (HL) dosed as a percentage of dry RAP mass.*
*-- DCB = density curve broke; DNB = density curve did not break, reported max density achieved*

## 8.3 Phase 2: SGC Moisture-Density Relationships

### 8.3.1 Gradations and Binder Blends Tested

Three gradations were tested to investigate their effects (if any) on moisture-density relationships. GF (fine gradation) and GC (coarse gradation) were constructed to approximate outer bands of literature gradations (Figure 2.1a). Three binder blends were also tested, targeting the US-49 cement and emulsion blends (SCBs) and a balanced blend of cement and emulsion (MCB). Mixing and compaction water was calculated as a percentage of dry solid material (i.e. RAP, emulsion residue, cement, and hydrated lime).

### 8.3.2 Phase 2 Test Matrices

The goal of testing was to evaluate the role of water during compaction of CIR mixtures with similar binder dosages as US-49. This was accomplished by monitoring dry density and moisture content of SGC-compacted specimens (100 mm diameter) at multiple gyration levels ($N_{gyr}$) and target moisture contents.

Phase 2 terms are: 1) target and actual moisture contents of an uncompacted mixture ($\omega_{mix,target}$ and $\omega_{mix,actual}$); 2) post-compaction SGC specimen moisture content ($\omega_{comp}$). They are expressed as a dry solids percentage. Three $\omega_{mix,target}$ values (6, 8, and 10%) were chosen to reasonably bracket all observed *OMC* values in Tables 8.1 and 8.2.

Two groups of specimens, *SGC-1* and *SGC-2*, were compacted to differing $N_{gyr}$ numbers. *SGC-1* was used to establish SGC moisture-density relationships, and *SGC-2* was used to verify them for additional materials. *SGC-1* evaluated R3(A/R), all binder blends, 3 $\omega_{mix,target}$ values, and 12 $N_{gyr}$ levels (5, 10, 15 and 15-150 in increments of 15). At one replicate, this yielded 108 *SGC-1* specimens. *SGC-2* evaluated all other materials (R1(A/R), R3(GF), and R3(GC)), all binder blends, 3 $\omega_{mix,target}$ values, and 4 $N_{gyr}$ levels (15, 30, 75, and 135). At one replicate, this yielded 108 *SGC-2* specimens.

After RAP, water, and binders were mixed, $\omega_{mix,actual}$ was obtained, and SGC specimens were compacted in 100 mm SGC molds. Immediately after compaction, mass and volume (by caliper dimensions) were recorded. The entire specimen was used to obtain $\omega_{comp}$ for $\gamma_d$ calculation.

To evaluate variability, two variability sets, *VS-1* and *VS-2*, were compacted to 30 gyrations. Based on *SGC-1* and *SGC-2* results, there appeared to be no added value in further testing 10% moisture. *VS-1* evaluated R1(A/R), all binder blends, and 6% and 8% $\omega_{mix,target}$; at six replicates, this yielded 36 *VS-1* specimens. *VS-2* was identical to *VS-1* except R3(A/R) was used instead of R1(A/R).

### 8.3.3 Phase 2 SGC Compaction Results

Figure 8.1 shows *SGC-1* results. Binders are shown as follows using Figure 8.1c as an example: 2.4c2e denotes 2.4% portland cement and 2% emulsion. R2G1 $\gamma_d$ increased with $N_{gyr}$ relatively consistently between $\omega_{mix,target}$ values. As $N_{gyr}$ increased, $\omega_{comp}$ decreased and converged between $\omega_{mix,target}$ values. For high $\omega_{mix,target}$ values, moisture was reduced considerably by 30 gyrations, which is a commonly documented $N_{gyr}$ for CIR (e.g. Cross, 2002, 2003), and moisture forced out of the gyratory mold was unavailable to aid in compaction. Furthermore, all $\omega_{mix,target}$ values yielded similar $\gamma_d$ at any $N_{gyr}$. The findings indicate $\gamma_d$ for *SGC-1* is essentially independent of moisture content in the range of moisture which encompasses the unstabilized Proctor-determined *OMC* of 7.8%.

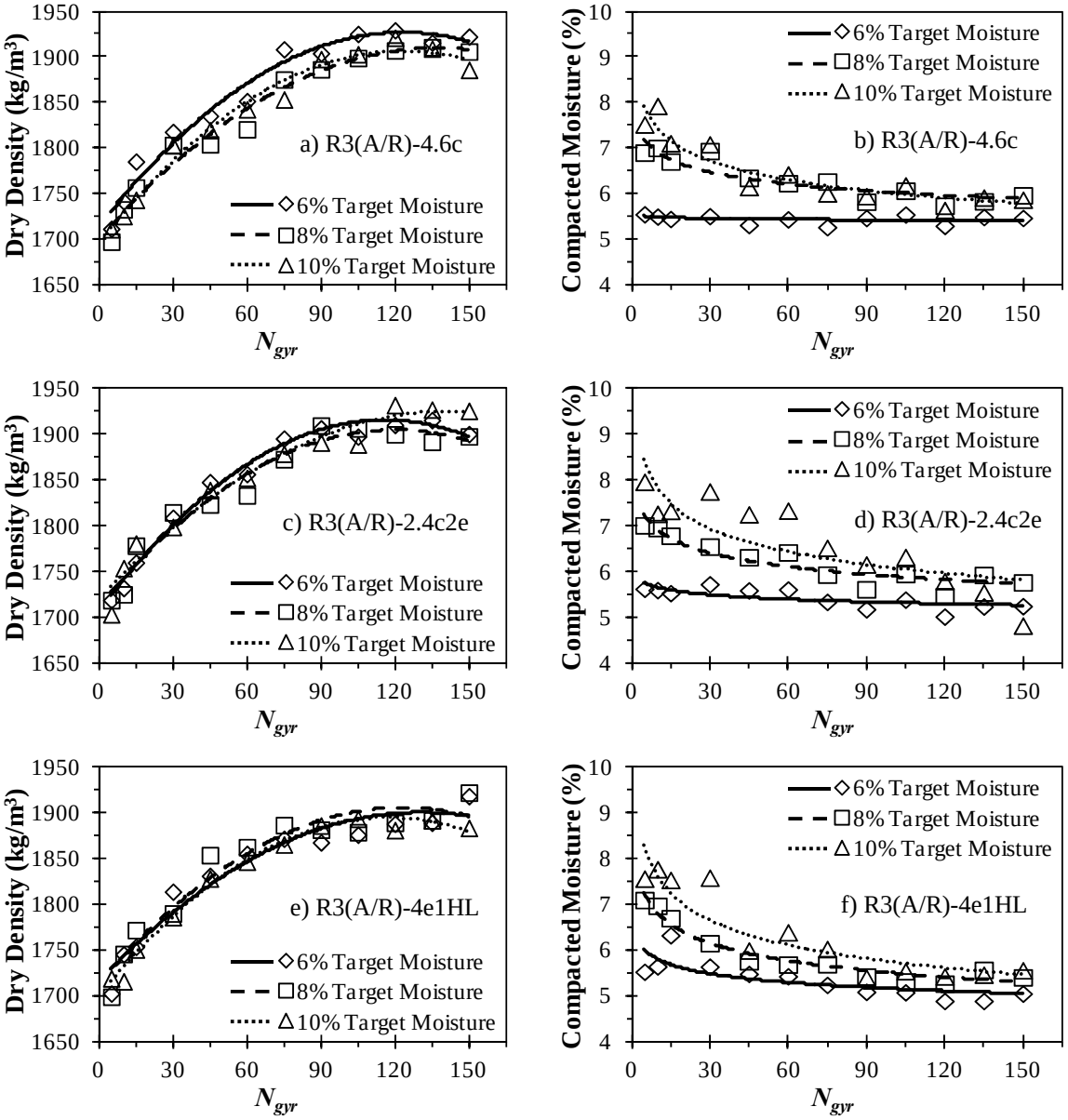


**Figure 8.1. Dry Density and Compacted Moisture versus $N_{gyr}$ for *SGC-1***

Dry density and $\omega_{comp}$ curves were fit with regression lines of the general form of Equations 8.1 and 8.2, respectively. Regression constants for *SGC-1* are shown in Table 8.3 as well as summary statistics to evaluate quality of fit.

$$\gamma_d = C_1\left(N_{gyr}\right)^2 + C_2\left(N_{gyr}\right) + C_3 \tag{8.1}$$

$$\omega_{comp} = C_4 N_{gyr}{}^{C_5} \tag{8.2}$$

Where,
$\gamma_d$ = dry density (kg/m$^3$)
$\omega_{comp}$ = moisture content after compaction (%)
$N_{gyr}$ = number of gyrations
$C_1$, $C_2$, $C_3$, $C_4$, $C_5$ = regression constants

**Table 8.3. Dry Density and Compacted Moisture Results for *SGC-1***

| R3(A/R) Mixture | $\omega_{mix,target}$ | Avg $\omega_{mix,actual}$ | 2nd Order Polynomial Fit Dry Density vs. $N_{gyr}$ (Eq. 8.1) | | | | | Power Fit $\omega_{comp}$ vs. $N_{gyr}$ (Eq. 8.2) | | | |
|---|---|---|---|---|---|---|---|---|---|---|---|
| | | | $C_1$ | $C_2$ | $C_3$ | $R^2$ | SSE | $C_4$ | $C_5$ | $R^2$ | SSE |
| 4.6c | 6 | 5.9 | -14.1 | 3.47 | 1713 | 0.97 | 1869 | 5.55 | -5 | 0.11[a] | 0.09 |
| | 8 | 8.3 | -11.0 | 3.03 | 1701 | 0.97 | 1696 | 7.91 | -59 | 0.81 | 0.46 |
| | 10 | 9.9 | -13.8 | 3.41 | 1696 | 0.98 | 1214 | 9.20 | -93 | 0.87 | 0.83 |
| 2.4c2e | 6 | 6.1 | -15.5 | 3.61 | 1706 | 0.99 | 758 | 6.01 | -27 | 0.52 | 0.26 |
| | 8 | 7.5 | -13.5 | 3.23 | 1711 | 0.96 | 2232 | 8.10 | -69 | 0.84 | 0.46 |
| | 10 | 10.4 | -10.1 | 2.89 | 1719 | 0.96 | 2163 | 10.08 | -110 | 0.65 | 3.71 |
| 4e1HL | 6 | 6.0 | -10.9 | 2.84 | 1715 | 0.95 | 2718 | 6.52 | -51 | 0.59 | 0.82 |
| | 8 | 8.0 | -12.7 | 3.12 | 1713 | 0.93 | 3627 | 8.43 | -93 | 0.95 | 0.23 |
| | 10 | 10.8 | -14.2 | 3.33 | 1699 | 0.99 | 542 | 10.11 | -123 | 0.84 | 1.96 |

*a) $R^2$ misrepresentative of fit quality due to shallow slope.* SSE *indicates good fit as shown in Fig. 8.1b.*
*-- SSE = sum of squared errors of prediction -- $R^2$ = coefficient of determination*

Table 8.4 shows density, moisture, and regression data for *SGC-2*. As in *SGC-1*, each material exhibited similar $\gamma_d$ regardless of $\omega_{mix,target}$ and similar trends for $\omega_{mix,target}$ versus $N_{gyr}$. For R1(A/R)-4.4c, $\gamma_d$ ranges from 1978 to 2030 kg/m$^3$ at 30 gyrations which is comparable to corresponding Table 8.1 and 8.2 $\gamma_{d,max}$ values. This is notable as it supports use of 30 design gyrations ($N_{des}$) as recommended by others (e.g. Cross, 2002, 2003). However, $N_{des}$ recommendations are not the purpose of this work.

Figure 8.2 provides equality plots comparing $\gamma_d$ at various $\omega_{mix,target}$ values for *SGC-1*, *SGC-2*, *VS-1*, and *VS-2*. Standard Deviation (S.D.) and coefficient of variation (COV) are relatively small for both variability sets. *VS-2* data was used to construct 95% confidence interval (C.I.) bands because *VS-2* had the lower S.D. which would provide a tighter confidence band. Most data lies within these bands. This indicates scatter around the equality line was due largely to RAP variability, not differing *MC*s.

As an independent check, 15 specimens of this experiment's 288 were selected in a stratified random approach by another researcher uninvested in this project. These were compacted on a different SGC (different model as well), and a paired *t*-test was conducted on the results. At a 5% significance level, the mean difference (3.8 kg/m$^3$) was not significant (*p-value* = 0.6190). All data collected concludes that moisture content within the range tested is irrelevant regarding $\gamma_d$.

**Table 8.4. Dry Density and Compacted Moisture Results for *SGC-2***

| Mixture | $\omega_{mix,target}$ | Avg $\omega_{mix,actual}$ | Dry Density (kg/m$^3$) at $N_{gyr}$ (15, 30, 75, 135) | 2nd Order Polynomial Fit $C_1$ | $C_2$ | $C_3$ | $R^2$ | SSE | $\omega_{comp}$ (%) at $N_{gyr}$ (15, 30, 75, 135) | Power Fit $C_4$ | $C_5$ | $R^2$ | SSE |
|---|---|---|---|---|---|---|---|---|---|---|---|---|---|
| R1(A/R)-4.4c | 6 | 6.03 | (1976, 2030, 2078, 2093) | -12.6 | 2.78 | 1946 | 0.97 | 251 | (5.3, 4.9, 4.2, 4.1) | 7.45 | -127 | 0.98 | 0.016 |
| | 8 | 7.94 | (1948, 1978, 2070, 2106) | -11.6 | 3.10 | 1900 | 0.99 | 43 | (5.8, 5.5, 4.3, 4.0) | 9.74 | -181 | 0.96 | 0.099 |
| | 10 | 9.71 | (1932, 1995, 2059, 2108) | -11.4 | 3.08 | 1898 | 0.98 | 348 | (6.0, 5.6, 4.5, 4.0) | 10.17 | -187 | 0.98 | 0.058 |
| R1(A/R)-2.3c2e | 6 | 6.23 | (1986, 2017, 2065, 2115) | -4.4 | 1.70 | 1965 | 0.99 | 42 | (5.1, 4.8, 3.9, 3.7) | 8.06 | -162 | 0.98 | 0.036 |
| | 8 | 8.85 | (1949, 1997, 2059, 2108) | -9.0 | 2.62 | 1917 | 0.99 | 127 | (5.6, 5.3, 4.1, 3.7) | 10.10 | -205 | 0.96 | 0.130 |
| | 10 | 10.26 | (1953, 1994, 2060, 2101) | -9.4 | 2.60 | 1919 | 0.99 | 37 | (6.0, 5.3, 4.2, 3.8) | 10.75 | -214 | 0.99 | 0.017 |
| R1(A/R)-4e1HL | 6 | 6.29 | (1959, 1991, 2060, 2094) | -9.4 | 2.54 | 1923 | 0.99 | 1 | (4.7, 4.3, 3.6, 3.2) | 7.90 | -182 | 0.99 | 0.015 |
| | 8 | 8.37 | (1943, 2001, 2059, 2094) | -11.8 | 2.95 | 1910 | 0.98 | 268 | (5.6, 4.6, 3.7, 3.3) | 10.47 | -237 | 0.99 | 0.020 |
| | 10 | 9.95 | (1949, 2001, 2056, 2110) | -7.9 | 2.45 | 1923 | 0.98 | 257 | (5.7, 4.7, 3.9, 3.2) | 11.20 | -250 | 0.99 | 0.017 |
| R3(GF)-4.6c | 6 | 5.92 | (1765, 1818, 1873, 1888) | -13.4 | 2.97 | 1730 | 0.98 | 190 | (5.7, 5.9, 5.6, 5.9) | 5.62 | 6 | 0.06[a] | 0.051 |
| | 8 | 7.96 | (1779, 1830, 1870, 1888) | -10.7 | 2.43 | 1754 | 0.96 | 293 | (7.7, 7.3, 6.8, 6.4) | 9.65 | -82 | 0.99 | 0.004 |
| | 10 | 9.98 | (1757, 1797, 1841, 1879) | -7.0 | 2.00 | 1734 | 0.98 | 141 | (8.2, 7.6, 6.5, 6.1) | 12.16 | -142 | 0.99 | 0.024 |
| R3(GF)-2.4c2e | 6 | 6.18 | (1801, 1821, 1872, 1908) | -4.7 | 1.61 | 1778 | 0.99 | 1 | (5.5, 5.7, 5.7, 5.3) | 5.84 | -14 | 0.16[a] | 0.090 |
| | 8 | 7.89 | (1767, 1802, 1868, 1915) | -7.7 | 2.37 | 1735 | 0.99 | 16 | (7.3, 7.3, 6.6, 5.9) | 9.80 | -96 | 0.87 | 0.179 |
| | 10 | 9.38 | (1747, 1785, 1839, 1875) | -8.0 | 2.22 | 1720 | 0.99 | 68 | (8.4, 8.0, 6.9, 6.7) | 11.51 | -112 | 0.98 | 0.046 |
| R3(GF)-4e1HL | 6 | 5.96 | (1790, 1826, 1893, 1913) | -11.4 | 2.72 | 1753 | 0.99 | 3 | (5.8, 5.9, 4.7, 4.5) | 8.69 | -135 | 0.87 | 0.228 |
| | 8 | 7.91 | (1774, 1825, 1887, 1921) | -11.5 | 2.89 | 1739 | 0.99 | 141 | (7.1, 7.0, 5.5, 5.2) | 11.43 | -163 | 0.92 | 0.297 |
| | 10 | 9.53 | (1778, 1815, 1885, 1917) | -10.6 | 2.73 | 1741 | 0.99 | 6 | (8.0, 7.4, 6.0, 5.4) | 13.56 | -188 | 0.98 | 0.107 |
| R3(GC)-4.6c | 6 | 5.53 | (1695, 1754, 1810, 1875) | -7.5 | 2.52 | 1669 | 0.98 | 401 | (5.1, 5.4, 5.2, 5.1) | 5.32 | -7 | 0.04[a] | 0.080 |
| | 8 | 7.68 | (1670, 1763, 1788, 1837) | -11.0 | 2.82 | 1653 | 0.87 | 1985 | (6.1, 6.3, 5.1, 5.2) | 8.12 | -95 | 0.76 | 0.281 |
| | 10 | 9.87 | (1659, 1698, 1815, 1825) | -19.8 | 4.41 | 1592 | 0.99 | 117 | (6.9, 6.1, 5.6, 5.3) | 9.23 | -115 | 0.98 | 0.037 |
| R3(GC)-2.4c2e | 6 | 5.58 | (1709, 1754, 1828, 1875) | -10.2 | 2.88 | 1672 | 0.99 | 51 | (5.4, 5.4, 5.4, 4.9) | 6.18 | -41 | 0.56[a] | 0.100 |
| | 8 | 6.85 | (1716, 1756, 1818, 1842) | -11.0 | 2.67 | 1682 | 0.99 | 27 | (6.8, 6.3, 5.8, 5.2) | 9.31 | -114 | 0.97 | 0.038 |
| | 10 | 9.89 | (1692, 1753, 1824, 1857) | -14.3 | 3.44 | 1652 | 0.99 | 213 | (6.6, 6.3, 6.0, 5.7) | 7.84 | -63 | 0.98 | 0.007 |
| R3(GC)-4e1HL | 6 | 5.87 | (1737, 1774, 1846, 1907[b]) | -6.7 | 2.40 | 1705 | 0.99 | 19 | (5.4, 5.1, 4.1, 3.8) | 8.77 | -169 | 0.97 | 0.067 |
| | 8 | 7.95 | (1764, 1769, 1837, 1851) | -7.6 | 1.94 | 1729 | 0.96 | 216 | (6.1, 5.6, 5.1, 5.1) | 7.58 | -85 | 0.90 | 0.064 |
| | 10 | 8.79 | (1744, 1719, 1836, 1852) | -9.1 | 2.48 | 1687 | 0.86 | 1849 | (6.4, 5.4, 4.8, 4.8) | 8.77 | -131 | 0.92 | 0.121 |

*a) $R^2$ value not representative of fit quality due to shallow slope.* SSE *indicates good fit.* *b) Data point questionable*

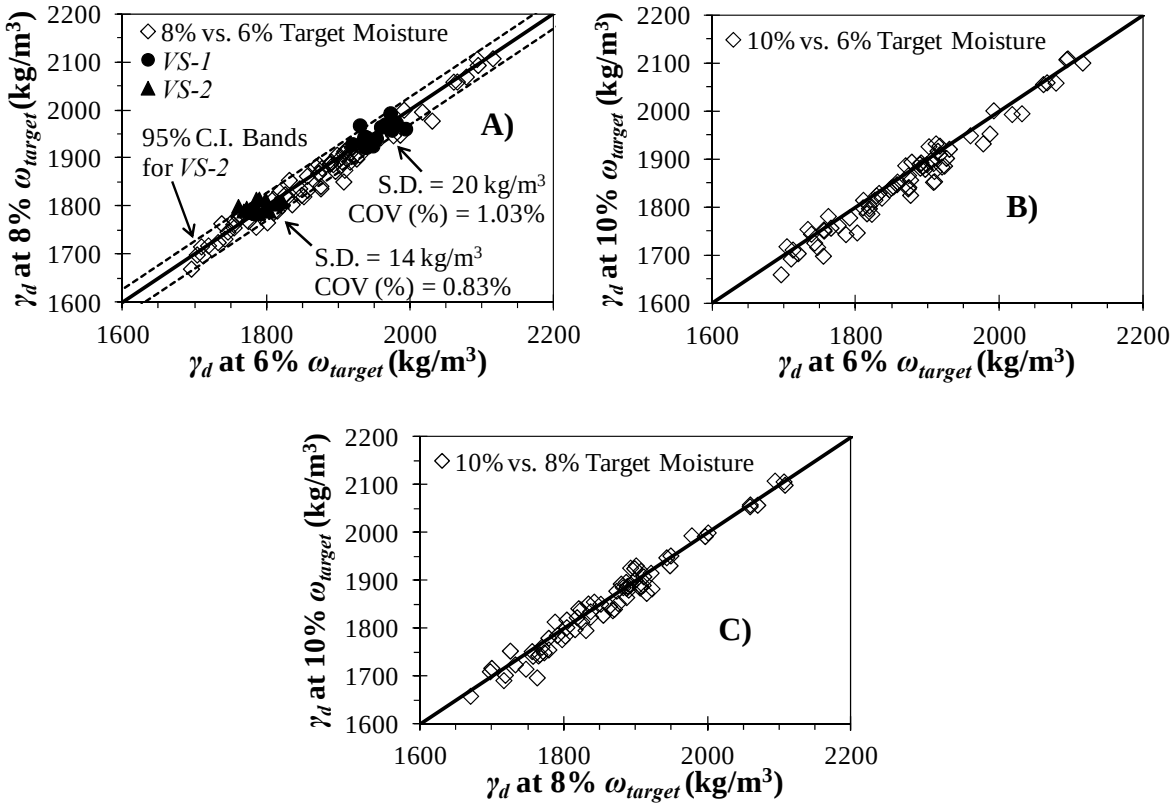


**Figure 8.2. Dry Density Equality Plots for All Specimens**

## 8.4 Summary of Density and Moisture Relations Investigation

Compaction of multiple materials at multiple gradations with various binding agent blends revealed no interaction between initial moisture content and dry density, at least in the range of moisture contents where Proctor compaction detected an *OMC*. From this chapter, the following observations are made.

- Because SGC dry density was indifferent to modest changes in moisture content, Proctor *OMC* does not appear as informative for CIR as for other materials. Therefore, the SGC is recommended for future use with CIR.
- For R1(A/R), the only material for which typically-shaped Proctor curves were obtained, 30 $N_{gyr}$ generally resulted in dry densities similar to standard Proctor values.
- When using the SGC for CIR compaction, more than 6% moisture content adds no value in terms of density gain for the mixtures tested. Because a wide variety of combinations was tested, it is likely that 6% maximum moisture is relevant to most CIR mixtures and is recommended. Additional work paralleling this work at lower than 6% moisture could be useful.

# CHAPTER 9 – PERFORMANCE TEST SCREENING

## 9.1 Overview of Performance Test Screening

The technical content contained in this chapter has been published by the American Society of Civil Engineers (ASCE) in the proceedings of the International Foundations Congress and Equipment Expo 2015 (Geotechnical Special Publication No. 256); accessible at: http://dx.doi.org/10.1061/9780784479087.037. With permission from ASCE the paper (Cox and Howard, 2015) was reformatted and reproduced in Cox (2015). This chapter also contains all relevant performance test screening from this work as it was collected for State Study 250.

CIR is not fully distinguished in terms of performance relative to, for example, traditional asphalt mixtures incorporating high RAP percentages. CIR introduces factors not present in plant recycling or traditional asphalt such as binders with vastly differing properties (e.g. cement and emulsion), cold mixing temperatures, use of mixing water, and similar. Therefore, while currently established design and testing procedures for traditional asphalt mixtures provide a logical starting point, they need to be evaluated and possibly modified to accommodate CIR differences relative to traditional asphalt.

The objective of this chapter is to evaluate CIR using several available durability and performance tests originally developed for asphalt concrete and, thus, assess their capability of characterizing CIR for a diverse array of binding agents. The screening of these performance tests is for development of a universal CIR characterization framework (presented in later chapters of this report) capable of accommodating multiple binder types as this does not seem to currently exist but would be an advancement for CIR technology. Current CIR design methods are binder-type specific (i.e. chemical or bituminous); a universal method could accommodate both types (SCBs) as well as MCB blends of the two (e.g. a balanced amount of cement and emulsion).

Six tests were evaluated herein. Each of these six tests is described in its own section following the evaluation criteria used, which are presented in Section 9.2. Tests were conducted on CIR stabilized with three binding agent blends consisting of a cement SCB, an emulsion SCB, and a cement-emulsion MCB. Binder blends utilized in this chapter are somewhat arbitrary in that they were selected solely to establish a reasonable framework in which to evaluate the six test methods. Unless otherwise stated, all specimens were SGC-compacted to 30 gyrations and cured in the humid oven (HO).

In all, approximately 100 specimens were tested in this chapter. Three RAP sources were utilized: R1, R3, and RAP milled from the surface of I-55 near Grenada, MS whose properties can be found in Cox and Howard (2015), though they are not especially important to this chapter. US-49's as received (A/R) gradation was evaluated, alongside a coarser gradation (GC); both are described in Chapter 3. Moisture for mixing and compaction was usually fixed at 6% (includes water in emulsion) based on Chapter 8 recommendations. The exception was that I-55 RAP specimens were produced with only the moisture in the emulsion utilized. Bulk dry density measurements were obtained via AASHTO T269.

## 9.2 Performance Test Evaluation Criteria

Given the overall focus of this chapter, four evaluation criteria (EC) were established as shown below to aid in systematic screening of the six performance tests evaluated. Tests which do not satisfy all criteria may not be optimal for further consideration in the context of a universal CIR design method.

EC1) Specimens must be feasibly producible. If specimens cannot be successfully fabricated, the corresponding performance test cannot be properly conducted.

EC2) The test must not be so harsh that all binder blends behave poorly. CIR mixtures with cement or emulsion binders have demonstrated satisfactory field performance in some applications. The goal of this evaluation is largely to characterize behavior of these current CIR designs, and a test that quickly destroys all specimens regardless of binder/dosage is not useful for this goal.

EC3) If reasonable results are achieved, the test must be capable of differentiating between cement and emulsion. In general, cement provides strength but is brittle, and emulsion provides flexibility but is less stable. Behavior of cement and emulsion blends are of secondary concern regarding EC3 since they were arbitrarily selected dosages. EC3 largely focuses on SCB systems.

EC4) The information gained from a test should be worth the testing effort. If a test provides a marginal result but requires intensive time, financial, and/or material resources to conduct, it may not be optimal for further consideration. It should be noted that EC4 is more of an indirect consideration rather than a strict criteria.

## 9.3 Cantabro Testing

Cantabro testing is described in Section 2.9.1 and Section 4.5.4. No documented case of CIR Cantabro testing was found by the authors. An initial CIR Cantabro investigation tested R3(A/R). Three replicate specimens (150 mm diameter by 115 mm tall) were cured 7 days and then tested. For 4.4c, 2.3c2e, and 4e1HL, respectively, average bulk dry densities were 1.79, 1.74, and 1.74 g/cm$^3$, and $M_L$ values were 99, 99, and 97%.

In attempts to further evaluate the Cantabro test, I-55 RAP was also tested. Prior to compaction, RAP was heated to 38 °C to assess temperature effects on $M_L$. Compaction effort was increased to 50 gyrations; average bulk dry densities (AASHTO T331) for 3, 4, and 5% emulsion, respectively, were 1.94, 1.97, and 2.00 g/cm$^3$. Specimens were cured at room temperature and humidity until constant mass was achieved (37 days). Average $M_L$ values were 99, 95, and 84% for 3, 4, and 5% emulsion, respectively. Even with 5% emulsion and additional compaction, $M_L$ was not informative; therefore, additional testing was not conducted. Based on these results, the Cantabro test does not satisfy EC2.

## 9.4 Bending Beam Rheometer Testing

BBR testing is described in Section 2.9.2 and 4.5.5. As with Cantabro testing, no documented case of CIR BBR mixture beam testing was found by the authors. BBR sawing procedures were attempted on R3(A/R) specimens (115 mm tall) for three binder blends and two cure times (7 and 28 days). Bulk dry densities ranged from 1.71 to 1.81 g/cm$^3$. Vertical

saw cuts were extremely difficult and usually unsuccessful, and horizontal saw cuts were never successful (Figure 4.16 illustrates BBR beam sawing for asphalt concrete and CIR). Beams broke into multiple pieces during sawing regardless of binder or cure time. Based on these results, BBR specimen preparation (and thus testing) of CIR mixture beams does not satisfy EC1.

## 9.5 Hamburg Loaded Wheel Testing

Hamburg testing is described in Sections 2.9.3 and 4.5.6. No documented case of CIR Hamburg testing was found by the authors. R1(A/R), R3(A/R), and R3(GC) were tested at three binder blends, which were 4.4 to 4.6c, 2.3 to 2.4c2e, and 4e1HL. Specimens were cured 7 days. Two specimens comprise one replicate test, and only one replicate was tested for each combination of material and binder blend.

Test results are shown in Figure 9.1. It should be noted that R3(A/R)-4.6c terminated prematurely for unknown reasons, but this did not have a major impact on overall findings. Nearly all specimens failed quickly (i.e. approximately 14 mm rut depth). For comparison, all specimens (except for R3(A/R)-2.4c2e) fell considerably short of the Texas DOT criteria in Table 2.2. Based on these results, Hamburg testing does not satisfy EC2.

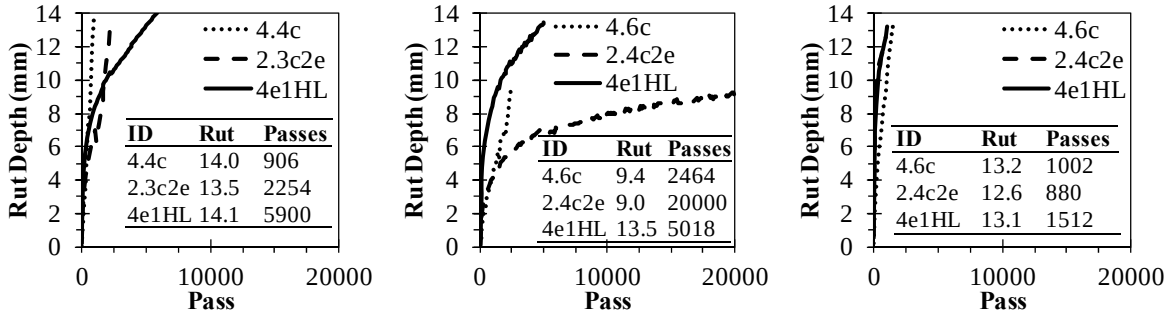


*a) R1(A/R)* *b) R3(A/R)* *c) R3(GC)*

**Figure 9.1. Hamburg Test Results**

## 9.6 Loaded Wheel Fatigue Testing

Fatigue testing is described in Sections 2.9.4 and 4.5.7. CIR loaded wheel fatigue testing does not appear to be documented in literature. Fatigue beam specimens were sawn from LAC slabs; because of slab compaction material demands, only R3(A/R) was initially considered. Two replicates of all binder blends were tested at two cure times (7 and 56 days) and two loads. Tests were conducted as described in Section 4.5.7.

Test results are shown in Figure 9.2 in which several general trends can be observed. For example, the 1100 N load was largely uninformative. Generally, 56-day fatigue data is more informative than 7-day data, which is not surprising considering fatigue is typically considered a longer-term performance issue. For the 445 N load at 56 days, 2.4c2e failed after very few cycles in comparison to 4.6c and 4e1HL.

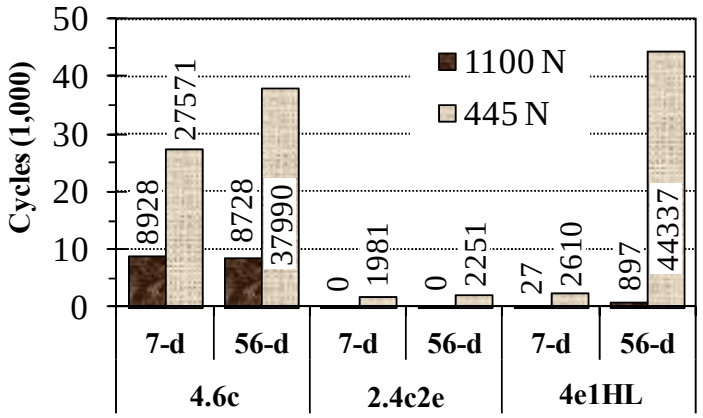


**Figure 9.2. Average Fatigue Test Results for R3(A/R)**

Although shorter fatigue life is plausible with 2.4c2e, the overwhelming differences between 2.4c2e and 4.6c or 4e1HL bring several items to question. First, strains induced by the applied loads are not explicitly considered. Appropriate CIR strain levels are not well-established and are also modulus-dependent (and to some extent application-dependent), which is not currently known for these materials. Using loads which induce realistic strain levels may, but also may not, result in reasonable comparisons for all binder blends. Second, fatigue resistance at a given load likely requires some threshold minimum strength. IDT results presented later suggest 2.4c2e strength may be a concern at early cure times (recall the 2.4c2e blend of cement and emulsion was an arbitrarily selected MCB system). At present, loaded wheel fatigue results appear somewhat inconclusive but not greatly promising. Given the marginal acceptance of loaded wheel fatigue tests for traditional asphalt combined with these results and labor intensive specimen preparation, CIR loaded wheel fatigue testing is not believed to be optimal based on EC4.

## 9.7 APA Loaded Wheel Testing

APA testing is described in Sections 2.9.6 and 4.5.8. R1(A/R), R3(A/R), and R3(GC) were tested at the same three binder blends as HLWT testing. Specimens were cured 7 days. Two specimens compose one replicate test, and only one replicate was tested for each combination of material and binder blend.

Test results are shown in Figure 9.3; 4.4 to 4.6c exhibits negligible rutting, while 4e1HL exhibits moderate rutting; 2.4c2e exhibits rutting closer to that of 4.4 to 4.6c. Depending on the pass/fail criteria used (Section 2.9.6), 4e1HL may be borderline unacceptable in terms of rutting. Figure 9.3 demonstrates the ability of cement to improve rutting resistance, which is a common reason for its use. Based on these results, the APA satisfies EC1 through EC4.

A small experiment was conducted on R1(A/R)1-4e1HL at 60 and 80% of the full 445 N load to account for pavement depth within a typical pavement structure (CIR overlaid with asphalt concrete). Figure 9.4 shows $RD_{APA}$'s were 7.0 and 7.6 mm, which were not meaningfully different from the 7.1 mm full-load $RD_{APA}$.

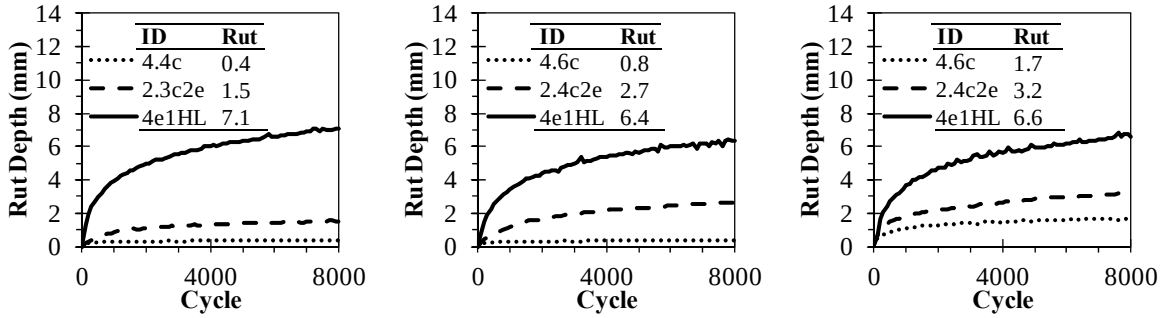


*a) R1(A/R)* *b) R3(A/R)* *c) R3(GC)*

**Figure 9.3. APA Test Results**

Based on Figure 9.4, the final $RD_{APA}$ appears to be indifferent to the load applied, which was somewhat unexpected. However, it should be noted that 55 to 65% of the total rut depth occurred by 1,000 cycles, and 0.32 mm rut per 1,000 cycles, on average, was accumulated between 2,000 and 8,000 cycles. This suggests that initial mixture densification, perhaps due to higher air voids than asphalt concrete, drives the final rut depth more than mixture rutting (defined as mixture shear failure). Further, all loads tested appeared comparable in terms of their effect on mixture densification.

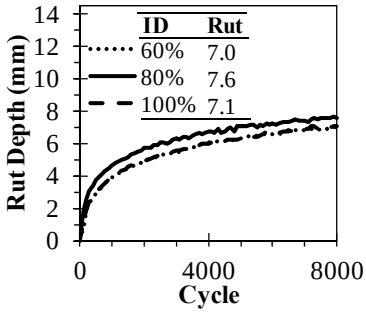


**Figure 9.4. Reduced and Full Load APA Test Results for R1(A/R)1-4e1HL**

## 9.8 Instrumented Indirect Tensile Testing

Instrumented IDT testing is described in Sections 2.9.11 and 4.5.11. Testing in this chapter was conducted at 25 °C (most intermediate temperature instrumented IDT testing was conducted at 20 °C in this report) and a load rate of 50 mm/min.

R1(A/R), R3(A/R), and R3(GC) were tested at the same three binder blends as HLWT testing. Specimens were cured 7 days. Three replicates were tested for each combination of material and binder blend. Three parameters thought to be informative for this chapter were derived from IDT testing (Table 9.1). These were tensile strength at fracture ($S_{t,f}$), horizontal strain at fracture ($\varepsilon_f$), and area under the stress-strain curve which is referred to in this chapter as a cracking index (*CI*).

*CI* is distinguished from the term FE used in later chapters primarily because of the slight differences in CIR testing protocols used in this chapter, given this chapter was an exploratory and preliminary investigation. Conceptually, *CI* and FE are identical, but the authors chose to distinguish between them in this chapter since instrumented IDT testing

protocols were still being refined at the time of this testing. As with FE, *CI* was calculated by numerical integration using Simpson's trapezoidal rule.

**Table 9.1. Average IDT Results**

| | R1(A/R) | | | R3(A/R) | | | R3(GC) | | |
|---|---|---|---|---|---|---|---|---|---|
| | **4.4c** | **2.3c2e** | **4e1HL** | **4.6c** | **2.4c2e** | **4e1HL** | **4.6c** | **2.4c2e** | **4e1HL** |
| **No. Replicates** | 6 | 6 | 6 | 6 | 5 | 6 | 2 | 5 | 6 |
| **$S_{t,f}$ (kPa)** | 476 | 293 | 354 | 433 | 221 | 339 | 221 | 154 | 303 |
| **$\varepsilon_f$ (με)** | 190 | 719 | 4289 | 248 | 1005 | 3068 | 1022 | 1069 | 4477 |
| ***CI* (kJ/m$^3$)** | 0.06 | 0.17 | 1.32 | 0.07 | 0.18 | 0.83 | 0.21 | 0.14 | 1.17 |

*-- 3 replicates were tested with 2 instrumented faces totaling 6 data points absent any testing errors.*
*-- For R3(GC)-4.6c, one specimen (two data points) broke prior to testing.*
*-- Testing errors occurred with some R3 blends. Review of data collected from these tests suggests one or more gage points may have become unbonded during testing. This incident occurred primarily with 4.6c blends (cement only), was generally a result of cemented material flaking off specimen faces.*
*-- R3(GC)-4.6c average results may be misleading given only two data points were available.*

Results show that 4.4 to 4.6c, with the exception of R3(GC)-4.6c $S_{t,f}$ and *CI*, exhibited the highest $S_{t,f}$ and lowest $\varepsilon_f$ (i.e. flexibility) and *CI*. Binder combination 4e1HL was the opposite of 4.4 to 4.6c; 2.4c2e $\varepsilon_f$ and *CI* generally fell between that of the other blends but closer to that of 4.4 to 4.6c; interestingly, 2.4c2e exhibited the lowest $S_{t,f}$. Perhaps the same issue presented in the fatigue section occurred with $S_{t,f}$ where there is an insufficient amount of either cement or emulsion, and the whole system suffers. Based on these findings, this form of IDT testing satisfies EC1 through EC4. It appears promising for CIR with multiple binder types and warrants further consideration at longer test times and with a wider range of cement and emulsion combinations.

## 9.9 Discussion of Screening Test Results

Table 9.2 presents a summary of the six performance tests currently available for traditional asphalt concrete mixtures which were evaluated for use with CIR in this chapter. For a test to be considered appealing, it must reasonably satisfy the four evaluation criteria established herein. For CIR testing conducted herein, Cantabro, BBR, and HLWT testing were least optimal, while APA and IDT testing appeared most optimal.

**Table 9.2. Summary of Performance Test Evaluation**

| | Test | | | | | |
|---|---|---|---|---|---|---|
| **Criteria** | **Cantabro** | **BBR** | **HLWT** | **Fatigue** | **APA** | **IDT** |
| EC1 | ✓ | × | ✓ | ✓ | ✓ | ✓ |
| EC2 | × | n/a | × | ● | ✓ | ✓ |
| EC3 | n/a | n/a | n/a | ● | ✓ | ✓ |
| EC4 | n/a | n/a | n/a | × | ✓ | ✓ |

*n/a = not applicable ✓ = Good ● = Moderate × = Bad*

Stresses and loads applied in traditional asphalt concrete tests may be irrelevant when testing CIR. In light of this issue, reduced loads were considered for fatigue and APA testing. Fatigue results were more informative with the reduced 445 N load; however, CIR loaded wheel fatigue testing is not believed to be optimal based on EC4.

APA results were not distinguishably different at 60 and 80% of the standard 445 N load. As stated previously, initial densification under load due to typically higher air voids than asphalt concrete appears to be a larger factor in the overall APA rut depth than shear failure of the mixture (i.e. rutting). Therefore, reduced load protocols do not appear more informative than current APA test protocols. Instead, establishing alternative maximum rut depth criteria for CIR could be more useful than reduced load protocols as this would allow CIR $RD_{APA}$'s to be directly compared to asphalt concrete $RD_{APA}$'s. Overall, APA testing satisfied all criteria and can be informative for CIR in its current state (i.e. 445 N load at 689 kPa hose pressure). IDT testing satisfied all criteria and should be further studied for CIR.

# CHAPTER 10 – CIR DENSITY CHARACTERIZATION

## 10.1 Overview of CIR Density Characterization

The key findings of this chapter have been previously published as a journal article in Issue 2444 of the Transportation Research Record: Journal of the Transportation Research Board (TRB). The original paper may be accessed at http://dx.doi.org/10.3141/2444-02. With permission from TRB, the paper (Cox and Howard, 2014) was reformatted and reproduced in Cox (2015) with minor modifications. There are no substantial differences in technical content between these three sources, though this chapter does contain a modest amount of additional information relative to the other documents.

CIR is a method which invokes mixed DOT responses. A recently-accessed FHWA survey (FHWA, 2011) where 42 DOT's responded revealed 22 states use CIR to some degree, and of those, 17 claimed to use CIR routinely or have a special provision or standard specification. Seventeen DOT's indicated they had no interest or enough concerns to prevent CIR use in the near future.

Survey results indicate CIR has merit within certain areas of pavement rehabilitation and that gaps within mix design and quality control procedures are what led to the majority of the observed criticism. This is evidenced by approximately one-third of surveyed DOT's reporting successful CIR use, but their success appears to depend largely on experience or within-state methods, not standard methods. Of the issues mentioned, density control and subsequent method variability was of particular interest for this chapter. Responses included 100% of T180 $\gamma_{d,max}$, 98% density, 94% of lab-compacted dry density, 98% of test strip density, 96% of Marshall briquette density, and 95% of Marshall density measured by vacuum sealing. Also, there were variations of these methods (e.g. 96% to 98% of test strip density). Some entities used a method-based specification, and others had no means of controlling density. Agencies would benefit both in mix design and quality control/assurance from a consistent standard for controlling density.

This chapter's objective is to present a method for controlling CIR density that is derived from volumetrics (i.e. $G_{mm}$ and $G_{mb}$) and uses vacuum sealing (i.e. CoreLok®). Vacuum sealing's simplicity, quickness, and reliability, alongside its ability to alleviate key testing issues, were the basis for its central role in the method presented. Also, vacuum sealing, with nominal effort, could be implemented in quality control/assurance programs. $G_{mm}$ is a well-accepted asphalt reference property that is independent of compaction procedures (unlike other CIR density methods). Herein, RAP $G_{mm}$ measured by ASTM D6857 (vacuum sealing method) is evaluated against AASHTO T209 (traditional method, also termed Rice gravity). An equation was developed to estimate CIR $G_{mm}$ (i.e. post binder(s) addition) using RAP $G_{mm}$ (i.e. pre binder(s) addition) and binder specific gravities (e.g. emulsion and cement) to further simplify the process. CIR $G_{mb}$ is measured by a modified version of AASHTO T331 (vacuum sealing method) and evaluated against AASHTO T166 (saturated surface dry, or SSD, method) and T269 (dimensional measurement method).

Once the CIR $G_{mm}$ equation was developed, some additional effort was put forth to investigate the robustness of the approach. This method, while not necessarily fully refined, seeks to demonstrate concept feasibility at a laboratory scale. The approach presented is currently only applicable to CIR using 100% RAP.

## 10.2 Density Characterization Laboratory Details

### 10.2.1 Materials Tested

Nine material and gradation combinations were evaluated in this chapter, the specifics of which are provided in Chapters 3 and 4. A variety of conditions were investigated to evaluate the difference in $G_{mm}$ due to, for example, physical state of RAP materials. Asphalt concrete slabs were processed in the laboratory to create: 1) loose mix (AC7 and AC8) by heating slabs until just workable, then removing saw-cut edges and separating slabs; and 2) a simulated, crushed RAP (denoted CrRAP) (CR1 or CR2) by freezing slabs overnight (saw-cut edges intact), then using a jaw crusher. CrRAP was sieved into multiple sizes for batching. R1, R3, and R4 were also evaluated in this chapter.

Note that AC8, CR2, and R4 were all taken from *Hwy 41*. R4 was sampled directly from the milling machine near the slab-cutting site to minimize material differences. As evidenced by a large asphalt content ($P_{AC}$) discrepancy, R4 greatly differed from AC8 and CR2 (also affirmed by differences in $G_{mm}$). Segregation within the milling drum is a likely explanation as there were several issues with the machine during the sampling period. The machine was repeatedly stopped and started because of mechanical issues, yet timing constraints prevented sampling postponement.

Three binder blends (Table 10.1) were used in Chapter 10 for R1(A/R) and R3(A/R). These blends were identical to those used in Chapters 8 and 9 and consisted of a cement SCB, an emulsion SCB, and a cement-emulsion MCB. Both SCB systems were used on US-49 (source of R1), and the MCB system was arbitrarily selected as a balanced blend of emulsion and cement.

**Table 10.1. Dosage Rates for CIR Blends for Density Evaluation**

| **Material** | **R1(A/R)** | | | **R3(A/R)** | | |
|---|---|---|---|---|---|---|
| **Blend** | **4.4c** | **2.3c2e** | **4e1HL** | **4.6c** | **2.4c2e** | **4e1HL** |
| Cement (%) | 4.4 | 2.3 | 0 | 4.6 | 2.4 | 0 |
| Emulsion (%) | 0 | 2 | 4 | 0 | 2 | 4 |
| Hydrated Lime (%) | 0 | 0 | 1 | 0 | 0 | 1 |

### 10.2.2 Testing Details

$G_{mm}$ RAP samples and water were mixed according to Section 4.4.1 with 6% moisture. Samples were cured in ambient laboratory conditions (Section 4.4.3.4) approximately seven days before testing.

T209 and D6857 precision statements (Table 10.2) were used as an acceptability reference. The one-sigma limit (1*s*) is the maximum allowable standard deviation of a group of results, and the difference two-sigma limit (d2*s*) is the maximum allowable difference between two test results. The maximum acceptable range of individual measurements when ten results are averaged ($Max\ Range_{10}$) is 14.1 times 1*s*. ASTM C670 (standard practice for preparing precision and bias statements) only reports a 1*s* multiplier up to ten replicates. Although these precision statements were not used according to their intended purpose, they do provide reasonable comparison boundaries for subjective assessment.

**Table 10.2. Relevant AASHTO and ASTM Precision Statements**

| Test & Type Index | AASHTO T209-05 | | | AASHTO T209-11 | | | ASTM D6857-03 | | |
|---|---|---|---|---|---|---|---|---|---|
| | **1*s*** | **d2*s*** | ***Max Range*$_{10}$** | **1*s*** | **d2*s*** | ***Max Range*$_{10}$** | **1*s*** | **d2*s*** | ***Max Range*$_{10}$** |
| Single-operator Precision (*SOP*) | 0.0040 | 0.011 | 0.056 | 0.0051 | 0.014 | 0.072 | 0.0070 | 0.020 | 0.099 |
| Multilaboratory Precision (*MLP*) | 0.0064 | 0.019 | 0.090 | 0.0084 | 0.024 | 0.118 | --- | --- | --- |

$G_{mb}$ specimens were mixed with *MC*s of 6%, 8%, or 10%, compacted to 30 or 75 gyrations, and cured using various protocols. While these variables could noticeably affect $G_{mb}$, the measurement methods of interest can measure $G_{mb}$ irrespective of the curing protocol employed.

$G_{mb}$ testing was performed using T269 and T331 as described in Section 4.4.4.2. T269 $G_{mb,wet}$ was calculated immediately after mold extrusion and converted to $G_{mb}$ using *MC*. To keep specimens intact, *MC* was estimated from *MC* vs. gyration curves which were developed in Chapter 8. A curve corresponding to each unique CIR mixture was constructed for completeness; Figure 8.1 demonstrates R3(A/R) curves, and Table 8.4 contains all data used to construct curves for other mixtures.

T331 was conducted post-curing. Depending on curing type and length, residual moisture was likely present in the specimen, resulting in a moist $G_{mb}$. Its *MC* was then measured directly to convert to dry $G_{mb}$ and obtain $V_a$. The goal of this research component was to investigate potential T331 use for moist specimens. Specimens could be moist vacuum sealed, tested if desired (e.g. indirect tensile), and then used to obtain *MC*. Recall that moisture state of a specimen (wet, moist, dry) did not meaningfully affect T331 volume measurements as described in Section 4.4.4.2.

### 10.2.3 Test Plan

Testing was divided into three components: 1) T209 (and T209$_{SSD}$) and D6857 testing to assess D6857, 2) D6857 testing to develop and refine a CIR $G_{mm}$ estimation equation, and 3) $G_{mb}$ testing to assess T331 use for moist CIR specimens. In all, 396 tests were conducted: 168 for Component 1 (i.e. pre binder(s) addition); 56 (plus 16 tests at additional cement dosages) for Component 2 (i.e. post binder(s) addition); and 156 for Component 3.

## 10.3 Test Results

### 10.3.1 RAP $G_{mm}$ Test Results

Figure 10.1 displays $G_{mm}$ test results. For T209/D6857 and T209$_{SSD}$/D6857, results from two respective data sets were combined and analyzed (e.g. 12 T209 replicates and 12 D6857 replicates). Practically, T209 and D6857 result in similar mean $G_{mm}$ values for each material (Figure 10.1a). T209$_{SSD}$ generally provides the lowest mean $G_{mm}$. For T209/D6857, $G_{mm}$ increases 0.012 and 0.010 when going from AC7 to CR1 and AC8 to CR2, respectively; however, T209$_{SSD}$ results remain practically the same.

AC8 and CR1 have very low $G_{mm}$ values with respect to the Figure 2.3 MDOT database. However, $G_{mm}$ values for all 7 materials are within the 95% confidence interval.

The database is useful in showing that such low $G_{mm}$ values exist in Mississippi which demonstrates that AC8 and CR1 results are possible.

Regarding Table 10.2, T209$_{SSD}$ and T209$_{SSD}$/D6857 are the only test categories that violate multilaboratory 1*s* limits in some way (Figure 10.1b). The current T209-11 *MLP* 1*s* is violated in only two cases. It is not surprising, though, to find more variability within dry-back procedures. In Figure 10.1c, all violations of multilaboratory d2*s* limits occur with T209$_{SSD}$ or T209$_{SSD}$/D6857 except for one case with T209/D6857 for R1(A/R) (which still does not violate the current T209-11 limit). Note again that d2*s* limits correspond to the maximum allowable difference in two results; both twelve and twenty-four results are analyzed herein. For those cases which do exceed d2*s* limits, the *Max Range*$_{10}$ limits were easily satisfied.

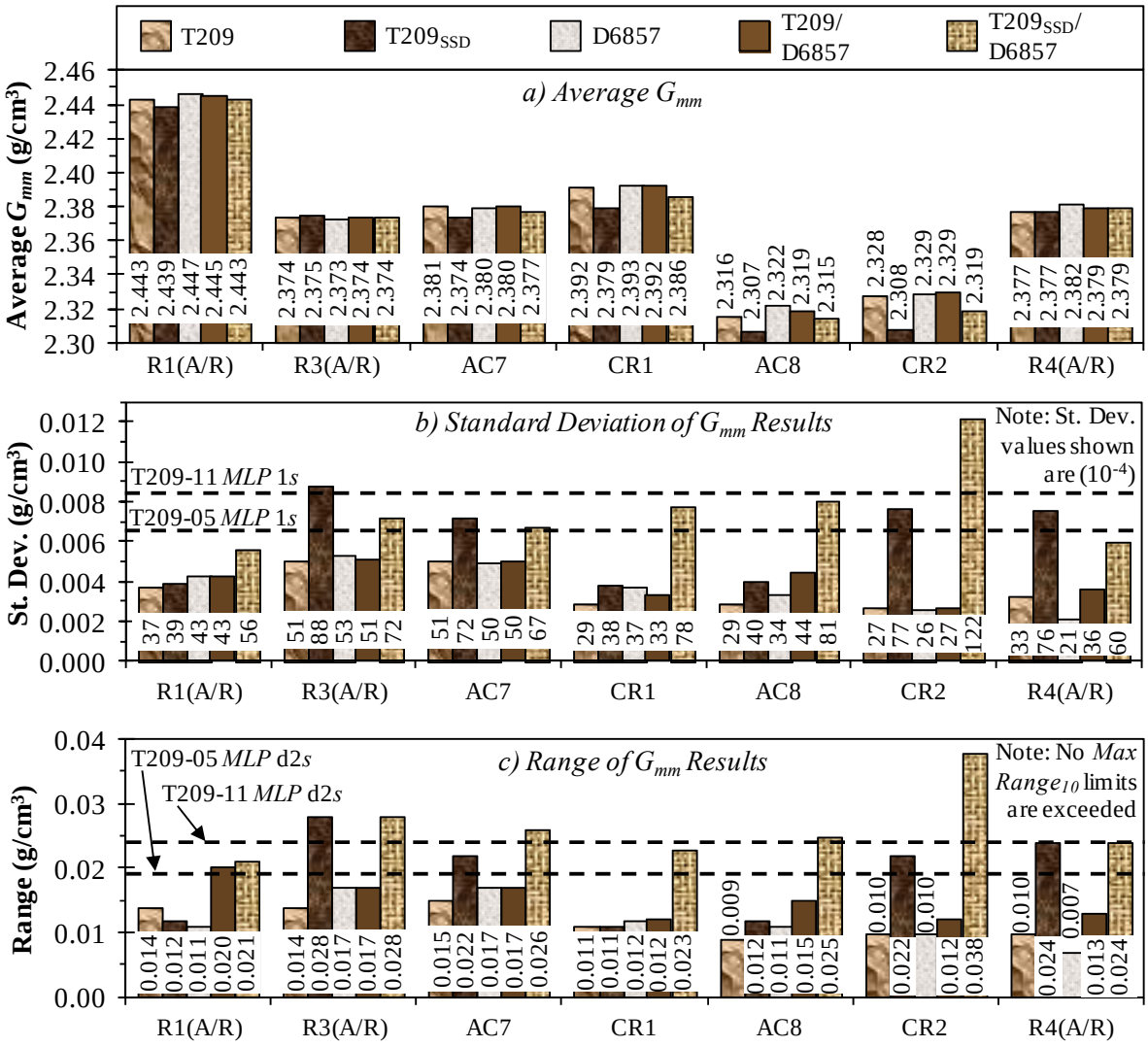


**Figure 10.1. $G_{mm}$ Test Results**

Table 10.3 shows statistical analysis. T209 and D6857 were not significantly different, except for AC8. T209$_{SSD}$ and D6857 were significantly different for all materials except R3(A/R). For *Hwy 41* and *Hwy 45*, going from AC to CrRAP yielded significantly

different results via T209 and D6857. This did not occur for *Hwy 41* $T209_{SSD}$. *Hwy 45* $T209_{SSD}$ was statistically (not practically) different from AC to CrRAP. Overall, there were some differences in measuring RAP and AC $G_{mm}$ between and sometimes within methods.

**Table 10.3. Two-Sample *t*-test Comparison of $G_{mm}$ Results**

| Material | Comparison | *n* | Mean | St. Dev. ($10^{-3}$) | *p*-value | Variances Equal?[a] | Sig. Different?[b] |
|---|---|---|---|---|---|---|---|
| R1(A/R) | T209 | 12 | 2.443 | 3.7 | 0.0502 | Yes | No |
| | D6857 | 12 | 2.447 | 4.3 | | | |
| | $T209_{SSD}$ | 12 | 2.439 | 3.9 | 0.0001 | Yes | Yes |
| | D6857 | 12 | 2.447 | 4.3 | | | |
| R3(A/R) | T209 | 12 | 2.374 | 5.1 | 0.7381 | Yes | No |
| | D6857 | 12 | 2.373 | 5.3 | | | |
| | $T209_{SSD}$ | 12 | 2.375 | 8.8 | 0.6997 | No | No |
| | D6857 | 12 | 2.373 | 5.3 | | | |
| AC7 | T209 | 12 | 2.381 | 5.1 | 0.7196 | Yes | No |
| | D6857 | 12 | 2.380 | 5.0 | | | |
| | $T209_{SSD}$ | 12 | 2.374 | 7.2 | 0.0342 | No | Yes |
| | D6857 | 12 | 2.380 | 5.0 | | | |
| CR1 | T209 | 12 | 2.392 | 2.9 | 0.4302 | Yes | No |
| | D6857 | 12 | 2.393 | 3.7 | | | |
| | $T209_{SSD}$ | 12 | 2.379 | 3.8 | <0.0001 | Yes | Yes |
| | D6857 | 12 | 2.393 | 3.7 | | | |
| AC8 | T209 | 12 | 2.316 | 2.9 | 0.0001 | Yes | Yes |
| | D6857 | 12 | 2.322 | 3.4 | | | |
| | $T209_{SSD}$ | 12 | 2.307 | 4.0 | <0.0001 | Yes | Yes |
| | D6857 | 12 | 2.322 | 3.4 | | | |
| CR2 | T209 | 12 | 2.328 | 2.7 | 0.2291 | Yes | No |
| | D6857 | 12 | 2.329 | 2.6 | | | |
| | $T209_{SSD}$ | 12 | 2.308 | 7.7 | <0.0001 | No | Yes |
| | D6857 | 12 | 2.329 | 2.6 | | | |
| R4 | T209 | 12 | 2.377 | 3.3 | 0.0007 | No | No |
| | D6857 | 12 | 2.382 | 2.1 | | | |
| | $T209_{SSD}$ | 12 | 2.377 | 7.6 | 0.0570 | No | Yes |
| | D6857 | 12 | 2.382 | 2.1 | | | |
| *Hwy 45* AC and CrRAP | T209 AC | 12 | 2.381 | 5.1 | <0.0001 | No | Yes |
| | T209 CrRAP | 12 | 2.392 | 2.9 | | | |
| | D6857 AC | 12 | 2.380 | 5.0 | <0.0001 | No | Yes |
| | D6857 CrRAP | 12 | 2.393 | 3.7 | | | |
| | $T209_{SSD}$ AC | 12 | 2.374 | 7.2 | 0.0392 | No | Yes |
| | $T209_{SSD}$ CrRAP | 12 | 2.379 | 3.8 | | | |
| *Hwy 41* AC and CrRAP | T209 AC | 12 | 2.316 | 2.9 | <0.0001 | Yes | Yes |
| | T209 CrRAP | 12 | 2.328 | 2.7 | | | |
| | T209 AC | 12 | 2.316 | 2.9 | <0.0001 | Yes | Yes |
| | T209 RAP | 12 | 2.377 | 3.3 | | | |
| | T209 CrRAP | 12 | 2.328 | 2.7 | <0.0001 | Yes | Yes |
| | T209 RAP | 12 | 2.377 | 3.3 | | | |
| | D6857 AC | 12 | 2.322 | 3.4 | <0.0001 | No | Yes |
| | D6857 CrRAP | 12 | 2.329 | 2.6 | | | |
| | D6857 AC | 12 | 2.322 | 3.4 | <0.0001 | No | Yes |
| | D6857 RAP | 12 | 2.382 | 2.1 | | | |
| | D6857 CrRAP | 12 | 2.329 | 2.6 | <0.0001 | Yes | Yes |
| | D6857 RAP | 12 | 2.382 | 2.1 | | | |
| | $T209_{SSD}$ AC | 12 | 2.307 | 4.0 | 0.8443 | Yes | No |
| | $T209_{SSD}$ CrRAP | 12 | 2.308 | 7.7 | | | |
| | $T209_{SSD}$ AC | 12 | 2.307 | 4.0 | <0.0001 | Yes | Yes |
| | $T209_{SSD}$ RAP | 12 | 2.377 | 7.6 | | | |
| | $T209_{SSD}$ CrRAP | 12 | 2.308 | 7.7 | <0.0001 | Yes | Yes |
| | $T209_{SSD}$ RAP | 12 | 2.377 | 7.6 | | | |

*a) Homogeneity of variances tested at the 95% confidence level.* --- $p_{critical} = 0.05$

*b) Significance testing performed at the 95% confidence level.*

### 10.3.2 CIR $G_{mm}$ Test Results

Table 10.4 shows D6857 CIR results. CIR differs from RAP materials discussed in the previous section in that binders (cement, emulsion, or a combination) have been incorporated. The St. Dev. and range of all results are within T209-05 multilaboratory and single-operator precision. Because of the time required to obtain $G_{mm}$ for a single CIR mixture (approximately one week of ambient laboratory curing), a simple but accurate estimation of $G_{mm}$ would be useful.

The approach used herein parallels parts of Superpave (AI, 2001). Equation 10.1 is the Superpave aggregate blending equation in general form, and Equation 10.2 was developed for determination of CIR $G_{mm}$ (identical to Equation 4.3). Equation 10.2 takes on a similar form to Equation 10.1 but was adapted to accommodate binders. In order to estimate $G_{mm}$ of a dry CIR mix, the emulsion water is treated as evaporated (i.e. only emulsion residue was included in the estimation). Conversely, some portion of mixing water is devoted to cement hydration; therefore, it permanently adds mixture mass and volume, reducing $G_{mm}$. For example, Feldman (1972) reported a specific gravity of 2.35 for fully hydrated cement. Specific gravity decrease due to hydrated water is accounted for in Equation 10.2 by the term non-evaporable water-cement ratio ($w_{NE}/cm$).

**Table 10.4. ASTM D6857 $G_{mm}$ Results for CIR Mixtures**

| Mixture | D6857 RAP $G_{mm}$ | Mean | *n* | St. Dev. | Range |
|---|---|---|---|---|---|
| R1(A/R)-4.4c | 2.447 | 2.451 | 4 | 0.0040 | 0.009 |
| R1(A/R)-2.3c2e | | 2.414 | 4 | 0.0029 | 0.006 |
| R1(A/R)-4e1HL | | 2.369 | 4 | 0.0050 | 0.011 |
| R3(A/R)-4.6c | 2.373 | 2.386 | 4 | 0.0028 | 0.006 |
| R3(A/R)-2.4c2e | | 2.344 | 4 | 0.0045 | 0.010 |
| R3(A/R)-4e1HL | | 2.303 | 4 | 0.0042 | 0.010 |
| R3(GF)-4.6c | 2.367 | 2.378 | 4 | 0.0018 | 0.004 |
| R3(GF)-2.4c2e | | 2.330 | 4 | 0.0033 | 0.007 |
| R3(GF)-4e1HL | | 2.295 | 4 | 0.0050 | 0.010 |
| R3(GC)-4.6c | 2.383 | 2.395 | 4 | 0.0051 | 0.011 |
| R3(GC)-2.4c2e | | 2.354 | 4 | 0.0051 | 0.010 |
| R3(GC)-4e1HL | | 2.314 | 4 | 0.0020 | 0.005 |

$$G_{sb} = \frac{P_1 + P_2 + \cdots + P_N}{\frac{P_1}{G_1} + \frac{P_2}{G_2} + \cdots + \frac{P_N}{G_N}} \tag{10.1}$$

Where,
$G_{sb}$ = bulk specific gravity for the total aggregate
$P_1$, $P_2$, $P_N$ = individual percentages by mass of aggregate
$G_1$, $G_2$, $G_N$ = individual (e.g. coarse, fine) bulk specific gravity of aggregate

An experiment was conducted where Type I portland cement paste (water-cement ratio of 0.5) was sealed in containers and cured on a lab bench for 1, 3, and 7 days. After curing, the container was placed in an oven overnight to determine the amount of non-evaporable water. Average $w_{NE}/cm$ for 1-, 3-, and 7-day cures (4 replicates each) was 0.13,

0.14, and 0.16, respectively. These numbers are likely higher than for CIR mixtures since CIR is not cured in a sealed container with this much free water. A $w_{NE}/cm$ of 0.10 worked well for the mixtures tested as indicated by Figure 10.2. Figure 10.2 is an equality plot of predicted vs. measured (Table 10.4) $G_{mm}$, where sum of squares error (SSE) and coefficient of determination ($R^2$) values indicate good correlation.

$$G_{mm,CIR} = \frac{1 + \left[P_{cm} + w_{NE/cm} P_{cm}\right] + P_{HL} + P_{Em} P_{Res}}{\frac{1}{G_{mm,RAP}} + \left[\frac{P_{cm}}{G_{cm}} + \frac{w_{NE/cm} P_{cm}}{G_w}\right] + \frac{P_{HL}}{G_{HL}} + \frac{P_{Em} P_{Res}}{G_b}} \quad (10.2)$$

Where,
$G_{mm,CIR}$ = estimated maximum specific gravity for the CIR mixture
$P_{cm}$ = percent of cement by mass of RAP
$w_{NE}/cm$ = non-evaporable water-cement ratio
$P_{HL}$ = percent of hydrated lime by mass of RAP
$P_{Em}$ = percent of emulsion by mass of RAP
$P_{Res}$ = percent of asphalt residue by mass of emulsion
$G_{mm,RAP}$ = D6857 maximum specific gravity of RAP
$G_{cm}$ = specific gravity of portland cement
$G_w$ = specific gravity of water = 0.997 g/cm$^3$ at 25 °C
$G_{HL}$ = specific gravity of hydrated lime
$G_b$ = specific gravity of asphalt binder

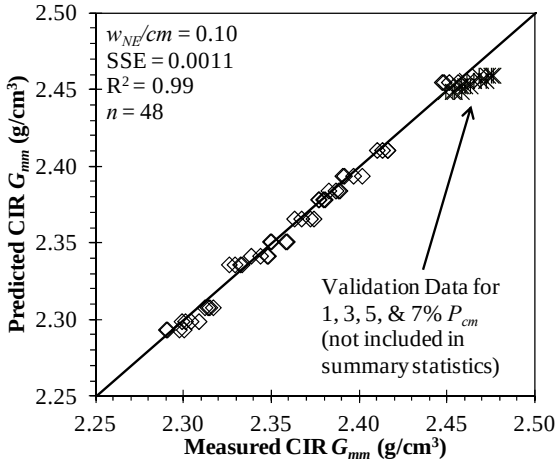


**Figure 10.2. Predicted vs. Measured CIR $G_{mm}$**

A second experiment was conducted to validate Equation 10.2 and the 0.10 $w_{NE}/cm$ value for a wide range of cement contents. Four replicates of R1(A/R) with $P_{cm}$ of 1, 3, 5, and 7% were tested by D6857. The average predicted minus measured $G_{mm}$ values for the 1, 3, 5, and 7% cement mixtures were 0.005, 0.007, 0.011, and 0.014, respectively. The $w_{NE}/cm$ component discussed thus far likely has room for improvement, but the concept is promising, reasonable, and appears implementable based on Figure 10.2. As discussed later in this chapter, some efforts to improve $w_{NE}/cm$ occurred later in State Study 250 (i.e. after Equation 10.2 was developed).

### 10.3.3 CIR $G_{mb}$ Test Results

Figure 10.3a shows that, on average, T269 air voids were 1.1% greater than T331. Howard and Doyle (2014) found that $V_{a(T269)}$ minus $V_{a(T331)}$ ranged from 0.9 to 2.6% for air voids of 4 to 10%. CIR $V_{a(T269)}$ minus $V_{a(T331)}$ was on the lower end of this range despite air voids ranging from approximately 18 to 28%. Bang et al. (2011) noted the SGC typically produced smooth sides on CIR specimens; reducing surface texture reduces the difference between $V_{a(T269)}$ and $V_{a(T331)}$. Figure 10.3a indicates T269 and T331 have relationships on the order of those observed by Howard and Doyle (2014) when measured in a moist condition (*MC* ranged 0.1 to 6.9%) and converted to dry $G_{mb}$ values. Figure 10.3b demonstrates that the relationship between T269 and T331 is similar regardless of gyration level.

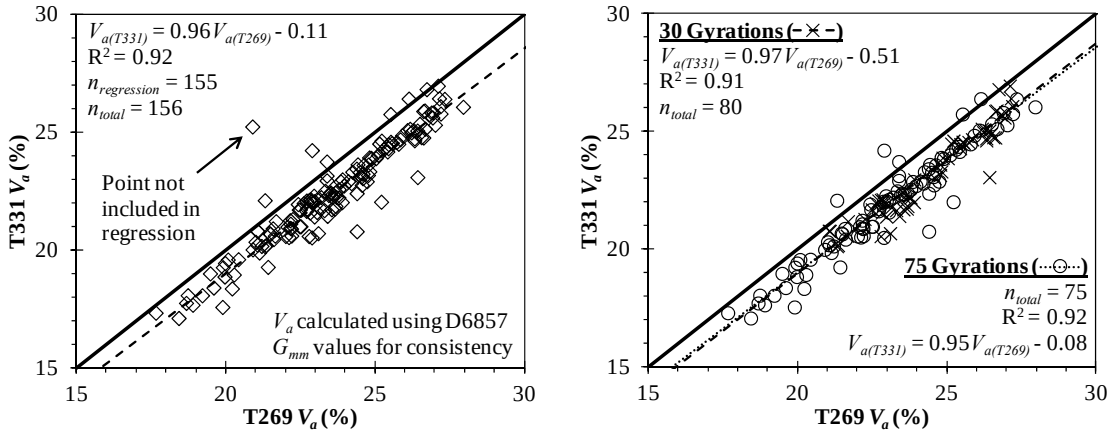


*a) 30 and 75 Gyration Data Combined* *b) 30 and 75 Gyration Data Separated*

**Figure 10.3. Air Voids Equality Plot Using T331 and T269 $G_{mb}$ Data**

## 10.4 Discussion of Results

RAP $G_{mm}$ test data indicates T209 and D6857 yield practically and statistically similar results. This is supported by AASHTO and ASTM precision statements (Table 10.2). *Hwy 45* and *Hwy 41* results confirm there are significant differences between $G_{mm}$ of AC and CrRAP. As recommended by Sholar et al. (2005), data indicates a dry-back procedure alleviates this difference. Obtaining dry-back results for D6857, however, is likely problematic. It is difficult to remove all material from a vacuum sealing bag, though it is a critical aspect of the dry-back procedure. Even though the dry-back procedure cannot be easily performed with D6857, it still has advantages over T209 in that it requires approximately 17 fewer minutes per test, and fines loss in the water bath is more easily controlled.

Additionally, the error caused by not performing the dry-back procedure for CrRAP or RAP is small relative to other variability factors currently within CIR. For *Hwy 45* D6857 results, the change in $G_{mm}$ from AC to CrRAP is 0.012. For *Hwy 41* D6857 results, the change in $G_{mm}$ from AC to CrRAP (AC to RAP is not discussed due to $G_{mm}$ discrepancies) is 0.010. The inherent difference in $G_{mm}$ when testing RAP instead of AC would result in increased air voids for a compacted mixture with a fixed $G_{mb}$. For a $G_{mb}$ of 1.937 (corresponding $G_{mb}$ for lowest Figure 10.2 $V_a$ value), an increase in RAP $G_{mm}$ of 0.012 from 2.380 to 2.392 (CIR $G_{mm}$ increase would be slightly less than 0.012) yields a $V_a$ increase of

0.41%. Likewise, evaluating 127 data points from (Bang et al., 2011) indicates a similar 0.012 $G_{mm}$ increase yields a $V_a$ increase of 0.35 to 0.50%. This difference in $V_a$ as a consequence of measuring $G_{mm}$ of RAP instead of AC appears manageable for CIR density control, especially since it seems to consistently increase calculated air voids.

Equation 10.2 provides reasonable CIR $G_{mm}$ predictions based on data presented herein. Equation 10.2 assumes RAP does not absorb any of the virgin binders into its pores and that the cement hydration process does not create inaccessible pore space (i.e. the volume considered in $G_{mm}$ measurement remains constant). It also assumes that no cement paste volume change occurs during hydration. All of these assumptions are probably violated to some extent, but none of the data indicates that use of these assumptions meaningfully affects results. Validation data indicates $w_{NE}/cm$ may not be constant for all cement dosages. Errors due to an incorrect $w_{NE}/cm$ appear manageable, and the following paragraphs describe additional efforts performed in this report to investigate Equation 10.2, $w_{NE}/cm$ in particular.

Two additional experiments were performed to further investigate $w_{NE}/cm$. First, a follow-up cement past experiment was conducted similar to the first except cure times were 120 and 360 days to approximate the upper end potential for $w_{NE}/cm$. Average $w_{NE}/cm$ at 120 and 360 days was 0.22 and 0.33, respectively.

Second, additional CIR D6857 testing was conducted with laboratory-crushed R3(A/R) and R4(A/R) at multiple cement contents (2, 4, and 6%) and cure times (3, 7, 14, 28, 56, and 120 days of ambient laboratory curing) to investigate $w_{NE}/cm$ trends. Paired testing was conducted for laboratory-crushed R3(A/R) where each $G_{mm}$ sample was mixed and then split; half was SGC compacted to 30 gyrations and humid oven cured, while the other half was ambient laboratory cured in a loose state. Paired testing was conducted to determine effects, if any, of measuring $G_{mm}$ on compacted then broken up samples.

Key findings from this experiment are as follows. Compacted then broken up $G_{mm}$ was 0.006 g/cm$^3$ lower on average than loose-cured $G_{mm}$, which is likely because compacted specimens are fairly difficult to fully break up to the extent they resemble loose-cured samples. This difference is not practically meaningful. Increasing cement content from 2 to 4 and 4 to 6% increased $G_{mm}$ by 0.010 and 0.015 g/cm$^3$, respectively. $G_{mm}$ trends over time were not apparent; any changes in $G_{mm}$ appeared due to test variability as all results for a given material and cement content were well within Table 10.2 $Max\ Range_{10}$ limits. Likewise, trends with respect to $w_{NE}/cm$ were not clearly evident. Therefore, at present, no changes to the $w_{NE}/cm$ of 0.10 are recommended.

Based on literature, T166 use for CIR is difficult to justify. However, both T269 and T331 appear to be feasible for high $V_a$ mixtures (e.g. most CIR mixtures). The ability to vacuum seal moist specimens would allow for both $G_{mb}$ and another property (e.g. $S_t$ or UCS) to be measured on one specimen.

## 10.5 Summary and Key Density Characterization Findings

CIR variability appears at least partly due to lack of standard and reliable density control methods. $G_{mm}$ and $G_{mb}$ have remained largely undisputed as reliable means of determining asphalt concrete density. Based on the data presented, CIR would also benefit from their use as $G_{mm}$ provides a consistent reference density and $G_{mb}$ encompasses the intent of other common bulk density properties in use (e.g. $\gamma_d$). $G_{mm}$ differences for AC and RAP do not appear significant enough to discourage the use of RAP $G_{mm}$ as a reference density.

Vacuum sealing is recommended for determination of CIR $G_{mm}$ where 100% RAP is used. For RAP $G_{mm}$, it provides at least as reliable measurements as T209 but with greater ease and less time. Differences between AC and RAP $G_{mm}$ are consistent between D6857 and T209. Directly measuring $G_{mm}$ of loose CIR mixtures (as opposed to compacted then broken up mixtures) is most reliable but is more difficult. The proposed CIR $G_{mm}$ estimation equation appears reasonable and efficient, though the $w_{NE}/cm$ concept might be improved.

Given the typically high CIR $V_a$ levels from literature, $G_{mb}$ measurement with T269 or T331 is more appropriate than T166. While T331 is recommended for most accurate results, T269 is more efficient and cost-effective and, because of the relatively consistent offset between the two methods, could be used almost interchangeably with T331. This chapter's findings indicate determining CIR $G_{mm}$ and $G_{mb}$, as determined by the CoreLok and Equation 10.2, comprise a reliable, convenient, and implementable approach to controlling density and likely reducing performance variability. This approach's ease could accommodate more frequent field testing to better control density longitudinally as material change in the direction of traffic has been a notable hindrance to previous density control measures.

# CHAPTER 11 – CIR EARLY-AGE AND CURING INVESTIGATION

## 11.1 Overview of the Early Age and Curing Investigation

To further understand how to continue improving CIR for existing applications, and expand to new applications, better techniques are needed with regard to interfacing design and construction. Moisture is one key area where design and construction are often disconnected. To this end, this chapter's primary objective is to evaluate moisture and associated early-age strength/stability aspects of CIR with the intention of better representing actual construction conditions during design within a framework that can consider hydraulic cement, bituminous emulsion, or combinations of both binders. A universal CIR design framework that can accommodate any binder or combination of binders while representing early-age field conditions has advantages for an agency, not only in its reasonable characterization of the construction process, but also in facilitating competition and creativity in the process of selecting materials and proportions. One secondary objective of this chapter is to provide early age strength data in a variety of manners for better overall understanding of the subject.

A major component of the overall framework presented in State Study 250 is provision for both SCB systems (cementitious *or* bituminous) and MCB systems (cementitious *and* bituminous). In a universal framework like the one envisioned in this study, moisture must be more carefully considered since moisture effects on performance properties are ordinarily different between cementitious and bituminous binders. Generally, laboratory design protocols favor either binder's performance with respect to moisture considerations. In the context of universal design, more appropriate moisture-related laboratory procedures may perhaps be those which represent field conditions (i.e. moisture conditions not necessarily optimal for any binder type). In light of the larger research goal, another secondary objective of this chapter is to evaluate CIR moisture from a balanced perspective considering both cementitious and bituminous binders.

Results from this chapter are presented in four phases. Phase 1 details the instrumentation and field monitoring of the US-45Alt cement CIR project described in Section 5.3. Phase 2 evaluates moisture's role during compaction using US-45Alt data to provide guidance on laboratory moisture content (*MC*) selection methods, particularly those which traditionally yield high *MC*s (e.g. Proctor methods). Phase 3 evaluates moisture during curing using US-45Alt field data alongside laboratory evaluation of multiple curing protocols using R1 and R2 (i.e. the two CIR project materials). Phase 4 details a laboratory-focused early-age strength investigation in which several small experiments were conducted with R2.

## 11.2 Phase 1: US-45Alt Instrumentation and Field Monitoring

During construction, US-45Alt was instrumented with Ruggedized GS3 sensors as described in Section 5.3.2.3. Following construction, US-45Alt was monitored through 14 days of curing. During and after construction, GS3 instrumentation data was recorded, and multiple samples and cores were attained and tested in the laboratory.

Figure 11.1 presents unprocessed GS3 data in the form of analog-to-digital counts (ADC). Figure 11.1a plots vertical lines for each roller pass crossing GS3 sensors during construction. In all, 46 roller passes were required to attain 1879 kg/m$^3$ dry density by *NG*.

This number of roller passes is not likely to occur throughout CIR projects on a widespread scale, and it should be noted that less compactive effort is likely on most projects. For comparison, laboratory SGC compaction presented in Phase 4 (Section 11.5) required 43 gyrations, on average, to reach field densities. Field densities were recorded after each roller pass except for some cases where consecutive passes were insufficiently spaced to facilitate a reading.

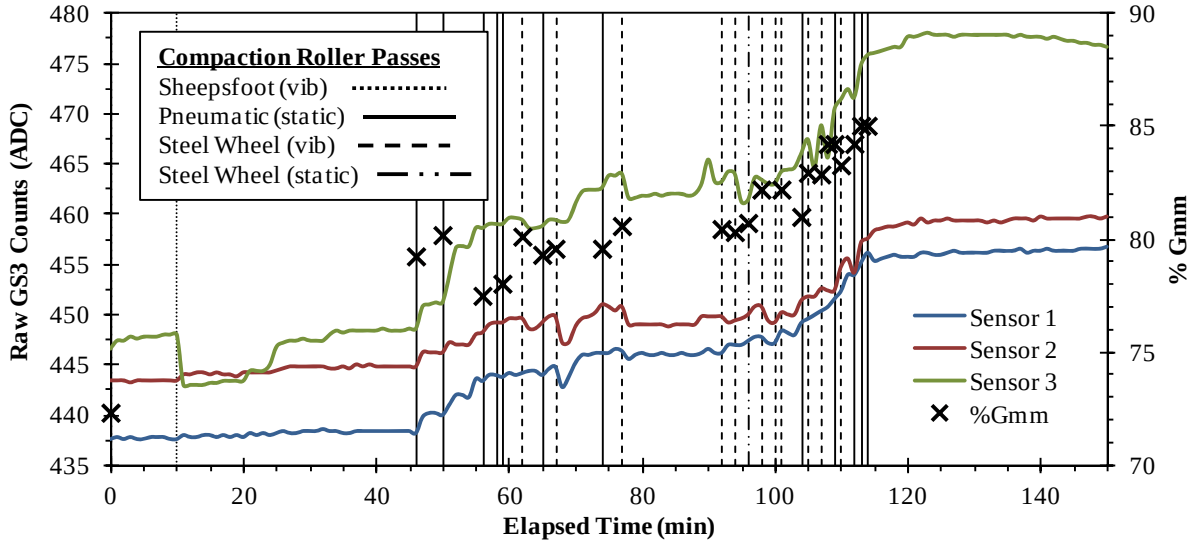


*a) Unprocessed GS3 Data During Compaction Alongside Roller Passes and Corrected NG Densities*

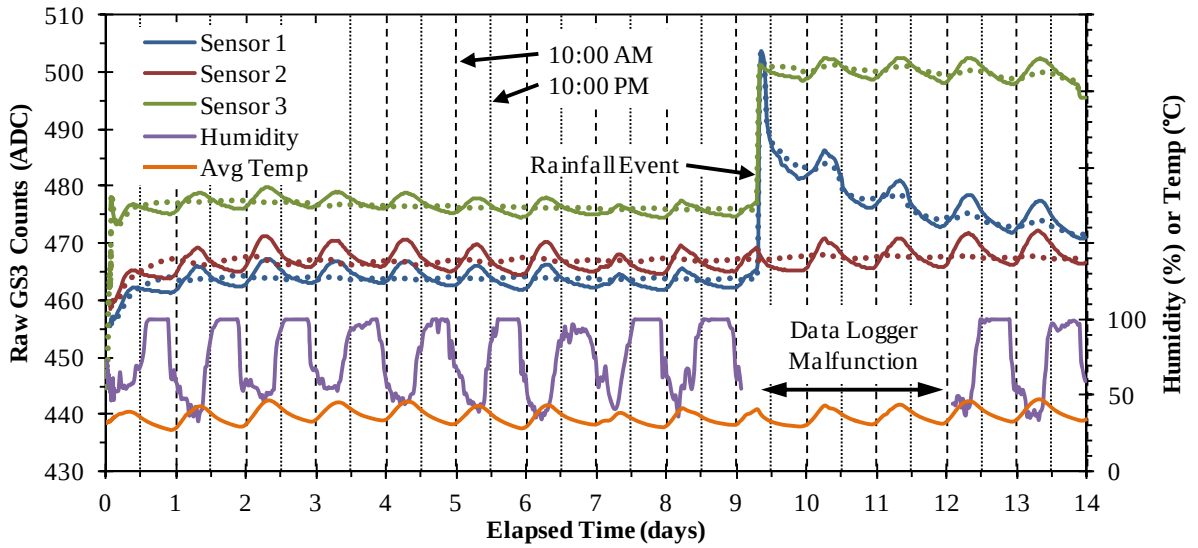


*b) Unprocessed GS3 Data During 14-Day Curing Period Alongside Temperature and Humidity*

**Figure 11.1. Unprocessed GS3 Moisture Data from US-45Alt**

The final *NG* density was 1885 kg/m$^3$; however, laboratory-measured dry density of cores averaged 2026 kg/m$^3$. Therefore, all *NG* densities were corrected by a simple offset factor of 141 kg/m$^3$. Corrected densities are plotted in Figure 11.1a as a percentage of $G_{mm}$. Final densities were 85% of $G_{mm}$, or 15% $V_a$. Figure 11.1a shows GS3 readings are directly proportional to roller passes and *NG* density changes.

Figure 11.1b presents GS3 raw data and temperature as well as ambient humidity throughout the first 14 days of curing. Oscillations corresponding to daily temperature fluctuations are observed in GS3 data. Similar oscillations were also observed in Lee et al. (2009), Kim and Lee (2011b), and Woods et al. (2012). Temperature corrections were applied according to Equation 11.1, which is similar to electrical conductivity temperature corrections in Kizito et al. (2008). Attempts were made to systematically determine the fitted constant in Equation 11.1 ($\beta$), but no trends were observed. Instead, $\beta$ was adjusted for each sensor until smoothing of the oscillations was visually optimized. Temperature-corrected readings are depicted by dotted lines in Figure 11.1b.

$$GS3_{i,corrected} = GS3_i + \beta \times \left(T_r - T_i\right) \tag{11.1}$$

Where,
$GS3_{i,corrected}$ = temperature-corrected GS3 reading at time $i$, ADC
$GS3_i$ = observed raw GS3 reading at time $i$, ADC
$\beta$ = fitted constant (0.31, 0.40, and 0.24 for sensors 1, 2, and 3, respectively)
$T_r$ = reference temperature, °C (14-day average GS3 temperature = 35.8 °C)
$T_i$ = temperature at time $i$, °C

As in Lee et al. (2009), Kim and Lee (2011b), and Woods et al. (2012), GS3 sensors detected rainfall. Sensor 2's location did not appear infiltrated by water based on Figure 11.1b. Water appeared to infiltrate sensor 1's location but was able to drain over time. Water appeared to infiltrate sensor 3's location but was not able to drain well. Aside from rainfall, the most notable change in GS3 readings occurred within 24 hours after construction and is thought to be related to cement setting reactions.

To calibrate raw GS3 output to *MC*, raw GS3 readings were converted to bulk dielectric permittivity ($\varepsilon_{bulk}$) using calibration data supplied by Decagon. Observed raw GS3 readings ranged from 430 to 510 ADC; in this range, a second-order polynomial described the ADC-to-dielectric relationship (Equation 11.2) satisfactorily ($R^2 = 0.999$).

$$\varepsilon_{bulk} = 8.8\times10^{-5}\left(GS3_{i,corrected}\right)^2 - 2.4\times10^{-2}\left(GS3_{i,corrected}\right) - 1.68 \tag{11.2}$$

The complex refractive index model (CRIM) (Leng, 2011) was used to derive *MC* from $\varepsilon_{bulk}$. Essentially, CRIM (Equation 11.3) calculates weighted averages of a certain power of constituent material dielectric constants based on volume proportions. Volumetric equations (discussed further in Phase 2 results) were substituted to obtain Equation 11.4. Rearranging for *MC* yields Equation 11.5.

$$\varepsilon_{bulk}^{\,1/\alpha} = \varepsilon_{CIR}^{\,1/\alpha} V_{CIR} + \varepsilon_{water}^{\,1/\alpha} V_{water} + \varepsilon_{air}^{\,1/\alpha} V_{air} \tag{11.3}$$

$$\varepsilon_{bulk}^{\,1/\alpha} = \varepsilon_{CIR}^{\,1/\alpha} \frac{G_{mb}}{G_{mm}} + \varepsilon_{water}^{\,1/\alpha} \frac{G_{mb}\omega}{G_w} + \varepsilon_{air}^{\,1/\alpha} \left(1 - \frac{G_{mb}}{G_{mm}} - \frac{G_{mb}\omega}{G_w}\right) \tag{11.4}$$

$$\omega = \frac{G_w\left(\varepsilon_{bulk}^{1/\alpha} - \varepsilon_{CIR}^{1/\alpha}\frac{G_{mb}}{G_{mm}} - \varepsilon_{air}^{1/\alpha}\left(1-\frac{G_{mb}}{G_{mm}}\right)\right)}{G_{mb}\left(\varepsilon_{water}^{1/\alpha} - \varepsilon_{air}^{1/\alpha}\right)} \quad (11.5)$$

Where,
$\alpha$ = empirical power parameter equal to 2 in CRIM
$\varepsilon_{CIR}$ = CIR dielectric constant
$V_{CIR}$ = CIR volume fraction
$\varepsilon_{water}$ = dielectric constant of water (74.7 at $T_r$)
$V_{water}$ = water volume
$\varepsilon_{air}$ = dielectric constant of air (1)
$V_{air}$ = air volume (equal to $V_a$ if $V_{water}$ is zero)
$G_{mb}$ = bulk mixture specific gravity
$\omega$ = gravimetric moisture content (also, $MC$)
$G_w$ = water specific gravity (0.994 at $T_r$)

In Equation 11.5, $\varepsilon_{CIR}$ is unknown; however, since $MC$ and $G_{mb}$ are known where direct $MC$s were obtained (i.e. where cores were obtained at 1, 3, 7, and 14 days), $\varepsilon_{CIR}$ can be iteratively estimated. Excel's Solver function was used to calculate $\varepsilon_{CIR}$ for each GS3 (note that, because $\varepsilon_{water}$ and $G_w$ are temperature-dependent, their values at $T_r$ were used). For sensors 1 to 3, $\varepsilon_{CIR}$ was 2.77, 2.88, and 3.53, respectively. Although $\varepsilon_{CIR}$ would generally be constant, using best-fit $\varepsilon_{CIR}$ values was deemed reasonable since $\varepsilon_{CIR}$ for each sensor was fit to field average direct $MC$ measurements. With $\varepsilon_{CIR}$ estimated, $MC$ was calculated where $G_{mb}$ was known.

A separate laboratory calibration experiment was also conducted in attempts to determine $\varepsilon_{CIR}$ through another means. A slot was machined into a 150 mm diameter SGC compaction mold (Figure 11.2a) so that a GS3 sensor could be compacted into CIR specimens. A sheet metal bracket (Figure 11.2b) was fabricated to aid in holding the GS3 in the center of the mold (Figure 11.2c) while allowing vertical travel and also protection of the cable. The GS3 was placed at the mid-depth of material in the mold and then compacted. Figure 11.2d shows a GS3 compacted inside a CIR specimen (top half of the specimen was removed to reveal GS3).

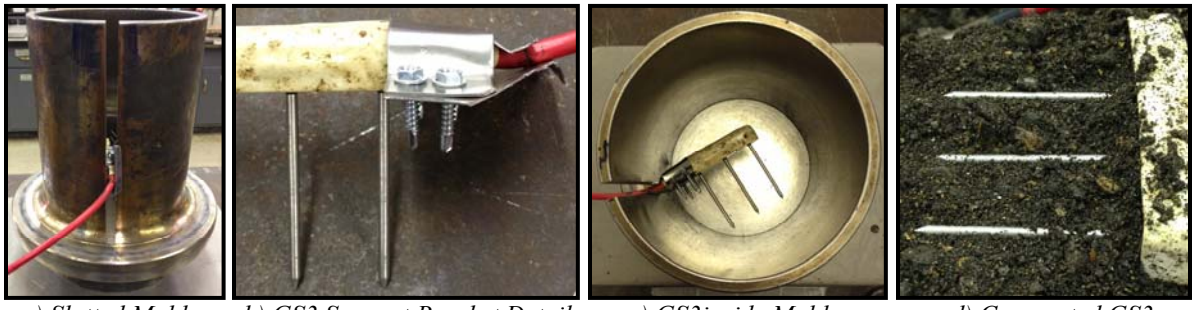

*a) Slotted Mold* *b) GS3 Support Bracket Detail* *c) GS3inside Mold* *d) Compacted GS3*

**Figure 11.2. GS3 Laboratory Calibration Experiment Photographs**

Multiple variations of $MC$ and $N_{gyr}$ were investigated. Results for trials with R2(A/R)-4.2c compacted at 8.2% $MC$ and 43 gyrations are presented herein. Three replicates were

tested; each replicate was tested twice. Compacted density was estimated accounting for GS3 volume, a GS3 raw reading was obtained, and then compacted *MC* was measured using material surrounding the GS3. This process was repeated a second time for each replicate without adding additional moisture. Data was input into Equation 11.5, and the best-fit $\varepsilon_{CIR}$ was iteratively determined to be 3.88, which was slightly higher than field-calibrated values which ranged from 2.77 to 3.53. Using the laboratory-determined $\varepsilon_{CIR}$ of 3.88 would result in reported GS3 *MC*s being approximately 1.1% lower. Ultimately, the laboratory calibration did not provide additional clarity, and the authors elected to use field-calibrated $\varepsilon_{CIR}$ values.

Figure 11.3 presents processed GS3 data. Figure 11.3a shows GS3 *MC* was, for all meaningful purposes, constant during compaction despite *MC* immediately before compaction being 8.2%. Figure 11.1a unprocessed data appeared to increase during compaction, but Figure 11.3a indicates these increases were related to density changes (accounted for in Equation 11.5) rather than *MC* changes.

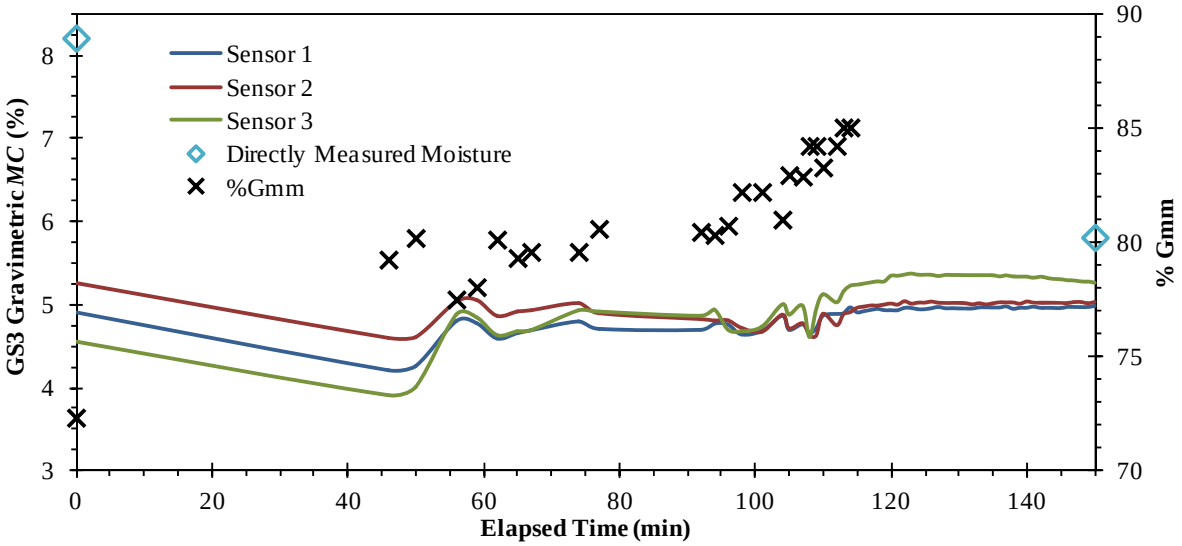


*a) GS3 Gravimetric Moisture Data During Compaction Alongside Corrected NG Densities*

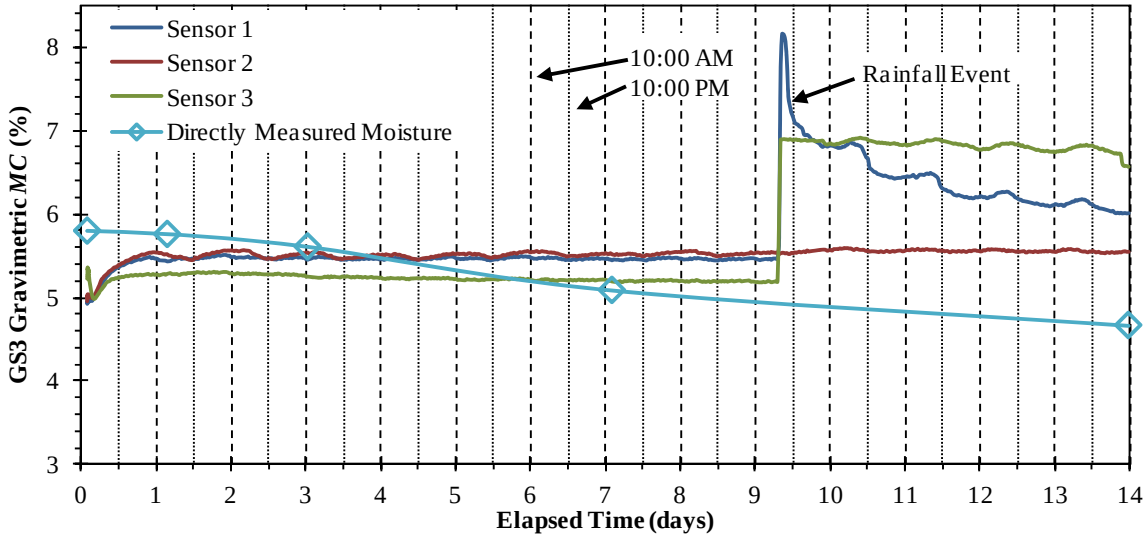


*b) GS3 Gravimetric Moisture Data During 14-Day Curing Period Alongside Core Properties*

**Figure 11.3. Processed GS3 Moisture Data from US-45Alt**

Figure 11.3b shows GS3 *MC*, which was mostly constant through curing (excluding exceptions previously mentioned) and did not follow *MC*s directly measured on cores. GS3 measurement radius is approximately 2 cm, meaning GS3 data represented the middle 4 cm of the 20 cm layer; whereas, directly-measured *MC*s nearly represented the entire layer. Therefore, directly-measured *MC*s may have been affected by drying near the layer's surface which was outside GS3 measurement range.

Recall from Section 5.3.3.2 that intact 0-day cores for *MC* measurements were not successfully obtained. Coring attempts broke the freshly-compacted layer into loose mix, and heat produced in coring appeared to dry the mix, yielding an average 4.8% *MC*, which was on the order of *MC* measured at 14 days. Alternatively, a third-order polynomial was fit to 1- to 14-day *MC*s ($R^2 > 0.99$), and the 0-day (0.079 days actual) *MC* was calculated to be 5.8%. Given the small change in *MC* over 14 days, omitting the 0-day *MC* only affected GS3 *MC* calibrations by 0.1 to 0.2%; therefore, this approach seemed reasonable.

Table 11.1 provides results of US-45Alt field testing. UCS and $S_t$ did not progressively increase with time, which appears partly due to $V_a$ variability. An analysis of variance (ANOVA) determined $V_a$'s were statistically different between coring lanes (marked in the transverse direction on Figure 5.12f). Therefore, SGC-compacted UCS versus $V_a$ data (Figure 11.9) was used to normalize $V_a$ effects. SGC-compacted UCS versus $V_a$ data is summarized by Equation 11.6 ($R^2 = 0.99$) where UCS output is in kPa. Relative correction factors (*CF*) were determined based on the difference between Table 11.1 $V_a$'s and US-45Alt's overall average $V_a$ of 15.5%. For example, Equation 11.6 produces a UCS of 2,670 kPa at 15.5% $V_a$ and a UCS of 3,200 kPa at 13.7% $V_a$, which results in a *CF* of 16.5%, or (1-2670/3200) times 100%, for Table 11.1's 3-day UCS value (i.e. UCS needed to be reduced 16.5%). Corrected UCS values ($UCS_{corr}$) were calculated by adjusting UCS by the relative *CF* percentage. Although fairly approximate, $S_t$ values were corrected ($S_{t,corr}$) using the same procedure since no laboratory IDT testing was available to perform corrections.

$$UCS = 24.3 \times V_a^{\,2} - 1004 \times V_a + 12394 \tag{11.6}$$

**Table 11.1. Results of US-45Alt Field Core Testing**

| | Cure Time (days) | | | |
|---|---|---|---|---|
| **Property** | **1** | **3** | **7** | **14** |
| Avg *MC* (%) | 5.8 | 5.6 | 5.1 | 4.7 |
| UCS (kPa) | --- | 2410 | 3050 | 1910 |
| $V_a$ (%) | --- | 13.7 | 13.5 | 16.7 |
| *CF* (%) | --- | 16.5 | 18.3 | -11.0 |
| $UCS_{corr}$ (kPa) | --- | 2010 | 2500 | 2120 |
| $S_t$ (kPa) | 359 | 565 | 262 | 372 |
| $V_a$ (%) | 16.0 | 14.6 | 17.0 | 16.8 |
| *CF* (%) | -4.7 | 8.4 | -13.7 | -11.9 |
| $S_{t,corr}$ (kPa) | 375 | 518 | 298 | 417 |

## 11.3 Phase 2: Moisture Considerations during Compaction

Phase 2 uses data presented in Phase 1 and discusses implications of moisture during compaction. Figure 11.3a shows directly-measured *MC* dropped from 8.2% to 5.8% during compaction. This agrees with findings in Chapter 8. For example, *MC* dropped from 7.9% to 5.5% for R1(A/R)-4.4c when SGC-compacted to 30 gyrations.

For practical purposes, GS3 *MC*s did not change during compaction and were around 5%, which is slightly lower when compared to directly-measured *MC*s. Regardless, GS3 *MC* slopes are flat, suggesting a considerable amount of moisture was expelled early during compaction. GS3 data aligns with findings in Chapter 8 that *MC* was greatly reduced early in SGC compaction, suggesting this trend is also applicable to field compaction.

Figure 11.4 presents an idealized phase diagram to volumetrically investigate compactibility as a function of *MC*. Consider US-45Alt's initial 8.2% *MC*. Suppose the weight of CIR ($W_{CIR}$) is 100 g (41.9 cm$^3$ with 2.384 $G_{mm}$), then weight of water ($W_w$) equals 8.2 g (approximately 8.2 cm$^3$). If 100% saturation is assumed during compaction (i.e. all voids between CIR particles are water-filled), 16.4% of the total volume ($V_{total}$) would be water, which, from a dry density perspective, would correspond to 16.4% air volume ($V_{air}$). Therefore, the minimum achievable $V_a$ is 16.4% if *MC* truly remains at 8.2% throughout compaction and 100% saturation is assumed. However, US-45Alt $V_a$'s averaged 15.5% and were as low as 13.5%, which would not be possible unless water was expelled during compaction.

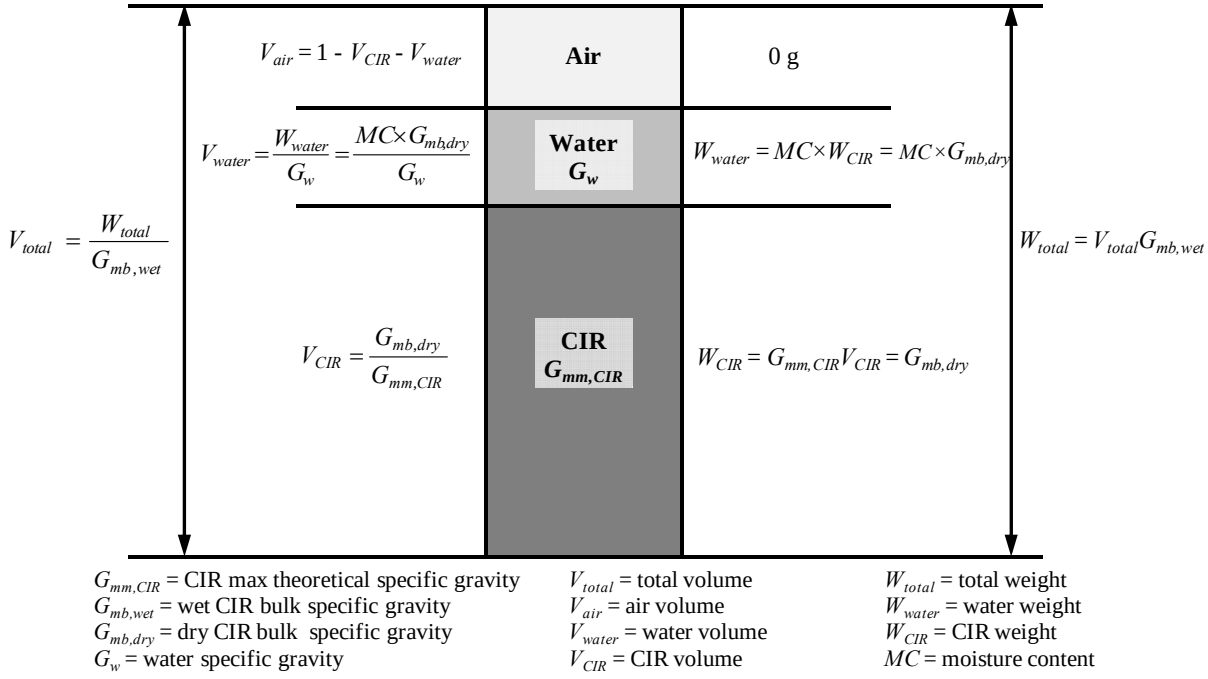


**Figure 11.4. CIR Phase Diagram**

From a different perspective, the maximum allowable *MC* to permit 15.5% average $V_a$ would be 7.7% (6.5% for the lowest-observed 13.5% $V_a$ value) under the ideal 100% saturation assumption. As a reference, additional analysis of data used in Chapter 8 showed saturation values immediately following SGC compaction generally ranged from 50 to 60%. Although field and laboratory saturation levels likely differ, the exercise provides insight to reasonable degrees of saturation to be expected. Therefore, with saturation values likely closer to 50 to 60% rather than 100%, the 5.8% directly-measured *MC* after compaction does not appear unreasonable.

Other caveats must also be considered. For example, it is almost certain some moisture would be present in the pavement prior to reclamation. Most of this moisture would

exist in the void structure, but some may be absorbed into RAP pores (i.e. volume considered within $G_{mm}$). This would effectively open voids in the mixture, potentially allowing it to take on slightly more water for a given $V_{air}$ than volumetrics might indicate. Effects of these factors are likely small and, for the calculations herein, would be offset by errors with the 100% saturation assumption, suggesting the phase diagram remains a useful theoretical or estimation tool. Ultimately, phase diagram and US-45Alt findings generally agree with Chapter 8 in discouraging the need for Proctor-level *MC*s for CIR compaction, consequently supporting standardized-*MC* practices as in Mamlouk and Ayoub (1983), Khosla and Bienvenu (1996), and Kim et al. (2011).

## 11.4 Phase 3: Moisture Considerations during Curing

### 11.4.1 Phase 3 Materials Tested

In addition to field curing data collected on US-45Alt in Phase 1, R1 (RAP from US-49 CIR project) and R2 (RAP from US-45Alt CIR project) were tested in the laboratory in Phase 3. Three binder blends were tested for each RAP source (Table 11.2) and included a cement SCB, an emulsion SCB, and a balanced cement-emulsion MCB. The R1 cement (4.4c) and emulsion (4e1HL) SCBs were the same as those used on US-49; the R2 cement SCB (4.2c) was that used on US-45Alt. The R1 emulsion SCB dosages were also used for the R2 emulsion SCB. The R1 MCB (2.5c2e) was the same as that used later in Chapter 13, and the R2 MCB (2.1c2e) was obtained by balancing cement and emulsion SCBs. The R2(A/R)-4.2c mixture was tested with and without the AE-P prime coat applied at a rate of 0.91 L/m$^2$.

**Table 11.2. CIR Blends Tested**

| **Material** | **R2(A/R)** | | | | **R1(A/R)** | | |
|---|---|---|---|---|---|---|---|
| **Blend** | **4.2c** | **4.2c*** | **2.1c2e** | **4e1HL** | **4.4c** | **2.5c2e** | **4e1HL** |
| Cement (%) | 4.2 | 4.2 | 2.1 | 0 | 4.4 | 2.5 | 0 |
| Emulsion (%) | 0 | 0 | 2 | 4 | 0 | 2 | 4 |
| Hydrated Lime (%) | 0 | 0 | 0 | 1 | 0 | 0 | 1 |
| Water (%) | 8.2 | 8.2 | 8.2 | 8.2 | 6.0 | 6.0 | 6.0 |
| Prime Coat Applied? | No | Yes | No | No | No | No | No |

*-- Note that (A/R) denotes the as-received gradation for a given RAP source. Recall from Chapter 3 that R1 and R2, though both tested at the as-received gradation, had difference as-received gradations.*

### 11.4.2 Phase 3 Laboratory Testing Details

Two curing experiments were conducted in Phase 3. In the first experiment, R2(A/R) LAC slabs were compacted according to Section 4.4.2.2. Four slabs per Table 11.2 binder blend were compacted at 8.2% moisture (US-45Alt field *MC* immediately prior to compaction). Slab bottoms and sides were sealed with petroleum jelly to limit water evaporation to the surface. One slab per binder blend was cured in four environments: OD ($OD_1$ in Table 4.1), HO, DO, and CR. One core (150 mm diameter) was dry-cut from each slab at 1, 3, 7, and 14 days (four total cores per slab) and tested for *MC*, $V_a$, and $S_t$.

A second curing experiment was conducted with R1(A/R) at the three Table 11.2 binder blends. Specimens (150 mm diameter) were compacted 30 gyrations with 6% *MC* based on Chapter 8 findings. Specimens were cured 3, 7, and 14 days with OD ($OD_2$ in Table

4.1), HO, and DO protocols (CR and 1-day curing were not considered based on R2 results). Recall that timing of $OD_1$ and $OD_2$ was coordinated so that curing conditions were similar. R1 differed in that specimens were not sealed but were cured traditionally with all sides exposed to air.

R1 specimens were tested for *MC*, $V_a$, and $S_t$ as with R2. APA rut testing was also conducted as well as instrumented IDT testing. APA specimens were conditioned 6 hours for consistency (T340 allows 6 to 24 hours). Instrumented IDT protocols were similar, but slightly refined, relative to those in Chapter 9; therefore, FE is reported in this chapter (and all subsequent chapters) as opposed to *CI*.

### 11.4.3 Phase 3 Results

Figure 11.5 presents R2 laboratory curing experiment results. Average $V_a$'s for 4.2c, 4.2c*, 2.1c2e, and 4e1HL binder systems were 15.6%, 15.2%, 14.2%, and 13.2%, respectively. $V_a$'s for 4.2c and 4.c2* binder systems were similar to US-45Alt field $V_a$'s. Figure 11.5 dashed bars represent values from US-45Alt field cores. Figure 11.5 shows *MC* decreased and $S_t$ increased over time for nearly all curing environments and binder blends.

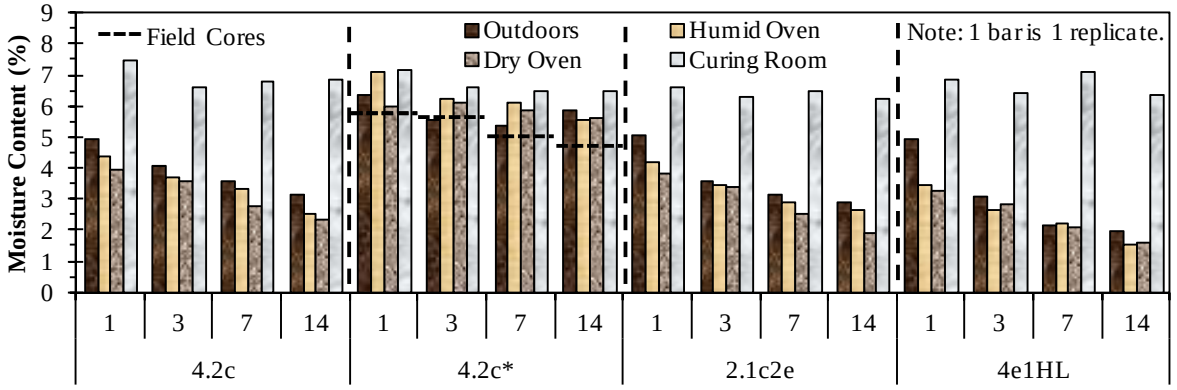


*a) Moisture Content Data by Blend and Cure Time*

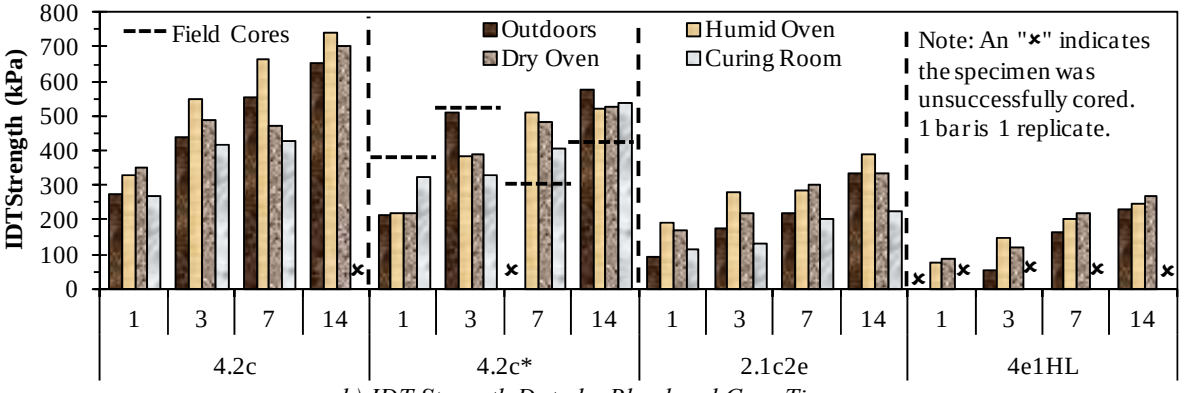


*b) IDT Strength Data by Blend and Cure Time*

**Figure 11.5. R2(A/R) Laboratory Curing Experiment Results**

Figure 11.6 presents R1 laboratory curing experiment results. Figure 11.6a displays similar *MC* trends as Figure 11.5a except Figure 11.6a *MC*s are approximately five times

lower on average, likely because moisture loss was not restricted to the top surface. However, *MC*s were not expected to be as low as those in Figure 11.6a when developing this experiment.

Figure 11.6b shows 4.4c $S_t$ changes over time were not as pronounced as 4.2c $S_t$ changes in Figure 11.5b, likely because less moisture was available throughout curing for cement hydration. Overall, OD and DO curing appeared closely related while HO curing generally yielded lower $S_t$ values.

Figure 11.6c and 11.6d show FE and APA rut depth increase considerably from 4.4c to 4e1HL as in Chapter 9. Curing protocol differences with respect to FE and APA results are difficult to identify visually. Overall, R1 *MC*s were low regardless of curing time or protocol resulting in few meaningful differences in performance properties.

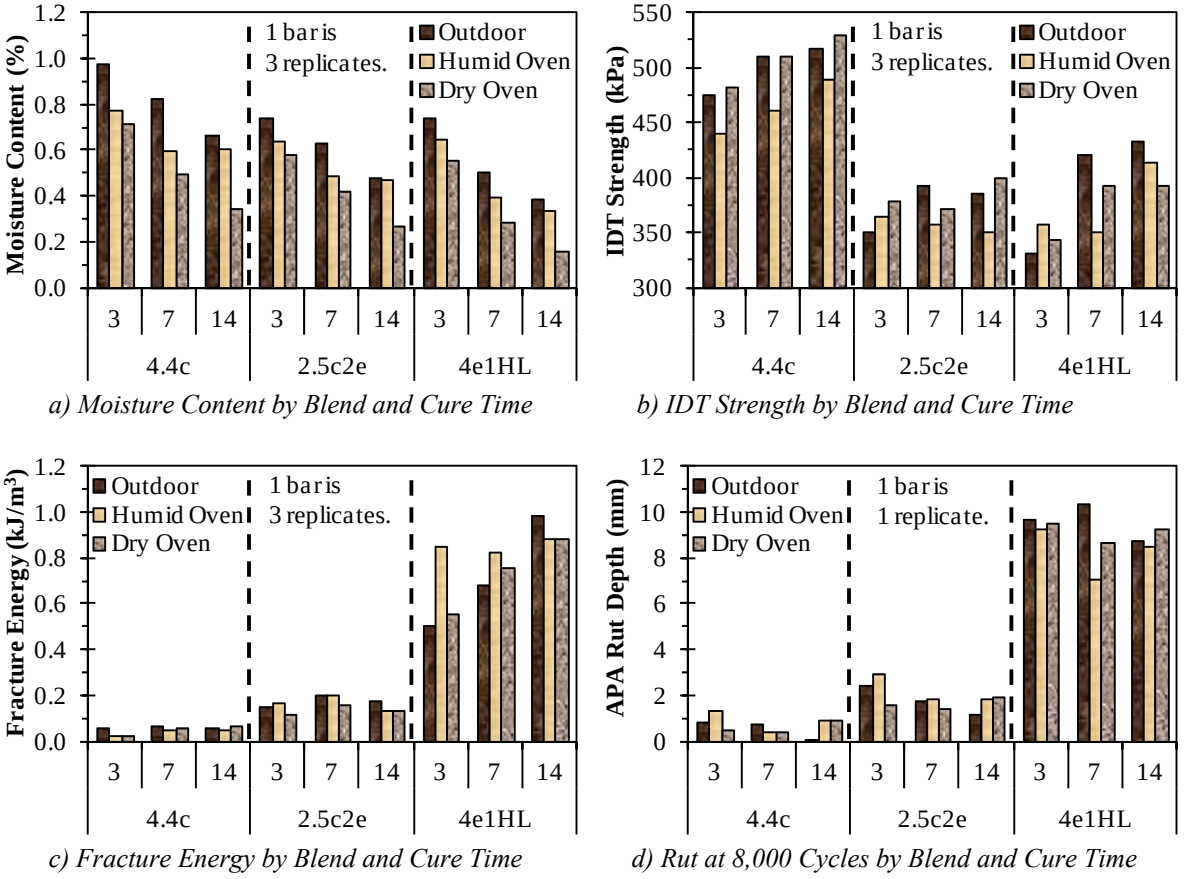


*a) Moisture Content by Blend and Cure Time*

*b) IDT Strength by Blend and Cure Time*

*c) Fracture Energy by Blend and Cure Time*

*d) Rut at 8,000 Cycles by Blend and Cure Time*

**Figure 11.6. R1(A/R) Laboratory Curing Experiment Results**

Figure 11.7 compares curing protocols studied to OD curing using Figure 11.5 and 11.6 data. Figures 11.7a and 11.7b discourage CR curing in the context of a universal design framework. Note that the CR $S_t$ trendline is misleading because all R2(A/R)-4e1HL CR cores were not able to be successfully obtained and are therefore not represented. Aside from CR, Figure 11.7 suggests HO and DO curing reasonably approximate OD curing and are not greatly different from each other.

Two-factor randomized complete bock ANOVAs were conducted for all Figure 11.7 data except CR data. Data was blocked by cure time since results were expected to vary by

cure time; curing method and binder blend were the two factors studied for each response variable (e.g. *MC*, $S_t$). ANOVAs were significant (*p-value* < 0.05) in all cases; curing method and binder blend did not interact except in Figure 11.7c data.

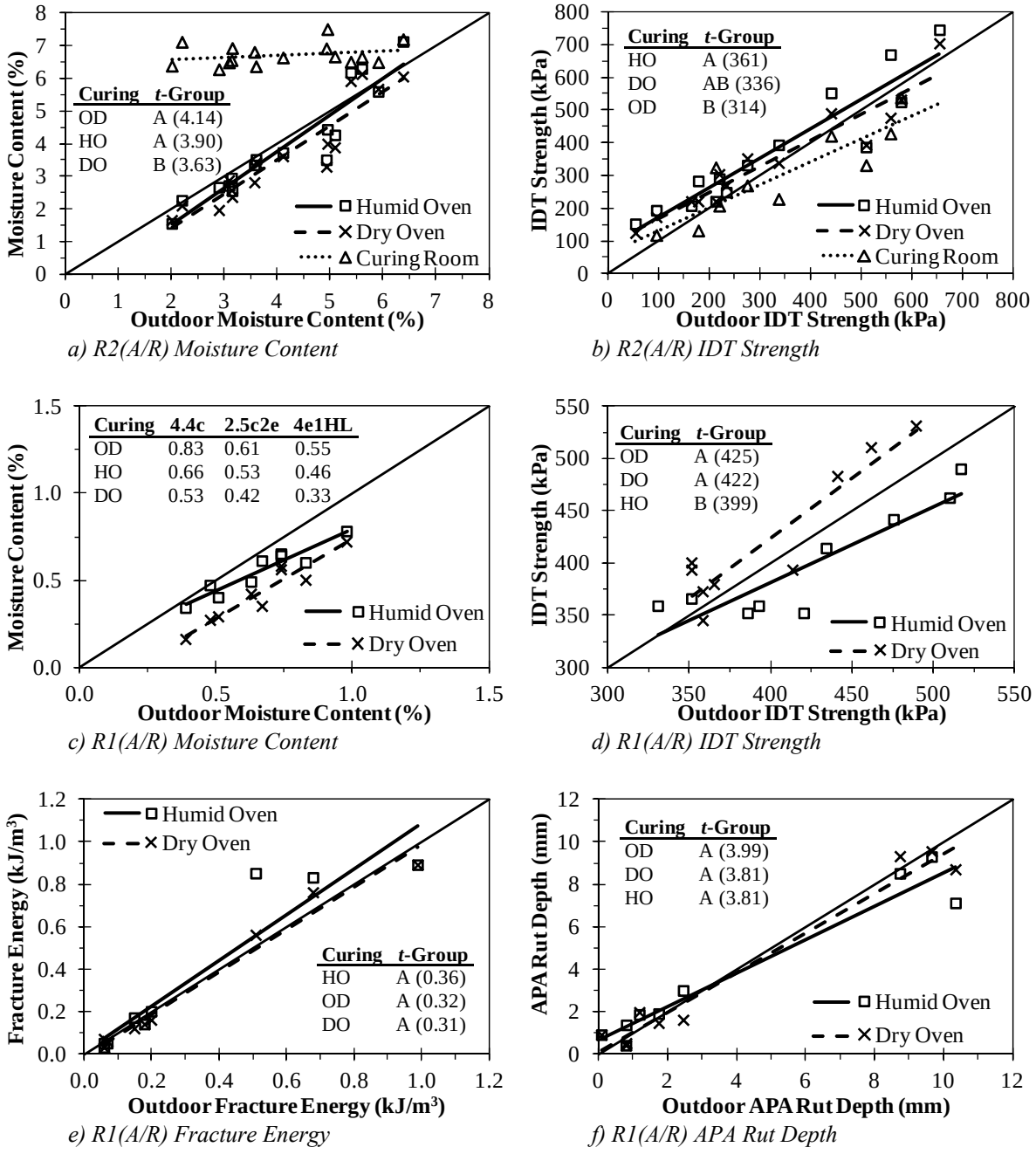


*a) R2(A/R) Moisture Content* *b) R2(A/R) IDT Strength*

*c) R1(A/R) Moisture Content* *d) R1(A/R) IDT Strength*

*e) R1(A/R) Fracture Energy* *f) R1(A/R) APA Rut Depth*

**Figure 11.7. Comparison of Various Curing Methods to Outdoor Curing**

Multiple comparisons rankings of curing methods (shown in Figure 11.7) were conducted using the LSMEANS statement in PROC GLM in SAS 9.3. Curing methods are ranked by response variable mean values (in parentheses) and are assigned *t*-Group letters. Curing methods assigned different letters are significantly different while those with identical

letters are not. Where interaction was encountered (Figure 11.7c), mean *MC* values for each blend are shown. While *t*-Group letters are not applicable in Figure 11.7c, curing methods did significantly rank in the order presented.

OD curing always ranked highest with respect to *MC*. With respect to $S_t$, curing method rankings changed between R1 and R2. In both cases, DO and OD curing were not significantly different from each other. Curing methods were not significantly different with respect to FE and APA results. Overall, statistical analysis did not identify a single curing method which best represents outdoor curing in all categories studied, implying humid and dry oven curing are both options worth considering.

## 11.5 Phase 4: Laboratory-Focused Early-Age Strength Behaviors

Phase 4 consisted of a laboratory-focused early-age strength investigation (all UC tests were conducted at the 1.27 mm/min load rate unless otherwise noted) with US-45Alt (R2) materials in which four experiments of interest to State Study 250 were conducted. The first experiment evaluated PM-P compaction both in the field and laboratory to investigate the PM-P for potential use in CIR quality control applications. Field-compacted PM-P specimens were those described in Section 5.3.3.2 which were field-cured in plastic molds and tested at 1, 3, 7, and 14 days. Figure 11.8 presents all as-measured results (i.e. no correction factors) for PM-P specimens (three replicates tested in all cases except for 14-day field PM-P specimens where 5 replicates were tested). Discussion focuses on three key items of interest: 1) $V_a$ levels achievable for PM-P compaction of CIR; 2) laboratory- and field-compacted PM-P comparisons; and 3) overall feasibility of PM-P use with CIR.

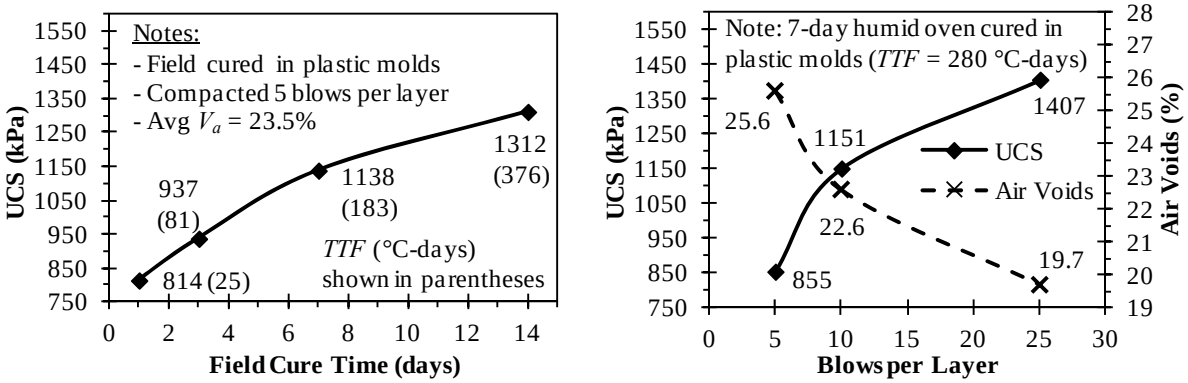


*a) Field-Cured UCS versus Cure Time* *b) Laboratory UCS versus PM-P Compaction*

**Figure 11.8. R2(A/R)-4.2c Field and Laboratory PM-P Investigation**

Field PM-P $V_a$'s were 23.5% on average, which is considerably higher than the average in-place US-45Alt $V_a$ of 15.5%. This difference is meaningful and suggests PM-P compaction of CIR following State Study 206 (Howard et al., 2013c) protocols would not be representative of field compaction. Greater compactive efforts were considered in laboratory PM-P compaction to better understand the relationship between compactive effort and $V_a$. Up to 25 blows per layer were evaluated in laboratory testing, yielding an average $V_a$ of 19.7%. Projecting the compaction-density trend to US-45Alt $V_a$ levels of 15.5%, required blows per layer would be approximately 100. For day-to-day quality control applications, 100 blows per layer (300 total blows per specimen) with a modified Proctor hammer is not ideal.

Compaction effort meaningfully affected UCS in addition to $V_a$. At 5 blows per layer, 7-day laboratory UCS (855 kPa) was approximately 75% of 7-day field UCS (1,138 kPa), though laboratory $V_a$ at 5 blows per layer was approximately 2% greater. At 23.5% laboratory $V_a$ (approximately 8 blows per layer in Figure 11.8b), laboratory UCS was approximately 1,060 kPa, or approximately 93% of the 7-day field UCS. The gap between field and laboratory UCS values becomes larger when curing maturity is considered (temperature-time factors (*TTF*s) were determined by calculating accumulated temperature reported as °C-days). The 7-day field UCS at 23.5% $V_a$ was greater than the 7-day laboratory UCS at 23.5% $V_a$ even though the 7-day field *TTF* (183 °C-days) was only 65% of the 7-day laboratory *TTF* (280 °C-days).

Ultimately, PM-P testing in a 7.6 cm diameter mold with CIR was deemed to be less informative than for soil-cement for which it was developed. The PM-P mold geometry was developed for soil-cement gradations where almost all particles are finer than a No. 8 (2.36 mm) sieve. It is not especially surprising for compaction to be difficult when only 25% of R2's gradation was finer than 2.36 mm. This was largely an exploratory effort; note larger PM-P style molds might be worth considering. In summary, 7.6 cm diameter PM-P compacted $V_a$'s were too high (19.7 to 25.6%) compared to the average in-place field $V_a$ of 15.5%, and UC strengths were too low (814 to 1,407 kPa) compared to Table 11.1 cores of 1,910 to 3,050 kPa (2,010 to 2,500 kPa corrected).

The second experiment evaluated R2(A/R)-4.2c UCS and $V_a$ as a function of SGC compaction (100 mm diameter and 115 mm tall specimens; 1.15:1 h/d ratio). Figure 11.9 presents results of specimens (three replicates per gyration level) which were humid oven cured for 7 days. Gyration levels considered were 15, 30, 75, and 135 as in *SGC-2* in Chapter 8. At 30 gyrations, an average $V_a$ level of 16.4% was obtained, which was within 1% of the 15.5% in-place $V_a$ measured on cores. The in-place core $V_a$ value was achieved at approximately 43 gyrations in Figure 11.9; recall that the number of roller passes used in US-45Alt construction was likely more than would be used for most projects. UCS corresponding to 43 gyrations (i.e. 15.5% $V_a$) was approximately 2,700 kPa, which was on the order of Table 11.1 $UCS_{corr}$ at 7 days (2,500 kPa). Overall, Figure 11.9 provides general strength and density trends for SGC-compacted and humid oven cured cement SCB systems.

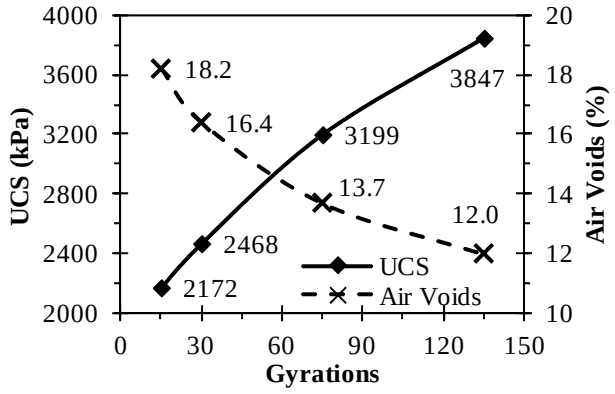


**Figure 11.9. R2(A/R)-4.2c Strength and Density versus Gyrations**

The third experiment evaluated UCS and $V_a$ of R2(A/R)-4e1HL as a function of emulsion content. Since R2 was from a field CIR project, one goal of this experiment was to further evaluate hypotheses regarding $V_a$ discrepancies with R1 and R3 first encountered in Chapter 7 but also present throughout this report. Figure 11.10 presents results of SGC specimens compacted to 30

gyrations (100 mm diameter and 115 mm tall) and humid oven cured for 7 days. Air voids decreased with increasing emulsion content, which is not surprising, but were on the order of 30-gyration air voids presented in this report for R1. Air voids for R1 and R2 being considerably lower than for R3 supports the idea that RAP obtained in traditional manners (e.g. mill and fill projects) exhibits different compaction characteristics than RAP obtained during CIR reclamation activities. The UCS at 4% emulsion (the emulsion content used on US-49 and arbitrarily applied to US-45Alt testing) was 1,331 kPa, which is approximately half that of the 30-gyration 4.2c UCS in Figure 11.9. Further, Figure 11.10 UCS did not continually increase with increasing binder content. In Figure 11.10, UCS peaks and then decreases with 5% emulsion, which would typically indicate the optimum emulsion content has been exceeded.

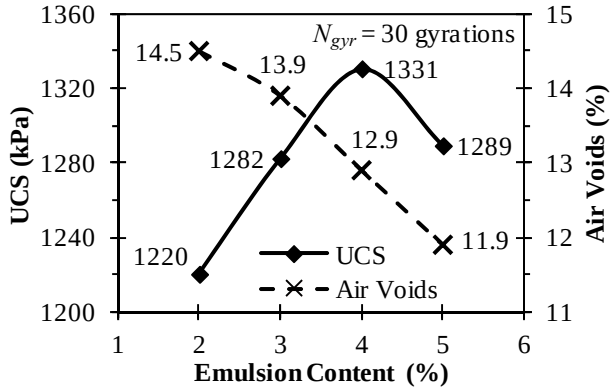


**Figure 11.10. R2(A/R)-4e1HL Strength and Density versus Emulsion Content**

The fourth experiment investigated the effects of UC load rate on R2(A/R)-4.2c specimens compacted to 30 gyrations and humid oven cured for 7 days. Table 11.3 presents a summary of test results. Average $V_a$'s for either group were similar and were between 16 and 17%. COV values were reasonable at approximately 10% or less. On average, UCS when measured with a 5.08 mm/min load rate was 1.25 times greater than when UCS was measured with a 1.27 mm/min load rate. Though this relationship likely varies from test to test or with different binder systems, it is helpful in establishing a general basis for comparison.

**Table 11.3. Load Rate Effects on UCS**

| Load Rate (mm/min) | Avg $V_a$ (%) | UCS (kPa) | | | Avg UCS Ratio (5.08 to 1.27 mm/min) |
|---|---|---|---|---|---|
| | | Avg | St. Dev. | COV (%) | |
| 1.27 | 16.4 | 2466 | 252.9 | 10.3 | 1.25 |
| 5.08 | 16.8 | 3084 | 176.1 | 5.7 | |

*-- R2(A/R)-4.2c specimens tested at three replicates per load rate.*

## 11.6 Key Early Age and Curing Findings

Field testing and instrumentation of a cement CIR project was used in conjunction with laboratory testing to investigate key aspects of CIR design and construction which involve moisture: compaction, curing, and early-age strength. Special consideration was given to moisture as it would relate to either cementitious or bituminous SCB systems as well as cementitious and bituminous MCB systems. Key findings are:

- Moisture sensors were successfully installed in a field CIR project and were able to obtain data not only during curing but also during compaction.
- US-45Alt field *MC*s (directly-measured and GS3-measured) support previous laboratory findings that unnecessary excess water is expelled early during compaction. Volumetric calculations agree and suggest excess moisture, if not able to escape, could hinder compaction. Results herein affirm the recommended 6% maximum *MC* in Chapter 8. As in Chapter 8, Proctor-based *MC* determination for CIR is discouraged. Use of a fixed CIR *MC* appears reasonable and would allow laboratory design efforts to primarily focus on selection of appropriate binder blends.
- Humid oven curing (40 °C and 35 to 50% humidity) and dry oven curing (40 °C) appear to reasonably represent outdoor curing conditions in the Mississippi summer and were not greatly different from each other. Either humid or dry oven curing are candidates for universal design; however, given field conditions (specifically in the southeast US) are humid (Table 5.1), the humid oven appears a more logical choice at present for use in a universal CIR design framework.

# CHAPTER 12 – US-49 PERFORMANCE EVALUATION

## 12.1 Overview of US-49 Performance Evaluation

The American Society of Civil Engineers (ASCE) has recently promoted a sustainability triple bottom line encompassing economics, environment, and social well-being. In-service performance of highways certainly affects all triple bottom line aspects. In-place recycling of existing pavements is one rehabilitation technique with potential to positively impact the triple bottom line. Relative to traditional construction, recycling pavements in place usually reduces emissions and costs since fewer virgin materials are used and transported. Likewise, social benefits often include shorter construction delays relative to traditional reconstruction and extended performance relative to other rehabilitation techniques (e.g. overlay, mill-and-fill).

CIR is the primary focus of this chapter (FDR is a secondary focus). Both are mature concepts which have existed for decades. While mature, however, in-place recycling should not be mistaken for a fully-developed technology, especially since in-place recycling markets have been expanding in recent years to include higher-traffic routes. Hansen (2015) discusses the state of the $425 billion (2006 dollars) US highway system stating, among other details, that 14% of major US roads are in poor condition. With the highway system operating in this context, it is reasonable to expect in-place recycling markets to continue expanding.

The primary objective of this chapter is to present a performance evaluation of US-49 through 53 months of service (nominally 4.5 years). US-49 performance is characterized herein using road profiler distress survey data, pavement core properties, and FWD data. Note that field performance data for FDR portions of US-49 are provided in Volume 1 of the State Study 250 report and reference is made to this document where pertinent. Pavement distress survey results are presented in Section 12.2; thereafter core property results are presented in Section 12.3, and FWD results are presented in Section 12.4.

A secondary objective is to provide a path forward for in-place recycling using lessons learned from US-49. Specifically, guidance is presented in the context of improving the triple bottom line by better optimizing in-place recycling binders, especially for CIR which should not be mistaken for a fully-optimized technology in regards to economics and performance. Traditionally, two binder types, cementitious and bituminous, are used for in-place recycling as discussed in Section 2.3. Cementitious binders are mostly used for FDR but have been used for CIR in some cases (e.g. US-49), and bituminous binders are most commonly used for CIR.

Generally, most CIR design methods are binder-type-specific, resulting in designs which utilize only one binder type (in some cases a small amount of a secondary binder type is used but is generally not fully represented during design). This practice may result in unbalanced designs with respect to expected distresses (or individual components of the triple bottom line). For example, a cement CIR design may have excess rutting resistance but insufficient capacity with respect to cracking. Practically, there is little need for reserve capacity of one distress when other distresses are well past capacity (e.g. no rutting but cracking which exceeds design criteria).

Ideally, a CIR design with just enough capacity within each distress type to satisfy design criteria would yield a more economical and optimized design with respect to overall performance and the triple bottom line. This result could be achievable with more balanced

blending of binder types (e.g. 2.5% portland cement with 2% emulsion), though this is largely neglected in practice due (at least in part) to the current lack of universal design protocols which accommodate both binder types. Study of the US-49 project, having both cement and emulsion CIR sections, provides field data useful in considering the MCB design approach and its potential regarding CIR cost and performance optimization.

## 12.2 Pavement Distress Survey Results

Table 12.1 presents distress survey results for US-49 Sections 2 through 6 as defined in Section 5.2.2.4. Note results for Section 1 (FDR) are presented in Volume 1 of the State Study 250 report.

All sections rated "good" according to PCR values and MDOT's rating categories for four-lane routes. PCR values were not meaningfully different between sections. Practically, all sections were similar with respect to average MRI and all severity levels. Section 4 (23 cm cement CIR over full-depth HMA) MRI was very slightly better than that of other sections. The average MRI for each section was well below the 2.37 mm/m threshold separating low and medium severity levels.

**Table 12.1. Summary of US-49 Distress Survey at 53 Months**

| Distress | Avg or Severity | US-49 Section No. 2 | 3 | 4 | 5 | 6 |
|---|---|---|---|---|---|---|
| PCR | Avg | 86 | 85 | 86 | 86 | 87 |
| MRI | Avg (mm/m) | 1.06 | 1.06 | 0.95 | 1.06 | 1.15 |
| | L (%) | 84.5 | 83.6 | 89.1 | 85.5 | 80.5 |
| | M (%) | 14.4 | 15.6 | 9.8 | 12.0 | 17.6 |
| | H (%) | 1.2 | 0.8 | 1.0 | 2.3 | 1.8 |
| Rutting | Avg (mm) | 2.0 | 2.4 | 2.0 | 1.8 | 1.0 |
| | L (%) | 86.1 | 76.3 | 78.2 | 86.8 | 97.7 |
| | M (%) | 13.3 | 23.7 | 20.7 | 12.3 | 2.1 |
| | H (%) | 0.6 | 0.0 | 1.1 | 0.6 | 0.2 |
| Fatigue Cracking | L (%) | 0.2 | 0.3 | 0.4 | 0.3 | 0.4 |
| | M or H (%) | 0.0 | 0.0 | 0.0 | 0.0 | 0.0 |
| Block Cracking | L (%) | 0.0 | 0.0 | 2.3 | 4.5 | 0.9 |
| | M or H (%) | 0.0 | 0.0 | 0.0 | 0.0 | 0.0 |
| Longitudinal Cracking | L (%) | 37.8 | 53.6 | 40.4 | 55.9 | 30.6 |
| | M (%) | 2.7 | 0.9 | 5.4 | 3.0 | 2.8 |
| | H (%) | 0.1 | 0.0 | 0.5 | 0.2 | 0.0 |
| Transverse Cracking | L (%) | 11.5 | 8.1 | 20.4 | 13.4 | 27.5 |
| | M (%) | 1.5 | 1.5 | 2.2 | 0.7 | 2.9 |
| | H (%) | 0.1 | 0.0 | 0.2 | 0.0 | 0.4 |

*-- L = low, M = medium, H = high*
*-- For PCR, Very Good ≥ 89, 82 ≤ Good < 89, 73 ≤ Fair < 82, 63 ≤ Poor < 73, Very Poor < 63*
*-- For MRI, L: MRI < 2.37 mm/m, M: 2.37 < MRI < 4.74 m/m, H: MRI > 4.74 mm/m*
*-- For rutting, L: 1.6 < Rut < 3.2 mm, M: 3.2 < Rut < 6.4 mm, H: Rut > 6.4 mm*
*-- Fatigue and block cracking values were figured using 3.66 m lane widths*
*-- Edge cracking, patching, potholes, raveling, and bleeding were not detected*

MDOT also measured MRI in September of 2011 (after 10 months of service); however, much of the northern portion of the project was not surveyed as discussed in

Section 5.2.3.2. Average MRI where measured ranged from 0.87 to 1.04 mm/m. Differences between 10- and 53-month MRI values (in cases where both were measured) ranged from 0.05 to 0.32 mm/m, resulting in a 5 to 31% increase within 43 months.

Rutting was manageable for each section. On average, Section 6 exhibited slightly less rutting (i.e. classifying in the "null" rating), while all other sections were in the "low" rating on average. Based on severity level percentages, Section 6 appeared to have less rutting than Sections 2, 4, and 5, which had less than Section 3. It is interesting that the traditionally-constructed Section 3 exhibited the highest rutting with nearly 25% of the section classifying as medium severity. Overall, however, rutting in any section did not appear to be of concern.

All observed fatigue cracking classified as low severity. Section 2 (emulsion CIR) appeared slightly better than all cement-stabilized sections. Overall, some trends are observed, but differences are slight. Block and fatigue cracking results were similar. All block cracking observed was low severity, and there was a gap between Sections 2 and 3 (emulsion CIR and traditional construction) and all cement-stabilized sections. This gap was slightly wider for block cracking than fatigue cracking as no block cracking was observed in Sections 2 and 3 while a modest amount was observed in cement-stabilized sections.

Longitudinal cracking results were less straightforward than other distresses. Three general groups were observed. Section 6 exhibited around 30% low severity cracking, Sections 2 and 4 exhibited around 40%, and Sections 3 and 5 exhibited more than 50%. Cement-stabilized sections were observed in all three groups, and Sections 2 and 3 fell in the middle and worst groups. Overall, Section 6 exhibited the least longitudinal cracking.

Transverse cracking results appear as expected, especially when all caveats of US-49 are considered. Sections 2 and 3 exhibited the least amount of low-severity cracking while more cracking was generally observed in cement-stabilized sections. Recall that Sections 2 and 6 have concrete slabs underneath the CIR layers; therefore, at least some of the observed transverse cracking was likely attributed to reflective cracking at slab joints. Section 6, which is the worst section, would likely be closer to other cement CIR sections if reflective cracking from underlying concrete was not present. Likewise, Section 2 would likely exhibit less transverse cracking than Section 3 if reflective cracking could be factored out of the final results.

Recall that Section 4 is where tack coat application delays were likely experienced as discussed in Section 5.2.2.4, resulting in shrinkage cracking tendencies. It is likely that the high amount of transverse cracking at 53 months was a factor of shrinkage cracking occurring immediately after construction. If Section 4 shrinkage cracking and Section 6 reflective cracking could be factored out of transverse cracking results, it is possible Sections 4, 5, and 6 would converge somewhat relative to their actual observed differences. Overall, cement stabilization appears to yield noticeably more transverse cracking than emulsion stabilization, which is neither an unexpected nor unreasonable finding.

When considering survey results as a whole, all sections appear to be performing satisfactorily, including Section 1 (FDR) which was discussed in Volume 1 of the State Study 250 report. Section 1 also rated "good" according to its PCR and exhibited an MRI of 1.09 mm/m, which was on the order of all other MRI's measured. Rutting was of no concern, and block and fatigue cracking were low severity. Section 1 did, however, have around 30% low severity longitudinal cracking and around 20% low severity transverse cracking. Overall,

performance of Sections 1 and 2 was slightly better than other sections. Section 1 exhibited less rutting, but more cracking, than Section 2, and vice versa.

## 12.3 Core Property Results

### 12.3.1 Layer Thicknesses

Layer thicknesses were fairly variable between as well as within US-49 sections. Figure 5.4 showed representative photographs of US-49 cores where layer thickness variability can be observed (arrows indicate layer interfaces). Note that Section 1 was shown for reference (Figure 5.4a), and two cores from Section 2 (Figures 5.4b and 5.4c) were presented showing the differences between when concrete was and was not present.

Figures 5.4b and 5.4e show pre-existing asphalt materials remaining underneath CIR layers, which appear to be bituminous materials originally serving as a base. Figure 5.4c and 5.4f show CIR above concrete. Figure 5.4c shows recycling depths extending to the top of the concrete while Figure 5.4f shows recycling depths which did not reach the top of the concrete. This type of layer thickness variability was very common within each section and across US-49.

Table 12.2 summarizes layer thicknesses for Sections 2, 4, 5, and 6 to provide an understanding of the variability present (Section 1 is discussed in Volume 1 of the State Study 250 report and Section 3 was not cored). Note that all layers, specifically those underneath recycled layers, were not retrieved for all cores since the main goal was to retrieve the AC and CIR (or FDR) layers unless the core was taken at an FWD location. For example, concrete was only retrieved for 4 of the 17 Section 6 cores; concrete thickness statistics for Section 6 describe all concrete cores retrieved. Also note that Section 4 variability appears very low, which is primarily because only two cores were cut in Section 4 and were cut in close proximity to each other.

Aside from Section 4, thickness of the AC surface course ($AC2_{FC}$) was, on average, close to the targeted 3.8 cm thickness; however, thicknesses still varied considerably from 3.2 to 7.0 cm (not including Section 4). In Section 4, $AC2_{FC}$ thicknesses were nearly double the target. Overall, 57% of all cores exhibited $AC2_{FC}$ thicknesses within 0.5 cm of the target thickness. Similarly, 61% were between 3 and 4 cm, 28% were between 4 and 5 cm, and 11% were greater than 5 cm.

Aside from Section 4, HMA base course ($AC1_{FC}$) thicknesses were also, on average, close to the targeted thickness (7.6 cm); however, thicknesses still varied considerably from 5.7 to 10.2 cm (not including Section 4). In Section 4, $AC1_{FC}$ thicknesses were greater than the target as with $AC2_{FC}$ although the difference was not as great. Overall, 30% of all cores exhibited $AC1_{FC}$ thicknesses within 0.5 cm of the target thickness. Further, 28% were between 6 and 7 cm, 30% were between 7 and 8 cm, and 32% were greater than 8 cm.

Section 2, 5, and 6 target thicknesses were 15 cm, but average as-built thicknesses were 13.1, 12.7, and 8.4 cm, respectively. Section 6 thicknesses were considerably lower than the target and, as shown in Figure 5.4f, could have been modestly greater before reaching underlying concrete. Thicknesses varied considerably from 4.4 to 15.9 cm for all three 15 cm targeted sections. For Sections 2, 5, and 6 combined, 29% of CIR thicknesses were less than 10 cm, 21% were between 10 and 12 cm, 31% were between 12 and 14 cm,

and 19% were greater than 14 cm. Section 4 CIR, at 19.4 cm on average, was also slightly less than its 23 cm target thickness.

**Table 12.2. US-49 Cored Layer Thicknesses**

| Section | Statistic | $AC2_{FC}$ (Surface) | $AC1_{FC}$ (Base) | CIR | Underlying Layers | |
|---|---|---|---|---|---|---|
| | | | | | Asphalt[a] | Concrete |
| 2 | Avg (cm) | 4.1 | 9.2 | 13.1 | 7.6 | 20.3 |
| | Min (cm) | 3.2 | 7.0 | 9.5 | 2.5 | 19.1 |
| | Max (cm) | 7.0 | 10.2 | 15.9 | 16.5 | 22.9 |
| | COV (%) | 25 | 14 | 19 | 101 | 11 |
| 4 | Avg (cm) | 7.5 | 10.0 | 19.4 | --- | --- |
| | Min (cm) | 7.3 | 9.5 | 19.1 | --- | --- |
| | Max (cm) | 7.6 | 10.5 | 19.7 | --- | --- |
| | COV (%) | 3 | 7 | 2 | --- | --- |
| 5 | Avg (cm) | 3.6 | 7.9 | 12.7 | 8.5 | --- |
| | Min (cm) | 3.2 | 5.7 | 8.9 | 7.6 | --- |
| | Max (cm) | 4.8 | 10.2 | 14.0 | 8.9 | --- |
| | COV (%) | 13 | 23 | 11 | 9 | --- |
| 6 | Avg (cm) | 4.1 | 7.6 | 8.4 | 3.1 | 20.8 |
| | Min (cm) | 3.8 | 6.4 | 4.4 | 1.3 | 20.3 |
| | Max (cm) | 5.1 | 8.3 | 12.7 | 6.4 | 21.6 |
| | COV (%) | 9 | 6 | 31 | 59 | 3 |

*a) may be bituminous base or hot mix asphalt, primarily depending on whether concrete slabs were or were not present*

Table 12.2 illustrates considerable construction variability with respect to layer thicknesses. As recommended in Strickland (2010), more extensive pre-construction coring could be beneficial towards reducing thickness variability. However, distress survey results presented in the previous section indicate US-49 is performing well despite this variability.

### 12.3.2 Air Voids

Table 12.3 summarizes US-49 CIR $V_a$'s for Sections 2, 5, and 6. Results shown are for all test specimens sliced from cores. In addition to analyzing all specimens simultaneously, top and bottom pairs were compared to investigate density gradients where cores were thick enough to obtain two test specimens from a single core. Paired *t*-tests were conducted to investigate statistical differences between top and bottom layer air voids at a 5% significance level.

Table 12.3 shows Section 2 $V_a$'s were 10.0% on average compared to Section 5 and 6 $V_a$'s of 13.8 and 15.3%, respectively. Trends between emulsion and cement CIR are similar to laboratory-compacted specimens with similar binder systems and dosages in this report. They appear reasonable primarily because emulsion is likely to facilitate compaction more so than cement and because emulsion fills more volume than cement due to specific gravity differences (1.03 versus 3.15) (i.e. emulsion occupies more voids in mineral aggregate than cement for similar dosages by mass).

Top and bottom layers were significantly different with respect to $V_a$ for all three sections. Section 2 $V_a$'s were significantly lower at the top of the layer than the bottom, while

the opposite was true for Sections 5 and 6. Material segregation may have led to the observed Section 5 and 6 density gradients, though the cause is unknown. Note that for Section 6, only 3 pairs were available primarily because the Section 6 CIR was fairly thin and typically only yielded one test specimen per core.

**Table 12.3. Summary of US-49 CIR Air Voids**

| | All Specimens | | | Top- and Bottom-Layer Paired Specimens | | | | |
|---|---|---|---|---|---|---|---|---|
| **Section** | ***n*** | **Avg $V_a$ (%)** | **COV (%)** | ***n*** | **Avg Top $V_a$ (%)** | **Avg Bottom $V_a$ (%)** | ***p-value*** | **Sig Diff?** |
| 2 | 18 | 10.0 | 20 | 8 | 8.6 | 11.7 | <0.001 | Yes |
| 5 | 19 | 13.8 | 9 | 7 | 14.8 | 12.9 | 0.008 | Yes |
| 6 | 18 | 15.3 | 7 | 3 | 16.7 | 15.0 | 0.033 | Yes |

*-- $V_a$ values were calculated using $G_{mm}$ values of 2.366 (Section 2) and 2.455 (Sections 5 and 6), which were obtained following protocols of Section 4.4.4.1 and Equation 4.3 (this same equation is repeated as Equation 10.2). This approach calculates CIR $G_{mm}$ based on RAP $G_{mm}$ and individual binder specific gravities and dosages. $G_{mm}$ values measured on cored materials obtained during a 41-month pilot investigation on US-49 were 2.335 (Section 2) and 2.376 (Sections 5 and 6). Internal investigation to date has led the authors to the perspective that field $G_{mm}$ values measured on compacted and broken up materials after several years of service may not be as reliable as values measured according to Equation 4.3 (or 10.2), especially for cement CIR sections where cement hydration over time likely affects $G_{mm}$ measurement ability (lower values expected from broken up cores). A considerable amount of effort was put forth to develop Equation 4.3 (or 10.2) in Chapter 10, and, until more information is available, the author recommends use of this method to determine CIR $G_{mm}$ when possible.*

### 12.3.3 Strength and Performance Properties

Table 12.4 presents laboratory-measured properties for the HMA surface course, HMA base course, and CIR materials from Sections 2, 5, and 6. Note that $S_t$ was measured on both 100 and 150 mm diameter cores, and tensile strengths are denoted $S_{t,\ 100\ mm}$ and $S_{t,\ 150\ mm}$, respectively. Properties tested for Section 1 (FDR) are summarized herein for comparison but differed slightly from those in this report. Section 1 core properties were, on average, as follows: elastic modulus (ASTM C469) was approximately 1.4 GPa (200 ksi), UCS was approximately 2.8 MPa (400 psi), $S_{t,100\ mm}$ was approximately 517 kPa (75 psi), and APA rut depths were less than 1 mm.

AC mixture properties are presented first for comparison with other CIR properties. $M_r$ for both AC mixtures was similar at approximately 7.5 GPa. $S_{t,\ 100\ mm}$ and $S_{t,\ 150\ mm}$ were relatively similar for either diameter. $S_t$ values for AC surface and base courses were approximately 1,400 and 1,100 kPa, respectively. Mixture cracking susceptibility was characterized via FE (larger FE suggests better cracking resistance), which was 2.72 and 0.65 kJ/m$^3$ for surface and base courses, respectively. The surface FE appears reasonable, but the base FE is of concern. Although no errors were found in data files, the 0.65 kJ/m$^3$ FE is not believed to be correct and should be interpreted accordingly. APA rut depths for surface and base courses were 2.2 and 4.0 mm, respectively.

Section 2 emulsion CIR properties were considerably different from that of the AC mixtures, which is reasonable. $M_r$, $S_t$, and FE were approximately 3.2 GPa, 600 kPa, and 1.3 kJ/m$^3$, respectively; all of which were slightly less than half of corresponding AC properties. At 11.8 mm, APA rut depths were approximately 3 to 5 times greater than that of AC mixtures. Overall, the comparison between emulsion CIR and AC is reasonable in that $M_r$, $S_t$, and FE were all lower while APA rut depth was greater.

**Table 12.4. Summary of US-49 AC and CIR Core Properties at 53 Months**

| Property | | $AC2_{FC}$ (Surface) | $AC1_{FC}$ (Base) | CIR Section No. 2 | 5 | 6 |
|---|---|---|---|---|---|---|
| $M_r$ | Avg | 7.6 | 7.4 | 3.2 | 13.9 | 11.8 |
| (GPa) | *n* | 6 | 6 | 6 | 6 | 6 |
| | COV (%) | 23 | 23 | 10 | 17 | 20 |
| | Avg $V_a$ (%) | 6.3 | 6.6 | 9.2 | 14.1 | 15.6 |
| $S_{t,\ 100\ mm}$ | Avg | 1386 | 952 | 648 | 1145 | 1020 |
| (kPa) | *n* | 16 | 8 | 6 | 8 | 7 |
| | COV (%) | 17 | 34 | 14 | 13 | 21 |
| | Avg $V_a$ (%) | 7.1 | 7.0 | 10.1 | 14.0 | 15.1 |
| $S_{t,\ 150\ mm}$ | Avg | 1413 | 1200 | 621 | 1041 | 1096 |
| (kPa) | *n* | 6 | 6 | 6 | 6 | 6 |
| | COV (%) | 19 | 38 | 18 | 22 | 20 |
| | Avg $V_a$ (%) | 6.3 | 6.6 | 9.2 | 14.1 | 15.6 |
| FE | Avg | 2.72 | 0.65 | 1.29 | 0.11 | 0.09 |
| ($kJ/m^3$) | *n* | 6 | 6 | 6 | 6 | 6 |
| | COV (%) | 53 | 34 | 26 | 58 | 33 |
| | Avg $V_a$ (%) | 6.3 | 6.6 | 9.2 | 14.1 | 15.6 |
| $RD_{APA}$ | Avg | 2.2 | 4.0 | 11.8 | 0.9 | 1.2 |
| (mm) | *n* | 6 | 6 | 6 | 2 | 2 |
| | COV (%) | 20 | 3 | 3 | --- | --- |
| | Avg $V_a$ (%) | 6.4 | 7.6 | 10.8 | 12.8 | 14.9 |
| UCS | Avg | --- | --- | --- | 3.70 | 3.80 |
| (MPa) | *n* | --- | --- | --- | 3 | 3 |
| | COV (%) | --- | --- | --- | 13 | 10 |
| | Avg $V_a$ (%) | --- | --- | --- | 13.4 | 15.4 |

*-- For $M_r$, six replicates were tested yielding 24 $M_r$ values (two faces, two axes per replicate). Trimming 10% removed the highest and lowest 10% of values (3 readings in this case).*

*-- For FE, 6 replicates were tested yielding 12 FE values (two faces per replicate). Of the 12 values, probable outliers were removed and then the highest and lowest 10% of values were trimmed (2 readings in this case).*

Sections 5 and 6 cement CIR properties demonstrated clear contrasts with emulsion CIR properties. $M_r$ was approximately 13 GPa on average, which was nearly two and four times greater than AC and emulsion CIR $M_r$, respectively. $S_t$ was approximately 1,100 kPa, which approaches that of AC $S_t$ but is approximately twice that of the emulsion CIR. FE was approximately 0.10 $kJ/m^3$, which, at 10% and 5% of emulsion CIR and AC FE values, was considerably lower. APA rut depths, at approximately 1 mm, were almost negligible relative to AC and emulsion CIR rut depths. UCS was determined for cement CIR only and was approximately 3.75 MPa, which is reasonable considering the US-49 cement CIR design required 2.1 MPa after 7 days of moist curing. Overall, cement CIR properties were effectively opposite of emulsion CIR properties in that cement CIR provided higher $M_r$ and $S_t$, considerably greater rutting resistance, but considerably less fracture resistance.

Table 12.5 presents properties for US-49 underlying asphalt materials (i.e. asphalt materials present underneath CIR layers). Underlying asphalt materials exhibited $M_r$ on average of 4.5 GPa, $S_t$ of approximately 670 kPa on average for either 100 or 150 mm diameter specimens, and FE of 0.71 $kJ/m^3$ on average. As with the AC base course FE, the underlying asphalt FE is relatively low, though no apparent testing issues were encountered other than considerable variability.

**Table 12.5. US-49 Underlying Asphalt Properties**

| Property | Avg | *n* | COV (%) |
|---|---|---|---|
| $M_r$ (GPa) | 4.5 | 3 | 21 |
| $S_{t,\ 100\ mm}$ (MPa) | 675 | 4 | 16 |
| $S_{t,\ 150\ mm}$ (MPa) | 668 | 3 | 6 |
| FE (kJ/m$^3$) | 0.71 | 3 | 54 |

Table 12.6 presents properties for US-49 underlying concrete materials. Underlying concrete was tested for ASTM C469 elastic modulus (*E*) and compressive strength. Specimens were 100 mm in diameter and were sawn to target heights of 200 mm. Actual heights were restricted by total concrete layer thickness in several cases and ultimately ranged from 180 to 200 mm. *E* and UCS were adjusted to a 2:1 h/d ratio using ASTM C39 correction factors; factors used ranged from 0.98 to 1.00. All available cores were tested, and two were tested for UCS only in order to establish target loads for *E* testing for all other specimens. On average, *E* and UCS were 43.7 GPa and 84.7 MPa, respectively.

**Table 12.6. US-49 Underlying Concrete Properties**

| Property | Avg | *n* | COV (%) |
|---|---|---|---|
| E (GPa) | 43.7 | 5 | 9 |
| UCS (MPa) | 84.7 | 7 | 18 |

*-- E = ASTM C469 elastic modulus*
*-- E and UCS adjusted to 2:1 h/d ratio by ASTM C39*

Table 12.7 presents US-49 subgrade material properties, which were grouped into six composite samples based on visual appearance and tested as described in Section 5.2.3.3. Table 12.7 indicates whether a given subgrade sample was obtained in a location where concrete slabs were present. For materials visually assessed to be sands, Atterberg limits were not performed, but a more detailed gradation was reported. AASHTO classification is reported alongside typical $M_r$ values from Table 11-10 in the *MEPDG* Manual (2008).

**Table 12.7. US-49 Subgrade Soil Properties**

| **Sample** | 1 | 2 | 3 | 4 | 5 | 6 |
|---|---|---|---|---|---|---|
| **Description** | Reddish Sand | Brown Fine Grained Soil | Greyish-Brown Fine Grained Soil | Reddish Sand | Greyish-Brown Fine Grained Soil | Brown Fine Grained Soil |
| **Concrete Present?** | Yes | No | No | No | Yes | Yes |
| **Liquid Limit** | --- | 37 | 34 | --- | 35 | 33 |
| **Plastic Limit** | --- | 23 | 23 | --- | 24 | 22 |
| **Plasticity Index** | --- | 14 | 11 | --- | 11 | 11 |
| **$P_{10}$ (%)** | 81.9 | --- | --- | 74.8 | --- | --- |
| **$P_{40}$ (%)** | 49.6 | --- | --- | 59.8 | --- | --- |
| **$P_{60}$ (%)** | 29.5 | --- | --- | 51.7 | --- | --- |
| **$P_{200}$ (%)** | 9.0 | 94.5 | 87.6 | 45.8 | 79.7 | 90.6 |
| **AASHTO Classification** | A-1-b | A-6 | A-6 | A-4 to A-7 | A-6 | A-6 |
| **Typical $M_r$ (GPa)** | 0.12 to 0.26 | 0.10 to 0.12 | 0.10 to 0.12 | --- | 0.10 to 0.12 | 0.10 to 0.12 |

Sample 1 classified as an A-1-b material, which is a gravel or sand with $M_r$ ranging from 0.12 to 0.26 GPa. Samples 2, 3, 5, and 6 classified as an A-6 material, which is a clayey

soil with typical $M_r$ values ranging from 0.10 to 0.12 GPa. Sample 4 was originally believed to be a sandy material based on visual assessment; however, it would classify as an A-4 to A-7 material based on gradation. Since Atterberg limits were not performed for Samples 1 and 4, the actual AASHTO classification and typical $M_r$ values could not be determined.

As suggested by pavement distress survey results presented in Section 12.2, all US-49 sections are performing satisfactorily though slight distinctions can be observed between sections (e.g. more cracking in cement CIR sections than in emulsion CIR sections). Properties measured on cores support distinctions observed in the distress survey, particularly regarding cement versus emulsion. Trends observed in strength and performance properties may serve as a foretelling of the expected progression of distresses on US-49. For example, the gap between cracking distresses in cement-stabilized and emulsion-stabilized sections will likely grow, and the gap between rutting distresses may grow slightly.

## 12.4 Falling Weight Deflectometer Results

Figure 12.1 presents FWD $d_{0\text{-}20}$ deflections with time for all FWD locations tested by MDOT through the first 53 months of service. Note 1 mil is equivalent to 0.0254 mm. Plots in Figure 12.1 also show $d_{0\text{-}20}$ data for locations which were not tested by MDOT over time but were added during the 53-month investigation for various reasons, mainly to collect more data in sections where there were less than three FWD locations. No FWD testing was conducted in Section 4 prior to the 53-month investigation; therefore, Section 4 data was included in Figure 12.1c with Section 5 since the two were similar other than layer thickness.

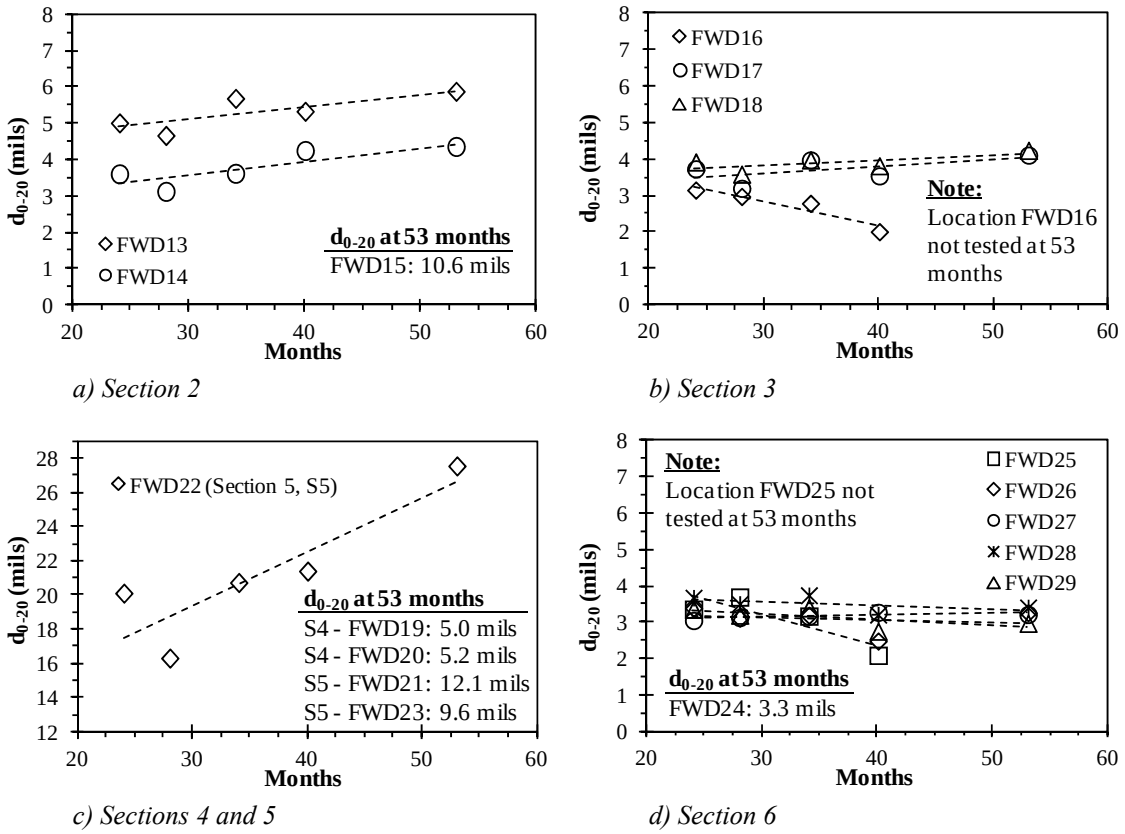


**Figure 12.1. FWD Deflection Data**

FWD22 (Figure 12.1c) deflections were considerably higher because FWD22 was located in an area of localized severe rutting and wheel path cracking (Figure 12.2). The cause of this distress is unknown, but it was limited to an area approximately 15 m long and was not representative of Section 5 as a whole. FWD22 was not included in further analysis or discussion.

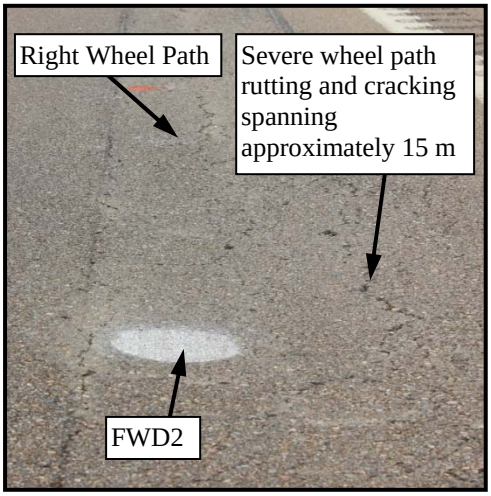


**Figure 12.2. Distresses at FWD22 Location**

Figure 12.3 summarizes Figure 12.1 data (excluding FWD22) by averaging all FWD locations and test times. Deflections generally ranged from 3 to 6 mils for all sections except Section 5 where deflections were around 11 mils. Figure 12.3 distinctly shows a notable difference between Section 5 and all others; this difference is discussed further in the following paragraphs.

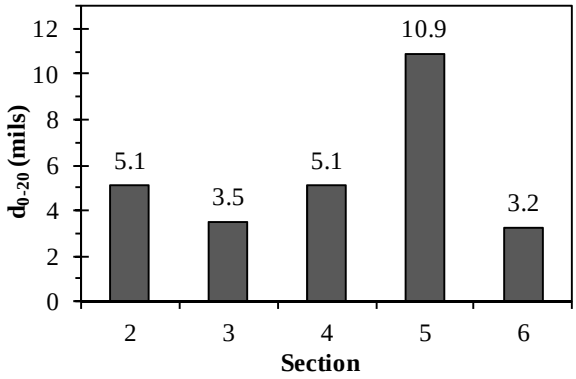


**Figure 12.3. Average FWD Deflections by Section**

Initially, a more involved FWD analysis was considered herein, such as the one used for FDR data in Volume 1 of the State Study 250 report. However, when all available FWD data was processed, FDR data (Section 1) was fairly symmetrical and suitable for the AASHTO (1993) analysis, while all other data was less symmetrical and less conducive to a detailed (yet reliable) analysis. For example, Section 1 was effectively a two-layer pavement structure with a higher-modulus material over a lower-modulus material, which yields a

fairly straightforward analysis. In contrast, other sections consisted of up to four layers (Table 12.2) with the highest-modulus material encountered on US-49 (i.e. concrete) comprising the lowest layer. The types of pavement structures encountered in Sections 2 through 6 complicate analysis considerably relative to Section 1. When layer properties were coupled with the high layer thickness variability observed, the suitability of a sophisticated FWD analysis to meet this report's needs was questioned, and it was decided that a more approximate analysis approach would be utilized.

As an initial reasonableness assessment, layer thicknesses and material modulus values were input into the multi-layer linear elastic analysis KENLAYER program to calculate pavement surface deflections at the center of loading. Generally, KENLAYER parameters were set to the default, idealized case (e.g. fully-bonded layers). Calculated deflections for Sections 2 to 6 ranged from 4.4 to 7.2 mils, which support FWD-measured deflections as generally in line with expected deflections calculated with these layer properties and thicknesses.

It is important to note that the Section 5 KENLAYER deflection was 6.6 mils, whereas the average FWD $d_{0\text{-}20}$ was 10.9 mils (excluding FWD22). This discrepancy is likely due to two issues. First, linear elastic calculations provide an ideal result; second, calculations are dependent on material properties. In coring Section 5, one out of every three cores, on average, was cracked. However, only intact cores were tested, meaning laboratory test results were the best possible representation of Section 5. Therefore, Table 12.4 properties may not necessarily align with Section 5 FWD deflections. Likewise, KENLAYER cannot appropriately consider this issue.

A second FWD assessment was conducted by comparing Table 2.9 literature values to US-49 FWD data in Figure 12.4 where deflection is plotted against $SN_{eff}$. Note all in-place recycling sections (1, 2, 4, 5, and 6) were considered in Figure 12.4. For US-49 data, approximate $SN_{eff}$ values were calculated by summing layer thicknesses multiplied by corresponding layer coefficients (AASHTO, 1993). Table 12.2 average layer thicknesses were used, and layer coefficients were assigned as follows: 0.44 (AC), 0.30 (in-place recycling), and 0.20 (all underlying pavement layers). Layer coefficients used are undoubtedly approximate but were considered sufficient given the analysis was intended to show trends from many studies in several states over time. Figure 12.4 shows that US-49 and literature trends are relatively similar.

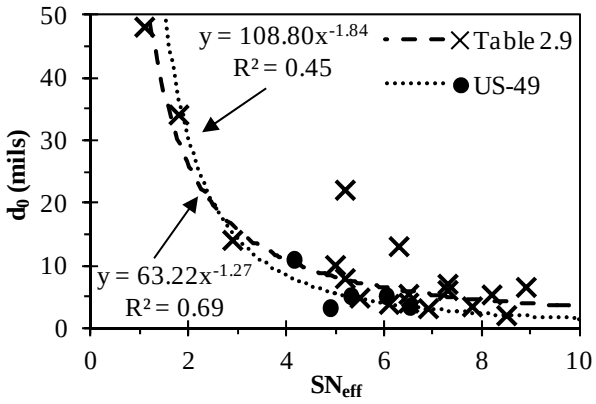


**Figure 12.4. $d_0$ versus $SN_{eff}$ for Literature and US-49**

Figure 12.4 also assists in identifying Section 5 as the most structurally deficient. Compared to Section 4, the CIR layer is thinner, and compared to Section 6, underlying layers are considerably less stiff (i.e. no concrete is present). Therefore, it is likely that Section 5 has accumulated greater fatigue damage than Sections 4 and 6. This could support the high coring failure rate as well as the higher FWD deflections. It also suggests Section 5 performance may begin to deteriorate at a faster rate relative to other US-49 sections.

Overall, though an approximate analysis was conducted, FWD testing generally concluded that US-49 is performing well from a structural capacity perspective. However, Section 5 is the one notable exception and, structurally, is of greater concern than other sections. This finding generally agrees with the distress survey. Core testing does not support this finding, yet that is likely because only intact (i.e. un-cracked) cores were tested.

## 12.5 Discussion of Results and Path Forward

Essentially all findings within this chapter support the notion that US-49 is performing well regardless of the section considered (including Section 1 FDR). Further, the performance of recycled sections is comparable to or slightly better than that of the traditionally constructed section after 53 months of service. Differences between the properties of cement-stabilized and emulsion-stabilized cores are distinct when directly measured, but based on distress survey and FWD results, those differences have not yet meaningfully manifested themselves within overall pavement performance as of 53 months in service (note some differences have been observed, such as with Section 5 structural capacity).

Given the current, relatively satisfactory performance of all US-49 sections, discussion focuses primarily on concepts which could be taken from this study and applied to future in-place recycling projects to better the triple-bottom line (i.e. economics, environment, and social well-being). Several of the immediate benefits, such as fewer costs and emissions due to fewer virgin materials needed or shorter construction delays, have already been discussed. However, US-49 results provide evidence that economics and performance, which ultimately affect social wellbeing, can be further optimized.

With regard to economics, Table 12.8 presents US-49 cost information by section and also includes Section 1 for comparison. Costs per lane-km (and per lane-mile) were calculated two ways: for only the base layer and for the base layer and AC overlay. The term base layer refers to cement FDR (Section 1), emulsion CIR (Section 2), crushed stone (Section 3), and cement CIR (Sections 4, 5, and 6).

When comparing only base layers, Table 12.8 shows that emulsion CIR was around twice the cost of cement CIR. Cement FDR was only slightly more cost effective than emulsion CIR, mainly due to the greater recycling depth. The crushed stone base layer used in Section 3 was nearly 1.5 times the cost of emulsion CIR (both targeted 15 cm depths). As an aside, Table 12.8 illustrates the potential economic benefit of CIR or FDR in general relative to crushed stone bases, specifically for Mississippi where crushed stone materials are typically transported from neighboring states. Regarding CIR, cement CIR demonstrates considerable economic benefits relative to emulsion CIR and would likely be preferred if only economics were considered.

**Table 12.8. US-49 Cost Information**

| | | Cost per lane-km | | Cost per lane-mile | |
|---|---|---|---|---|---|
| **Section** | **Description** | **Base** | **Base & HMA** | **Base** | **Base & HMA** |
| 1 | Cement FDR (41 cm) | $39,000 | $114,000 | $63,000 | $183,000 |
| 2 | Emulsion CIR (15 cm) | $44,000 | $119,000 | $71,000 | $191,000 |
| 3 | Traditional Construction | $62,000 | $200,000 | $100,000 | $323,000 |
| 4 | Cement CIR (23 cm) | $25,000 | $99,000 | $40,000 | $160,000 |
| 5 or 6 | Cement CIR (15 cm) | $22,000 | $97,000 | $36,000 | $156,000 |

*-- Costs calculated using bid unit prices for applicable pay items.*
*-- Emulsion cost = $0.64 per liter ($2.42 per gallon)*
*-- Hydrated lime cost = $201 per metric ton ($182 per ton)*
*-- Cement cost = $114 per metric ton ($103 per ton)*

Cement stabilization in general was also preferred by MDOT engineers during US-49 construction. MDOT engineers felt that cement was easier to work with than emulsion in that mix designs were easier to obtain, early-age properties were more predictable, and traffic could be returned to the pavement in less time. For example, during a 2012 cement FDR project on State Route 14 in Issaquena County, MS, MDOT allowed traffic on the FDR layer within three hours of compaction. Details of the project are as follows: 23 cm recycling depth (18 cm HMA plus 5 cm cement-treated base), 5% cement dosage by volume, 700 AADT, $19,000 per lane-km FDR cost, and double chip seal surfaced. These characteristics could be considered to positively impact social well-being.

Pavement performance also impacts social well-being, and recycling techniques which prolong pavement life would have a considerable positive impact on social well-being. Results in this chapter indicate cement FDR and emulsion CIR have slightly outperformed cement CIR sections up to 53 months, and based on core properties, it would not be surprising for the performance gap to increase over time. Cement FDR and emulsion CIR may provide better long-term performance, which justifies higher initial costs within a triple bottom line framework.

Results in this chapter suggest the idea of multiple component CIR binder systems has merit with respect to the triple bottom line. For US-49, emulsion CIR could be said to have sufficient rutting capacity and excess reserve cracking capacity, at a high cost relative to cement CIR. Cement CIR, however, is more economical, perhaps more convenient from a construction perspective, and could be said to have excess reserve rutting capacity but not excess cracking capacity. Utilizing a balanced binder blend of cement and emulsion could better optimize economics and distress capacities, in turn benefiting the triple bottom line. For example, 2.5% emulsion and 2% cement should be better balanced (i.e. adequate rutting resistance, adequate cracking resistance, sufficient constructability, and mid-range economics). To this end, Chapter 13 provides further guidance regarding cost and performance optimization using MCB systems for CIR.

## 12.6 Summary of US-49 Project Findings Related to CIR

The objective of this chapter was to present a field performance evaluation of US-49 through the first 53 months of service and provide discussion on implications of US-49 relating to better meeting the triple bottom line of economics, environment, and social well-being in future in-place recycling projects. US-49 consisted of six sections which were

discussed herein and can be largely grouped into four categories: traditional construction, cement-stabilized FDR, cement-stabilized CIR, and emulsion-stabilized CIR. Key findings are as follows:

- Pavement distress survey results at 53 months indicate all sections of US-49 are performing satisfactorily. Recycled sections are performing comparably to, or slightly better than, the completely reconstructed section. For specific distresses, slight differences can be observed, particularly between cement stabilization and emulsion stabilization. For example, emulsion CIR exhibited less cracking than cement-stabilized sections. Overall, the cement FDR and emulsion CIR sections are performing the best based on survey results.
- US-49 coring revealed considerable variation underneath the pavement surface. Layers varied considerably (e.g. concrete slabs were sometimes present in the emulsion CIR Section 2 and were sometimes not present). Layer thicknesses varied considerably. Density (or air void) gradients were significant within CIR layers. Despite these factors, US-49 is performing relatively well, which is encouraging.
- Properties of US-49 cores demonstrated distinct differences between cement and emulsion stabilization. Emulsion CIR exhibited greater cracking resistance, while cement CIR exhibited greater modulus, strength, and rutting resistance. These trends have not yet manifested themselves meaningfully within the overall pavement's performance (i.e. distress survey results) but are likely to become more apparent over time.
- FWD data demonstrated that most US-49 sections are structurally sound through 53 months. It did, however, suggest Section 5's (cement CIR) structural capacity is low relative to the rest of US-49. This is potentially an indication of fatigue damage that, relative to other sections, may result in more rapid performance deterioration.
- Cost data and overall performance findings from US-49 suggest the triple bottom line could be positively impacted relative to current CIR practices by exploring MCB systems (e.g. balanced amounts of cement and emulsion). Generally, SCB systems often result in excess reserve capacity with respect to one or more distresses while perhaps resulting in insufficient capacity with respect to another distress. MCB systems could potentially address this issue as well as provide economically-competitive alternatives.

# CHAPTER 13 – SINGLE AND MULTIPLE COMPONENT BINDER RESULTS

## 13.1 Overview of Single and Multiple Component Binder Results

CIR has been used for decades as a pavement rehabilitation technique. During this time, single component binder (SCB) systems have governed the CIR market. Recall that SCB systems, as defined in this report, are those with one binder (or two if the secondary binder dosage is 1% or less). Two SCB examples are 4% portland cement or 3% asphalt emulsion with 1% hydrated lime. In contrast, this chapter focuses efforts on multiple component binder (MCB) systems. An MCB example is 2.5% emulsion with 2% cement.

CIR, in general, is of interest with respect to the ASCE sustainability triple bottom line, which focuses on economics, environment, and social well-being. While traditional CIR mixtures with SCB systems have demonstrated positive impacts on the triple bottom line as demonstrated in Chapter 12, CIR mixtures with MCB systems exhibit the potential for even greater triple bottom line impacts. To this end, this chapter aims to contribute to the CIR knowledge base in three key areas (KA):

KA1. Universal Design Framework: Present a CIR specimen preparation, curing, and testing framework which can be universally applied to any mixture irrespective of the bituminous or cementitious stabilization materials. This type of framework is needed for unbiased side-by-side comparisons of various binder types and does not currently exist. Further, this type of framework could offer agencies (e.g. departments of transportation, DOTs) flexibility to continue SCB use or consider MCB use.

KA2. MCB Sustainability Advantages: Provide evidence within a universal design framework that CIR incorporating MCB systems, when conditions warrant, is more likely to positively affect the triple bottom line than almost exclusive reliance on SCB systems, which is the current state of practice. Specifically, MCB systems could optimize economics and performance on a project-by-project basis. For example, economic and field performance data in Chapter 12 indicated emulsion SCB sections of US-49 were less economical and rut resistant, but more crack resistant, than cement SCB sections. A balanced MCB system is believed to be able to provide adequate cracking and rutting resistance with mid-range economics.

KA3. Extensive SCB and MCB Characterization: Present data for a broad spectrum of SCB and MCB binder blends. Specifically, incremental adjustments in MCB emulsion and cement contents herein provide resolution regarding MCB trends. In contrast, current literature typically compares limited numbers of binder blends for a given highway's exiting materials.

Data presented in this chapter is the culmination of all previous chapters. For this reason, components of the presented design framework discussed in previous chapters are summarized herein. Chapters prior to this one focused on foundational aspects of a universal design framework (e.g. curing protocols) which were applicable to SCB or MCB systems. This chapter provides an extensive characterization of SCB and MCB systems within a universal design framework.

## 13.2 Review of Universal Framework Components

Work towards components of the universal design method presented in previous chapters is summarized in this section. Together, components presented comprise the mix characterization approach that was used throughout this chapter.

### 13.2.1 Moisture in Compaction

Chapter 8 and 11 evaluated moisture's role during compaction and its effect on compacted density. SGC dry densities in Chapter 8 were indifferent to *MC* between 6 and 10%, and *MC*s were around 6% by 30 gyrations regardless of initial *MC*. A 6% maximum *MC* was recommended and supported by Chapter 11 findings and was used in this chapter.

### 13.2.2 Moisture during Curing

Chapter 11 also addressed moisture as it relates to curing in a universal design protocol since existing curing protocols are considerably different for bituminous and cementitious binders. Overall, Chapter 11 concluded either humid or dry oven curing are candidates for a universal design method although the humid oven appears to be a more logical choice at present, at least in Mississippi and much of the southeast US where field conditions are humid. Humid oven curing was used in this chapter.

### 13.2.3 Density and Air Voids

Chapter 10 sought after more reliable maximum and bulk specific gravity ($G_{mm}$ and $G_{mb}$) measurement for $V_a$ determination. Vacuum sealing (CoreLok®) was used to measure $G_{mm}$ and $G_{mb}$. Air voids reported in this chapter were measured according to the $G_{mm}$ and $G_{mb}$ approach developed in Chapter 10; Equation 10.2 was used to determine $G_{mm}$.

### 13.2.4 Performance Characterization Tests

Chapter 3 performed an initial assessment of performance tests available for AC with potential to characterize CIR for a diverse array of binding agents. Findings were APA wheel tracking following traditional protocols was informative, and IDT testing ($S_t$ and FE) appeared promising.

Research in Chapters 8 through 11 established key aspects of a universal design framework: mixing and compaction moisture recommendations (6% maximum *MC*), curing recommendations (40 °C at 35 to 50% humidity), a method to measure $G_{mm}$, $G_{mb}$, and $V_a$, and a screening of various performance tests. However, Chapters 8 through 11 did not fully evaluate performance characteristics of SCB and MCB systems. This chapter builds on the prior chapters by addressing this issue.

## 13.3 Laboratory Testing Details

CIR specimens were produced in this chapter with R1 (US-49 RAP) using nine binder combinations which are shown in Table 13.1. The 4.4c and 4e1HL blends were the

US-49 CIR design blends and, thus, were the initial SCBs considered. Cement and emulsion were adjusted in 1% increments to produce all other blends. Three cement and three emulsion SCB blends were tested. Emulsion SCBs always included 1% hydrated lime as in the US-49 design. Three cement-emulsion MCB blends were tested to provide a symmetrical progression between US-49 SCB design blends. Note that 3.5c1e is, by definition, an SCB; however, it was used herein as an MCB for a more symmetrical matrix of MCB binder blends.

**Table 13.1. SCB and MCB Binder Combinations Tested**

| | Cement SCB | | | Cement/Emulsion MCB | | | Emulsion SCB | | |
|---|---|---|---|---|---|---|---|---|---|
| **Blend ID** | **2.5c** | **3.5c** | **4.4c** | **3.5c1e** | **2.5c2e** | **1.5c3e** | **4e1HL** | **3e1HL** | **2e1HL** |
| Cement (%) | 2.5 | 3.5 | 4.4 | 3.5 | 2.5 | 1.5 | 0 | 0 | 0 |
| Emulsion (%) | 0 | 0 | 0 | 1 | 2 | 3 | 4 | 3 | 2 |
| Hydrated Lime (%) | 0 | 0 | 0 | 0 | 0 | 0 | 1 | 1 | 1 |

CIR specimens were either 30-gyration SGC specimens compacted according to Section 4.4.2.1 or LAC slabs compacted according to 4.4.2.2. Specimens were humid oven cured for various cure times (3, 7, 14, 28, 56, 90, and 180 days). Note that a small set of R1(A/R)-4.4c specimens were also CR cured. For all SGC $V_a$'s, 95% confidence intervals were calculated and are reported as follows: 16.3 to 18.4% (cement SCBs), 13.6 to 17.2% (emulsion SCBs), and 14.9 to 17.7% (MCBs). SCB and MCB systems were characterized using the following test methods: APA wheel tracking, PW wheel tracking, MSP-$L_L$ permeability, D7369 $M_r$, T322 creep compliance, IDT strength, and FE.

## 13.4 Wheel Tracking and Permeability Results

Figure 13.1 presents APA, PW, and permeability results. Cement SCB APA $RD_{APA}$'s, at approximately 1 mm, were practically negligible. $RD_{APA}$ ever so slightly decreased as cement content increased. Chapter 9 cites various $RD_{APA}$ threshold criteria of 4 to 6 and 12 mm for high-traffic and standard- and medium-traffic routes in MS as well as 8 mm. Cement SCB $RD_{APA}$'s were well below both these thresholds and are also well below AC values presented in Chapter 6. Emulsion SCB $RD_{APA}$'s fall among Chapter 6 AC values but also among cited thresholds, indicating discretion is warranted regarding emulsion SCB rutting.

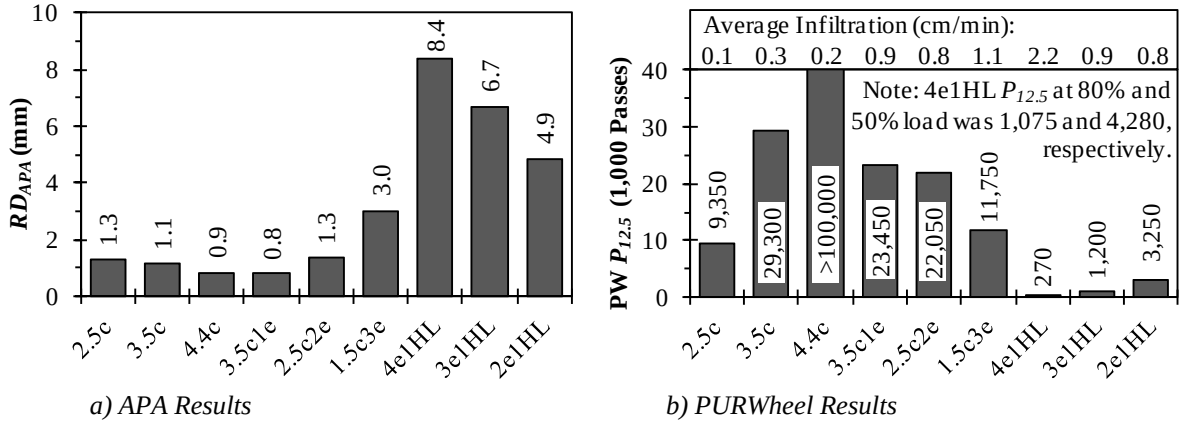


*a) APA Results* *b) PURWheel Results*

**Figure 13.1. Wheel Tracking and Infiltration Results**

MCB results demonstrated an exponential trend from insignificant (4.4c) to considerable (4e1HL) rutting. Relative to 4e1HL, 1.5c3e exhibited a considerable $RD_{APA}$ decrease; 2.5c2e exhibited another noticeable decrease at which point $RD_{APA}$ was similar to all other blends including cement. APA results indicate rutting concerns with emulsion SCBs are completely eased with cement SCBs or can be comfortably managed with emulsion-dominated MCBs.

PW results are slightly more pronounced than APA results due to the presence of moisture. Chapter 6 AC $P_{12.5}$'s ranged from approximately 5,500 to 8,000 passes, and all cement SCB $P_{12.5}$'s exceeded AC values. The 4.4c blend did not meaningfully degrade through 100,000 passes where testing was eventually terminated ($P_{12.5}$ for 4.4c at 28 days was also >100,000 passes). The 2.5c and 3.5c blends experienced degradation (rather than densification or shear failure). Emulsion SCB $P_{12.5}$'s were well below AC values and decreased with increasing emulsion content. As with the APA, MCBs demonstrated ability to balance wheel tracking performance.

Permeability, as characterized by infiltration (*Inf*), was measured on LAC slabs prior to PW testing as a durability index. *Inf* ranged from 0.1 to 2.2 cm/min with cement SCB *Inf*'s being distinctly lower than emulsion SCB or MCB *Inf*'s. Volume 3 of the State Study 250 report documents average *Inf*'s for field-compacted asphalt concrete ranging from 0.5 to 4.2 cm/min. CIR *Inf* values appear reasonable if not lower than expected given its high $V_a$'s (the LAC may produce relatively sealed slab surfaces). Based on results presented, permeability does not seem to be of greater concern than for typical asphalt concrete.

## 13.5 Resilient Modulus Results

Figure 13.2a presents $M_r$ results for 14-day humid oven cured specimens, which were generally 20 to 30% of Chapter 6 AC $M_r$ results. Cement SCB $M_r$, ranging from approximately 3 to 9 GPa, generally increased with cement content and was relatively insensitive to temperature. Emulsion SCB $M_r$ was considerably temperature-dependent. At 20 °C, $M_r$ was approximately 1.8 GPa for all emulsion contents. At lower temperatures, differences between emulsion contents were more apparent. MCB $M_r$ exponentially decreased and became increasingly temperature-dependent when progressing from 4.4c to 4e1HL. MCB results illustrate ability to affect $M_r$; however, 2.5c2e was the only MCB blend that, at 20 °C, yielded an $M_r$ which meaningfully balanced cement and emulsion SCB $M_r$'s (i.e. 4.4c and 3.5c1e or 1.5c3e and 4e1HL were not practically different).

Variability was investigated at 20 °C and 14 days of curing for 4.4c, 2.5c2e, and 4e1HL. Five tests (15 specimens) were conducted for each blend yielding between-test coefficients of variation (COVs) of 3.4, 11.7, and 5.7%, respectively. This degree of variability is very manageable for CIR (D7369 within-laboratory repeatability 1*s* (i.e. COV) is 7% for AC).

Figure 13.2b presents $M_r$ results at 20 °C for 14 to 180 days of humid oven curing. In this case, only 4.4c, 4e1HL, and MCB blends were tested. Aside from 180-day $M_r$, 4.4c $M_r$ generally increased with time, likely due to cement hydration. Similarly, 4e1HL $M_r$ increased over time, likely due to a combined effect of emulsion curing at early ages and aging at later ages. $M_r$ for 3.5c1e and 2.5c2e was variable, and 3.5c1e $M_r$ generally decreased over time, though $M_r$ would be expected to increase with curing. This trend is not understood at present.

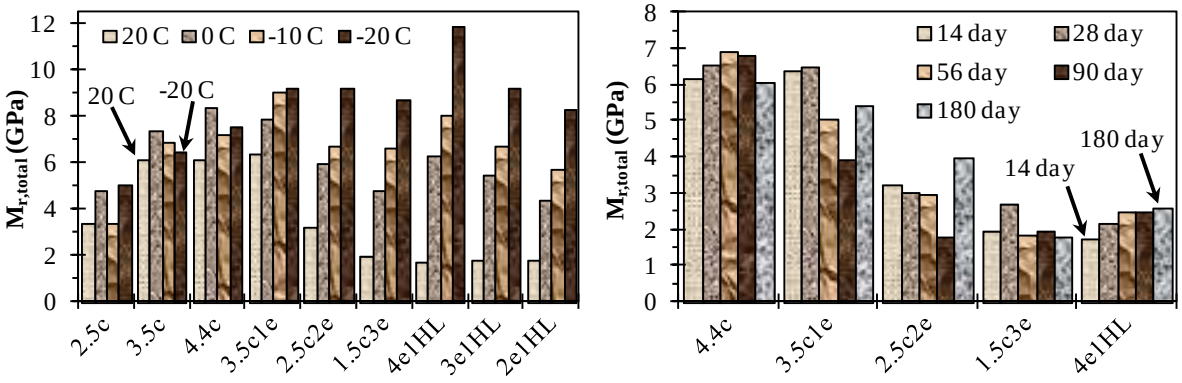


*a) 14-day $M_r$ Results* *b) Long-term 20 °C $M_r$ Results*

**Figure 13.2. Resilient Modulus Results**

## 13.6 Creep Compliance Results

Figure 13.3 presents $T_{crit}$ results derived from creep compliance testing. LTSTRESS calculates $S_{t,f}$ for $T_{crit}$ determination as 78% of $S_{t,ult}$, which is based on a relationship presented in NCHRP Report 530 (Christensen and Bonaquist 2004). Figure 13.3 results used the 78% relationship, but results (in brackets) were also calculated using the directly-measured $S_{t,f}$ to $S_{t,ult}$ relationship for CIR, which was 89% on average. Though this shifts $T_{crit}$ results slightly, overall trends are not affected. Results are discussed in terms of LTSTRESS calculated values.

At between 4 and 5 °C, cement SCB $T_{crit}$ values were similar for all dosages. Emulsion SCB $T_{crit}$ values, ranging from -21.6 to -17.8 °C, were considerably lower (which is better) and varied by emulsion content. MCB $T_{crit}$ values fell in between SCB values and improved as MCB blends progressed from 4.4c to 4e1HL. MCBs demonstrate ability to improve thermal cracking performance relative to cement SCBs, which are typically of greater concern regarding cracking.

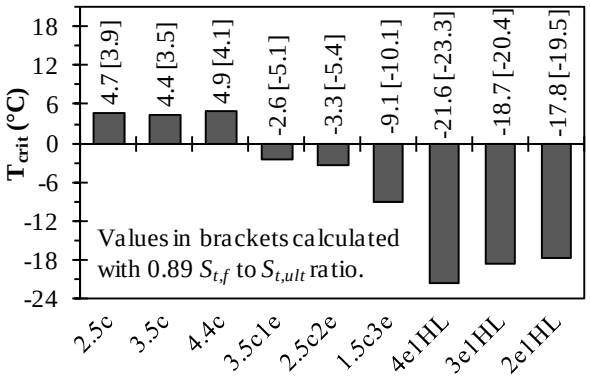


**Figure 13.3. Critical Cracking Temperature Results**

## 13.7 Strength and Fracture Energy Results

Figure 13.4a presents $S_{t,ult}$ results for 14-day humid oven cured specimens, which were on average 15 to 25% of Chapter 6 AC $S_{t,ult}$ results depending on temperature. As with

$M_r$, Figure 13.4a results increased as temperature decreased. The low-temperature (0 °C and below) $S_{t,ult}$'s, however, were primarily used for calculation of $T_{crit}$ values discussed in the previous section. When used in mix design methods or for mixture characterization, intermediate-temperature (e.g. 20 °C) $S_{t,ult}$'s are primarily used and are the focus of remaining discussion.

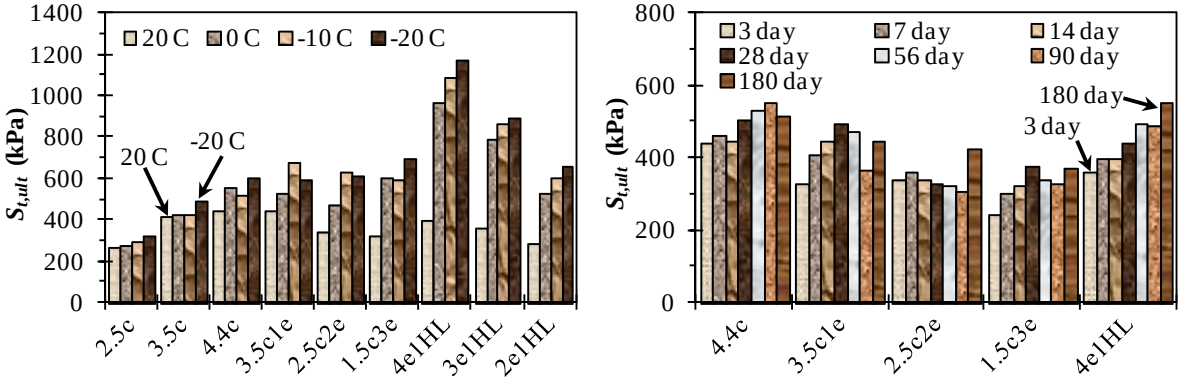


*a) 14-day $S_{t,ult}$ Results* *b) Long-term 20 °C $S_{t,ult}$ Results*

**Figure 13.4. Indirect Tensile Strength Results**

For 20 °C results, trends among SCBs and MCBs were less distinct than for other properties (e.g. $T_{crit}$). Consequently, $S_{t,ult}$'s are alternatively discussed in reference to the Table 2.2 literature criteria of 276 to 310 kPa minimum. All binder systems except 2.5c and 2e1HL yielded $S_{t,ult}$'s greater than 310 kPa. At 269 and 283 kPa, 2.5c and 2e1HL $S_{t,ult}$'s are concerning but are also reasonable given these blends have the lowest binder dosages. MCB $S_{t,ult}$'s, namely for 2.5c2e and 1.5c3e, were approximately 20% lower than for the US-49 design SCB blends (4.4c and 4e1HL). This result seems counterintuitive and perhaps could be further investigated in future research efforts, but these $S_{t,ult}$'s were slightly above Table 2.2 thresholds nonetheless.

Variability was investigated at 20 °C and 14 days of curing for 4.4c, 2.5c2e, and 4e1HL. Five tests (15 specimens) were conducted for each blend yielding between-test COVs of 5.1, 3.4, and 3.0%, respectively. This degree of variability is very manageable for CIR (at 25 °C, ASTM D6931 suggests a single-laboratory standard deviation of 80 kPa for AC, corresponding to approximately 20% COV in this case).

Figure 13.4b presents $S_{t,ult}$ results at 20 °C for 3 to 180 days of humid oven curing. As with $M_r$, only 4.4c, 4e1HL, and MCB blends were tested. $S_{t,ult}$ increased over time for both 4.4c and 4e1HL SCBs. Generally, $S_{t,ult}$ over time increased for MCBs though trends were less intuitive and more variable with 2.5c2e.

Figure 13.5a presents FE results for 14-day humid oven cured specimens. Cement SCB FE values were low, ranging from 0.03 to 0.07 kJ/m$^3$ for all cement contents and temperatures. In contrast, emulsion SCB FE values decreased considerably with temperature and varied by emulsion content. At 20 °C, FE ranged from 0.87 kJ/m$^3$ with 4e1HL to 0.29 kJ/m$^3$ with 2e1HL (AC FE values in Chapter 6 were 2.6 kJ/m$^3$ on average). Overall, 4e1HL FE values at 20 °C were more than an order of magnitude greater than for 4.4c. MCB FE values exponentially increased from 4.4c to 4e1HL and also increased in temperature dependence.

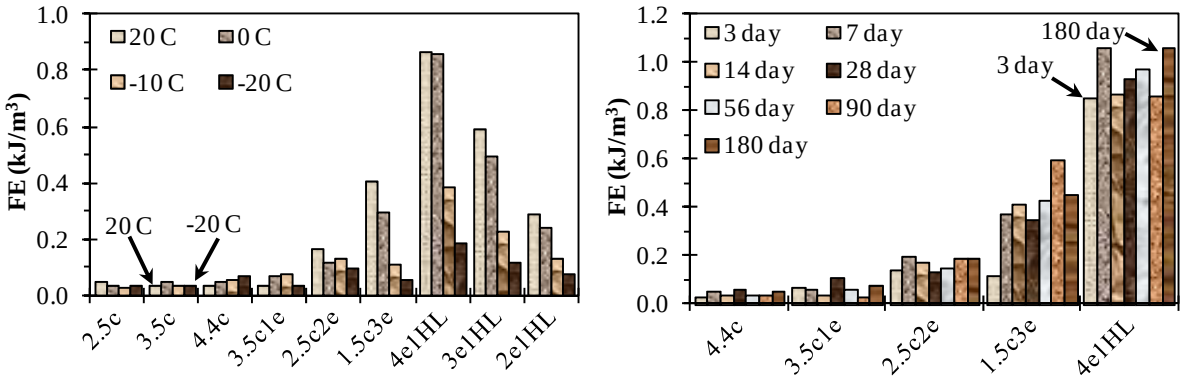


*a) 14-day FE Results* *b) Long-term 20 °C FE Results*

**Figure 13.5. Fracture Energy Results**

Variability was investigated at 20 °C and 14 days of curing for 4.4c, 2.5c2e, and 4e1HL. Five tests (15 specimens) were conducted for each blend yielding between-test COVs of 22.0, 26.3, and 8.8%, respectively. Though this variability is greater than for $M_r$ and $S_{t,ult}$, it could still be deemed manageable for CIR.

Figure 13.5b presents FE results at 20 °C for 3 to 180 days of humid oven curing. Overall, FE appeared relatively constant over time though some variability was present and the 1.5c3e FE seemed to increase slightly.

For the 4.4c blend, several tests were performed on specimens CR cured for comparison to HO curing. Figure 13.6 presents $S_{t,ult}$ and FE results from 3 to 56 days of curing. At 56 days, CR $S_{t,ult}$ was approximately 1.5 times greater than HO $S_{t,ult}$ and exhibited an increasing trend; whereas, HO strength gain seemed relatively constant in comparison. FE results were similar. Figure 13.6 highlights noticeable differences between CR and HO curing. Specifically, it demonstrates the usefulness of a universal design framework to treat various binder systems identically for direct comparisons. Without a universal framework, direct comparisons of cement SCB and emulsion SCB properties are not possible.

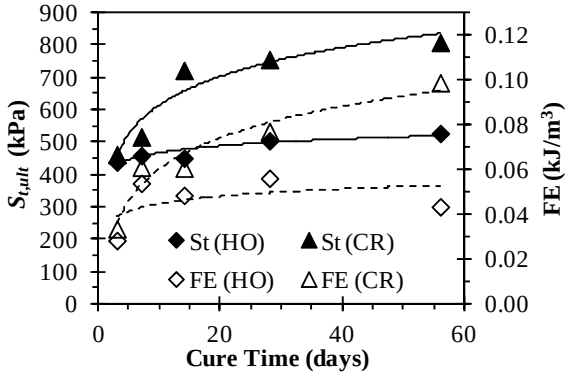


**Figure 13.6. Humid Oven versus Curing Room for R1(A/R)-4.4c**

## 13.8 Discussion of SCB and MCB Characterization Results

Perhaps with the exception of $S_{t,ult}$, differences between cement SCB and emulsion SCB systems were distinct for all properties presented. Cement SCB systems offered

superior wheel tracking performance and higher $M_r$ values, while emulsion SCB systems offered superior critical cracking temperatures and greater FE values. CIR wheel tracking results were comparable to AC results presented in Chapter 6; however, CIR $M_r$, $S_{t,ult}$, and FE results were considerably lower than Chapter 6 AC results. MCB results demonstrated promise in that MCBs were able to more optimally utilize useful attributes of cement and emulsion SCBs by balancing rutting and cracking properties.

With regard to the three key contribution areas (KAs), the tests evaluated herein were informative within a universal design framework (KA1) in that most tests were able to differentiate cement and emulsion binders and dosages. APA wheel tracking was insightful, and results were supported by additional, and arguably more severe, PURWheel testing. The APA, being a common test, could be incorporated into agency design methods for rutting characterization with relative ease. $M_r$ and $T_{crit}$ results were informative and could be used in universal design as they already are by some agencies (Table 2.2).

Though $S_{t,ult}$ was not generally capable of distinguishing binder systems, minimum strength requirements could still be useful in a design method. FE results were informative and capable of distinguishing binder blends. Further, $T_{crit}$ and FE results supported each other, which is encouraging. While FE is less practical for mix design operations than the commonly specified Marshall stability, FE data exhibits greater value and can be obtained with little additional effort when $T_{crit}$ testing is required as is currently the case with several agency specifications.

Regarding MCB advantages (KA2), MCBs were able to balance desirable and less desirable traits of SCBs. As supported by the field study of US-49 cement and emulsion SCB sections in Chapter 12, SCB systems may result in excess reserve capacity for one distress and no reserve capacity of another. For example, the US-49 cement SCB section exhibits no rutting concerns (excess reserve capacity) but is showing modest cracking distresses at 53 months of service (lesser reserve capacity). Based on results presented herein, MCB systems could offer a more balanced solution to this issue, positively impacting ASCE's triple bottom line. Given the differences in emulsion and cement costs, MCB economic impacts could also be important.

Figure 13.7 uses FE and APA data from this chapter, as well as cost data from Chapter 12, to illustrate an example mix design plot and evaluate optimization abilities with MCBs. Note that other results (e.g. $T_{crit}$) could have been shown with similar implications. Rutting and cracking are best balanced around 1.5c3e (i.e. a small dosage of cement can considerably improve rutting while a larger dosage of emulsion is needed to maintain cracking resistance). This finding alone is not necessarily unique as many agencies already incorporate a small amount of cement or hydrated lime. However, the Figure 13.7 concept is unique with respect to its potential value, partly due to the symmetrical distribution of MCBs tested (KA3). The following paragraph discusses examples in which Figure 13.7 provides flexibility for an agency (KA1).

Since Figure 13.7 incorporates cracking, rutting, and cost data, multiple parameters can be considered on a project-by-project basis, taking into account route type, traffic level, anticipated surface (e.g. chip seal, thin AC overlay, thick AC overlay), and current material costs. In one case, an agency may have many routes in need of repair and might opt for cement-dominated binders so that a fixed budget can repair more lane miles. In another case, an agency may opt for reserve rutting capacity (cement-dominated) and tolerate more cracking so that a chip seal surface can be used without major rutting concerns since it is

typically a greater safety concern than cracking. Lastly, for a lightly-trafficked route where rutting distresses would take longer to develop, an agency may elect to spend more for reserve cracking capacity (emulsion-dominated) in hopes of a longer service life.

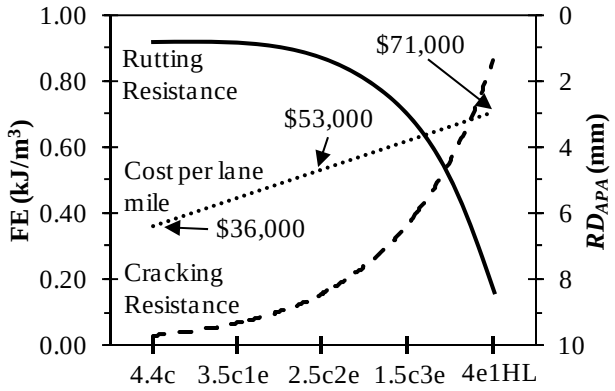


**Figure 13.7. CIR Optimization with MCB Systems**

In all cases, Figure 13.7 could likely be used to make more informative decisions. Additionally, agencies could continue using current design blends (e.g. emulsion SCB) but would also have the flexibility to explore other options if desired. Lastly, the Figure 13.7 approach could prevent repeat occurrences such as the one documented by Thomas et al. (2000) in Kansas (see Section 2.5) and would more effectively promote a fair and competitive bidding process. Rather than having to predetermine CIR binder type in order to specify a design method, agencies could establish and specify performance criteria and allow bidders to bid any binder combination, SCB or MCB, they choose as long as it satisfies the criteria. This would be conceptually similar to some agencies allowing hot and warm mix asphalt to be bid interchangeably.

## 13.9 Key SCB and MCB Characterization Findings

A major goal of this chapter was to utilize a universal design framework for CIR that is indifferent to binder type and can accommodate cementitious and bituminous binder types either individually (SCB) or collectively (MCB). By studying a broad range of cement SCB, emulsion SCB, and cement-emulsion MCB systems, this chapter demonstrated potential advantages of MCB systems. Key findings from this chapter are as follows:

- A universal CIR design framework is capable of providing direct comparisons between cement and emulsion SCB systems and accommodating MCB systems, offering increased flexibility to agencies.
- The framework presented (applicable to CIR with 100% RAP) entails SGC compaction (30 gyrations) of CIR materials at 6% *MC* (Chapters 8 and 11) followed by curing in a 40 °C oven at 35 to 50% humidity (Chapter 11) for an established cure time (14 days was the predominant cure time herein). Specimen $V_a$ is determined by the vacuum sealing method (both $G_{mm}$ and $G_{mb}$), which is capable of interfacing with construction (Chapter 10). Design binder blends are determined based on several parameters: rutting, cracking, and cost (Chapter 13).

- For SCB systems, cement blends offered low cracking resistance, high rutting resistance, and lower costs. Emulsion blends yielded the opposite. Both were similar regarding $S_{t,ult}$.
- For MCB systems, rutting, cracking, and cost can be balanced by proportioning cementitious and bituminous binders, which can positively impact the triple bottom line. Overall, the 1.5c3e blend, while not the most economical blend tested, appeared to offer the best balance between rutting and cracking.

# CHAPTER 14 – SUMMARY, CONCLUSIONS, AND RECOMMENDATIONS

## 14.1 Summary

This report focused on cold in-place recycling (CIR) and presented laboratory and field data collected during this multi-year study. The contents of this report are intended for in-place recycled material consisting only of asphalt concrete and gradations resembling Figure 2.1a. The primary objective of this report was to characterize CIR properties that are important to design, construction, and performance in high traffic applications. This objective was met, and the findings should provide MDOT with information to aid in their future CIR endeavors. This report considers single component binder (SCB) or multiple component binder (MCB) systems used to stabilize RAP to produce CIR.

This report can be divided into three groups of information: 1) research literature and current practice that represent the state of the art for CIR (Chapters 2 and 7); 2) material properties and experimental methods utilized in this project (Chapters 3 through 6); and 3) the universal characterization framework capable of considering any type of binder that is the main contribution of the CIR efforts of State Study 250 (Chapters 8 through 13). Chapters 2 and 7, when viewed together, clearly show a gap in current practice that Chapters 8 through 13 aimed to help fill. Stated simply, a framework capable of encompassing any cementitious or bituminous binder within one protocol in an unbiased way did not exist prior to completion of the activities presented in this report to the authors' knowledge. A framework of this nature would allow an agency such as MDOT to establish and specify performance criteria, allowing bidders to bid any binder combination, SCB or MCB, as long as it satisfies specified criteria. This would be conceptually similar to MDOT allowing hot and warm mix asphalt to be bid interchangeably, would prevent MDOT from having to predetermine a binder type in order to specify a design method, and would promote an overall fair bidding process. The following sections provide the conclusions and recommendations from this report.

## 14.2 Conclusions

The primary conclusion from this report is that a framework capable of systematically addressing single or multiple component binder systems in an unbiased manner for CIR is feasible technically and from the standpoint of implementation. Also, there seems to be an opportunity to improve the Mississippi highway system from the perspectives of economics and performance by utilizing in-place recycling where this report's universal framework is applied in some way. The most relevant conclusions from this work moving forward are provided in the following list, while findings that are more specific in nature are mostly left for the summary sections of Chapters 7 through 13.

1. Existing state DOT design methods are reasonable for cement SCB systems, existing state DOT design methods are worth reconsidering for emulsion SCB systems, and none of the design methods in existence appear ideal for a universal CIR design framework capable of handling any binder system (SCB or MCB).
2. CIR materials are more suitably compacted with the Superpave Gyratory Compactor (SGC) than with a Proctor hammer.

3. Asphalt Pavement Analyzer (APA) wheel tracking via typical MDOT protocols and instrumented indirect tensile (IDT) testing were the most promising characterization methods for a universal CIR framework based on several evaluation criteria.
4. CIR benefits from use of bulk and maximum specific gravity ($G_{mb}$ and $G_{mm}$) principles as $G_{mm}$ provides a consistent reference density and $G_{mb}$ encompasses the intent of other common bulk density properties in use (e.g. maximum dry density from Proctor testing).
5. Humid oven curing (40 °C and 35 to 50% humidity) and dry oven curing (40 °C) appear to reasonably represent outdoor curing conditions in the Mississippi summer and were not greatly different from each other.
6. Pavement distress survey results at 53 months indicate all sections of US-49 are performing satisfactorily. Recycled sections are performing comparably to, or slightly better than, the completely reconstructed section.
7. Properties of US-49 cores demonstrated distinct differences between cement and emulsion stabilization. Emulsion exhibited greater cracking resistance, while cement exhibited greater modulus, strength, and rutting resistance. These trends have not yet manifested themselves meaningfully within the overall pavement performance but are likely to become more apparent over time.
8. FWD data demonstrated that most US-49 sections are structurally sound through 53 months. It did, however, suggest Section 5 (cement CIR) structural capacity is low relative to the rest of US-49.
9. Cost data and overall performance findings from US-49 suggest the triple bottom line of environment, economics, and social well-being could be positively impacted relative to current CIR practices by exploring more balanced multiple component binder blends (e.g. balanced amounts of cement and emulsion). Generally, single component binder blends often result in excess reserve capacity with respect to one or more distresses while perhaps resulting in insufficient capacity with respect to another distress. Multiple component binder systems could potentially address this issue as well as provide economically-competitive alternatives. US-49 base layer costs ranged from $22,000 to $62,000 per lane kilometer (Table 12.8), and the data presented in this report suggests these costs could be better optimized with respect to rutting and cracking performance.
10. Overall, a blend of 1.5% cement and 3% emulsion by mass, while not the most economical blend tested, appeared to offer the best balance of rutting and cracking.

## 14.3 Recommendations

The primary recommendation from this report is for MDOT to consider constructing a full scale test section or test sections that contain a cement-dominated SCB system, an emulsion-dominated SCB system, and one or two MCB systems. The universal framework presented in this report should be used to select dosages for all test sections. These sections should be monitored during construction and over time. Specific recommendations are provided in the following list.

1. MDOT should implement the universal framework presented herein and not adopt design methods from other states so that a wider array of binders can be considered to meet the diverse needs of CIR projects.

2. CIR specimen preparation during design should utilize a total moisture content of 6%; i.e. Proctor optimum moisture content determination should be abandoned.
3. CIR compaction during design in the 30 to 40 gyration range is recommended until more data is available. Nothing observed during this study led the authors to believe that a design gyration level of 30 (the most prevalent value in research literature and current practice) was problematic. Data in Chapter 8 suggested 30 gyrations resembled Proctor density for US-49 material, while data in Chapter 11 suggested 43 gyrations replicated in-place density for the US-45Alt cement CIR project that used a very large number of roller passes.
4. Vacuum sealing is recommended for determination of CIR $G_{mm}$ where 100% RAP is used; specifically, Equation 10.2 is recommended for use with the note that the equation should be studied further and refined if warranted.
5. AASHTO T269 or T331 is recommended for CIR; T166 is not recommended.
6. Humid oven curing (40 °C, 35 to 50% humidity) for 7 days is recommended for CIR.
7. APA rut depth, indirect tensile strength, and fracture energy should be used as response criteria after curing. Rut testing is recommended at 64 °C, and indirect tensile strength and fracture energy (measured on the same specimens) testing is recommended at 20 °C for MDOT's climate.

# CHAPTER 15 – REFERENCES


AASHTO (1993). *Guide for Design of Pavement Structures*, Washington, D.C.

AASHTO (1998). *Cold Recycling of Asphalt Pavements*. Task Force 38 Report, Joint Committee AASHTO-AGC-ARTBA.

AI (2001). *Superpave Mix Design: Superpave Series No. 2 (SP-2)*. 3rd Edition. Asphalt Institute, Lexington, KY.

Alabama (2009). *Laboratory Design of Soil-Cement and Full-Depth Reclamation Mixes*. ALDOT Procedure ALDOT-416, Alabama Department of Transportation.

Alcoke, W.H., Robbins, E.G., Taylor, J.E., (1979). "Cold Recycling of Failed Flexible Pavements with Cement," *Transportation Research Record: Journal of the Transportation Research Board*, 734, pp 22-27.

Allen, D., Hicks, R.G., Rogge, D.F., Scholz, T.V. (1992). "Use of Asphalt Emulsions for In-Place Recycling: Oregon Experience," *Transportation Research Record: Journal of the Transportation Research Board*, 1342, pp 95-102.

Anderson, D.A., Luhr, D.R., Larh, M. (1985). *Cold In-Place Recycling of Low-Volume Roads in Susequehanna County, Volume I: Technical Report.* Report No. FHWA/PA-84/020, Pennsylvania Department of Transportation, Harrisburg, PA.

Apeagyei, A.K., Diefenderfer, B.K. (2013). "Evaluation of Cold In-Place and Cold Central-Plant Recycling Methods Using Laboratory Testing of Field-Cored Specimens," *Journal of Materials in Civil Engineering*, 25(11), pp 1712-1720.

Artamendi, I., Khalid, H. (2006). "A Comparison between Beam and Semi-Circular Bending Fracture Tests for Asphalt," *Road Materials and Pavement Design*, 7(1), pp 163-180.

Aschenbrener, T. (1995). "Evaluation of the Hamburg Wheel-Tracking Device to Predict Moisture Damage in Hot Mix Asphalt," *Transportation Research Record: Journal of the Transportation Research Board*, 1492, pp 193-201.

Babei, K., Walter, J.P. (1989). *Evaluation of the Performance of Cold-Mix Recycled Asphalt Concrete Pavement in Washington*. Report WA-RD 201.1, Washington State Department of Transportation, Olympia, WA.

Bandyopadhyay, S.S. (1982). "Structural Performance Evaluation of Recycled Pavements by Using Dynamic Deflection Measurements," *Transportation Research Record: Journal of the Transportation Research Board*, 888, pp 38-43.

Bang, S., Lein, W., Comes, B., Nehl, L., Anderson, J., Kraft, P., deStigter, M., Leibrock, C., Roberts, L., Sebaaly, P., Huft, D. (2011). *Quality Base Material Produced Using Full Depth Reclamation on Existing Asphalt Pavement Structure – Task 4: Development of FDR Mix Design Guide*. Final Report FHWA-HIF-12-015. U.S. Department of Transportation, Washington, D.C.

Badaruddin, S.R., McDaniel, R.S. (1992). "Cold In-Place Recycling for Rehabilitation and Widening of Low-Volume Flexible Pavements in Indiana," *Transportation Research Record: Journal of the Transportation Research Board*, 1342, pp 13-19.

Berthelot, C., Haichert, R., Podborochynski, D., Wandzura, C., Taylor, B., Guenther, D. (2010). "Cement Stabilization of Reclaimed Asphalt Pavement Materials," CD-ROM, *Transportation Research Board 89th Annual Meeting*, Washington, D.C. Paper 10-1803.

Birgisson, B., Montepara, A., Romeo, E., Roque, R., Roncella, R., Tebaldi, G. (2007). "Determination of Fundamental Tensile Failure Limits of Mixtures," *Journal of the Association of Asphalt Paving Technologists*, 76, pp 303-344.

Birgisson, B., Soranakom, C., Napier, J.A.L., Roque, R. (2003). "Simulation of Fracture Initiation in Hot-Mix Asphalt Mixtures," *Transportation Research Record: Journal of the Transportation Research Board*, 1849, pp 183-190.

Bradbury, A., Kazmierowski, T., Raymond, C., Cheng, S. (1991). "Cold In-Place Recycling In Ontario – A Case Study," *Proceedings of the 36th Annual Conference of Canadian Technical Asphalt Association*, Ottawa, Ontario, pp 153-170.

Braham, A., Howard, I.L., Barham, J., Cox, B.C. (2014). "Characterizing Emulsion Effects on Aged Asphalt Concrete Surfaces Using Bending Beam Rheometer Mixture Beams," *International Journal of Pavement Engineering*, 16(7), pp 620-631.

Brown, E.R., Kandhal, P.S., Zhang, J. (2001). *Performance Testing for Hot Mix Asphalt*. NCAT Report 01-05, National Center for Asphalt Technology, Auburn, AL.

Brown, S.F., Needham, D. (2000). "A Study of Cement Modified Bitumen Emulsion Mixtures." *Journal of the Association of Asphalt Paving Technologists*, 69, pp 92-121.

Buchanan, M.S., White, T.D., Smith, B.J. (2004). *Use of the Asphalt Pavement Analyzer to Study In-Service Asphalt Mixture Performance*. Report No. FHWA/MS-DOT-RD-04-155, Mississippi Department of Transportation, Jackson, MS.

Buttlar, W.G., Roque, R., Kim, N. (1996). "Accurate Asphalt Mixture Tensile Strength," *Proceedings of the 4th Materials Engineering Conference: Materials for a New Millennium*, Washington, D.C., pp 163-172.

California (2005). *Method of Test for Determining the Percent of Emulsified Recycling Agent to Use for Cold Recycling of Asphalt Concrete*. Lab Procedure No. 8, California Department of Transportation.

California (2013). *Full Depth Reclamation Using Cement*. Caltrans Division of Maintenance, California Department of Transportation.

Carter, A., Feisthauer, B., Lacroix, D., Perraton, D. (2010). "Comparison of Cold In-Place Recycling and Full-Depth Reclamation Materials," CD-ROM, *Transportation Research Board 89th Annual Meeting*, Washington, D.C., Paper 10-1325.

Chan, P., Tighe, S.L., Chan, S. (2010). "Exploring Sustainable Pavement Rehabilitation: Cold In-Place Recycling with Expanded Asphalt Mix," CD-ROM. *Transportation Research Board 89th Annual Meeting*, Washington, D.C., Paper 10-1542.

Chen, D.H. (2007). "Field and Lab Investigations of Prematurely Cracking Pavements." *Journal of Performance of Constructed Facilities*, 21(4), pp 293-301.

Chen, D.H., Hong, F., Zhou, F. (2011). "Premature Cracking from Cement-Treated Based and Treatment to Mitigate Its Effect." *Journal of Performance of Constructed Facilities*, 25(2), pp 113-120.

Chen, D.M., Heitzman, M., Hosin, L., Jahren, C.T., Jungyong, K. (2010). "Long-Term Field Performance of Cold In-Place Recycled," *Journal of Performance of Constructed Facilities*, 24(3), pp 265-274.

Christensen, D. (1998). "Analysis of Creep Data from Indirect Tension Test on Asphalt Concrete." *Journal of the Association of Asphalt Paving Technologists*, 67, pp 458-492.

Christensen, D.W., Bonaquist, R.F. (2004). *Evaluation of Indirect Tensile Test (IDT) Procedures for Low-Temperature Performance of Hot Mix Asphalt*. NCHRP Report 530.

Cox, B.C. (2015). *Cold In-Place Recycling Characterization Framework for Single or Multiple Component Binder Systems*. PhD Dissertation, Mississippi State University, Mississippi State, MS.
http://sun.library.msstate.edu/ETD-db/theses/available/etd-10092015-130829/

Cox, B.C., Howard, I.L. (2013). *Cold In-Place Recycling and Full-Depth Reclamation Literature Review*. White Paper Number CMRC WP-13-1, Construction Materials Research Center, Mississippi State University, Starkville, MS.
http://www.cee.msstate.edu/downloads/(2013)CoxandHoward-CMRCWP13-1-LitReviewofCIRandFDR.pdf

Cox, B.C., Howard, I.L. (2014). "Vacuum Sealing Based Volumetric Density Measurement Approach for Cold In-Place Recycling," *Transportation Research Record: Journal of the Transportation Research Board*, 2444, pp 11-19.

Cox, B.C., Howard, I.L. (2015). "Merits of Asphalt Concrete Durability and Performance Tests When Applied to Cold In-Place Recycling," *Proceedings of IFCEE 2015* (GSP 256), San Antonio, TX, 2015, pp 369-379.

Cox, B.C., Howard, I.L., Jordan III, W.S. (2015a). "Recommendations for Seal Treatment Rejuvenation Specifications Based on Bending Beam Rheometer Testing of mixture Beams," *Transportation Research Record: Journal of the Transportation Research Board*, 2473, pp 23-32.

Cox, B.C., Howard, I.L., Battey, R. (2015b). "In-Place Recycling Moisture-Density Relationships for High-Traffic Applications," *Proceedings of IFCEE 2015* (GSP 256), San Antonio, TX, pp 349-358

Cross, S.A. (1999a). *Evaluation of Cold In-Place Recycled Mixtures on US-283*. Final Report KS-99-4, Kansas Department of Transportation, Topeka, KS.

Cross, S.A. (1999b). "Experimental Cold In-Place Recycling with Hydrated Lime," *Transportation Research Record: Journal of the Transportation Research Board*, 1684, pp 186-193.

Cross, S.A (2002). *Determination of $N_{design}$ for CIR Mixtures Using the Superpave Gyratory Compactor*. Final Report FHWA Agreement No. DTFH61-98-X-00095, RMRC Research Project 15, Federal Highway Administration, Washington D.C.

Cross, S.A. (2003). "Determination of Superpave® Gyratory Compactor Design Compactive Effort for Cold In-Place Recycled Mixtures," *Transportation Research Record: Journal of the Transportation Research Board, 1819*, pp 152-160.

Cross, S.A., Kearney, E.R., Justus, H.G., Chesner, W.H. (2010). *Cold-In-Place Recycling in New York State*. Report C-06-21, New York State Department of Transportation, Albany, NY.

Cross, S.A., Ramaya, B.M. (1995). "Evaluation of Cold In-Place Recycling in Kansas," *Transportation Research Board Conference Proceedings: 6th International Conference on Low-Volume Roads*, Minneapolis, MN, pp 195-206.

Doyle, J.D., Howard, I.L. (2011). "Evaluation of the Cantabro Durability Test for Dense Graded Asphalt," *Geotechnical Special Publication No. 211*, pp 4563-4572.

Doyle, J.D., Howard. I.L. (2013a). "Rutting and Moisture Damage Resistance of High RAP Warm Mixed Asphalt: Loaded Wheel Tracking vs. Conventional Methods," *Road Materials and Pavement Design*, Special Issue from 88th Association of Asphalt Paving Technologists' Annual Meeting, 14(S2), pp 148-172.

Doyle, J.D., Howard, I.L. (2013b). "Thermal Cracking Potential of High RAP-WMA Evaluated with Bending Beam Rheometer Mixture Beam Test," *Journal of Testing and Evaluation*, 41(2), pp 236-246.

Doyle, J.D., Howard, I.L. (2014). *Linear Asphalt Compactor Operator's Manual*. Manual Number CMRC M 10-1, Version 2, Construction Materials Research Center, Mississippi State University, Starkville, MS.

Doyle, J.D., Howard, I.L. (2016). “Characterization of Dense-Graded Asphalt with the Cantabro Test,” *Journal of Testing and Evaluation*, 44(1), pp 1-12.

Doyle, J.D., Howard, I.L., Robinson, W.J. (2012). “Prediction of Absorbed, Inert, and Effective Bituminous Quantities in Reclaimed Asphalt Pavement,” *Journal of Materials in Civil Engineering*, 24(1), pp 102-112.

Du, J., Cross, S.A. (2006). “Rut Depth Prediction Model for Cold In-Place Recycled Mixtures by Gray System,” *Transportation Research Board 85th Annual Meeting*, Washington, D.C., Paper 06-0281.

Du, J.C., Cross, S.A. (2007). “Cold In-Place Recycling Pavement Rutting Prediction Model Using Grey Modeling Method,” *Construction and Building Materials.* 21(5), pp 921-927.

Dudley, S.W., Majidzadeh, K., Kaloush, K. (1987). “The Recycling of Cold-Mix, In-Place Asphalt for Low-Volume Roads in Ohio,” *Transportation Research Record: Journal of the Transportation Research Board*, 1106, pp 163-172.

Epps, J.A., (1980). “State-of-the-Art Cold Recycling.” *Transportation Research Record: Journal of the Transportation Research Board*, 780, pp 68-100.

Feldman, R.F. (1972). “Density and Porosity Studies of Hydrated Portland Cement,” *Cement Technology*, 3(1), pp 5-13.

FHWA. (2011). *Cold In-place Recycling (CIR) Survey Summary*. Office of Asset Management, Pavement, and Construction. Federal Highway Administration. https://www.fhwa.dot.gov/Pavement/recycling/cir/cir01.cfm. Accessed July 18, 2013.

Forsberg, A., Lukanen, E., Thomas, T. (2002). “Engineered Cold In-Place Recycling Project: Blue Earth County State Aid Highway 20, Minnesota,” *Transportation Research Record: Journal of the Transportation Research Board*, 1813, pp 111-123.

Montepara, A., Giuliani, F. (2001). “The Role of Cement in the Recycling of Asphalt Pavement Cold-Stabilized with Bituminous Emulsions,” *Second International Symposium on Maintenance and Rehabilitation of Pavements and Technological Control*, Auburn, AL.

Gumbert, R., Harris, G. (1993). *Field Evaluation of Cold In-Place Recycling of Asphalt Concrete*. Final Report HR-303, Iowa Department of Transportation, Ames, IA.

Hansen, J. (2015). “Good Roads, Healthy America,” *Asphalt Pavement Magazine*, 20(4), pp 47-51.

Head, R.W. (1974). “An Informal Report of Cold Mix Research Using Emulsified Asphalt as a Binder,” *Journal of the Association of Asphalt Paving Technologists*, 43, pp 110-131.

Hilbrich, S.L., Scullion, T. (2011). "Evaluation of the Laboratory Mix Design and Field Performance of an Asphalt Emulsion and Cement Stabilized Full-Depth Reclamation Project in Texas," CD-ROM, *Transportation Research Board 87th Annual Meeting*, Washington, D.C., Paper 08-2439.

Howard, I.L., Cox, B.C. (2016). "Multi-Year Laboratory and Field Performance Assessment of High-Traffic US Highway 49 Full-Depth Reclamation," *Submitted to the 95th Annual Meeting of the Transportation Research Board*, Paper 16-6963.

Howard, I.L., Doyle, J.D. (2014). "Investigating the Consistency of Asphalt Density Measurement Methods Over a Wide Range of Air Voids," *Journal of Testing and Evaluation*, 42(3), pp 1-12.

Howard, I.L., Doyle, J.D., Cox, B.C. (2013a). "Merits of Reclaimed Asphalt Pavement-Dominated Warm Mixed Flexible Pavement Base Layers," *Road Materials and Pavement Design*, Special Issue from 88th Association of Asphalt Paving Technologists' Annual Meeting, 14(S2), pp 106-128.

Howard, I.L., Jordan, III, W.S., Barham, J.M., Alvarado, A., and Cox, B.C. (2013b). *Performance Oriented Guidance for Mississippi Chip Seals-Volume I*. Report No. FHWA/MS-DOT-RD-13-211-Volume I, Mississippi Department of Transportation, Jackson, MS.

Howard, I.L., Sullivan, W.G., Anderson, B.K., Shannon, J., Cost, T. (2013c). *Design and Construction Control Guidance for Chemically Stabilized Pavement Base Layers*. Report No. FHWA/MS-DOT-RD-13-206, Mississippi Department of Transportation, Jackson, MS.

Howard, I.L., Doyle, J.D., White, T.D., Ivy, J., Booth, O. (2010). *PURWheel Laboratory Wheel Tracker Operator's Manual*. Manual Number CMRC M 10-2, Version 1, Construction Materials Research Center, Mississippi State University, Starkville, MS.

Howard, I.L., Payne, B.A., Bogue, M., Glusenkamp, S., Baumgardner, G.L., Hemsley, J.M. (2012). *Full Scale Testing of Hot-Mixed Warm-Compacted Asphalt for Emergency Paving*, SERRI Report 70015-011, U.S. Department of Homeland Security.

Howard, I.L., Warren, K.A. (2009). "Finite Element Modeling of Instrumented Flexible Pavements under Stationary Transient Loading," *Journal of Transportation Engineering*, 135(2), pp 53-61.

Illinois (2012). *Special Provision for Cold In-Place Recycling (CIR) with Emulsified Asphalt*. Special Provision LR 400-5, Illinois Department of Transportation.

Iowa (2008). *Mix Design Method for CIR with Engineered Emulsion*. Matls IM 504 Appendix B, Iowa Department of Transportation.

Kandhal, P.S., Koehler, W.C. (1987). "Cold Recycling of Asphalt Pavements on Low-Volume Roads," *Transportation Research Record: Journal of the Transportation Research Board*, 1106, pp 156-163.

Kansas (2014). *Mix Design Procedures for CIR (Cold in Place Recycling) Material*. Kansas Department of Transportation Construction Manual, Part V, Section 5.3.4., Kansas Department of Transportation.

Kavussi, A., Modarres, A. (2010a). "A Model for Resilient Modulus Determination of Recycled Mixes with Bitumen Emulsion and Cement from ITS Testing Results," *Construction and Building Materials*, 24, pp 2252-2259.

Kavussi, A., Modarres, A. (2010b). "Laboratory Fatigue Models for Recycled Mixes with Bitumen Emulsion and Cement," *Construction and Building Materials*, 24, pp 1920-1927.

Khosla, N.P., Bienvenu, M.E. (1996). *Design and Evaluation of Cold In-Place Recycled Pavements*. Report No. FHWA/NC/97-006. North Carolina Department of Transportation, Raleigh, NC.

Kim, Y., Im, S., Lee, H. (2011). "Impacts of Curing Time and Moisture Content on Engineering Properties of Cold In-Place Recycling Mixtures using Foamed or Emulsified Asphalt," *Journal of Materials in Civil Engineering*, 23(5), pp 542-553.

Kim, Y., Lee, H. (2006). "Development of Mix Design Procedure for Cold In-Place Recycling with Foamed Asphalt," *Journal of Materials in Civil Engineering*, 18(1), pp 116-124.

Kim, Y., Lee, H. (2008). "Influence of Reclaimed Asphalt Pavement Temperature on Mix Design Process of Cold In-Place Recycling Using Foamed Asphalt," CD-ROM, *Transportation Research Board 87th Annual Meeting*, Washington, D.C., Paper 08-3028.

Kim, Y., Lee, H. (2011a). "Influence of Reclaimed Asphalt Pavement Temperature on Mix Design Process of Cold In-Place Recycling Using Foamed Asphalt," *Journal of Materials in Civil Engineering*, 23(7), pp 961-968.

Kim, Y., Lee, H. (2011b). "Measurements of Moisture Conditions of Cold In-place Recycling Layer," CD-ROM, *Transportation Research Board 90th Annual Meeting*, Washington, D.C., Paper 11-3129.

Kim, Y., Lee, H., Heitzman, M. (2007). "Validation of New Mix Design Procedure for Cold In-Place Recycling with Foamed Asphalt," *Journal of Materials in Civil Engineering*, 19(11), pp 1000-1010.

Kim, Y., Lee, H., Heitzman, M. (2008). "Laboratory Evaluation of Cold In-place Recycling Mixtures using Foamed Asphalt Based on Dynamic Modulus and Repeated Dynamic Load Tests," CD-ROM, *Transportation Research Board 87th Annual Meeting*, Washington, D.C., Paper 08-2300.

Kim, Y., Lee, H., Heitzman, M. (2009). "Dynamic Modulus and Repeated Load Tests of Cold In-Place Recycling Mixtures Using Foamed Asphalt," *Journal of Materials in Civil Engineering*, 21(6), pp 279-285.

Kim, J., Lee, H.D., Jahren, C.T., Heitzman, M., Chen, D. (2010). "Long-Term Field Performance of Cold In-Place Recycled Roads in Iowa," *Journal of Performance of Constructed Facilities*, 24(3), pp 265-274.

Kim, Y., Wen, H. (2002) "Fracture Energy from Indirect Tension Testing," *Journal of the Association of Asphalt Paving Technologists*, 71, pp 779-793.

Kizito, F., Campbell, C.S., Campbell, G.S., Cobos, D.R., Teare, B.L., Carter, B., Hopmans, J.W., (2008). "Frequency, Electrical Conductivity and Temperature Analysis of a Low-Cost Capacitance Soil Moisture Sensor," *Journal of Hydrology*, 352, pp 367-378.

Koh, C., Roque, R. (2010). "Use of Nonuniform Stress-State Tests to Determine Fracture Energy of Asphalt Mixtures Accurately," *Transportation Research Record: Journal of the Transportation Research Board*, 2181, pp 55-66.

Lee, K.W., Brayton, T.E., Gress, D., Harrington, J. (2001). "A Performance-Based Mix-Design Method for Cold In-Place Recycling of Bituminous Pavements for Maintenance Management," *Proceedings of the 9th Maintenance Management Conference*, 23, pp 11-19.

Lee, H., Kim, Y. (2003). *Development of a Mix Design Process for Cold-In-Place Rehabilitation Using Foamed Asphalt*. Final Report for TR-474 Phase I, Iowa Department of Transportation, Ames, IA.

Lee, H., Kim Y., Hwang S. (2009). "Is 1.5% Moisture Content a Necessary Condition Before Overlaying the CIR Layer?" CD-ROM, *Proceedings of the 6th International Conference on Maintenance and Rehabilitation of Pavements and Technological Control*, Turin, Italy.

Leng, Z. (2011). *Prediction of In-Situ Asphalt Mixture Density Using Ground Penetrating Radar: Theoretical Development and Field Verification*. PhD Dissertation, University of Illinois at Urbana-Champaign, Urbana, Illinois.

Lewis, D.E., Jared, D.M., Torres, H., Matthews, M. (2006). "Georgia's Use of Cement-Stabilized Reclaimed Base in Full-Depth Reclamation," *Transportation Research Record: Journal of the Transportation Research Board*, 1952, pp 125-133.

Litzka, J., Haslehner, W. (1995). "Cold In-Place Recycling on Low-Volume Roads in Austria," *Transportation Research Board Conference Proceedings: 6th International Conference on Low-Volume Roads*, Minneapolis, MN, pp 189-194.

Lytton, R.L., Uzan, J., Fernando, E.G., Roque, R., Hiltunen, D., Stoffels, S. (1993). *Development and Validation of Performance Prediction Models and Specifications for Asphalt Binders and Paving Mixes*, Report SHRP-A-357, Strategic Highway Research Program, Washington, D.C.

Mallick, R.B., Bonner, D.S., Bradbury, R.L., Andrews, J.O., Kandhal, P.S., Kearney, E.J. (2002a). "Evaluation of Performance of Full-Depth Reclamation Mixes." *Transportation Research Record: Journal of the Transportation Research Board*, 1809, pp 199-208.

Mallick, R.B., Kandhal, P.S., Brown, E.R., Bradbury, R.L., Kearney, E.J. (2002b). *Development of a Rational and Practical Mix Design System for Full Depth Reclaimed (FDR) Mixes.* Final Report for Subcontract No. 00-373. The Recycled Materials Resource Center, Univ. of New Hampshire, Durham, NH.

Mallick, R.B., Teto, M.R., Kandhal, P.S., Brown, E.R., Bradbury, R.L., Kearney, E.J. (2002c). "Laboratory Study of Full-Depth Reclamation Mixes," *Transportation Research Record: Journal of the Transportation Research Board*, 1813, pp 103-110.

Mamlouk, M.S. (1991). *Low-Volume Roads Rehabilitation Strategies*. Report FHWA-AZ91-840, Arizona Department of Transportation, Phoenix, AZ.

Mamlouk, M.S., Ayoub, N.F. (1983). "Evaluation of Long-Term Behavior of Cold Recycled Asphalt Mixture (Abridgment)," *Transportation Research Record: Journal of the Transportation Research Board*, 911, pp 64-66.

Marasteanu, M.O., Velasquez, R., Falchetto, A.C., Zofka, A. (2009). *Development of a Simple Test to Determine the Low Temperature Creep Compliance of Asphalt Mixtures*. Final Report, Highway IDEA Project 133, Transportation Research Board, Washington, D.C.

Marasteanu, M., Zofka, A., Turos, M., Li, X., Velasquez, R., Li, X., Buttlar, W., Paulino, G., Braham, A., Dave, E., Ojo, J., Bahia, H., Williams, C., Bausano, J., Gallistel, A., McGraw, J. (2007). *Investigation of Low Temperature Cracking in Asphalt Pavements*. Report No. NM/RC 2007-43, Minnesota Department of Transportation, St. Paul, MN.

Marcandali da Silva, A.H., Vasconcelos, K.L., Aranha, A.L., Bernucci, L.B., Chaves, J.M. (2013). "Laboratory and Field Evaluation of Cold In-Place RAP Recycling," *Transportation Research Board 92nd Annual Meeting*, Washington, D.C., Paper 13-4178.

Martinez, A.H., Miró, R., Pérez-Jiménez, F. (2007). "Spanish Experience with Gyratory Compactor and Indirect Tensile Test in Design and Control of Cold Recycled Asphalt Pavement," *Transportation Research Record: Journal of the Transportation Research Board*, 2001, pp 163-168.

MDOT (2004). *Mississippi Standard Specifications for Road and Bridge Construction*. Mississippi Department of Transportation, Jackson, MS.

Miller, J.S., Bellinger, W.Y. (2003). *Distress Identification Manual for the Long-Term Pavement Performance Program (Fourth Revised Edition)*. Report No. FHWA-RD-03-031, Federal Highway Administration, McLean, VA.

Mississippi (2010a). *Roadbed Reclamation with Emulsified Asphalt*. Special Provision 907-425-1, Mississippi Department of Transportation.

Mississippi (2010b). *Roadbed Reclamation with Portland Cement*. Special Provision 907-499-1, Mississippi Department of Transportation.

Modarres, A., Nejad, F.M., Kavussi, A., Hassani, A., Shabanzadeh, E. (2011). "A Parametric Study on the Laboratory Fatigue Characteristics of Recycled Mixes," *Construction and Building Materials*, 25, pp 2085-2093.

Montana (2015). *Cold In-Place Recycling (Partial Depth) Mixture Design*. Special Provision 405-2, Montana Department of Transportation.

Moore, T., Davidson, J.K., Kucharek, A.S., Esenwa, M. (2011). "Early Stage Curing Characteristics of Partial Depth Cold Recycling," *Proceedings of the 56th Annual Conference of the Canadian Technical Asphalt Association*, Quebec, Canada, pp 171-184.

Mull, M., Othman, A., Mohammad, L. (2006). "Fatigue Crack Growth Analysis of HMA Employing the Semi-Circular Notched Bend Specimen," *Transportation Research Board 85th Annual Meeting*, Washington, D.C., Paper 06-1665.

Mohammad, L.N., Cooper, S., King, B., Raghavendra, A. (2013). *Characterization of HMA Mixtures Containing High Reclaimed Asphalt Pavement Content With Crumb Rubber Additives*. Report FHWA/LA 09/465, Louisiana Transportation Research Center, Baton Rouge, LA.

Molenaar, A., Scarpas, A., Liu, X., Erkens, S. (2002). "Semi-Circular Bending Test; Simple but Useful?" *Journal of the Association of Asphalt Paving Technologists*, 71, pp 794-815.

Morian, D.A., Solaimanian, M., Scheetz, B., Jahangirnejad, S. (2012). *Developing Standards and Specifications for Full-Depth Pavement Reclamation*. Report FHWA-PA-2012-004-090107, Pennsylvania Department of Transportation, Harrisburg, PA.

Niazi, Y., Jalili, M. (2009). "Effect of Portland Cement and Lime Additives on Properties of Cold In-Place Recycled Mixtures with Emulsion," *Construction and Building Materials*, 23, pp 1338-1343.

New York (2014). *Geotechnical Engineering Manual: Design and Construction Guidelines for Full Depth Reclamation of Asphalt Pavement*. GEM-27, New York State Department of Transportation.

Noureldin, S., Zhu, K., Harris, D., Li, S. (2005). *Non-Destructive Estimation of Pavement Thickness, Structural Number, and Subgrade Resilience Along INDOT Highways*. Report No. FHWA/IN/JTRP-2004/35, Indiana Department of Transportation, Indianapolis, IN.

O'Leary, M.D., Williams R.D. (1992). "In Situ Cold Recycling of Bituminous Pavements with Polymer-Modified High Float Emulsions," *Transportation Research Record: Journal of the Transportation Research Board*, 1342, pp 20-25.

Pasetto, M., Bortolini, G., Scabbio, F., Carta, I. (2004). "Experiments on Cold Recycling with Foamed Bitumen of Bituminous Emulsion and Cement," *Proceedings of the 3rd Eurasphalt & Eurobitume Congress*, Vienna, 1, pp 494-503.

Rajagopal, A., Crago, D. (2007). *A Comparative Evaluation of the CoreLok Device in Determining Reliable Bulk Specific Gravity and Maximum Specific Gravity Test Results*. Final Report FHWA/OH-2007/07, Columbus, OH.

Rand, D.A. (2006). *Hamburg Wheel Test*. Technical Advisory Dated August 16, 2006, Texas Department of Transportation Construction and Bridge Division.

Rogge, D.F., Hicks, R.G., Scholz, T.V., Allen, D. (1992). "Use of Asphalt Emulsions for In-Place Recycling: Oregon Experience," *Transportation Research Record: Journal of the Transportation Research Board*, 1342, pp 1-8.

Roque, R., Birgisson, B., Drakos, C., Dietrich, B. (2004). "Development and Field Evaluation of Energy-Based Criteria for Top-Down Cracking Performance of Hot Mix Asphalt," *Journal of the Association of Asphalt Paving Technologists*, 73, pp 229-260.

Roque, R., Birgisson, B., Sangpetngam, B., Zhang, Z. (2002). "Hot Mix Asphalt Fracture Mechanics: A Fundamental Crack Growth Law for Asphalt Mixtures," *Journal of the Association of Asphalt Paving Technologists*, 71, pp 816-827.

Roque, R., Buttlar, W.G. (1992). "The Development of a Measurement and Analysis System to Accurately Determine Asphalt Concrete Properties Using the Indirect Tensile Mode," *Journal of the Association of Asphalt Paving Technologists*, 61, pp 304-332.

Roque, R., Buttlar, W.G., Ruth, B.E., Tia, M., Dickson, S.W., Reid, B. (1997). *Evaluation of SHRP Indirect Tension Tester to Mitigate Cracking in Asphalt Pavements and Overlays*. Report No. B-9885, Florida Department of Transportation, Tallahassee, FL.

Salomon, A., Newcomb, D.E. (2000). *Cold In-Place Recycling Literature Review and Preliminary Mixture Design Procedure*. Final Report No. MN/RC-2000-21, Minnesota Department of Transportation, St. Paul, MN.

Santagata, E., Chiapinelli, G., Riviera, P.P., Baglieri, O. (2010). "Triaxial Testing for the Short-Term Evaluation of Cold-Recycled Bituminous Mixtures," *Road Materials and Pavement Design*, 11(1), pp 123-147.

Scherocman, J.A. (1983). "Cold In-Place Recycling of Low-Volume Roads," *Transportation Research Record: Journal of the Transportation Research Board*, 898, pp 308-315.

Schmidt, R.J., Santucci, L.E., Coyne, L.D. (1973). "Performance Characteristics of Cement-Modified Asphalt Emulsion Mixtures," *Journal of the Association of Asphalt Paving Technologists*, 42, pp 300-319.

Scholz, T., Rogge, D.F., Hicks, R.G., Allen, D. (1991). "Evaluation of Mix Properties of Cold In-Place Recycled Mixes," *Transportation Research Record: Journal of the Transportation Research Board*, 1317, pp 77-89.

Schwartz, C.W., Khosravifar, S. (2013). *Design and Evaluation of Foamed Asphalt Base Materials*. Publication No. MD-13-SP909B4E. Maryland State Highway Administration, Baltimore, MD.

Shahin, M.Y. (2006). *Pavement Management for Airports, Roads, and Parking Lots*. 2nd ed., Springer, New York.

Sholar, G.A., Page, G.C., Musselman, J.A., Upshaw, P.B., Moseley, H.L. (2005). "Investigation of the CoreLok for Maximum, Aggregate, and Bulk Specific Gravity Tests," *Transportation Research Record: Journal of the Transportation Research Board*, 1907, pp 135-144.

Skok, G., Dai, S., Westover, T., Lukanen, E., Labuz, J. (2008). *Pavement Rehabilitation Selection*. Report No. MN/RC 2008-06. Minnesota Department of Transportation, St. Paul, MN.

Smith, C.R., Lewis, D.E., Turner, J., Jared, D.M. (2008). "Georgia's Use of Lime in Full-Depth Reclamation," *Transportation Research Record: Journal of the Transportation Research Board*, 2059, pp 89-94.

Spelman, S.R. (1983). "Rural Cold Recycling," *Transportation Research Record: Journal of the Transportation Research Board*, 898, pp 303-307.

Steward, D.A. (1987). "Cold, In-Place Asphalt Pavement Recycling," *Transportation Research Record: Journal of the Transportation Research Board*, 1106, pp 172-178.

Strickland, M.J. (2010). *Construction monitoring of full-depth reclamation in madison count for MDOT Project No. NH-008-03(032)*. Report Number FHWA/MS-DOT-FDR, TRID Accession Number 01340417, Mississippi Department of Transportation, Jackson, MS.

Stroup-Gardiner, M. (2011). *Recycling and Reclamation of Asphalt Pavements Using In-Place Methods: A Synthesis of Highway Practice*. NCHRP Synthesis 421, Transportation Research Board, Washington, D.C.

Sullivan, W.G. (2012). *Investigation of Compaction and Corresponding Thermal Measurement Techniques for Cementitiously Stabilized Soils.* Master's Thesis, Mississippi State University, Mississippi State, MS.
http://sun.library.msstate.edu/ETD-db/ETD-search/search

Sullivan, W.G., Howard, I.L., Anderson, B.K. Development of Equipment for Compacting Soil-Cement into Plastic Molds for Design and Quality Control Purposes. In *Transportation Research Record: Journal of the Transportation Research Board*, No. 2511, Transportation Research Board of the National Academies, Washington, D.C., 2015, pp. 102-111.

Terrel, R.L., Wang, C.K. (1971). "Early Curing Behavior of Cement Modified Asphalt Emulsion Mixtures," *Journal of the Association of Asphalt Paving Technologists*, 40, pp 108-125.

Texas (2004). *Cold In-Place Recycling of Asphalt Concrete Pavement*. Special Specification 3254, Texas Department of Transportation.

Thomas, T., Kadrmas, A. (2002). "Performance-Related Tests and Specifications for Cold In-Place Recycling: Lab and Field Experience," *Transportation Research Board 82nd Annual Meeting*, Washington, D.C., Paper 03-0658.

Thomas, T., Kadrmas, A., Huffman, J. (2000). "Cold In-Place Recycling on US-283 in Kansas," *Transportation Research Record: Journal of the Transportation Research Board*, 1723, pp 53-56.

Virginia (2014). *Special Provision for Cold In-Place Recycling (CIR)*. Special Provision S315X01-1214, Virginia Department of Transportation.

Wagoner, M.P., Buttlar, W.G. (2007). "Influence of Specimen Size on Fracture Energy of Asphalt Concrete," *Journal of the Association of Asphalt Paving Technologists*, 76, pp 391-426.

Watson, D.E., Cooley Jr., L.A., Moore, K.A., Williams, K. (2004). "Laboratory Performance Testing of Open-Graded Friction Course Mixtures," *Transportation Research Record: Journal of the Transportation Research Board*, 1891, pp 40-47.

Wood, J.F. (1980). "Cold-Asphalt Recycling Equipment," *Transportation Research Record: Journal of the Transportation Research Board*, 780, pp 101-102.

Wood, L.E., White, T.D., Nelson, T.B. (1988). "Current Practice of Cold In-Place Recycling of Asphalt Pavements," *Transportation Research Record: Journal of the Transportation Research Board*, 1178, pp 31-37.

Woods, A., Kim, Y., Lee, H. (2012). "Determining Timing of Overlay on Cold In-Place Recycling Layer: Development of New Tool Based on Moisture Loss Index and In-Situ Stiffness," *Transportation Research Record: Journal of the Transportation Research Board*, 2306, pp 52-61.

Wu, H., Huang, B., Shu, X. (2014). "Characterizing Fatigue Behavior of Asphalt Mixtures Utilizing Loaded Wheel Testers," *Journal of Materials in Civil Engineering*, 26(1), pp 152-159.

Wu, Z., Mohammad, L., Wang, L., Mull, M. (2005). "Fracture Resistance Characterization of Superpave Mixtures Using the Semi-Circular Bending Test," *Journal of ASTM International*, 2(3), pp 127-141.

Yan, J., Ni, F., Tao, Z., Jia, J. (2009). "Development of Asphalt Emulsion Cold In-Place Recycling Specifications," *Geotechnical Special Publication*, 190, pp 49-55.

Yan, J., Ni, F., Yang, M., Li, J. (2010). "An Experimental Study on Fatigue Properties of Emulsion and Foam Cold Recycled Mixes," *Construction and Building Materials*, 24, pp 2151-2156.

Zawadzki, J. (2000). “Some Properties of the Mineral-Portland Cement-Emulsion Mix.” *Proceedings of the 2nd Eurasphalt & Eurobitume Congress*, Barcelona, Spain, pp 678-685.

Zhang, Z., Roque R., Birgisson B., Sangpetngam B. (2001). “Identification and Verification of a Suitable Crack Growth Law,” *Journal of the Association of Asphalt Paving Technologists*, 70, pp 206-241.

Zhang, Z., Wu, Z., Matinez, M., Gaspard, K. (2008). “Pavement Structures Damage Caused by Hurricane Katrina Flooding,” *Journal of Geotechnical and Geoenvironmental Engineering*, 134(5), pp 633-643.

Zofka, A., Braham, A. (2009). “Comparison of Low-Temperature Field Performance and Laboratory Testing of 10 Test Sections in the Midwestern United States,” *Transportation Research Record: Journal of the Transportation Research Board*, 2127, pp 107-114.

Zofka, A., Marasteanu, M., Li, X., Clyne, T., McGraw, J. (2005). “Simple Method to Obtain Asphalt Binders Low Temperature Properties from Asphalt Mixtures Properties,” *Journal of the Association of Asphalt Paving Technologists*, 74, pp 255-282.